INVESTIGATING INTERACTION PARTNERS OF YEAST UBPS AND HUMAN USP7 DEUBIQUITINASES

SARA SADAT CHAVOSHI

A DISSERTATION SUBMITTED TO
THE FACULTY OF GRADUATE STUDIES
IN PARTIAL FULFILLMENT OF THE REQUIREMENTS
FOR THE DEGREE OF

DOCTOR OF PHILOSOPHY

GRADUATE PROGRAM IN BIOLOGY
YORK UNIVERSITY
TORONTO, ONTARIO

February 2018

Abstract

Ubiquitin-specific proteases (USPs; Ubps in yeast) are the most abundant family of deubiquitinating enzymes. Their involvement in various cellular processes, which are implicated in development and diseases such as cancer, have made them an important subject of investigation. Protein function correlates with its three-dimensional fold; therefore, structural studies can help identify evolutionary conserved features, catalytic mechanisms and provide clues to specificity and interactions. We examined the expression of soluble *Saccharomyces cerevisiae* deubiquitinating enzymes in *E. coli* for structural studies. Following extensive optimizations Ubp1, the Ubp6 catalytic domain and the Ubp12 N-terminal domain crystallized. The Ubp6 crystals led to the determination of its three-dimensional structure and revealed that the catalytic triad residues are arranged in an active conformation. We showed that the Ubp6 catalytic domain superimposes well with that of USP14, its human homologue. This suggests a similar regulatory mechanism for yeast Ubp6 as compared to human USP14. Further, we investigated the mode of protein interaction of yeast Ubp15. Both *S. cerevisiae* Ubp15 and its human homologue, USP7, harbor a highly conserved DWGF motif in their N-terminal domains. The DWGF motif in USP7-NTD efficiently binds substrates or interacting proteins containing (E/P/A)XXS sequences. We showed that similar to USP7-NTD, the DWGF motif in Ubp15-NTD mediates interaction with (E/P/A)XXS motifs.

To establish latency, human herpesviruses (HHVs) have evolved various mechanisms for host immune evasion. Proteins expressed by some members of the HHV family interfere with the USP7-p53-Hdm2 pathway. They competitively bind to USP7, block USP7-substrate interaction and suppress p53 mediated apoptosis. We identified an EGPS motif in both vIRF1 protein (expressed by Kaposi's sarcoma-associated herpesvirus; KSHV) and pp71 protein (expressed by human cytomegalovirus; HCMV). This motif is identical to the sequence reported in EBNA1 (of Epstein-Barr virus) and ORF45 (of KSHV) responsible for mediating their interaction with USP7-NTD. We demonstrated that both vIRF1 and pp71 interact with USP7-NTD *in vitro* and characterized the interaction using functional studies. The crystal structures of the USP7-NTD:vIRF1 and USP7-NTD:pp71 peptide complexes revealed identical modes of binding as that of the EBNA1 EGPS peptide to USP7-NTD. Our results support new roles for vIRF1 and pp71 through deregulation of the deubiquitinating enzyme USP7, which destabilize p53 and inhibit cellular antiviral responses.

Acknowledgments

First, I would like to express my sincere gratitude to my supervisor and mentor Dr. Vivian Saridakis. This work would not have been possible without your insight and constant feedback. Thanks for letting me be part of your lab and giving me the opportunity and freedom to try, experiment and learn just like a real scientist! After I became a mother of two myself, I truly began to appreciate your hard work and achievements as a mother and a professor with a highly demanding position, and I look up to you as my role-model. Your guidance not only helped me through my research but also writing this thesis. Let me thank-you for all your thorough reviews and insightful critique of my work. Thanks for commenting on my ideas, highlighting the inconstancies, placing back in the missing commas and dashes, and pointing out the grammar mistakes that even my fancy grammar checking program couldn't identify!

My sincere thanks also go to my advisory committee Dr. Bayfield and Dr. White for their thorough review of my work and their insightful critique and suggestions. I'm truly grateful for your time and continuous support. I would like to extend a special thank-you to Dr. Yi Sheng for her help and advice over the past years. Also, I would like to thank my examining committee for their time and insight.

Throughout my project, I have been extremely fortunate to work alongside some of the most supportive, talented and fun lab mates. I am so glad that I got to share all of the ups and downs of the grad school with you, my friends: John Mandawe, Hong Zhen, Ira Lacdao, Niharika Luthra, Leila Ashurov, Rahima Khatun, Stephanie Lombardo, Anthony LaDelpha, Mihai Sfranciog, Jaewon Hwang, Feroz Sarkari, Roland Pfoh, Anna Troshchynsky, Olga Egorova, Sahar Farhadi, Khotira Baryolay, Varvara Gagarina, Hossein Davarinejad, Agnessa Shahla, Lesia Szyca, Farabi Nur, Thaarshinee Thevabalan and all the past and present lab members. You have been the best listeners, study buddies and the perfect scientific minds to discuss ideas with. Thanks for being there for me not only on my happy days but also on those long and stressful days when experiments seem never to work. I'm truly grateful for all your assistance and taking over my experiments when I had to rush out to care for my little ones. I will greatly miss working with you all.

And above ground, I am indebted to my family, my supportive parents, my loving husband and my genius brothers. My dear parents, Shahin and Hassan, there are not enough words to describe how thankful I am for your endless support and love. My dear Laith thanks for blessing me with a life of joy in the hours when the lab lights were off. Your love and endless encouragements have meant the world to me. My dear Sina and Saeid it has truly been a blast growing up with you by my side. Your great achievements have always inspired me. And last but not least, my little angels, Jonas and Maya, thank you for coming into my life and filling it with the greatest joy and happiness I've known.

Table of Contents

List of Tables

Chapter 2

Chapter 3

Chapter 4

List of Figures

Chapter 1

Chapter 2

Chapter 3

Chapter 4

List of Abbreviations

AKT	Protein Kinase B
Ala	Alanine
AMP	Adenosine Monophosphate
APC	Anaphase Promoting Complex
APC/C	Anaphase Promoting Complex /Cyclosome
ARF1	ADP-Ribosylation Factor 1
Arg	Arginine
Asn	Asparagine
Asp	Aspartic Acid
ATM	Ataxia Telangiectasia-Mutated
ATP	Adenosine Triphosphate
ATR	Ataxia Telangiectasia and Rad3-Related Protein
BAX	BCL2 Associated X
BER	Base Excision Repair
BRISC	BRCC36 Isopeptidase Complex
CHFR	Checkpoint with Forkhead and Ring Finger Domains
CRL	Cullin-RING Ligases
CSN	COP9 Signalosome
Cys	Cysteine
CTD	C-Terminal Domain
CYLD	Cylindromatosis Deubiquitinase
DAXX	Death Domain Associated Protein
DNA	Deoxyribonucleic Acid
DTT	Dithiothreitol
DUB	Deubiquitinating Enzyme
DUSP	Domain Present in USPs
EBV	Epstein-Barr Virus
ESCRT	Endosomal Sorting Complex Required for Transport
FANC	Fanconi Anemia Complementation
FITC	Fluorescein Isothiocyanate
GEF	Guanine Nucleotide Exchange Factor
Gln	Glutamine
Glu	Glutamic acid
Gly	Glycine
GMPS	Guanosine 5'-Monophosphate Synthase
GST	Glutathione S-Transferase
GTP	Guanosine Triphosphate
HAUSP	Herpesvirus Associated USP
HCMV	Human Cytomegalovirus
HECT	Homologous to the E6-AP COOH Terminus
HHV	Human Herpesvirus
His	Histidine
HOIP	HOIL-1L-Interacting Protein

HPV	Human Papillomavirus
HRP	Horseradish Peroxidase
HSQC	Heteronuclear Single Quantum Coherence
HSV	Herpes Simplex Virus
IFN	Interferon
IKK	Inhibitor-of-κB Kinase
Ile	Isoleucine
IPTG	Isopropyl β-D-1-Thiogalactopyranoside
IRF	Interferon Regulatory Factor
JAMM	JAB1/MPN/Mov34 Domain
KSHV	Kaposi's Sarcoma Associated Herpesvirus
LANA	Latency-Associated Nuclear Antigen
Leu	Leucine
LUBAC	Linear Ubiquitin Chain Assembly Complex
Lys	Lysine
MALT	Mucosa-Associated Lymphoid Tissue
MATH	Meprin and TRAF-C Homology
MCM-BP	Minichromosome Maintenance Complex Binding Protein
Met	Methionine
MINDY	Motif Interacting with Ub-containing Novel DUB Family
MJD	Machado Joseph Disease/Josephin Domain
NEMO	NF-κB Essential Modulator
NMR	Nuclear Magnetic Resonance
NTD	N-Terminal Domain
OTU	Ovarian Tumor Domain
p/CAF	p300/CBP Associated Factors
PCNA	Proliferating Cell Nuclear Antigen
PCR	Polymerase Chain Reaction
PEG	Polyethylene Glycol
Phe	Phenylalanine
PKB	Protein Kinase B
PML	Promyelocytic Leukemia
PML-NB	Promyelocytic Leukemia Nuclear Bodies
PMSF	Phenylmethylsulfonyl Fluoride
Pro	Proline
PTEN	Phosphatase and Tensin Homolog
PUMA	p53 Upregulated Modulator of Apoptosis
Rb	Retinoblastoma
RBR	RING1, in between RING, RING2
RING	Really Interesting New Gene
RISC	RNA Induced Silencing Complex
RMSD	Root Mean Standard Deviation
RNA	Ribonucleic Acid
RTA	Immediate-Early Transactivator
SAGA	Spt–Ada–Gcn5 Acetyltransferase
SCF	Skp/Cullin/F-Box

SDS	Sodium Dodecyl Sulfate
Ser	Serine
SMAD	Homologues of the *Drosophila* Protein, Mothers Against Decapentaplegic (Mad) and the *Caenorhabditis elegans* Protein (Sma)
STAM	Signal Transducing Adaptor Molecule
STAT	Signal Transducer and Activator of Transcription
SUMO	Small Ubiquitin-related Modifier
TEV	Tobacco Etch Virus
TGF	Transforming Growth Factor
Thr	Threonine
TLR	Toll-Like Receptor
TLS	Translesion Synthesis
TNF	Tumor Necrosis Factor
TRAF	TNF Receptor-Associated Factor
Trp	Tryptophan
Tyr	Tyrosine
Ub	Ubiquitin
UBA	Ubiquitin Associating Domain
UBB	Ubiquitin B Gene
UBC	Ubiquitin C Gene
UBD	Ubiquitin Binding Domain
Ubl	Ubiquitin-Like
Ubp	Ubiquitin Binding Protein
UCH	Ubiquitin C-Terminal Hydrolase
UIM	Ubiquitin Interacting Motif
ULD	UCH37-Like Domain
USP	Ubiquitin Specific Protease
Val	Valine
vIRF	Viral Interferon Regulatory Factor
VZV	Varicella-Zoster Virus

Chapter 1: Literature Review

Specific Proteolysis:

Proteins in cells are highly dynamic, constantly being modified, degraded and remade. Intracellular degradation of proteins is common and essential in all organisms including bacteria. In 1973 Schimke in his comprehensive review of protein turnover proposed that there must be a system or systems involved in protein degradation in contrast to non-specific lysosomal proteolysis (Schimke 1973). Almost two decades later it was demonstrated by Hershko, Ciechanover and Rose that the system involved in targeted protein degradation in most cases is the ubiquitin-proteasome pathway, which led to their 2004 Nobel prize in Chemistry (Wilkinson 2005; Hershko & Ciechanover 1992).

Ubiquitin-mediated proteolysis is highly complex and regulated and is involved in crucial cellular processes such as signal transduction, cell cycle progression, destruction of abnormal proteins, transcriptional regulation, antigen presentation and growth control (Finley et al. 2012; Glickman & Ciechanover 2002). Ubiquitination modifies the surface of the substrate protein affecting its stability, activity, interactions or subcellular localization. With so many pathways involved, it is not unexpected to see that deregulations in the ubiquitin proteolytic pathways have been implicated in many human diseases including malignancies, neurodegenerative disorders, cystic fibrosis, Angelman syndrome as well as immune and inflammatory responses (Hao et al. 2015; Margolis et al. 2015; Deng et al. 2011; Ciechanover 2003; Glickman & Ciechanover 2002).

Ubiquitin-Proteasome Pathway:

Ubiquitin:

Ubiquitin (Ub) is a 76 amino acid long protein engaged in post-translational modification of cellular proteins (Finley et al. 2012). Ubiquitin involvement in crucial cellular processes, such as well-studied proteasome-dependent protein degradation and more recently discovered endocytosis, transcriptional regulation, protein trafficking and cell cycle progression, has made it one of the central elements of eukaryotic cell physiology (Grice & Nathan 2016). The structure of ubiquitin resembles a ß-grasp fold (consisting of a β-sheet with 5 anti-parallel β-strands and an alpha helix that connects β-strands 2 and 3) with a flexible C-terminal tail ending with two signature glycine residues (Burroughs et al. 2012). The Ub structure is conserved and identical

among all eukaryotes from yeast to plants and mammals (Burroughs et al. 2012; Wilkinson et al. 1986). It is suggested that the compact structural architecture, conserved hydrophobic core and extensive hydrogen bonding of ubiquitin is responsible for its unusual heat stability and pH resistance (Callis 2014).

The Ub molecule is one of the most conserved proteins among all eukaryotes to the extent that budding yeast ubiquitin differs in only three amino acids from its human homologue (Zuin et al. 2014). All eukaryotic organisms carry almost identical ubiquitin coding sequences which show extremely low divergence even among very distant species. This observation indicates that the incorporation of any mutations into the ubiquitin coding sequence has been blocked throughout evolution (Zuin et al. 2014). In fact, it was shown that a vector expressing *Arabidopsis thaliana* ubiquitin could fully replace *Saccharomyces cerevisiae* (*S. cerevisiae*) ubiquitin without any phenotypic abnormalities (Ling et al. 2000). Extreme conservation of the amino acid sequence and structural fold of ubiquitin has led to evolutionary conservation of its surface features as well. Many Ub interacting proteins and enzymes involved in the ubiquitin pathway have evolved structurally distinct ubiquitin binding domains (UBDs) that contact conserved surface regions on ubiquitin (Husnjak & Dikic 2012). For instance, ubiquitin core residues around Ile44, known as the Ile44 hydrophobic patch (consists of Leu8, Ile44, His68 and Val70), are essential for Ub-proteasome interaction and Ub mediated endocytosis, while mutagenesis of these residues has no effect on ubiquitin-protein conjugation (Fig. 1-1) (Kulathu & Komander 2012; Haririnia et al. 2008). Another essential surface region on ubiquitin is around Phe4 (including Thr14 and Gln2 residues) which is important for Ub mediated endocytosis and protein internalization. Mutational studies indicated that Phe4 is not involved in Ub-protein conjugation or proteasomal degradation of ubiquitin-tagged proteins (Sloper-Mould et al. 2001). Further, extensive mutational analysis revealed that out of 63 surface residues on the ubiquitin Ile44 hydrophobic patch, the Phe4 patch and C-terminal tail are essential for viability (Zuin et al. 2014; Sloper-Mould et al. 2001). Other surface patches on ubiquitin worth mentioning are: the Ile36 patch, the Asp58 patch, the TEK box and the flexible loop (Fig. 1-1). The Ile36 hydrophobic patch, comprised of Ile36, Leu71 and Leu73, is involved in polyubiquitin chain formation (Suryadinata et al. 2014). The Asp58 polar patch binds the zinc finger UBD of Rabex-5 (guanine nucleotide exchange factor) (Fu et al. 2012). The TEK box surface patch is essential for UBE2S and UBE2C (E2 conjugating enzymes) mediated Lys11-linked Ub chains catalysis (Wickliffe et al. 2011). And lastly, the flexible loop, located between ß-strand1 and ß-strand2 of ubiquitin, contains Leu8 which based on the conformation of the loop can be part of the Ile44 or Ile36 patch. The orientation of the

loop towards the Ile44 patch was shown to be important in Lys33-linked ubiquitin chain synthesis. While leaning of the loop towards Ile36 was observed in Lys6-linked Ub chains (Kristariyanto, Choi, et al. 2015).

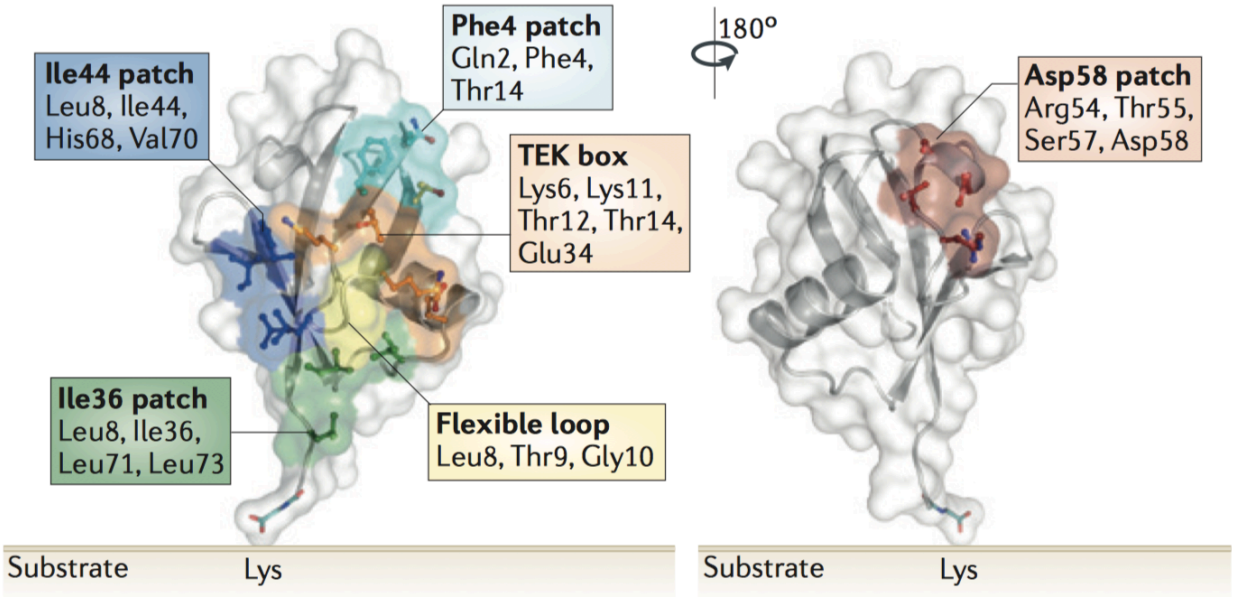

Fig. 1-1: Ubiquitin structure depicting conserved surface motifs. Ubiquitin surface and stick representation (Data bank ID: IUBQ) highlighting the surface patches including the hydrophobic Ile44, Ile36 and Phe4 patches; the polar Asp58 patch, the TEK box and the flexible loop. Residues involved in forming these motifs are identified. Ubiquitin surface patches are involved in protein-protein interactions where the Ile44 and Phe4 patches and di-glycine C-terminal residues have been found essential for viability. The C-terminal tail is imperative for Ub-substrate conjugation. (Reprinted by permission from Nature Publishing Group: Nature Reviews Molecular Cell Biology, (Kulathu & Komander 2012), copyright 2012).

Ubiquitin is exclusively expressed as a fusion protein across all eukaryotes. These precursors are either N-terminal ubiquitin fusions to ribosomal protein subunits or a chain of ubiquitins attached head to toe. UBA52 and RPS27A ubiquitin precursors in humans (Ubi1-Ubi3 in yeast) are fused to two ribosomal proteins L40 and S27a (L40 and S31 in yeast), while UBB and UBC (similar to Ubi4 in yeast) are expressed as a chain of ubiquitin multimers attached with no spacer sequence (Bianchi et al. 2015; Finley et al. 2012). Attachment of even one residue to the C-terminal tail of ubiquitin inhibits ubiquitin-protein conjugation therefore, cleavage of these ubiquitin precursors is essential for their function (Callis 2014; Finley et al. 2012). Abnormalities in expressed ubiquitin precursors are toxic to the cell and have been detected in Alzheimer's, Down syndrome and liver diseases (van Tijn et al. 2011; van Tijn et al. 2007).

Ubiquitination:

Ubiquitin-protein conjugation is achieved when the C-terminal glycine 76 of ubiquitin covalently binds to the amino group of a lysine residue on the substrate protein to form an isopeptide bond. Ligation of ubiquitin to a protein typically involves a three-step cascade mechanism: activation, conjugation and ligation (Callis 2014). Ubiquitination of the substrate protein is initiated when ubiquitin-activating enzyme E1 (Uba1 in yeast) adenylates Ub through an ATP-dependent transthiolation. This modification forms a high energy thioester bond with Ub glycine 76 and a thiol group of a cysteine residue in the E1 active site (Varshavsky 2012; Hochstrasser & Amerik 2004). Ub is then transferred to the active site cysteine residue of one of the ubiquitin-conjugating enzymes, E2 (or UBC) which in return catalyzes ubiquitination with the help of a ubiquitin-protein ligase, E3 (Finley et al. 2012). E3 ubiquitin-protein ligases catalyze the formation of an isopeptide bond between ε-amino group of a lysine residue on the substrate protein and the C-terminal glycine residue of ubiquitin (Fig. 1-2) (Finley et al. 2012). Depending on the type of E3 enzyme involved, ubiquitin can either directly transfer from E2 to the substrate or first form a thioester bond with the E3 ligase which is then transferred to the substrate.

Ubiquitin moieties can be conjugated to any lysine residue on the protein, and there is no known consensus sequence to predict the ubiquitination site (McDowell & Philpott 2013). In some cases, ubiquitination has been reported on specific lysine residues, while in others no particular specificity has been observed. For example, yeast iso-2-cytochrome *c* protein is almost exclusively ubiquitinated on Lys13 and mammalian IκBα protein degradation is induced by

polyubiquitination on Lys21 and Lys22 (Baldi et al. 1996; Sokolik & Cohen 1991). While in the case of the T-cell receptor zeta chain, c-Jun and cyclin B, any lysine residue, even if artificially inserted, can form an isopeptide bond with ubiquitin (McDowell & Philpott 2013; Hou et al. 1994). Typically ubiquitin forms an isopeptide bond with the ε-NH_2 group of lysine residues on the substrate, however, in multiple cases it was observed that removal of all surface lysine residues (either by substitution to arginine or by chemical reductive methylation) does not stop polyubiquitination and proteasomal degradation (Chicooree et al. 2013). Further, polyubiquitination of proteins such as $p16^{INK4a}$ (cell cycle inhibitor) and HPV-58 E7 (human papillomavirus oncoprotein) that naturally don't contain any lysine residues was reported (Ben-Saadon et al. 2004). Later it was shown that ubiquitin could also ligate to the N-terminal α-amino group of lysine-less proteins and some higher eukaryotic proteins such as MyoD (transcriptional activator), cyclin G1, ERK3 kinase and p21 (Noy et al. 2012; Li et al. 2009; Coulombe et al. 2004). Furthermore, in case of Pex5p (peroxisomal import receptor), a lysine-less protein, polyubiquitination and degradation were still observed even when the N-terminal α-amino group was blocked to inhibit its ubiquitination. It was demonstrated that Pex5p both in yeast and human is actually ubiquitinated on a cysteine residue (Platta et al. 2014). Ubiquitin ligation to serine, threonine or cysteine residues forming hydroxyester or thioester bonds has been observed both in yeast and higher eukaryotes (McDowell & Philpott 2013).

A single passage through the ubiquitination cascade leads to monoubiquitination of the substrate while attachment of single ubiquitin moieties to multiple lysine residues on one substrate is referred to as multi monoubiquitination. Catalysis of the isopeptide bond between a lysine residue on the substrate-anchored ubiquitin and free ubiquitin leads to the formation of the polyubiquitin chain (Fig. 1-2) (Finley et al. 2012). Polyubiquitination at Lys48 typically represents a signal for proteasomal degradation, while mono or multi-monoubiquitination in most cases is linked to protein trafficking, localization, DNA repair, transcriptional regulation and proteasomal independent degradation (Callis 2014; Kulathu & Komander 2012).

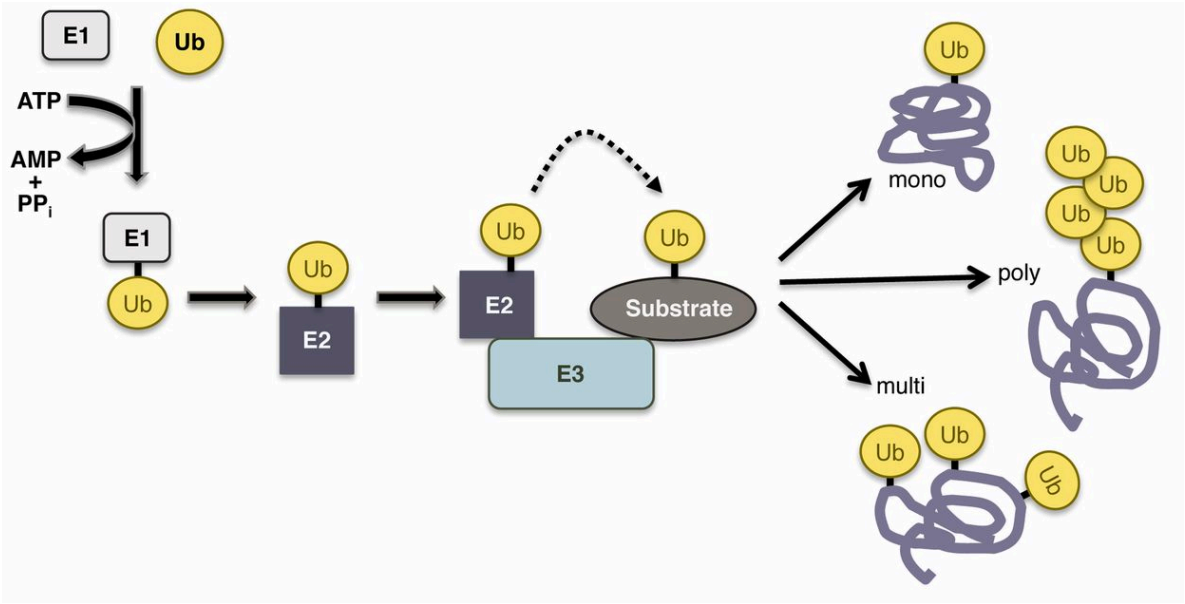

Fig. 1-2: Schematic representation of protein ubiquitination. The E1 activating enzyme in an ATP dependent step forms a thioester bond with ubiquitin (Ub) C-terminal glycine. Ubiquitin is then passed on to the active site of an E2 enzyme. E2 with the help of an E3 ligase enzyme catalyzes isopeptide bond formation between ε-amino group of a lysine residue on the substrate and terminal the carboxyl group of ubiquitin. Attachment of a single Ub moiety to the substrate is termed monoubiquitination while multiple rounds of ubiquitination lead to multi-monoubiquitination or polyubiquitination of the substrate. (Reprinted by permission from Genetics Society of America: Genetics, (Finley et al. 2012), copyright 2012).

E1 Activating Enzymes:

The E1 enzyme catalyzes the first step in the ubiquitination cascade. To activate ubiquitin, the E1 enzyme interacts with a ubiquitin and an ATP molecule. The Ub C-terminus initially forms a non-covalent Ub-adenylate bond with AMP which allows the E1 enzyme active site cysteine residue to attack this bond, form a high energy thioester bond and release the adenylate moiety (Groen & Gillingwater 2015). During the ubiquitin activation process, the E1 enzyme binds a second ubiquitin molecule non-covalently which is important for the E1 enzyme favorable conformational change to transfer Ub to an E2 conjugating enzyme (Schulman & Harper 2009). *S. cerevisiae* codes for one E1 enzyme, Uba1, which is essential for viability (Ghaboosi & Deshaies 2007). In humans two E1 activating enzymes have been identified, UBA1 and UBE1L2. The *UBA1* gene codes for two essential isoforms that show high expression in all cell types and are recognized as the main human E1 enzymes (Groen & Gillingwater 2015). UBE1L2, a recently identified E1 enzyme is more tissue-specific and is mostly expressed in testis (Pelzer et al. 2007). Pharmacological inhibition of UBA1 activity, similar to proteasome inhibition, leads to cell cycle arrest and apoptosis and has been well studied as a potential anti-cancer treatment (Lub et al. 2016; Xu et al. 2013).

E2 Conjugating Enzymes:

Thirty-eight ubiquitin-conjugating enzymes have been identified in humans (11 in yeast) (Stewart et al. 2016; Ghaboosi & Deshaies 2007). E2 enzymes contain a Ub conjugating catalytic domain (UBC) with a conserved cysteine residue in their active site. All E2s should be able to interact with the E1 activating enzyme and catalyze the transfer of ubiquitin to a thiol group in their active site. Further, they have to be able to interact with one or more E3 ligase enzymes and transfer Ub thioester bond to an amino group on the substrate or to the active site of some E3 ubiquitin ligases. (Ye & Rage 2011). Direct transfer of Ub from E2 to amino groups on the substrate has also been reported however, in the absence of E3 enzymes, E2s are typically inefficient in the transfer of ubiquitin (Ye & Rage 2011). E2s are more than just a mediator between E1 and E3 enzymes and show different mechanisms of action. The majority of E2 enzymes in complex with E3 ligases (RING domain type E3s) are able to transfer Ub from their active site to a lysine residue on the substrate, while some E2s transfer Ub to a cysteine residue in the E3 enzyme's active site (HECT domain type E3s, discussed below) (Stewart et al. 2016). For some E2s, such as UBE2G2 in humans (Ubc7 in yeast), transfer of polyubiquitin chain *en*

bloc to the substrate has been reported (Liu et al. 2014; Ravid & Hochstrasser 2007). Heterodimeric E2s, such as UBC13 in complex with Mms2 (catalytically inactive E2), promote Lys63-linked polyubiquitin chain formation by specifically transferring charged Ub to a substrate-anchored acceptor ubiquitin (Campbell et al. 2012). E2 enzymes have also been implicated in non-lysine ubiquitination of the substrate. In yeast, the Pex2 conjugating enzyme directly ubiquitinates Pex5p, a lysine-less protein, on a conserved cysteine residue (Williams et al. 2007). The UBE2J2 conjugating enzyme in humans can transfer ubiquitin to serine or threonine residues on substrate proteins. Similarly, its yeast homologue, Ubc6, is involved in ubiquitination of lysine-free Asi2 protein (Boban et al. 2015).

E2 enzymes help bring specificity to the ubiquitin pathway through selective interaction with different substrates and E3 ligase enzymes. For instance, depending on the type of E3 ligase it interacts with, Rad6/Ubc2 (UBE2A & B in humans) can promote mono or polyubiquitination (Imura et al. 2015). It monoubiquitinates histone H2B and proliferating cell nuclear antigen (PCNA), while it is also involved in N-end rule substrate polyubiquitination and degradation (protein degradation based on the N-terminal amino acid residues, where basic amino acids such as arginine and Lys are primary destabilizing due to their recognition by E3 ligases) (Kumar et al. 2010). Cdc34, an essential yeast E2 enzyme, and its human homologue, UBE2R1, are the main E2 ligases for the Skp/Cullin/F-Box (SCF) E3 ligase complex (Sandoval et al. 2015). While Cdc34 in complex with the San1 E3 ligase is involved in degradation of misfolded or damaged proteins (Finley et al. 2012). Yeast Ubc4 and Ubc5 (homologues of UBCH5 in humans) through interaction with Rsp5 E3 ligase recognize and monoubiquitinate misfolded proteins (Stoll et al. 2011). While Ubc4/Ubc5 interaction with Not4p E3 ligase mediates stress response (Mulder et al. 2007). Also, it has been shown that in yeast Ubc1 and Ubc4 work sequentially to polyubiquitinate proteins involved in cell cycle progression targeted by the anaphase promoting complex (APC) E3 ligase. While Ubc4 supports multi-monoubiquitination of APC substrates, Ubc1 (and its human homologue E2-25K) promotes APC-dependent Lys48-linked ubiquitin chain elongation (Rodrigo-Brenni & Morgan 2007).

E3 Ligase Enzymes:

E3 ubiquitin ligases are the largest group of enzymes involved in protein ubiquitination. They bring specificity to the pathway through selective substrate recognition. Based on the mechanism of ubiquitination and presence of the conserved domains that mediate ubiquitin transfer from E2

enzyme to the substrate, E3 enzymes are categorized into two major groups: The HECT domain (homologous to the E6-AP COOH terminus) E3 ligases and RING domain (really interesting new gene) E3 ligases (which also includes the U-box domain E3s) (Scheffner & Kumar 2014; Varshavsky 2012). The HECT domain E3s are named after human E6AP (E6 associated protein) enzyme which is deregulated by the E6 oncoprotein of certain human papillomaviruses. The HECT domain ligases mediate ubiquitination by first transferring Ub from the E2 enzyme to their active site's conserved cysteine residue. This generates a thioester intermediate prior to transfer of ubiquitin to the substrate protein (Scheffner & Kumar 2014). In case of the RING domain E3s, Ub is directly transferred from ubiquitin-charged E2 enzyme to the E3 ligase-bound substrate (Fig. 1-3) (Finley et al. 2012; Deshaies & Joazeiro 2009). To date, bioinformatics analysis has identified 617 E3 ligases in humans (80 in yeast) out of which only 28 (5 in yeast) belong to the HECT domain E3s (Finley et al. 2012; Deshaies & Joazeiro 2009; W. Li et al. 2008).

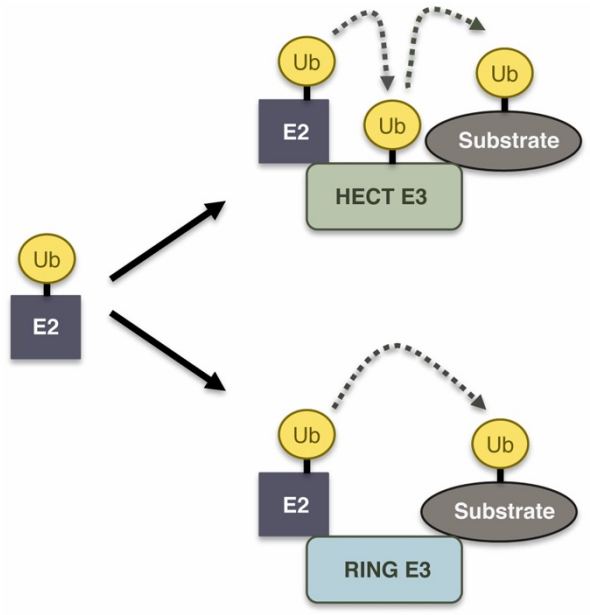

Fig. 1-3: The mechanism of ubiquitin ligation catalyzed by E3 enzymes. The HECT domain E3 ligases initially form a thioester bond with ubiquitin on their active site cysteine residue before transferring Ub to the substrate. While the RING domain E3 ligases provide a platform for E2 enzymes to directly transfer ubiquitin to the substrate. (Reprinted by permission from Genetics Society of America: Genetics, (Finley et al. 2012), copyright 2012).

The RING and U-box Domain E3 Ligases:

The RING E3 ligases belong to the zinc finger domain family of proteins that are typically involved in protein-protein or protein-DNA interaction. However, the RING-type zinc finger domain of E3s are often involved in the ubiquitin-mediated protein degradation pathway and especially recognize proteins such as E2 conjugating enzymes (Callis 2014). RING E3s contain seven cysteine and one histidine residues in their active site that coordinate two zinc ions (Deshaies & Joazeiro 2009). Ubiquitin-charged E2 enzymes initially interact with the zinc finger domain of RING E3 ligases which leads to destabilization of the Ub-E2 thioester bond and therefore promotes the transfer of Ub from E2 to the amino group of an E3-bound substrate (Das et al. 2013). U-box E3 ligases are structurally related to the RING domain E3 enzymes. The U-box motifs similar to the zinc finger domain, interact with Ub-charged E2 enzymes however, in their active site instead of zinc binding cysteines and a histidine residue, they contain charged and polar amino acids, such as glutamic acid and serine. These residues produce a strong network of hydrogen bonds and salt bridges that supports the E3 enzyme's structure and stabilizes its interaction with E2 enzymes (Callis 2014). Computational analysis and genome-wide screening have identified 300 genes in humans (47 in *S. cerevisiae*) that code for RING finger domain proteins, out of which only 8 code for U-box motif containing proteins (2 in yeast). Including RING domain containing E3 enzyme complexes, an estimate of 616 RING or U-box E3 ligases are identified in humans which comprises more than 95% of the total E3 ligase enzymes (W. Li et al. 2008). 26 RING finger domain E3 ligases are highly conserved in eukaryotes from yeast to plants and humans (W. Li et al. 2008). However, not all RING finger domain E3s identified through bioinformatics analysis have shown E3 ligase activity. For example, proteins such as Hdmx and BMI1 contain a RING domain but are not active ligases however, their interaction with an E3 ligase, Hdm2 and RING1B respectively, stimulates ubiquitination activity (McGinty et al. 2014; Shadfan et al. 2012).

The RBR Domain E3 Ligases:

A newly described family of the RING domain E3 enzymes with at least 14 members is referred to as the RBR (RING1, in between RING, RING2) domain E3 ligases (Deshaies & Joazeiro 2009). These enzymes that represent the second largest RING domain E3s, contain three RING-like domains each of which coordinates two Zn^{2+} ions. The N-terminal RING1 domain highly resembles a standard RING domain E3 ligase, while the mid region and the third

RING motifs are more variable and do not conform to the canonical RING E3 structure (Dove et al. 2016). The ubiquitin-charged E2 initially interacts with the RING1 domain however, similar to a HECT domain E3 ligase, the Ub thioester bond is transferred to a conserved cysteine residue in the RING2 domain prior to its transfer to an amino group on the substrate (Spratt et al. 2014). All three RING-like domains in the RBR E3s are required for ubiquitin ligase activity. The RBR E3 ligases are complex multidomain proteins. They typically contain protein-protein interaction motifs in their N or C-termini which are involved in the regulation of E3 enzyme's Ub chain assembly or have an inhibitory effect on the E3 activity (Spratt et al. 2014). The best studied RBR domain E3 ligase in humans is Parkin, which is essential for mitophagy (autophagy of mitochondria). Parkin contains an N-terminal ubiquitin like domain (Ubl) that contacts Parkin's RING1 domain and inhibits its interaction with the E2 enzymes. Phosphorylation of the Ubl domain suppresses its inhibitory effect. Mutations in the Parkin gene is linked to autosomal recessive Juvenile Parkinson's disease (Ham et al. 2016).

The Complex RING Domain E3s:

One of the most conserved and abundant multisubunit RING domain E3s is the SCF (Skp1-Cullin1-F-box) complex. Out of 616 RING-type ligases identified in humans about 287 genes code for SCF containing domains (W. Li et al. 2008). In SCF complexes, which are cullin-RING ligases (CRL), the E2 docking motifs and the substrate interaction motifs are on different subunits connected together with a cullin type protein scaffold (Zheng et al. 2016). A RING domain protein bound to cullin1 scaffold, such as RBX1 (RING box 1), recruits the Ub-charged E2 enzyme which in most cases is UBE2R1 (Cdc34 in yeast) (Sandoval et al. 2015). Skp1 (S phase kinase-associated protein 1) acts as a linker or adaptor that connects an F-box substrate binding protein to cullin1. Skp1 and cullin1 proteins are the invariant subunits of each SCF complex, while 69 F-box proteins that have been identified in humans bring specificity to the SCF complex (Gorelik et al. 2016).

The anaphase promoting complex/cyclosome (APC/C) is an essential and highly conserved multisubunit RING domain E3 ligase with more than ten core proteins and a minimum of 13 subunits. Conserved Apc11 and Apc2 are the RING and cullin subunits that recruit the Ub charged E2 enzymes (He et al. 2013). Interaction of the APC with different activator proteins directs the complex's ubiquitination activity towards certain substrates. The APC-substrate interaction is heavily regulated during mitosis mainly through phosphorylation. Its

phosphorylation by Cdk1 (cyclin-dependent kinase 1) in yeast during prophase to anaphase transition leads to the recruitment of Cdc20 activator protein. Cdc20 promotes the APC mediated destabilization of substrates such as securin and cyclin B which results in sister chromatin disjunction and triggers chromosome segregation (Hellmuth et al. 2015; Metzger et al. 2012; Deshaies & Joazeiro 2009). Replacement of the Cdc20 activator protein by Cdh1 in mitotic exit and G1 phase promotes the APC to target the Cdc20 itself, as well as, Aurora-A kinase and Cdc25 phosphatase. This leads to activation of important cell cycle regulators such as p21 and p27. Phosphorylation of the Cdh1 stimulates its dissociation from the APC complex and promotes cell cycle transition to S phase (Qiao et al. 2016; Metzger et al. 2012). The Cdc20 and Cdh1 activator proteins increase the APC/C activity by enhancing its interaction with the Ub charged E2 enzymes (Van Voorhis & Morgan 2014).

The polycomb repressive complex 1 (PRC1) is another RING domain E3 ligase complex. It is part of a family of multimeric complexes known as the polycomb group. Members of the polycomb group are involved in chromatin compaction and gene silencing and are essential for cell differentiation and development (Abdouh et al. 2016). The PRC1 complex is composed of RING1A, RING1B and BMI1 core proteins which together are involved in monoubiquitination of the histone H2A. The BMI1 RING finger protein is especially involved in heterochromatin formation in somatic cells, while RING1A/B perform ubiquitination of H2A (Lin et al. 2015). RING1B E3 ligase and its coactivator BMI1, recognize tri-methylated Lys27 on histone 3 (H3) and monoubiquitinate chromatin at H2A on Lys119. This leads to transcriptional silencing and has an established role in X chromosome inactivation (Vidal 2009).

The constitutive photomorphogenesis protein 1 (COP1) is a RING domain complex initially identified in *Arabidopsis* where it acts as a switch for plant growth underground in darkness versus growth under light exposure (Callis 2014). COP1 regulates plant's response to the infrared, blue and ultraviolet lights by downregulating transcription factors that bind light-responsive promoters (Callis 2014). In mammals, COP1 modulates glucose and lipid metabolism. Further, it regulates tumorigenesis through downregulation of substrates such as p53 and c-Jun (Sanchez-Barcelo et al. 2016). The COP1 mediated downregulation of tumor suppressors, such as p53, p27 and 14-3-3σ, induces cell cycle progression and has been linked to tumorigenicity (Sanchez-Barcelo et al. 2016).

The HECT Domain E3 Ligases:

The HECT domain E3 ligases contain a 350-residue long conserved motif at their C-termini which resembles human E6AP enzyme's C-terminus. The N-terminal extension of these enzymes contains different motifs or domains that mediate substrate specificity (Metzger et al. 2012). The HECT domain itself contains two sections: The N-lobe that recruits the Ub-charged E2 enzymes and the C-lobe that contains a highly conserved cysteine residue required for intermediate thioester bond formation with ubiquitin. Structural studies have revealed that the two lobes of the HECT domain are flexible. Upon Ub-E2 docking on the N-lobe, conformational change brings the two lobes to close proximity to allow transfer of the ubiquitin from the N-lobe to the conserved cysteine on the C-lobe (Scheffner & Kumar 2014). The linkage type of ubiquitin chain assembled by the HECT domain solely depends on the C-lobe and is not affected by the E2 enzyme involved (Kim & Huibregtse 2009). Based on the N-terminal extensions of the HECT E3 ligases they are divided into three subfamilies: the Nedd4-like E3s, the HECT and RCC1-like domain E3s (HERC) and the "others" (Metzger et al. 2012).

The Nedd4-like E3 ligases include nine members with a characteristic N-terminal calcium-dependent lipid binding domain (C2) followed by 2-4 WW domains (involved in protein-protein interaction) and a C-terminal E6AP homology domain (Scheffner & Kumar 2014). The Nedd4-like E3s have a significant role in cancer development through regulation of trafficking and stability of proteins that are linked to tumorigenesis, such as SMAD, p53 and Jun families (Chen & Matesic 2007). Nedd4 (Neural precursor cell-expressed developmentally downregulated gene 4) is the first member of this subfamily that was identified and is highly conserved and essential for viability among all eukaryotes. Nedd4 is mostly involved in the regulation of membrane proteins and promotes their endocytosis (Scheffner & Kumar 2014). It has been shown that viral matrix proteins expressed by Ebola virus, retrovirus and Epstein-Barr virus interact with Nedd4 leading to their ubiquitination and recognition by the cellular ESCRT complex (endosomal sorting complex required for transport) which is important for their eventual budding from the host cell (Sette et al. 2013; Blot et al. 2004).

The human HERC E3 subfamily has six members (HERC1-6). These unusually large proteins, reaching up to 500 kDa, harbor one to three RLDs (RCC1-like domains) and one E6AP homology domain (Sanchez-Tena et al. 2016). RCC1 (Regulator of chromosome condensation 1) is a guanine nucleotide exchange factor (GEF) for small GTP-binding protein (also known as

Ran). The RLDs consist of seven repeats of a 50-70 residue motif and have dual functions as a GEF and E3 ubiquitin ligase. One end of the RCC1 functions as GEF and interacts with the small GTP-binding protein, while the other end contacts histones to allow interaction with the chromatin (Hochrainer et al. 2005). HERC1 is the first identified member of the HERC E3 ligases. It's a 530 kDa protein that acts as a GEF for ARF1 (ADP-ribosylation factor 1, a GTP binding protein) however, it does not ubiquitinate ARF1 suggesting that HERC1 has separate substrates for the GEF and E3 ligase activities (Sanchez-Tena et al. 2016; Diouf et al. 2011).

The "others" members of the HECT domain E3 ligases do not contain the C2-WW-HECT structure of the Nedd4-like E3s or the RCC1-like domain of the HERCs. The best example of such HECT E3 enzyme is E6AP, the first HECT domain E3 ligase that was identified in HPV infected cells associated with cervical cancer (Scheffner & Kumar 2014). The E6AP (expressed from *UBE3A* gene) was found as a binding partner with the HPV E6 oncoprotein. In HPV infected cells, the E6 viral protein induces interaction of the E6AP E3 ligase with proteins that are not its cellular substrates, such as p53, and leads to their ubiquitination and degradation, which contributes to HPV mediated cervical cancer (Mortensen et al. 2015). E6AP is known to function as both coactivator and downregulator of the steroid hormone receptors, such as estrogen, progesterone and androgen (Ramamoorthy et al. 2012). Mutations in the E6AP gene that cripple its activity have been linked to Angelman syndrome, a neurodevelopmental disorder (Margolis et al. 2015).

E4 Ligase Enzymes:

A relatively new class of ubiquitin ligases known as E4, ubiquitin chain assembly factor, selectively interact with previously ubiquitinated proteins and catalyze elongation of the ubiquitin chain. These enzymes cannot ubiquitinate proteins that are not previously ubiquitinated by an E3 ligase enzyme (Micel et al. 2013). For instance, p300, an E4 enzyme, is involved in polyubiquitination of p53 following its mono or multi-monoubiquitination by Hdm2 (Crosas et al. 2006). Ufd2 is the first E4 ligase that was identified in yeast. Its human homologue, UBE4B (ubiquitin factor E4B), similar to the p300 is involved in polyubiquitination of p53 (Micel et al. 2013). It acts as a cofactor for Hdm2 and catalyzes elongation of Ub chains on p53, which leads to p53 instability and inhibition of its transactivation. Overexpression of the UBE4B is observed in colon cancer, breast cancer, promyelocytic leukemia and medulloblastoma, whereas deletion of the UBE4B gene results in apoptosis of cancer cells (X.-F. Zhang et al. 2016; Li et al. 2003).

Ubiquitin-Like Proteins:

In recent years, a number of ubiquitin-related family of proteins have been identified that share the same beta-grasp structure. Ub-like proteins (Ubls) employ a pathway homologous to the ubiquitination for conjugation to their substrates. These three-step enzymatic cascades, similar to ubiquitination, utilize E1, E2 and E3 enzymes specific to each type of Ubl involved (Ronau et al. 2016). Other than the Nedd8 the rest of the identified Ubls, such as SUMO, ISG15 and Fat10 do not show much sequence similarity to ubiquitin. SUMO (small ubiquitin-related modifier) is the most abundant Ubl in the cell after ubiquitin. Mixed linkages of SUMO-Ub have also been reported (Ronau et al. 2016). Nedd8 is highly related to the ubiquitin both in sequence and structure and similarly contains a conserved Ile44 hydrophobic patch, which is important for its protein-protein interaction (Soucy et al. 2009). Nedd8 interacts with the CRL (Cullin-RING ubiquitin ligase) enzyme complexes and facilities transfer of Ub to the substrate. Neddylation of the CRLs is essential for their enzymatic activity and substrate ubiquitination. In conjugation with the CRL enzymes, Nedd8 also regulates rate of substrate ubiquitination and degradation (Zhao & Sun 2013). Similar to the ubiquitination pathway Nedd8 is activated by Nedd8 activating enzyme. Activated Nedd8 is then transferred to Nedd8 specific E2 enzymes, UBC12 or UBE2F, through transthiolation. UBC12 or UBE2F process the transfer of Nedd8 to a conserved Lys residue at the C-terminal end of cullin protein of the CRL complex (Zhao & Sun 2013). Nedd8 interaction with the CRL complex leads to conformational changes that are necessary for CRL interaction with the Ub-charged E2 enzymes (Micel et al. 2013; Soucy et al. 2009).

Functional Diversity in Ubiquitination Patterns:

Ubiquitin contains seven lysine residues including: Lys6, Lys11, Lys27, Lys29, Lys33, Lys48 and Lys63 and a signature glycine-glycine C-terminal end (Fig. 1-4) (Trempe 2011). Each of these lysines can form an isopeptide bond with another ubiquitin to form a Ub-Ub chain of uniform linkage (homotypic) with seven possible linkage types. Ubiquitin can also bind the N-terminal amino group of another ubiquitin and form a Met-linked or linear linkage chain (Fujita et al. 2014; Trempe 2011; Dikic et al. 2009). Mixed-linkage (heterotypic) polyubiquitin chains have also been reported however, their significance is not well understood (Husnjak & Dikic 2012; Dikic et al. 2009). Ub-Ub linkage types lead to the formation of chains that are structurally different and produce distinct signals. Lys48-linked ubiquitin chains, which are essential for

viability, are the most abundant linkage-type both in humans (52%) and yeast (29%) however, Lys63 at 38% is the second most abundant in humans, while Lys11 at 28% forms the second most abundant linkage in yeast followed by Lys63 at 16% (Trempe 2011).

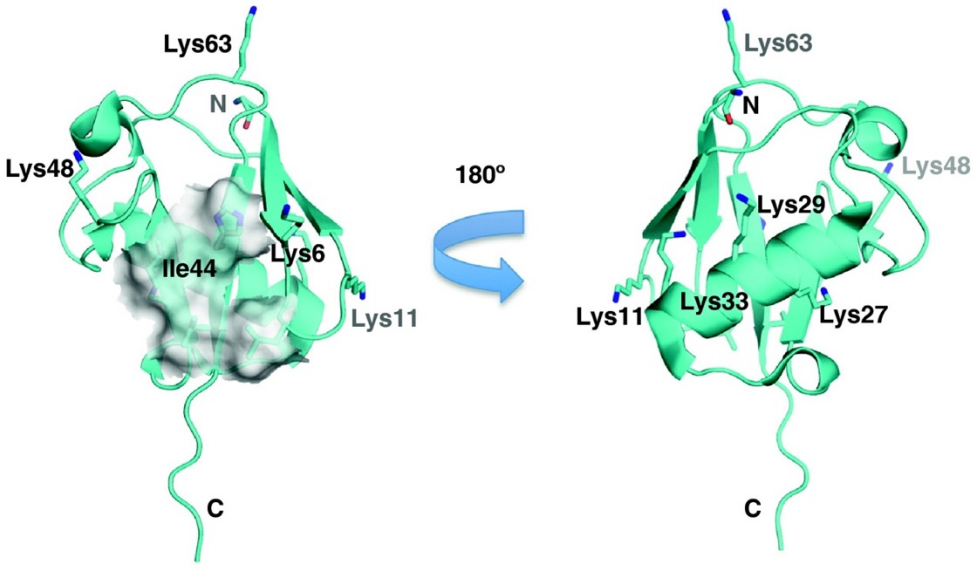

Fig. 1-4: The ubiquitin structure. Ubiquitin contains seven lysine (Lys) residues (shown as sticks). Each of these lysine residues can form an isopeptide bond with another ubiquitin to produce a Ub-Ub chain with seven possible structurally different linkage types. The white surface representation refers to the hydrophobic Ile44 patch. The N and C-terminal domains have been identified. (Reprinted by permission from Elsevier: Current Opinion in Structural Biology, (Trempe 2011), copyright 2011).

Monoubiquitination is the first step to start assembly of the polyubiquitin chain. On its own monoubiquitination in the majority of the known cases is implicated in protein localization, membrane receptor internalization, transcription regulation and DNA repair. For instance, RING1B component of the PRC1 E3 ligase complex monoubiquitinates histone H2A, which leads to chromatin compaction and gene silencing (Abdouh et al. 2016). Recent findings indicate that mono or multi-monoubiquitination of the substrate can also lead to proteasomal degradation. For instance, multi-monoubiquitination of cyclin B1 catalyzed by the APC complex along with the UBCH10, E2 ligase, results in its proteasomal degradation (Dimova et al. 2012). Further, it's been reported that monoubiquitination of small proteins (about 20 residues long) on their N-terminal α-amino group also leads to their rapid proteasomal degradation (Kravtsova-Ivantsiv & Ciechanover 2012).

Lys48-linked polyubiquitin chains of four or more ubiquitins are efficiently recognized by the 26S proteasome and target proteins for proteolytic degradation (Varshavsky 2012). Under physiological conditions, the hydrophobic Ile44 patch on the ubiquitin mediates compact Lys48-linked chain formation resulting in an intermolecular interface between the two joint ubiquitin molecules, which involves residues Leu8, Ile44 and Val70 of the hydrophobic patch (Fig. 1-5)(Suryadinata et al. 2014; Kulathu & Komander 2012). NMR studies have revealed a less favorable conformation for Lys48 linkage under acidic conditions (pH6.8) which is formed through the interaction of the Ile44 hydrophobic patch of one ubiquitin with the Ile36 patch of another (Suryadinata et al. 2014). The hydrophobic patch on the ubiquitin surface not only is essential for Lys48 compact chain formation, but it is also important for the interaction of these chains with the 26S proteasome subunits (Husnjak & Dikic 2012). Further, proteins known as proteasome shuttling receptors, such as Rad23 in yeast (HR23B in humans), specifically recognize Lys48-linked Ub chains and shuttle tagged proteins to the proteasome (Shi et al. 2016).

Lys63-linked Ub chains, both in humans and yeast, have non-proteolytic function and are implicated in DNA repair, intercellular protein trafficking, endocytosis and vacuolar protein sorting (Trempe 2011). Lys63 linkage has open conformation in which the two ubiquitin molecules are only connected through the linkage point (Fig. 1-5)(Kulathu & Komander 2012). Both Lys48 and Lys63 ubiquitinated proteins can bind pure proteasome with similar affinities *in vitro* however, Lys63 Ub chains do not affect the stability of the substrate proteins *in vivo* (Xu et al. 2009). Further, proteasome inhibition does not increase cellular levels of Lys63 linkage type,

confirming the non-proteolytic function of these chains (Kim et al. 2011). It was shown that compared to the Lys48-linked polyubiquitin chains, Lys63 chains are much faster disassembled from the tagged proteins, which inhibits their recognition by the proteasome (Nathan et al. 2013). Also, several proteins and complexes such as ESCRT0 have been identified that specifically and tightly interact with the Lys63-linked Ub chains and block their interaction with the proteasome (Nathan et al. 2013).

Lys11-linked polyubiquitin chains are mostly involved in the endoplasmic reticulum (ER) associated degradation and mitophagy (Grice & Nathan 2016). In addition, Lys11 linkage catalyzed by the APC E3 ligase complex on the cell cycle proteins, such as cyclin B1 and securin, has been found important for cell cycle progression (Min & Lindon 2012). Lys11-connected ubiquitins form a compact structure with an intermolecular interface mediated through the Ile36 patch (Fig. 1-5)(Kulathu & Komander 2012). It has been reported that the Ly11-linked Ubs do not efficiently lead to proteasomal degradation however, a recently identified heterotypic Ly11/Lys48 mixed chain catalyzed by the APC on the cell cycle proteins, such as cyclin A, is recognized by the proteasome and leads to downregulation of the tagged protein. Proteasome inhibition has led to the enrichment of the Lys11 chains indicating their proteolytic function (Swatek & Komander 2016; Ikeda & Dikic 2008). In contrast to steady levels of the Lys48 and Lys63 linkage types, cellular levels of the Lys11-linked Ub chains are cell cycle dependent and significantly increase following mitosis (Kulathu & Komander 2012).

Linear ubiquitin chains (also referred to as Met-linked) have open conformation in which Gly76 of one ubiquitin forms an isopeptide bond with the α-amino moiety of the methionine residue of another ubiquitin (Fig. 1-5) (Kulathu & Komander 2012). Linear ubiquitin chain assembly complex (LUBAC), an RBR E3 ligase, is the only identified E3 ligase that produces Met-linked polyubiquitin (Iwai 2011). The LUBAC mediated linear chains have been shown important in the regulation of the tumor necrosis factor (TNF) and activation of the nuclear factor κB (NF-κB) transcription factor. Linear-linked Ubs were identified on NEMO, a subunit of the Inhibitor-of-κB kinase (IKK), which further linked linear ubiquitination to the IKK degradation, NF-κB activation and cell death (Swatek & Komander 2016; Iwai et al. 2014). In addition, Met-linked polyubiquitination of certain proteins, such as PCNA (a replication clamp protein), NPL4 (nuclear protein localization4) and UFD1 (ubiquitin fusion degradation 1), efficiently promotes their proteasomal degradation (Kravtsova-Ivantsiv & Ciechanover 2012).

Lys6-linked ubiquitin chains form a compact structure mediated through the Ile44 and the Ile36 patches of each ubiquitin (Fig. 1-5). Proteasomal inhibition does not lead to accumulation of the Ly6-linked chains indicating their non-proteolytic function (Swatek & Komander 2016). One study showed that Lys6 and Lys33-linked chains largely increase upon UV stress, associating Lys6 ubiquitination with the DNA damage response (Elia et al. 2015). The Lys6 linkage has also been implicated in mitochondrial degradation. In fact, mutation of the ubiquitin's Lys6 resulted in the delay in mitophagy (Ordureau et al. 2015).

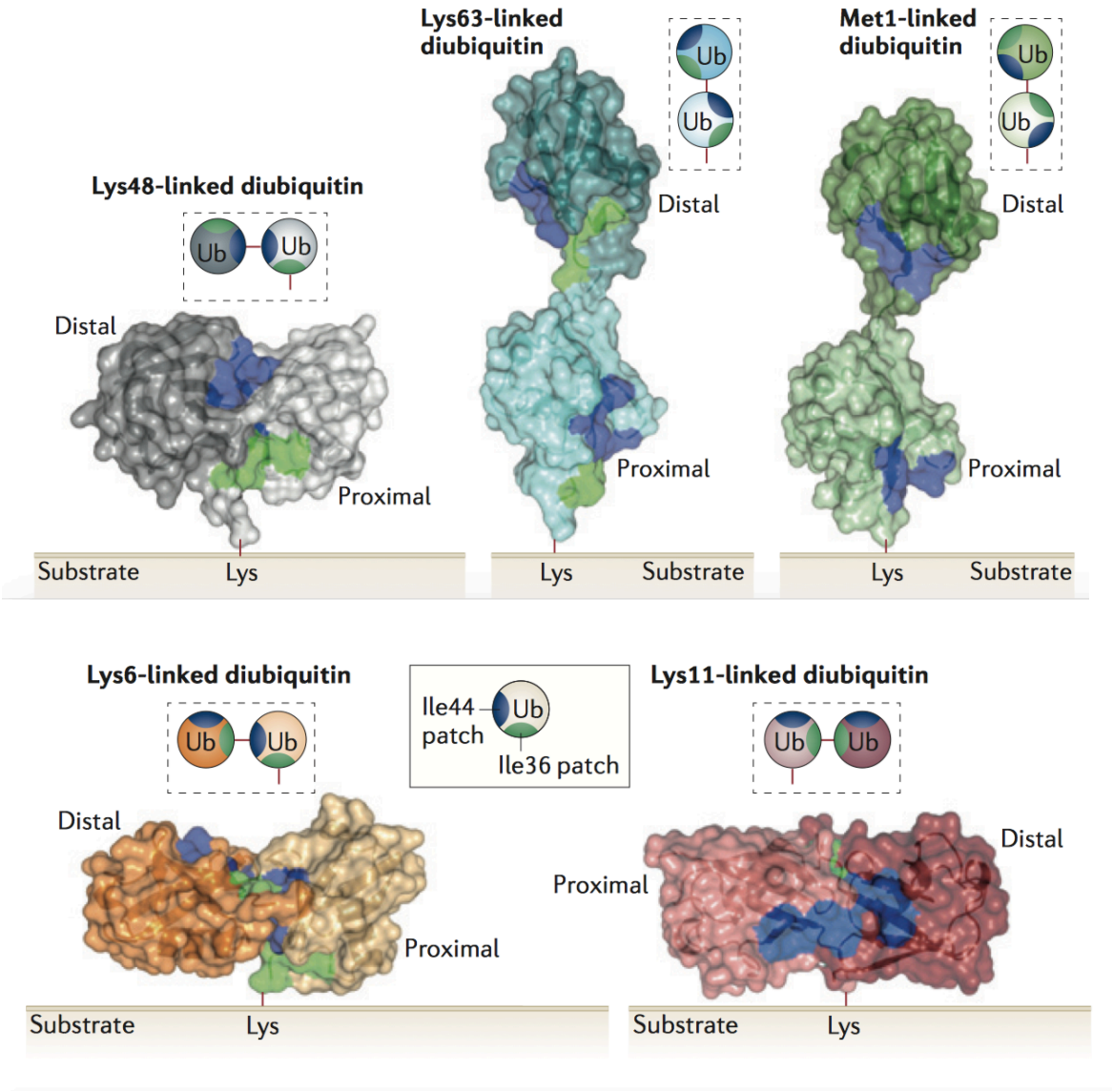

Fig. 1-5: Crystal structure of the different ubiquitin linkage types. Surface representation of the diubiquitins in varying linkage types including: Lys48, Lys63, Met-linked (or linear linkage), Lys11 and Lys6 are shown (Protein Data Bank IDs: 2XK5, 3NOB, 1AAR, 2JF5 and 2W9N). The hydrophobic Ile44 (in blue) and Ile36 (in green) patches involved in the intermolecular interactions are indicated. (Reprinted by permission from Nature Publishing Group: Nature Reviews Molecular Cell Biology, (Kulathu & Komander 2012), copyright 2012).

The other linkage types, Lys27, 29 and 33, have been detected in very low levels in the cell and their role in the proteasomal degradation is not well understood. Ring finger E3 ligase, RNF168, was shown to polyubiquitinate histone H2A with Lys27-linked ubiquitins, which was upregulated in response to DNA double-strand breaks. The Lys27 linkage is implicated in DNA damage response and leads to recruitment of DNA double-strand break response proteins such as p53 binding protein (53BP1) and breast cancer associated gene 1 (BRCA1) to DNA damage response foci (Gatti et al. 2015). Lys29-linked chains are assembled by UBE3C, a HECT domain E3 ligase, and have been linked to proteasomal degradation (Kristariyanto, Abdul Rehman, et al. 2015). Lys33-linked Ub chains are assembled by AREL1, HECT E3 ligase, and are implicated in Golgi membrane trafficking (Yuan et al. 2014).

Modifications of the Ubiquitin:

It has been noted that Ub itself can be further phosphorylated, acetylated or modified by the other Ubls (Swatek & Komander 2016). For instance, ubiquitin is targeted for SUMOylation on Lys6, Lys11, Lys27, Lys48 and Lys63. Proteasome inhibition leads to upregulation of the Lys6 and Lys27 SUMO-conjugated ubiquitins suggesting their role in protein degradation (Hendriks et al. 2014). Acetylation of the ubiquitin was readily detected on the Lys6 and Lys48. Even though acetylation did not interfere with the monoubiquitination, Lys11, Lys48 and Lys63 chain elongation of the Ac-Ub was interrupted. Histone H2B has been identified as a substrate for the Ac-Ub modification (Ohtake et al. 2015). PTEN induced protein kinase 1 (PINK1) phosphorylates ubiquitin on Ser65 as its main substrate. Phospho-ubiquitin is required for the optimal activation of Parkin, E3 ligase enzyme, and ubiquitination of the damaged mitochondria (Matsuda 2016).

The 26S Proteasome:

The proteasome is a 2.5 MDa complex with 33 identified subunits and two major sub-complexes: The 20S core particle (CP) and the 19S regulatory particle (RP) (Grice & Nathan 2016). The barrel-shaped CP contains two outer rings of subunits known as the alpha-rings (α1-7) and two inner beta rings (ß1-7). CP subunits ß1, ß2 and ß5, which form the proteolytic active site, are threonine proteases with chymotrypsin, trypsin and caspase-like proteolytic activity (Grigoreva et al. 2015). The 19S RP is composed of 10 base subunits and 9 lid subunits that are involved in ubiquitinated substrate recognition, ubiquitin tag removal as well as unfolding and

translocation of the protein through the proteasome gate. The 19S RP base subunits anchor the 19S RP to the alpha ring of the CP. The ATPase regulatory particles of the base subunits, Rpt1-6, form a heterohexameric ring that contacts the CP. They use ATP hydrolysis to unfold the substrate protein and transfer it through the open gate of the CP (Grigoreva et al. 2015; Finley 2009). Other than the 6 ATPase subunits of the RP, the non-ATPase (Rpn) subunits are only conserved in eukaryotes and are suggested to have evolved mostly for ubiquitinated substrate recognition and processing (Finley et al. 2012). Rpn1, 2 and 13 along with the 6ATPase subunits form the RP base (Grigoreva et al. 2015). The 19S RP lid is consists of the Rpn3 and Rpn5-12, which are mainly involved in the removal of the ubiquitin tag from the substrate. Rpn11 is a metalloprotease deubiquitinating enzyme that efficiently removes Ub tags from the substrate before protein translocation into the CP. Rpn10 (S5a) and Rpn13 subunits are known as the ubiquitin receptors. They bind ubiquitin chains in an ATP dependent manner with a very high affinity (Fig. 1-6A)(Hamazaki et al. 2015). It has been shown that Lys48-linked Ub-chains on the tagged proteins interact with the proteasome by initially contacting Rpn10 and Rpn13 subunits (Hamazaki et al. 2015). The 19S RP subunits also interact with the ubiquitin like domains of the shuttling proteins, such as Rad23 in yeast (hHR23A & B in humans), that contain Ubl-UBA (ubiquitin associating) domain. The Ubl domains of the shuttling receptors interact with the proteasome subunits, such as Rpn1 and Rpn13, while the UBA domain binds the ubiquitin chain on the substrate (Fig. 1-6B)(Grigoreva et al. 2015; Chen & Madura 2006).

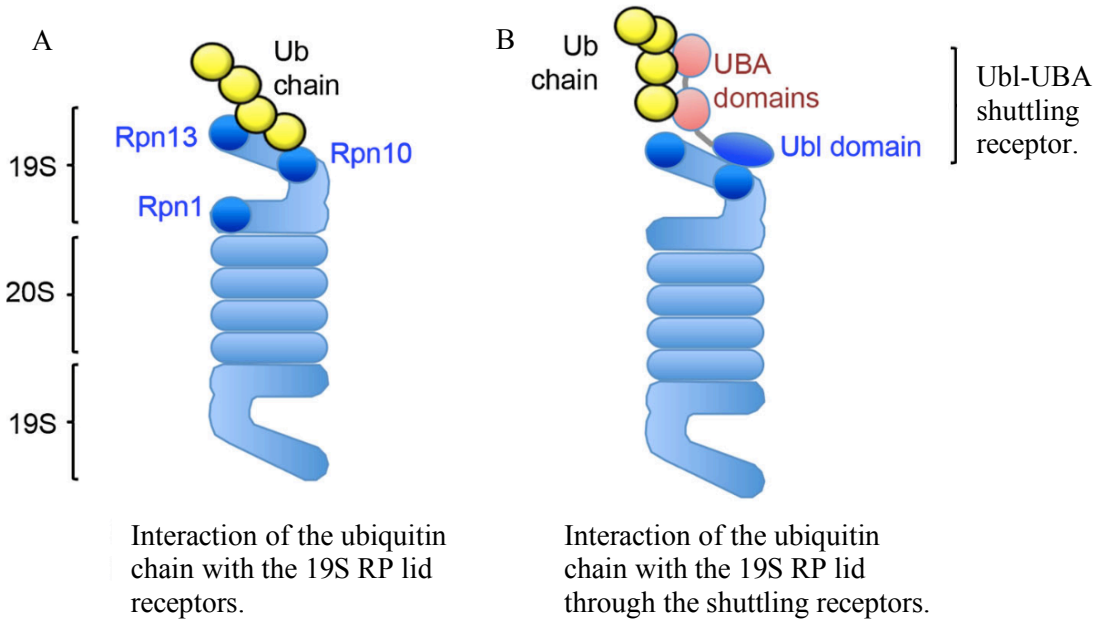

Interaction of the ubiquitin chain with the 19S RP lid receptors.

Interaction of the ubiquitin chain with the 19S RP lid through the shuttling receptors.

Fig. 1-6: Schematic representation of the proteasome ubiquitin receptors. A) Rpn10 and Rpn13 subunits of the 19S RP contact polyubiquitin chains on the substrate, specially Lys48-linked Ubs, with high affinity and in an ATP dependent manner. B) The Ubl domains of the shuttling receptors contact 19S RP subunits, such as Rpn1 and Rpn10, while their UBA domain binds ubiquitin chain on the substrate. (Reprinted by permission from Creative Commons (http://creativecommons.org/licenses/by/4.0/): Cellular and Molecular Life Sciences, (Grice & Nathan 2016), copyright 2016).

Deubiquitinating Enzymes:

Ubiquitin is a long-lived protein despite its covalent fusion to rapidly degrading substrates. This is due to the ubiquitin's efficient removal from the Ub-tagged proteins and disassembly of the ubiquitin chains by deubiquitinating enzymes (DUBs). DUBs catalyze the hydrolysis of the isopeptide bond between the carboxyl terminal glycine (Gly76) of the ubiquitin and the lysine residue of a tagged substrate protein or another ubiquitin (Phillips & Corn 2015; Hershko 2005). A computational bioinformatics analysis has identified 84 potential deubiquitinating enzymes in the human genome (20 in yeast *S. cerevisiae*) (Ye et al. 2009). Based on their conserved catalytic domains DUBs are grouped into five major families of thiol and metalloprotease (Fig. 1-7) (Wolberger 2014; Nijman et al. 2005). Four of the DUB families including, ubiquitin specific proteases (USP), ubiquitin C-terminal hydrolases (UCH), ovarian tumor domain-containing proteases (OTU) and Machado Joseph disease domain (MJD) are thiol proteases. They have similar catalytic activity to papain enzyme, a cysteine isopeptidase. The fifth family of DUBs are ubiquitin specific metalloproteases that are related to the JAB1/ MPN/Mov34 (JAMM) domain metalloenzymes (Sahtoe & Sixma 2015). In addition, a new family of DUBs named MINDY (motif interacting with Ub-containing novel DUB family) has been recently described that belongs to the cysteine proteases superfamily (Abdul Rehman et al. 2016).

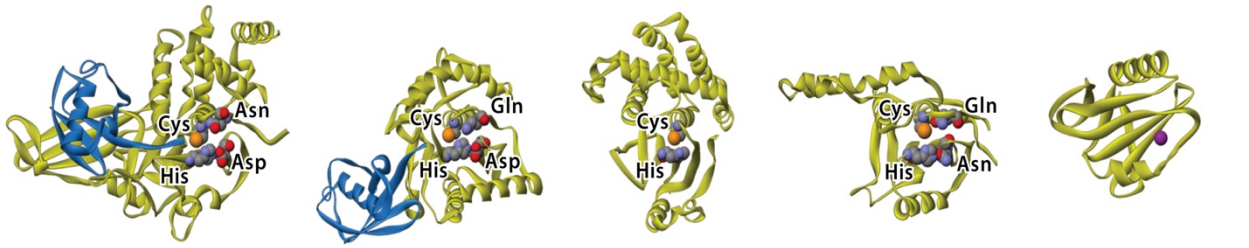

USP Domain UCH Domain OTU Domain MJD Domain JAMM Domain

Fig. 1-7: Five families of the deubiquitinating enzymes (excluding MINDY DUBs). Proteases are shown in green and Ub molecule in blue. Active site Cys, Asn, Asp and His residues are shown as Van der Waals spheres (with carbon in gray, nitrogen in blue, oxygen in red, sulfur in orange and zinc ion in purple). *USP*, ubiquitin specific proteases (USP7 structure, 1nbf); *OTU*, ovarian tumor domain proteases (OTUB2 structure, 1tff); *UCH*, ubiquitin C-terminal hydrolases (UCH-L3 structure, 1xd3); *MJD*, Machado Joseph disease domain proteases (Ataxin-3 structure, 1yzb); *JAMM*, JAB1/MPN/Mov34 domain metalloenzymes (AfJAMM structure, 1r5x). (Reprinted by permission from Elsevier: Cell, (Nijman et al. 2005), copyright 2005).

The activity of the cysteine proteases relies on the function of a highly-conserved cysteine, histidine and aspartate/asparagine catalytic triad. Polarized aspartic acid/asparagine assists histidine to deprotonate the thiol group of the cysteine residue. Then deprotonated cysteine launches a nucleophilic attack on the substrate's isopeptide carbonyl group carbon to form an intermediate thioester bond. Histidine then donates a hydrogen to the ε-amino group of the substrate's leaving Lys residue and tetrahedral intermediate collapses. Remaining acyl-enzyme intermediate is then hydrolyzed to free the enzyme and form a carboxylic acid group on the remaining distal ubiquitin (Fig. 1-8) (Eletr & Wilkinson 2014; Clague et al. 2013; Katz et al. 2010).

Metalloproteases coordinate a Zn^{2+} ion in their active site typically with the help of two histidines, an aspartic acid and a water molecule. The water molecule is bound to Zn^{2+} ion and a conserved glutamic acid. Glutamic acid deprotonates water and activates it into a potent nucleophile. Activated water molecule launches a nucleophilic attack on the substrate's isopeptide carbonyl group carbon. Then glutamic acid acts as a proton donor and transfers a hydrogen to the ε-amino group of the leaving protein's lysine residue. Tetrahedral intermediate collapses by forming a carboxylate group on the distal ubiquitin and releases the enzyme (Shrestha et al. 2014).

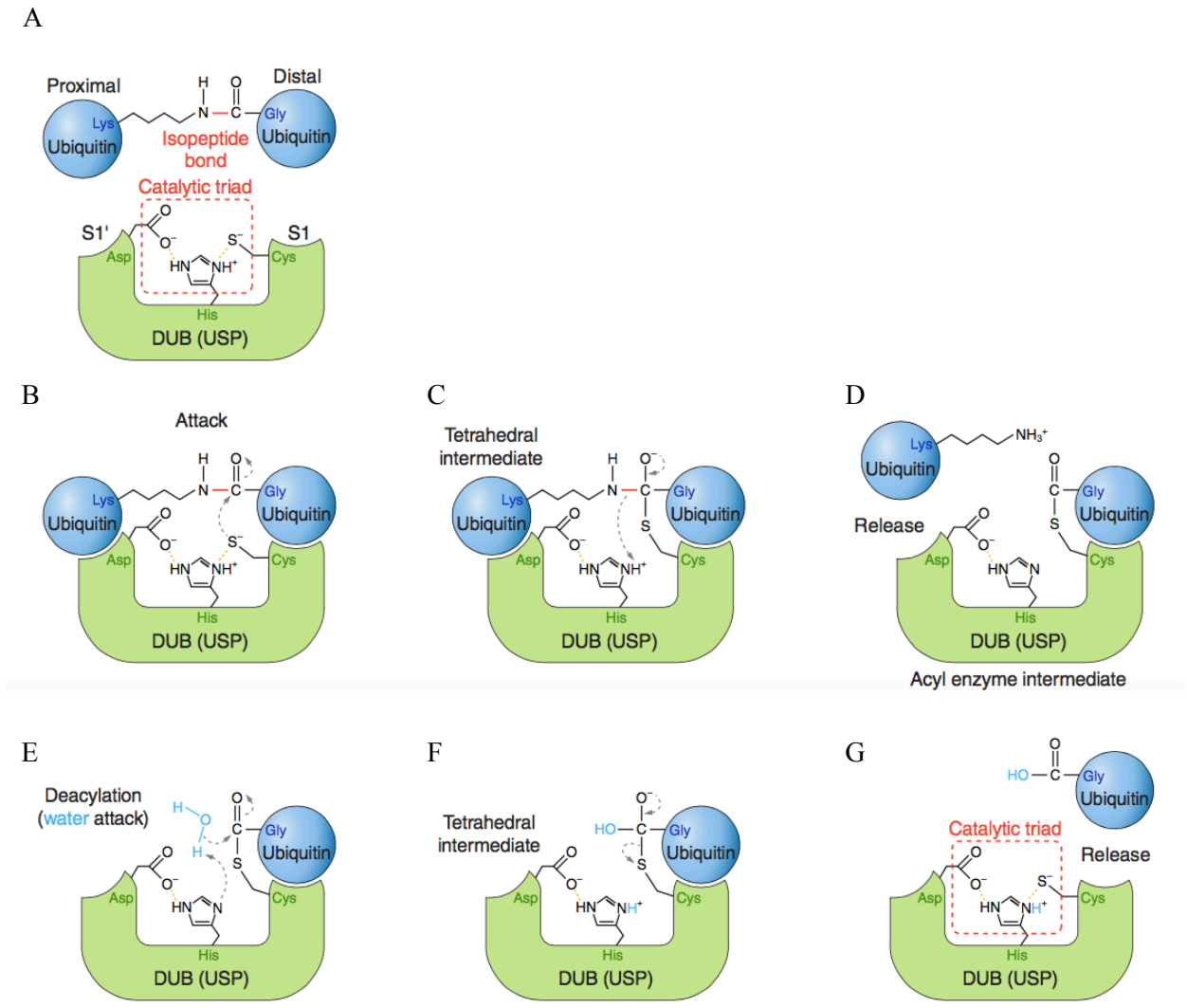

Fig. 1-8: Schematic representation of cysteine protease DUBs (USPs) mechanism in cleaving a diubiquitin chain. A) The catalytic triad residues, Asp, His and Cys, mediate cleavage of the isopeptide bond. B) Aspartic acid assists histidine to deprotonate the thiol group of the Cys, which in turn launches a nucleophilic attack on the substrate's isopeptide carbonyl carbon. C) A negatively charged tetrahedral intermediate forms. Then histidine donates a proton to the ε-amino group of the leaving Lys residue on the proximal ubiquitin. D) Tetrahedral intermediate collapses leading to the release of the proximal ubiquitin and leaving behind an acyl-enzyme intermediate. E-G) Acyl intermediate is hydrolyzed to free the enzyme and form a carboxylic acid group on the remaining substrate. Covalent bonds (in black), isopeptide bonds (in red) and noncovalent bonds (in yellow) are shown. (Reprinted by permission from APS Journals: Physiological Reviews, (Clague et al. 2013), copyright 2013).

Ubiquitin Specific Proteases (USP):

USPs (Ubps in yeast) represent the largest DUB subclass. Out of 84 DUBs identified in humans, 56 belong to the USP family (16 out of 20 DUBs in *S. cerevisiae*) (Davis & Simeonov 2015; Nijman et al. 2005). USPs/Ubps share two highly conserved motifs known as His and Cys boxes that contain the catalytic triad residues in the active site pocket. Research on yeast and mammalian cells indicate that despite highly conserved sequences in the USPs' catalytic domains, USPs/Ubps have diverse functions and show substrate specificity. This arises from different insertions in their catalytic domains and terminal extensions, which modulate their cellular localization and protein-protein interaction (Davis & Simeonov 2015). Resolved structures of the USP enzymes (except for CYLD, tumor suppressor protein) revealed a conserved extended right hand-like architecture consists of the thumb, palm and fingers subdomains (Sato et al. 2015). The active site is located in a cleft between the thumb and the palm structures and the fingers subdomain helps positon the ubiquitin C-terminal glycine within the active site (Reyes-Turcu et al. 2009). Some USP enzymes, such as USP7, have misaligned catalytic triad. Realignment of the catalytic resides is typically achieved through interaction with the ubiquitinated substrate or regulatory proteins (Faesen et al. 2012; Hu et al. 2002).

Ubiquitin C-Terminal Hydrolases (UCH):

Four UCH domain DUBs have been identified in humans (one in yeast). UCH-L1 and UCH-L3, which only consist of a catalytic domain (about 230 residues), are involved in the removal of short peptides from the C-termini of the ubiquitin precursors and cannot cleave polyubiquitin chains (Zhou et al. 2012). Also, UCH-L1 and UCH-L3 are implicated in the removal of accidental ubiquitin C-terminus thiol or amine adducts that are formed during the thioester intermediate bond formation (Clague et al. 2013). Large UCH enzymes, UCH37 and BRCA1-associated protein 1 (BAP1) with 100 and 500 residues extension at their C-termini respectively, are able to cleave polyubiquitin chains (Zhou et al. 2012). It was shown that UCH37, a proteasome-associated DUB in humans, can hydrolyze Lys48-linked ubiquitins. The ability of these enzymes to catalyze the cleavage of Ub chains depends on the length of the loops that hover over the UCH domain active sites. UCH37 and BAP1 compared to UCH-L1 and UCH-L3 have longer crossover loops (over 14 residues long), which provide more flexibility and larger access to the catalytic triad allowing them to cleave diubiquitins as well as polyubiquitin chains (Zhou et al. 2012).

Ovarian Tumor Related Proteases (OTU):

The OTU catalytic domain is about 150-350 residues long and resembles the ovarian tumor gene implicated in the development of fruit fly ovaries (Balakirev et al. 2003). Sixteen OTU DUBs have been identified in humans (two in yeast) which are further categorized into three classes: the OTUs, the Otubains and the A20-like OTUs. OTU DUB enzymes are typically involved in the regulation of the signaling pathways. For instance, A20, Cezanne and OTULIN regulate NF-κB signaling while OTUD5 regulates interferon signaling cascade (Mevissen et al. 2013). Further, OTU domain DUBs show high specificity towards cleaving one or two types of Ub linkages. For instance, human OTUB1, A20 and yeast Otu1 specifically recognize Lys48-linked Ub chains, while Cezanne cleaves Lys11-linked chains, TRABID recognizes Lys29 and Lys33 linkages and OTULIN hydrolyzes linear-linked Ubs (Mevissen et al. 2013).

Machado Joseph Disease/Josephin Domain (MJD) Proteases:

Four DUBs in humans contain the ~180 residue-long MJD domain, including Ataxin-3, Ataxin-3L, Josephin-1 and Josephin-2 (Costa & Paulson 2012). MJD domain DUBs have been implicated in the Machado-Joseph disease, the most common spinocerebellar ataxia and fatal neurodegenerative disorder caused by polyglutamine expansion (beyond ~ 44 glutamines) in Ataxin-3 (Costa & Paulson 2012). MJD DUBs contain a catalytic domain at their N-termini and multiple ubiquitin interacting motifs (UIM) at their C-termini. For instance, Ataxin-3 contains a Josephin domain at its N-terminus and two UIMs followed by polyglutamine chain and a third UIM at its C-terminus (Clague et al. 2013).

JAB1/ MPN/Mov34 Domain (JAMM) Proteases:

The JAMM domain DUBs are metalloproteases related to the MPN (Mpr1-Pad1-N-terminal) family of proteins, which are also conserved in prokaryotes (Eletr & Wilkinson 2014). Fourteen JAMM domain-containing proteins have been identified in humans, one in yeast (Rpn11) out of which only six have shown deubiquitinase activity, including BRCC36, Rpn11 (also known as POH1), CSN5, MYSM1, AMSH and AMSH-LP (AMSH-like protein) (Shrestha et al. 2014). The JAMM domain DUBs such as Rpn11, an essential proteasomal subunit, tend to cleave polyubiquitin chains in whole from the substrate and show a high preference for Lys63 linkage type. Also, they typically function as part of a large multisubunit complex (Clague et al. 2013).

For instance, Rpn11 is a subunit of the proteasome 19S RP, AMSH is a component of the ESCRT transport machinery, CSN5 functions as part of the COP9 signalosome (CSN), BRCC36 is associated with the BRISC and BRCA1-RAP180 complexes (involved in DNA repair) and MYSM1 is a histone H2A deubiquitinating enzyme that functions as part of the p/CAF complex (p300/CBP- associated factors, a histone acetyltransferase complex) (Bueno et al. 2015; Le Guen et al. 2015; Patterson-Fortin et al. 2010).

MINDY Domain Proteases:

MINDY is a recently described family of cysteine protease deubiquitinating enzymes with a high preference for Lys48-linked polyubiquitin chain hydrolysis. Its orthologues have been identified in humans as well as in plants and budding yeast (Abdul Rehman et al. 2016). Crystal structure of the MINDY-1 catalytic domain, a member of the MINDY DUBs, resembles a "light bulb", consisting of the base of the bulb "stalk" and the "bulb" (Fig. 1-9) (Abdul Rehman et al. 2016). The catalytic domain structure also revealed that catalytic Cys137 and His319 are not within the hydrogen bond distance and therefore are in an unproductive state. However, the structure of the MINDY-1 catalytic domain in complex with propargylated ubiquitin showed conformational change in a "Cys loop" that tends to occlude access to the active site and helped realign the active site residues into a productive conformation (Abdul Rehman et al. 2016).

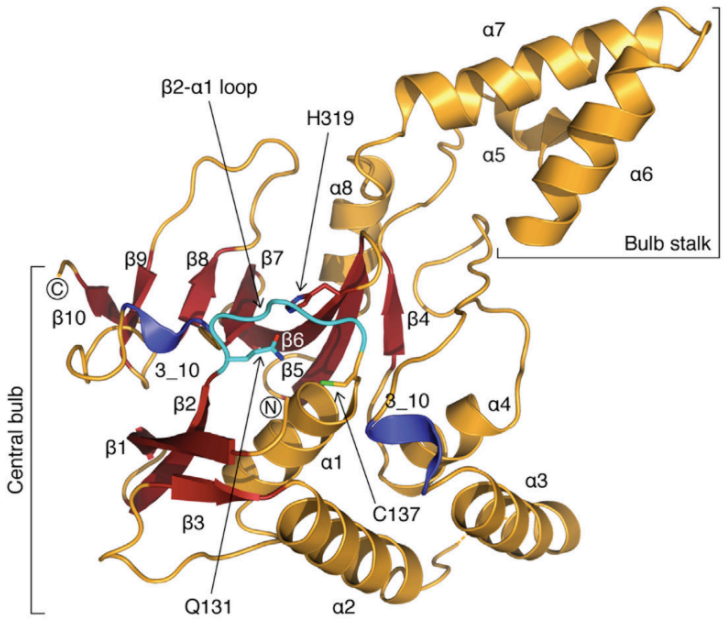

Fig. 1-9: MINDY-1 catalytic domain structure. Structure resembles a light bulb with two subdomains consisting of "bulb" and "bulb stalk". Catalytic Cys137 and His319 are identified. Blocking ß2- α1 loop (Cys loop) hovering over active site is shown in cyan. (Reprinted by permission from Creative Commons (Creative Commons Attribution License (CC BY)): Molecular Cell, (Abdul Rehman et al. 2016), copyright 2016).

Cellular Functions of DUBs:

The major role of the ubiquitin pathway is tagging proteins for proteolytic destruction therefore, deubiquitinating enzymes are essentially involved in protein stabilization. DUBs are important regulators of the ubiquitin-proteasome system. Prior to degradation of proteins by the 26S proteasome, DUBs remove polyubiquitin chains and assist in the unfolding of the protein and its translocation into the proteasome CP chamber (Finley 2009). Recycling of the Ub chains from the tagged proteins is essential for preserving available ubiquitin pool for cellular functions (Hochstrasser & Amerik 2004). Further, DUBs are known to deubiquitinate and stabilize enzymes that are involved in the ubiquitin-proteasome pathway, such as auto-ubiquitinating E3 ligases. In addition, ubiquitin is expressed with a C-terminal extension. Proper cleavage of the Ub precursors is essential for the production of functional ubiquitins (He et al. 2016). DUBs are also involved in nonproteolytic functions such as regulation of transcription through deubiquitination of histone H2A and H2B (Emre et al. 2005; Henry et al. 2003). Further, DUBs through the removal of Lys63-linked chains or single ubiquitin tags regulate cellular levels of proteins that are targeted for endocytosis and degradation in lysozymes (Dupre & Haguenauer-Tsapis 2001).

DUBs Associated with the Proteasomal Degradation:

Three DUBs are known to associate with the 26S proteasome in humans (two in yeast) including UCH37, USP14 (Ubp6 in yeast) and Rpn11 (also Rpn11 in yeast). UCH37 and USP14 transiently interact with the proteasome, while Rpn11 is an essential subunit of the 19S RP lid (Eletr & Wilkinson 2014).

UCH37, a UCH domain DUB, interacts with the C-terminal domain of Rpn13/Adrm1 ubiquitin receptor subunit of the 19S RP lid (Jiao et al. 2014). It has been shown that the C-terminal domain of the UCH37 has an inhibitory effect on its deubiquitination activity. Interaction of the UCH37 with Rpn13 releases the inhibition and brings UCH37 enzyme to close proximity of the polyubiquitin tag on the substrate, allowing it to remove distal ubiquitins from the chain (VanderLinden et al. 2015). The decrease in the cellular levels of UCH37 leads to increase in degradation of the proteasomal substrates suggesting a role for UCH37 in the stabilization of the ubiquitin-tagged proteins (Wang et al. 2014; Al-Shami et al. 2010).

USP14 and its yeast orthologue, Ubp6, are non-essential cysteine proteases. They contain a conserved Ubl domain in their N-termini which is necessary for their interaction with Rpn1 subunit of the 19S RP. The Ubl domain interaction with the proteasome increases USP14/Ubp6 ubiquitin-substrate hydrolysis activity by ~300-1000 folds (Selvaraju et al. 2015). USP14/Ubp6 similar to UCH37 remove single ubiquitin moieties from the distal end of a polyubiquitin chain with a high preference for Lys48 linkage. Deletion of the *USP14* gene in mice or *UBP6* gene in yeast leads to depletion of the free cellular ubiquitin pool indicating their important role in recycling ubiquitin (M. J. Lee et al. 2011). Ubp6 was shown to interact with and catalytically oppose the function of Hul5 (KIAA10 in mammals), a proteasome-associated HECT domain E3 ligase (Aviram & Kornitzer 2010). Knockdown of USP14 in human cells or deletion of Ubp6 in yeast increases proteolytic degradation of proteins (Bashore et al. 2016).

Rpn11/POH1, a metalloprotease, is essential for viability in yeast and cell growth in humans. RNA interference knockdown of Rpn11 leads to accumulation of ubiquitinated proteins and defect in proteasome function due to proteasomal instability and disruption its assembly (Saunier et al. 2013; Koulich et al. 2008). Rpn11 dependent deubiquitination activity requires ATP hydrolysis and an intact proteasome. Also, unlike UCH37 and USP14, Rpn11 acts as an endopeptidase and tends to cleave Ub-chains in whole from their proximal end. It was observed that Ubp6 interaction with the proteasome 19S RP strongly interferes with Rpn11 deubiquitination activity and helps stabilize substrates (Bashore et al. 2016; Koulich et al. 2008).

DUBs Associated with Endocytosis and Protein Trafficking:

Many membrane proteins, such as receptors (especially tyrosine kinases) and channels, are downregulated through endocytosis and trafficking to the lysosomes. Monoubiquitinated or Lys63-linked polyubiquitinated membrane proteins bind UBD of the ESCRT complex and form sorting endosomes which mature into multivesicular bodies (MVBs). MVBs fuse with the lysosome and release ubiquitinated proteins into the vacuole (Olmos & Carlton 2016; Carlton 2010). Ubiquitin tags must be removed prior to fusion of the MVBs with the lysosome. The ESCRT complex, is composed of four major subcomplexes, including ESCRT-0, I, II and III, and similar to the proteasome it tends to associate with deubiquitinating enzymes (Olmos & Carlton 2016). AMSH, a metalloprotease, and USP8 associate with multiple components of the ESCRT-0 and ESCRT-III subcomplexes. They both contain microtubule interacting and trafficking domains which play a role in intracellular trafficking and endosomal localization

(Olmos & Carlton 2016; MacDonald et al. 2014). AMSH is a Lys-63 specific DUB. It interacts with a subunit of the ESCRT-III and is involved in proof reading and stabilizing receptors prior to their fusion with the lysosome (Birol & Echalier 2014). USP8, which cleaves most types of ubiquitin linkages, stabilizes Hrs and STAM subunits of ESCRT-0. Depletion of USP8 leads to enlarged endosomes due to the accumulation of ubiquitinated proteins (MacDonald et al. 2014; De Ceuninck et al. 2013).

DUBs Involved in Activation and Stabilization of E3 Enzymes:

Many E3 ligase enzymes tend to undergo adventitious self-ubiquitination. Their interaction with a DUB is essential for their stabilization and rescue from proteasomal degradation (Ventii & Wilkinson 2008). For instance, Rho52, an oncoprotein and an E3 ligase, interacts closely with the USP4 deubiquitinating enzyme which helps stabilize Rho52 from self-ubiquitination in the absence of its substrates. Rho52 also tends to ubiquitinate USP4 however, USP4 is able to self deubiquitinate and stabilize itself (Wada & Kamitani 2006). Likewise, RING1B, E3 ligase subunit of the PRC1 complex, is targeted for degradation both by auto-ubiquitination and by E6AP, E6 associated E3 ligase. While E6AP forms Lys48-linked polyubiquitin chains on RING1B, its auto-ubiquitination leads to Lys6, Lys27 and Lys48 mixed and branched linkage types assembly. Interaction of RING1B with USP7 leads to removal of Ub chains and return of the protein to its native state (de Bie & Ciechanover 2011). DUBs can also alter or regulate E3 ligase activity through induction of conformational changes. For instance, a conserved lysine residue in cullin subunit of the SCF E3 ligase complex is conjugated to Nedd8, a Ubl protein. This conjugation stabilizes the C-terminus of cullin and increases the efficiency of the RING domain to ubiquitinate substrates. CSN5, a JAMM domain DUB and subunit of the COP9 signalosome (CSN), deneddylates cullin and removes Nedd8, which leads to conformational change, dissociation of Skp1 from the SCF complex and downregulation of the SCF activity (Mosadeghi et al. 2016; Enchev et al. 2012).

DUBs Involved in Modulating the Activity of E2 Enzymes:

Deubiquitinating enzymes can block the interaction of the E2 enzymes with the ubiquitin or inhibit E2 mediated transfer of the Ub to the E3 ligases or substrates. For instance, Parkin is a Parkinson disease-associated RBR domain E3 ligase. UBCH7, Parkin's cognate E2 enzyme, has to first transfer the ubiquitin intermediate to the active site of Parkin before Ub is transferred to

the substrate (Durcan et al. 2012). The ataxin-3 deubiquitinating enzyme is known to make a tight complex with Parkin and prevent the transfer of Ub from UBCH7 to the Parkin's active site (Durcan et al. 2012). Another example is OTUB1, an OTU domain deubiquitinating enzyme. It directly interacts with the Ub conjugated E2 enzymes, such as UBE2D2 (Hdm2 cognate E2 enzyme) and UBC13, and hinder their function (Sun & Dai 2014). Co-crystal structure of the OTUB1 with UBE2D2 revealed that OTUB1 binds this E2 enzyme through residues that are involved in interaction with Hdm2. Subsequently, OTUB1 inhibits Hdm2 mediated ubiquitination of p53 non-catalytically and leads to p53 stabilization (Sun & Dai 2014). Similarly, OTUB1/UBC13 structure revealed that OTUB1 binds UBC13 residues that are involved in the transfer of Ub to H2A through RNF168 E3 ligase (Wiener et al. 2012).

DUBs Involved in Processing and Recycling of Ubiquitin:

In all eukaryotic cells genes that express ubiquitin either code for head to tail linked polyubiquitin chains with a small C-terminal extension (*UBB* and *UBC* genes in humans) or a single ubiquitin fused to the ribosomal subunits (*UBA52* and *RPS27A/UBA80* genes in humans). In humans UCH-L3, and to a lesser extent USP9X and USP7, are the deubiquitinating enzymes involved in the cleaving of the ubiquitin precursors that are fused to the ribosomal subunits (L40 and S27A proteins) (Grou et al. 2015). In contrast, Otulin, an OTU domain DUB, displays remarkable preference for cleaving polyubiquitin chain precursors. Ub precursors are either expressed from the *UBB* gene, that codes for three ubiquitin monomers followed by a cysteine residue, or the *UBC* gene, that codes for nine ubiquitin monomers followed by a valine residue (Eletr & Wilkinson 2014). UCH-L3 complements Otulin function by removing amino acids or peptides from the C-terminus of the final ubiquitin in the poly Ub chain (Eletr & Wilkinson 2014). Further, UCH-L1 and specially UCH-L3 are also implicated in the removal of the adventitious nucleophile thiol or amine adducts that get conjugated to the C-terminal glycine of the ubiquitin through thiolester intermediate bond formation (Bishop et al. 2016; Sekiguchi et al. 2006). In humans at least two DUBs can act on one type of ubiquitin precursor indicating the importance of *de novo* free ubiquitin synthesis and robustness of this process (Grou et al. 2015).

To maintain cellular levels of the free ubiquitin pool polyubiquitin chains released from the protein substrates must be cleaved to single ubiquitins (Coyne & Wing 2016; Clague et al. 2013). USP5, also known as iso-peptidase T (Ubp14 in yeast), specifically recognizes and cleaves unanchored polyubiquitin chains (Grou et al. 2015). USP5 is a multidomain enzyme that can

hydrolyze varying Ub linkage types including Lys6, Lys29, Lys48, Lys63 and Met-linked ubiquitins. Full-length structure of the USP5 revealed four ubiquitin binding sites: two zinc finger ubiquitin-binding domains at its N-terminus and two UBA domains inserted within the catalytic domain (Avvakumov et al. 2012). Deletion of Ubp14 in yeast or knockdown of USP5 in human cells lead to accumulation of polyubiquitin chains, which interfere with proteasomal degradation of certain substrates (Grou et al. 2015).

DUBs Associated with Chromatin Modification:

In humans, 10% of the histone H2A is ubiquitinated at Lys119 and about 1% of the histone H2B is ubiquitinated at Lys120 (Atanassov et al. 2011). Histone H2B ubiquitination is linked to transcription activation, while H2A ubiquitination generally leads to silencing (Du 2012). DUBs such as MYSM1, USP16, USP21, BAP1, BRCC3 and USP10 recognize and deubiquitinate histone H2A. MYSM1/2A-DUB is a JAMM domain DUB that deubiquitinates H2A and leads to transcription activation of androgen receptor-regulated genes (Gatzka et al. 2015). USP16, which colocalizes with RING1B E3 ligase component of the PRC1 complex, works in oppose to the PRC1 by globally deubiquitinating H2A and maintaining gene expression during mitosis (Frangini et al. 2013). USP21 deubiquitinates H2A on Lys119 in mice especially during liver regeneration (Pannu et al. 2015). BAP1, a UCH domain DUB, is a major tumor suppressor protein and chromatin remodeling factor (Murali et al. 2013). BAP1 deubiquitinates H2A at Lys119 in oppose to the PRC1 function and leads to repression of genes such as human HOX genes (39 conserved genes that code for transcription factors involved in embryonic anterior-posterior patterning and development) (Yu et al. 2014). BRCC3, a JAMM domain metalloprotease with specificity for Lys63-linked Ub chains, antagonizes RNF8 mediated H2A ubiquitination during double-strand DNA breaks (Huang et al. 2015; Feng et al. 2010). USP10 specifically recognizes histone H2A.Z variant which is involved in thermosensory response and regulation of transcription. Deubiquitination of H2A.Z by USP10 leads to transactivation of androgen receptor-regulated genes such as prostate-specific antigen (Draker et al. 2011).

USP3 and USP22 (Ubp8 in yeast) can deubiquitinate both H2A and H2B. USP3 interacts with ubiquitinated H2A, gamma-H2AX (H2A variant) and H2B through its zinc finger ubiquitin-binding domains and opposes RNF168 E3 ligase activity (Sharma et al. 2014; Nicassio et al. 2007). USP22 and its yeast homologue, Ubp8, are histone deubiquitinating subunits of SAGA (transcriptional co-activator histone acetylation complex) (Cole et al. 2015). USP22

deubiquitinates H2B on Lys120 and Ubp8 on Lys123 (Melo-Cardenas et al. 2016). Ubp8 activity leads to recruitment of C-terminal kinase 1 (CtK1) which in turn phosphorylates RNA-polymerase II and initiates transcription (Wyce et al. 2007).

USP7, USP15, USP36 (Ubp10 in yeast), USP44 and USP49 are involved in deubiquitination of histone H2B. USP7 has been shown to interact with GMPS (guanosine 5'-monophosphate synthase), a metabolic enzyme involved in the final step of *de novo* guanine nucleotides synthesis. Together they are involved in H2B deubiquitination and act as transcriptional repressors. Depletion in the cellular levels of GMPS or USP7 leads to increase in monoubiquitinated H2B (Reddy et al. 2014; van der Knaap et al. 2010). USP15 was reported to directly interact with the RNF20-RNF40 E3 ligase complex, which is involved in histone H2B monoubiquitination. Further, the USP15 N-terminal DUSP (domain present in USPs) and Ubl domains interact with SART3 (Squamous cell carcinoma antigen recognized by T-cells 3) component of the splicing machinery. SART3 recruits USP15 to the nucleus for deubiquitination of histone H2B (Q. Zhang et al. 2016; Long et al. 2014). USP36 deubiquitinates Ub-H2B in *Drosophila* stem cells and its overexpression in humans is linked to ovarian cancer. Its yeast homologue, Ubp10, localizes to silent chromatin and has established a role in telomeric silencing. Ubp10 deubiquitinating activity leads to low levels of histone H3 Lys4 and Lys79 methylation which in turn leads to recruitment of Sir proteins and telomeric silencing (Reed et al. 2015; J. Li et al. 2008). USP44 antagonizes RNF20 E3 ligase function by deubiquitinating histone H2B. It was shown that USP44 levels are significantly downregulated during embryonic stem cells differentiation, which is important for activation of genes involved in the developmental process, such as DAAM2 (dishevelled associated activator of morphogenesis 2) (Fuchs et al. 2012). Lastly, USP49 forms a complex with RuvB-like1 ATPase and deubiquitinates H2B. USP49 activity is important for efficient splicing of a large set of exons (Zhang et al. 2013).

DUBs Involved in Signaling Cascades:

Reversible ubiquitination has a critical role in recruiting, activating and controlling stability of receptors and signal transducing proteins. Catalysis of the Lys63-linked Ub chains is important for recruiting signaling proteins such as kinases in a non-proteasome dependent manner, while Lys48-linked ubiquitination regulates the half-life of the signaling receptors and complexes (Clague et al. 2013). The best-studied signal transduction pathway dependent on the reversible

ubiquitination is that of nuclear factor κB (NF-κB) transcription factor which has well-established roles in innate and adaptive immunity and cell growth (Won et al. 2016). In an unstressed cell a family of inhibitory proteins, IκB, associate with NF-κB in the cytoplasm and hinder its nuclear localization and transactivation (Won et al. 2016). Signal engagement by receptors, such as Tumor Necrosis Factor (TNF), leads to recruitment of TRAF2 or TRAF6 (TNF receptor-associated factors), RING-type E3 ligases, and their Lys63 autoubiquitination and activation (Hoesel & Schmid 2013). TRAF E3s further catalyze Lys63-linked ubiquitin chains on the TNF complex components such as RIP1 and RIP2 (receptor interacting proteins). This acts as a signal to recruit TAK1-TAB2/3 kinase which in turn phosphorylates IκB Kinase (IKK) and leads to Lys63-linked ubiquitination of IKK regulatory subunit, NEMO (NF-κB essential modulator). Subsequently, activated IKK phosphorylates IκB on two N-terminal serine residues. The SCF E3 ligase complex (with a beta-transducing repeat-containing protein, ßTrCP) recognizes phosphorylated IκB and catalyzes its Lys48-linked ubiquitination and proteasomal degradation. IκB downregulation allows NF-κB to enter the nucleus and start its transactivation (Won et al. 2016; Hoesel & Schmid 2013). Two DUBs, A20 and CYLD, have been identified as downregulators of the NF-κB signaling pathway (Chen 2012). A20 is a novel enzyme with an OTU domain at its N-terminus and a zinc finger domain with E3 ligase activity at its C-terminus (Heyninck & Beyaert 2005). The A20 OTU domain specifically cleaves Lys63 Ub linkage. It hydrolyses Lys63-linked chains produced by TRAF E3 ligases on RIP1 and inhibits NF-κB signaling. Simultaneously A20 acts as an E3 ligase and catalyzes Lys48-linked ubiquitination of RIP1 which leads to its degradation. Mice with A20 deletion die shortly after birth due to continuous NF-κB signaling and organ inflammation (Won et al. 2016; Heyninck & Beyaert 2005). CYLD, another DUB involved in the NF-κB signaling, is a tumor suppressor with a USP catalytic domain which shows preference for Lys63 and linear-linked Ub chains. It inhibits IKK activation by hydrolyzing Lys63 chains from TRAF2, TRAF6, RIP1 and NEMO (Kobayashi et al. 2015). CYLD depletion leads to increase in ubiquitinated RIP1 levels and activation of NF-κB signaling (Chen 2012). Recently more DUBs have been implicated in NF-κB signaling such as Cezanne, USP21 and USP7. Cezanne (Cellular zinc finger anti-NF-κB) is an OTU domain DUB with a preference for Lys11 linkage hydrolysis. TNF signaling activates Cezanne and recruits it to TNF receptors (TNFR). In return, Cezanne cleaves Lys11-linked Ub chains from activated TNFR1 which suppresses ubiquitination of RIP1 and downregulates NF-κB signaling (Enesa et al. 2008). Likewise, USP21 is activated by TNF signaling. It downregulates NF-κB transactivation by associating with and deubiquitinating RIP1 (Xu et al. 2010). USP7 has also

been implicated as the negative regulator of the NF-κB pathway. It was shown that upon Toll-like receptor (TLR) or TNFR signal engagement USP7 translocates to the cytoplasm. It leads to downregulation of the NF-κB dependent inflammatory cytokine response through deubiquitination of the Lys63-linked Ub chains on TRAF6 E3 ligase and NEMO component of the IKK complex (Li et al. 2014; Daubeuf et al. 2009).

Other noteworthy signaling cascades that are tightly regulated by reversible ubiquitination are the Wnt and TGF-ß pathways. Wnt/ ß-catenin signaling is highly conserved and has a critical role in the development and adult tissue homeostasis. Wnt proteins interact with Frizzled transmembrane receptors and lead to signal transduction through ß-catenin transcription coactivator (Yun et al. 2015). The USP8 deubiquitinating enzyme, which is involved in endosomal trafficking, was shown to recycle ubiquitin-tagged Frizzled receptors, suppress their lysosomal trafficking and upregulate Wnt signaling (Mukai et al. 2010). Further, USP4, USP34 and TRABID (an OTU domain DUB) stabilize components of the Wnt signaling pathway such as ß-catenin, Axin and APC respectively and regulate Wnt signaling (Yun et al. 2015; Lui et al. 2011; Tran et al. 2008). TGF-ß signaling cascade involves a variety of cytokines and regulates different biological functions. Activated TGF-ß receptor, in turn, phosphorylates receptor-regulated SMAD proteins (R-SMADs) and leads to their transcription activation in association with SMAD4 (Juan Zhang et al. 2014). USP9X deubiquitinating enzyme (also known as FAM, *fat facets)* is recruited to this complex to activate SMAD4 by specifically removing monoubiquitin tags from SMAD4 Lys519. Monoubiquitinated SAMD4 cannot interact with R-SMADs and remains inhibited in the cytoplasm (Dupont et al. 2009). USP15 and USP4 also upregulate TGF-ß levels by deubiquitinating and stabilizing TGF-ß type I receptors (TßRI) (Aggarwal & Massague 2012).

DUBs Involved in the DNA Repair Pathways:

Many environmental factors, such as toxins, viruses and radiation, and cellular factors, such as metabolic byproducts and replication errors, can lead to DNA damage which is quite hazardous to the cell. DNA lesions caused by double-strand breaks, single-strand breaks (SSBs) and interstrand crosslinks activate the DNA repair pathways, which are crucial for preserving genomic integrity and health of the organism (Jasin & Haber 2016). DNA repair pathways are tightly associated with reversible ubiquitination. Effector proteins including E3 ligases are recruited to the DNA break lesions through the function of kinases, such as ATM, ATR, DNA-

PK, Chk1 and Chk2 (Li & Xu 2016). Subsequently, Lys63-linked Ub chains get accumulated through enzymatic activity of RNF8 and RNF168, RING finger E3 ligases. This leads to recruitment of the genome caretaker proteins, such as 53BP1, Pax transactivation domain-interacting protein (PTIP) and BRCA1 containing protein complex, which activate the DNA double-strand break pathway (Li & Xu 2016). RNF8 associates with HERC2, a large HECT domain E3 ligase, which helps RNF8 to specifically interact with UBC13 E2 ligase and form Lys63-linked Ub chains on histones at the site of the DNA damage. RNF8/HERC2 function further activates RNF168 which also with the help of UBC13 forms Lys63-linked polyubiquitin on histone H2A and H2AX (Jasin & Haber 2016; Bekker-Jensen & Mailand 2011). Deubiquitinating enzymes, USP3 and BRCC3, counteract the DNA repair signaling by cleavage of the Lys63-linked ubiquitins at the DNA break sites, while OTUB1 inhibits ubiquitination function of RNF168 by interacting with the UBC13 E2 ligase and blocking its interaction with E3 ligases (Nakada et al. 2010). Another DUB that has been identified as a major regulator of the DNA damage response is USP28. DNA double-strand breaks can lead to DNA damage induced apoptosis which in most cases is orchestrated through the Chk2 kinase-p53-PUMA pathway (Fong et al. 2016). In response to DNA damage, USP28 interacts with and stabilizes Chk2 kinase and other scaffolding proteins such as 53BP1, Claspin and mediator of DNA damage checkpoint 1. Depletion of USP28 decreases cellular levels of these proteins, weakens DNA damage response and inhibits IR induced p53 mediated apoptosis (Fong et al. 2016; Gupta et al. 2014). USP28 is also implicated in G2 DNA damage response checkpoint. To allow cell cycle progression in unstressed cells G2 checkpoint is silenced through ubiquitination and destabilization of Claspin. Plk1, a mitotic kinase, phosphorylates Claspin and leads to its recognition and downregulation by the SCF E3 ligase complex (containing a ßTrCP F-box subunit) (Bassermann et al. 2008). In case of DNA damage, the APC/C E3 ligase complex (along with Cdh1 component) ubiquitinates and destabilizes Plk1 kinase and therefore prevents mitosis. (Bassermann et al. 2008).

Naturally occurring compounds, such as reactive aldehydes, and exogenous chemicals, such as chemotherapeutic drugs, can give rise to intrastrand crosslink which leads to covalent bonding of the two DNA strands and blocks essential processes such as DNA transcription and replication (Lopez-Martinez et al. 2016). PCNA, Fanconi anemia complementation group D2 (FANCD2) and Fanconi anemia complementation group I (FANCI) are involved in the interstrand crosslinks repair pathway. These proteins are activated through monoubiquitination and further promote activation of the Fanconi anemia (FA) signaling cascade. Monoubiquitination of FANCD2 and

FANCI heterocomplex is important for their localization at the DNA repair foci and their subsequent interaction with repair factors such as BRCA1 and RAD51 recombinase, which are implicated in DNA repair through activation of the homologous recombination (Lopez-Martinez et al. 2016). The USP1 deubiquitinating enzyme is one of the most important regulators of the FA signaling in response to DNA damage. In complex with its activator, USP1-associated factor 1 (UAF1), USP1 deubiquitinates PCNA, FANCD2 and FANCI and suppresses FA signaling (Boisvert & Howlett 2014). UAF1, contains a WD40 domain at its N-terminus, which binds USP1, and two SUMO-like domains (SLDs) at its C-terminus, which interact with the highly conserved SUMO-like interacting motifs of FANCI (Yang et al. 2011). UAF1 SLD2 is also important for USP1 mediated deubiquitination of FANCD2-Ub and PCNA-Ub (Yang et al. 2011). In response to DNA damage, UAF1 targets USP1 to the FANCD2-FANCI heterocomplex. USP1/UAF1 deubiquitination of FANCD2 and FANCI is crucial for proper function of the FA pathway and is especially important for exit from S phase and recycling of FANCD2 (Boisvert & Howlett 2014; Murai et al. 2011). Even though USP1/UAF1 complex dampens the FA signaling, *USP1* gene deletion in mouse embryonic fibroblasts or DT40 chicken cells led to hypersensitivity to chemical cross-linking agents and defective homologous recombination repair (Boisvert & Howlett 2014). It was shown that USP1/UAF1 deubiquitination function also suppresses the non-homologous end-joining pathway which further promotes activation of homologous recombination repair in DNA double-strand breaks (Murai et al. 2011). The activity of the USP1/UAF1 complex is highly regulated. Upon exposure to DNA damaging agents, such as radiation, USP1 transcription is inhibited by p21, a cyclin-dependent kinase inhibitor, to allow accumulation of the monoubiquitinated FANCD2/FANCI and activation of the DNA damage response (Rego et al. 2012). At the same time USP1 undergoes autocleavage at an internal Gly-Gly motif which leads to its dissociation from UAF1 and eventual degradation (Huang et al. 2006).

Regulation of DUBs Activities:

Reversible ubiquitination has a critical role in many complex cellular functions. Any derangement in the activity of enzymes involved in this pathway disrupts cell homeostasis and is linked to many human cancers, disease and neurological disorders (Hanpude et al. 2015; Shi & Grossman 2010). Majority of DUBs are implicated in multiple and varying cellular functions at the same time they show timely activation and substrate specificity regarding each particular

function. DUBs activity must be tightly regulated. To date, many mechanisms have been identified that govern DUBs function and substrate specificity.

Regulation of DUBs Expression and Stability:

DUBs activity can be regulated by controlling their expression. For instance, repression effect of USP1 on the FA signaling pathway is downregulated upon DNA damage by inhibiting its transcription. Activated p21 terminates USP1 transcription and leads to its quick attenuation (Rego et al. 2012). Further, regulation of DUBs' activity also occurs through downregulation of their cellular levels. For instance, upon exposure to DNA damaging radiation USP1 autocleaves itself which leads to its degradation and activation of the FA signaling pathway (Huang et al. 2006). Another example is the case of A20, an OTU domain DUB, which itself is a substrate of mucosa-associated lymphoid tissue (MALT) protease (Martinez-Climent 2014). MALT cleaves A20 after Arg439 and suppresses its negative effect on the NF-κB pathway. Deletion or mutations in A20 or constitutively activated MALT leads to prolonged NF-κB signaling and is associated with MALT lymphoma (Martinez-Climent 2014; Du 2011).

Recently microRNAs (miRNAs) have also been implicated in the post-transcriptional regulation of DUBs' expression. miRNAs lead to mRNA silencing and decay by base-paring with the complementary sequences within 3' untranslated region of the mRNA molecules. This recruits RISC (RNA-induced silencing complex) to the mRNA transcript and triggers its decapping and deadenylation (Bartel 2009). USP14, a proteasome bound DUB, is upregulated in multiple human cancers such as leukemia, colorectal cancer and non-small cell lung cancer (Wu et al. 2013). It was shown that upregulation of MiR-4782-3p miRNA correlates with a decrease in USP14 expression in patients with non-small cell lung cancer (Wu et al. 2014). MiR-4782-3p has been successfully used to target USP14, decrease its expression and inhibit cell proliferation (Wu et al. 2014).

Substrate-Induced Regulation of DUBs Activities:

To avoid random and untimely hydrolysis of the substrates and as a safeguard mechanism, typically DUBs active site residues are in an inactive conformation. In case of the cysteine protease DUBs histidine must be within the hydrogen bond distance from cysteine (~3.8 Å) to deprotonate its thiol group (Jeffrey 1997). For instance, USP7 crystal structure revealed that catalytic residues are not in a productive state and that catalytic cysteine residue is about 10 Å

away from the catalytic histidine. Structure of the USP7 bound to ubiquitin aldehyde showed conformational change and realignment of the catalytic residues into an active conformation (Hu et al. 2002). Another example of active site realignment upon substrate interaction is seen in the case of the UCH-L1 enzyme. In the absence of the substrate catalytic histidine rotates about 7.7 Å away from the catalytic cysteine rendering the active site unproductive (Boudreaux et al. 2010). UCH-L1 bound to a suicide substrate, ubiquitin vinyl methyl ester, revealed two contact sites for ubiquitin. While the C-terminal glycine of ubiquitin contacts the active site, an N-terminal ß-hairpin loop of Ub contacts a hydrophobic patch on UCH-L1 about 17 Å away from the active site (Boudreaux et al. 2010). Ubiquitin interaction with UCH-L1 distal site leads to rearrangement of the active site residues into an active conformation (Ronau et al. 2016; Boudreaux et al. 2010). Another case is OTULIN, an OTU domain DUB, specific for cleavage of the linear ubiquitin chains. Crystal structure of the OTULIN revealed that catalytic Cys-His-Asn triad in the majority of the molecules is misaligned (Keusekotten et al. 2013). An Asp residue in the catalytic domain inhibits productive conformation by pulling active site histidine residue away from cysteine. However, in case of OTULIN's interaction with the linear ubiquitin chains, catalytic histidine residue is forced back to a hydrogen bond distance with the catalytic cysteine (Keusekotten et al. 2013). It was shown that Glu16 residue of the linear-chained proximal ubiquitin releases the inhibitory effect of Asp on the active site histidine and allows rearrangement of the catalytic triad into a productive conformation. Only in linear-linked ubiquitin chains Glu16 can contact OTULIN's Asp residue and release its inhibitory effect on the active site histidine, giving OTULIN its unique specificity (Elliott & Komander 2016; Keusekotten et al. 2013)

Regulation of DUBs Activity and Specificity Through Internal Loops and Domains:

Other than misaligned catalytic triad in some DUBs' internal loops crossing over or adjacent to the active site regulate ubiquitin access and catalytic activity. DUBs interaction with substrates or binding partners is important in relieving the obstruction. As mentioned before USP7 catalytic residues in the absence of ubiquitin are misaligned. It was shown that USP7's five C-terminal Ubl domains can fold back towards the catalytic domain. This allows Ubl4 & 5 to interact with a so-called "switching loop" close to the catalytic triad which leads to a significant conformational change in the loop and helps realign the catalytic residues (Faesen et al. 2011). Another example is the case of CSN5, a JAMM domain metalloprotease and a subunit of the COP9 signalosome (CSN). CSN5 recognizes and cleaves NEDD8 from the CRL E3 ligase complex and

downregulates CRL activity (Cope et al. 2002). However, outside the CSN complex CSN5 is essentially an inactive enzyme and access to its active site is inhibited by an internal loop, referred to as Ins1 (insertion loop 1). Within the holoenzyme, CNS6 forms a heterodimer with CSN5 and simultaneously contacts CSN4 subunit through a conserved ß-hairpin loop (Ins2) (Lingaraju et al. 2014). Upon the CSN complex interaction with neddylated CRL E3 ligase, CSN4 subunit interacts with CRL and undergoes significant remodeling, which is sensed by the Ins2 loop of the CSN6 subunit. Conformational change in the CSN6 Ins2 leads to considerable movement in the CSN5 Ins1 and removes its inhibitory effect from the CSN5 active site (Lingaraju et al. 2014). Therefore, the inhibitory effect of the Ins1 assures that CSN5 can only function within the CSN complex and in response to neddylated CRLs (Lingaraju et al. 2014). In case of the USP14 (functional homologue of yeast Ubp6), its crystal structure revealed that catalytic triad is in an active position however, the catalytic domain alone showed low affinity for Ub-substrate cleavage (Hu et al. 2005). It was observed that within the catalytic domain two surface loops, blocking loops 1 and 2 (BL1 and BL2) which are also conserved in yeast, occlude the ubiquitin binding pocket (Hu et al. 2005). Cocrystal structure of the USP14 catalytic domain bound to ubiquitin aldehyde revealed a significant conformational change in the position of BL1 and BL2 which leads to opening access to the active site (Hu et al. 2005). Further, the interaction of the yeast Ubp6 Ubl domain with Rpn1 subunit of the proteasome 19S RP results in considerable movement in BL1 and BL2 and removes their inhibitory effect from the Ubp6 active site (Bashore et al. 2016).

All four members of the UCH domain DUBs incorporate crossover loops that block the catalytic active site by joining an α-helix to a β-strand across the active site pocket. These crossover loops have a varying length (11-21 amino acids long) and contribute to substrate specificity (Clague et al. 2013). UCH-L1, the most abundant protein in the brain, contains the shortest crossover loop with a rigid structure that restricts access to the active site. Accordingly, it is involved in the removal of short peptides from the C-terminus of the ubiquitin precursors and accidental Ub C-terminus thiol or amine adducts that are formed during thioester intermediate bond formations (Bishop et al. 2016). UCH-L3 crystal structure revealed a 20 residue long crossover loop which was mostly disordered indicating its high flexibility (Misaghi et al. 2005). However, the steric constrain imposed by the crossover loop does not allow accommodation of large substrates. Therefore, UCH-L3 cannot cleave the isopeptide bond between two ubiquitins and instead shows a high preference for small ubiquitin C-terminal

leaving groups (Grou et al. 2015). It was shown that expansion of the UCH-L3 crossover loop by 5-10 glycine residues allows hydrolysis of Lys48 and Lys63 linked Ub chains (Popp et al. 2009).

Allosteric Regulation of DUBs Activity and Specificity:

Many deubiquitinating enzymes function as a subunit of a larger complex or through interaction with another binding partner. A global proteomic analysis of 75 DUBs identified 774 proteins associated with these enzymes (Sowa et al. 2009). DUBs typically show a low affinity towards the ubiquitinated substrate and only achieve optimal function through interaction with other proteins. In some cases interacting partners downregulate DUBs' activity or contribute to their substrate specificity (Reyes-Turcu et al. 2009). A notable example of the allosteric regulation is the case of USP1 and its coactivator UAF1, regulators of the FA DNA repair pathway. USP1 alone is essentially an inactive enzyme. Its interaction with UAF1 increases enzymatic activity (K_{cat}) by 35 folds while it does not affect ubiquitin binding (Villamil et al. 2013). Probing active site amino acids revealed that UAF1 interaction modulates active site residues and leads to their conformational change. Further, it was shown that in the USP1/UAF1 complex compared to the apoenzyme, pKa of the catalytic cysteine does not change however, upon UAF1 interaction pKa of the catalytic histidine decreases, which facilities its function as a general base (Villamil, Chen, et al. 2012; Cohn et al. 2007). Another example is the case of UCH37 (also known as UCH-L5) and BAP1. Similar to UCH-L1 and UCH-L3, UCH37 and BAP1 contain crossover loops that occlude the active site groove. However, in contrast to UCH-L1 & 3 that cleave small leaving groups and peptides, UCH37 hydrolyzes Lys48-linked Ub chains and BAP1 deubiquitinates histone H2A (Morrow et al. 2013). It was shown that interaction of UCH37 with Rpn13, ubiquitin receptor of the 19S RP, and BAP1 with ASXL1 (additional sex combs like 1) stimulates their catalytic activity (Ronau et al. 2016). Cocrystal structure of UCH37, Rpn13 and ubiquitin-propargyl (suicide inhibitor) revealed that upon UCH37 and Rpn13 interaction a segment of the crossover loop contacts Rpn13 and gets stabilized. Rpn13 also interacts with the C-terminal UCH37-like domain (ULD) of the UCH37 and holds it in a favorable position for binding with the ubiquitin (Sahtoe et al. 2015; Misaghi et al. 2009). INO80G is another binding partner of UCH37 which recruits it to INO80 chromatin remodeling complex (VanderLinden et al. 2015). While Rpn13 activates UCH37, INO80G interaction with the ULD domain inhibits UCH37 enzymatic activity. Crystal structure of UCH37 in complex with the INO80G revealed that upon interaction INO80G forces C-terminal end of the ULD towards the UCH37 active site and blocks access to the ubiquitin-binding groove

(Sahtoe et al. 2015; VanderLinden et al. 2015).

Allosteric regulation of DUBs has also been noted in the endocytic and autophagy pathways. AMSH, a JAMM domain DUB, is recruited to endosomes by STAM, a subunit of the ESCRT complex, which also enhances AMSH hydrolysis activity (Davies et al. 2013). While the AMSH catalytic domain interacts with the distal ubiquitin in a Lys63-linked Ub chain, the STAM Ub interacting motif (UIM) binds the Ile44 patch of the proximal ubiquitin. STAM interaction with the proximal Ub stabilizes the chain and increases AMSH enzymatic activity (Davies et al. 2013).

Post-Translational Modification of DUBs:

Similar to many well-studied cellular processes DUBs' activity is also fine-tuned through post-translational modifications, such as phosphorylation, SUMOylation and even ubiquitination. For instance, Ser313 phosphorylation of USP1 by Cdk1 kinase is critical for recognition and activation by its cofactor, UAF1. Mutation of Ser313 to alanine suppresses USP1/UAF1 complex formation and renders USP1 inactive (Villamil, Liang, et al. 2012). Another example is OTULIN which negatively regulates the NF-κB pathway by antagonizing the linear Ub chain assembly complex, LUBAC. HOIP, E3 ligase subunit of the LUBAC, interacts with the OTULIN's PUM interacting motif and recruits it to the LUBAC. It was shown that phosphorylation of the conserved Tyr56 within the PUM interacting motif of OTULIN abolishes its interaction with the LUBAC and inhibits its antagonizing effect on the NF-κB pathway (Schaeffer et al. 2014). Likewise, CYLD, tumor suppressor protein and a USP domain DUB, is regulated both through phosphorylation and SUMOylaltion. Retinoic acid induced SUMOylation of CYLD on Lys40 inhibits its substrate cleavage activity and upregulates the NF-κB signaling (Kobayashi et al. 2015). In addition, Ser418 phosphorylation of CYLD by IKKε (IκB kinase epsilon) oncoprotein inhibits its deubiquitination activity towards TRAF2 and is essential for IKKε mediated cell transformation (Hutti et al. 2009). DUBs' function can also be modified through ubiquitination. For instance, ubiquitination of ataxin-3 on Lys117 in reaction to the unfolded protein response (UPR) leads to enhanced hydrolysis of polyubiquitin chains while it does not affect on ataxin-3 preference for Lys63-linked ubiquitins (Tsou et al. 2013). Another example is the Josephin domain protein 1 (JosD1), a member of the JAM domain DUBs. JosD1 can hydrolyze Ub chains only after it is activated through monoubiquitination. Ubiquitination of JosD1 is also important for its plasma membrane localization and regulation of endocytosis (Seki et al. 2013).

Post-translational modification of DUBs can alter their cellular localization without affecting catalytic activity. For instance, BAP1 is multi-monoubiquitinated by an E2/E3 hybrid enzyme, UBE2O, close to its nuclear localization motif (Mashtalir et al. 2014). Such modification leads to the cytoplasmic sequestration of BAP1 and restricts its access to the nuclear substrates (Mashtalir et al. 2014). Similarly, USP4 phosphorylation by AKT kinase at Ser445 leads to its translocation to the cytoplasm and localization to the membrane where it can stabilize TßRI receptor and upregulates the TGF-ß signaling (Zhang et al. 2012).

Further, it has been noted that catalytic cysteine of DUBs can be modified and temporarily inactivated by reactive oxygen species. Many DUBs from USP, UCH and OTU family can undergo reversible oxidation by reactive oxygen species such as superoxides, hydrogen peroxides and hydroxyl radicals (Lee et al. 2013). Oxidation of DUBs catalytic cysteine produces cysteine sulphenic acid or sulphene amide which inhibits isopeptide bond hydrolysis activity (Lee et al. 2013). For instance, inhibition of the USP1 enzymatic activity by oxidation is essential for the PCNA monoubiquitination and activation under oxidative stress (Lee et al. 2013). USP1 is inactivated partly through oxidation of its catalytic cysteine residue, which leads to accumulation of the monoubiquitinated PCNA and activation of the translesion synthesis pathway (TLS). USP1 recovers from oxidative inhibition in a time-dependent manner and mostly through activation of the anti-oxidative genes (Lee et al. 2013). Another example is the case of A20 OTU domain deubiquitinating enzyme. High resolution structure of the A20 catalytic domain under different oxidation states (oxidation numbers) indicated that catalytic cysteine oxidizes into cysteine sulphenic acid which is stabilized by OTU catalytic center structure through hydrogen bond formation (Kulathu et al. 2013). It is suggested that cysteine modification to sulphenic acid intermediate may protect the active site from further oxidation (Kulathu et al. 2013).

Human USP7:

Human ubiquitin specific protease 7 (USP7/HAUSP) is a well-characterized cysteine protease deubiquitinating enzyme involved in stabilization, activation and localization of its substrates. An ever-expanding list of proteins has been identified as USP7 substrates or binding partners. USP7 modulation of tumor suppressors and transcription factors such p53, PTEN (phosphatase and tensin homolog), FOXO4 (forkhead Box O4) and retinoblastoma-associated protein (Rb)

family is essential for normal cellular stress response and regulation of cell cycle progression. USP7 is also implicated in the regulation of the DNA repair pathways, epigenetics and immune response (Pfoh, Lacdao & Saridakis 2015; Nicholson & Suresh Kumar 2011). Therefore, it is not surprising that aberrations in the USP7 activity are linked to tumorigenesis and human disease.

USP7 Domain Structure:

USP7 harbors a TRAF-like domain (Tumor necrosis factor receptor (TNFR) associated factor (TRAF)) in its N-terminus and five Ubl domains in its C-terminus (Fig. 1-10) (Sheng et al. 2006; Holowaty et al. 2003). A shallow groove on the surface of the USP7 N-terminus binds substrates or interacting proteins (E/P/A)XXS motifs where X stands for any amino acid with a higher preference for serine (Sarkari et al. 2010; Saridakis et al. 2005). All USP7 homologues in their TRAF-like domain binding pocket harbor a highly conserved ^{164}DWGF^{167} motif where Asp164 and Trp165 residues have been found essential for USP7-substrate interaction (Saridakis et al. 2005). USP7 C-terminal Ubl domains are also involved in protein-protein interaction. USP7-CTD structure revealed that the five Ubl domains are arranged in a 2-1-2 architecture where Ubl12 and Ubl45 form di-Ubls and Ubl3 shows limited contact (Faesen et al. 2011). USP7 C-terminal interacting proteins such as GMPS, UHRF1 and ICP0 recognize a negatively charged ^{758}DELMDGD^{764} motif on Ubl2 through their KXXXK sequence where the two lysine residues have been found important for interaction with USP7 Asp762 and Asp764 (Pfoh et al. 2015).

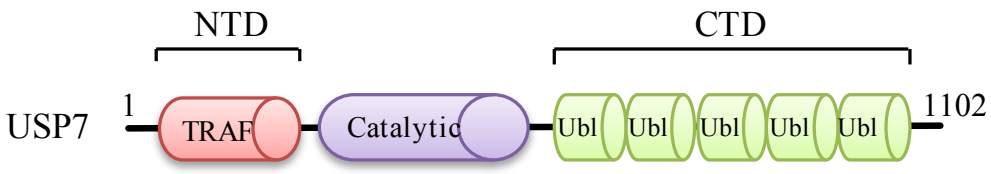

Fig. 1-10: The domain arrangement of human USP7. USP7 contains an N-terminal substrate binding TRAF domain, a catalytic domain and a C-terminal domain that comprises five ubiquitin-like (Ubl) sub-domains.

The USP7 catalytic domain resembles an extended right hand composed of the fingers, palm and thumb subdomains. The active site residues are located in a cleft between the thumb and palm structures while the finger subdomain helps position the ubiquitin C-terminal glycine within the active site cleft (Fig. 1-11) (Hu et al. 2002). USP7 crystal structure revealed that the catalytic Cys223 is about 9.7 Å away from the catalytic His464 rendering the active site unproductive (Hu et al. 2002). However, the USP7 catalytic domain structure bound to ubiquitin aldehyde showed conformational change and realignment of the catalytic cysteine to 3.6 Å distance from histidine (close to a hydrogen bond distance) (Hu et al. 2002). Further, it was noted that realignment of the catalytic triad is reinforced by the C-terminal Ubl4 and 5. The USP7 Ubl domains show considerable flexibility between Ubl123 and Ubl45 and can fold back towards the catalytic domain (Faesen et al. 2011). Consequently, a peptide extension beyond Ubl45 contacts the "switching loop" close to the catalytic triad and results in a significant conformational change in the loop. This leads to the realignment of the catalytic triad and increases catalytic activity by 100 fold (Faesen et al. 2011).

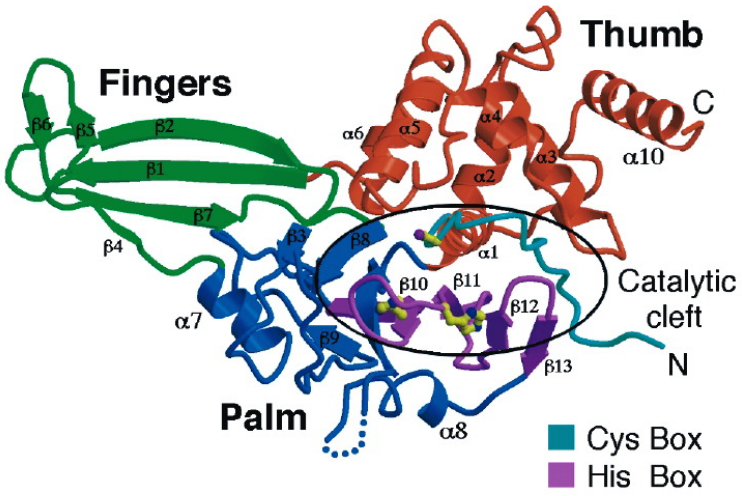

Fig. 1-11: USP7 catalytic domain structure depicting the fingers (in green), thumb (in red) and palm (in blue) subdomains. Cys and His boxes include the active site residues in a cleft between Thumb and Palm structure. (Reprinted by permission from Elsevier: Cell, (Hu et al. 2002), copyright 2002).

Regulation of the USP7 Activity and Stability:

The active conformation of the USP7 catalytic triad is further stabilized with the help of allosteric activator proteins such as GMPS and ABRO1(Abraxas brother 1). GMPS induces USP7 activation and is required for its histone H2B deubiquitination, while USP7 has no effect on GMPS stability or *de novo* GMP synthesis (van der Knaap et al. 2010). GMPS is typically sequestered in the cytoplasm owing to its monoubiquitination by TRIM21, an autoimmune associated RING domain E3 ligase (Reddy et al. 2014). Upon genomic stress TRIM21 dissociates from GMPS, allowing unubiquitinated GMPS to localize in the nucleus where it allosterically activates USP7 and stabilizes USP7-p53 complex. Nuclear accumulation of GMPS is required for USP7 mediated stabilization and transactivation of p53 (Reddy et al. 2014). GMPS contacts USP7 C-terminal Ubl123 and specifically interacts with ^{758}DELMDGD^{764} sequence on Ubl2. It promotes compact confirmation of USP7 by forcing Ubl45 to reach the "switching loop" and therefore leads to realignment of the catalytic residues (Fig. 1-12)(Pfoh, Lacdao, Georges, et al. 2015; Faesen et al. 2011). ABRO1, another protein implicated in the USP7 activation, is a component of the BRISC complex which is a multisubunit DUB involved in Lys63-linked Ub hydrolysis (Jianhong Zhang et al. 2014). Upon oxidative stress or DNA damage signal, ABRO1 which is typically cytoplasmic localizes to the nucleus. It was shown that ABRO1 simultaneously interacts with the USP7 C-terminal domain and p53 and promotes formation of the ABRO1-USP7-p53 complex. ABRO1 enhances USP7 deubiquitination activity and mediates stability and transactivation of p53 in a USP7 dependent manner (Jianhong Zhang et al. 2014). Apart from USP7 activators there are cellular proteins that downregulate USP7 and inhibit its contact with cellular substrates. For instance, TSPYL5 (testis-specific protein, Y-encoded-like 5) selectively binds the USP7 N-terminal TRAF domain, impairs USP7-p53 interaction and leads to p53 instability (Yang et al. 2013; Epping et al. 2011).

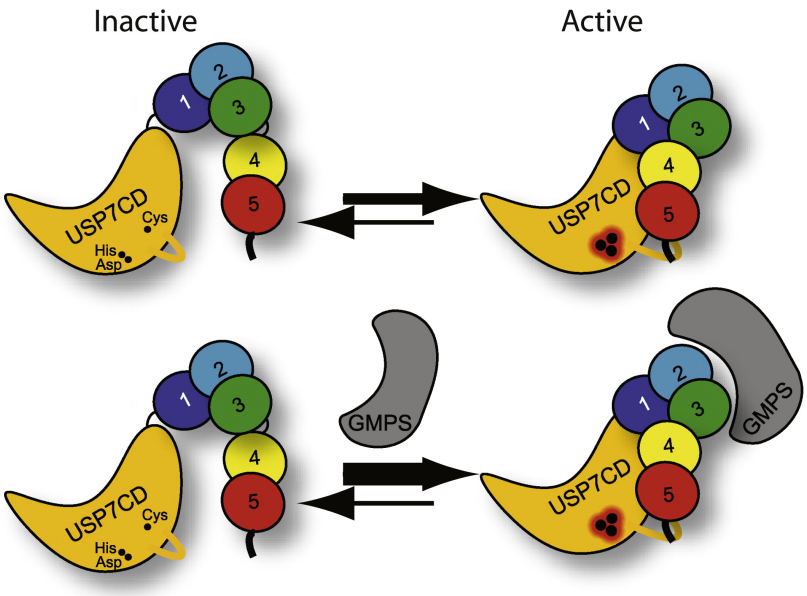

Fig. 1-12: Schematic representation of USP7 activation by Ubl45. Upon folding of the USP7 C-terminal Ubl domains a peptide extension beyond Ubl45 contacts the “switching loop” close to the catalytic active site and mediates realignment of the catalytic triad. The compact conformation of USP7 is further stabilized through the interaction of GMPS with USP7 Ubl123. (Reprinted by permission from Elsevier: Molecular Cell, (Faesen et al. 2011), copyright 2011).

Other than allosteric regulation of its activity, USP7 stability is also regulated through post-translational modifications. 60-70% of the cellular USP7 exists as a phosphorylated isoform (Khoronenkova et al. 2012). Under normal cellular conditions, CK2 kinase (Casein kinase II) phosphorylates USP7 on Ser18 and stabilizes it by inhibiting USP7 ubiquitination and proteasomal degradation (Khoronenkova et al. 2012). However, upon exposure to ionizing radiation ATM kinase phosphorylates and activates PPM1G phosphatase (protein phosphatase, Mg^{2+}/Mn^{2+} dependent, 1G) which in turn dephosphorylates and downregulates USP7. The decrease in the cellular levels of phosphorylated USP7 was followed by Hdm2 downregulation and p53 transactivation (Khoronenkova et al. 2012).

USP7 Regulation of the p53-Hdm2 Pathway:

One of the most extensively studied functions of USP7 is regulating the stability of p53 and its negative regulator, Hdm2. p53 provoked cell cycle arrest or apoptosis upon a variety of stress signals including, DNA damage, viral infection or oncogenic activation is crucial for DNA repair and tumor suppression (Shadfan et al. 2012). p53 and Hdm2 both interact with the USP7-NTD DWGF motif through their (P/A)XXS sequence, which is important for their deubiquitination and stabilization (Sheng et al. 2006). However, Hdm2 is the USP7 preferred substrate and makes more extensive contact with the N-terminal TRAF domain. It was noted that reduction in the cellular levels of USP7 leads to instability of p53 while its total removal results in destabilization of Hdm2 and in turn stabilizes p53. Therefore, under normal cellular homeostasis stabilized Hdm2 maintains p53 at low levels to allow cell cycle progression (Sheng et al. 2006; Meulmeester et al. 2005). Further, it was observed that despite deletion of the p53 TRAF binding sequence, USP7 was still able to stabilize it. Both p53 and Hdm2 also interact with the USP7 C-terminal domain, which is sufficient for their deubiquitination and stabilization (Ma et al. 2010; Brooks et al. 2007). Hdmx, Hdm2 homologue, is another known USP7 substrate implicated in the p53-Hdm2 pathway. It interacts with the USP7 N-terminal domain (NTD) through its AHSS motif (Sarkari et al. 2010). Hdmx does not show E3 ligase activity however, it forms a heterodimer with Hdm2 through its RING domain and stabilizes Hdm2 by inhibiting its autoubiquitination. Under stress signal ATM kinase is activated through autophosphorylation and subsequently phosphorylates Hdm2, Hdmx and p53 (Chao 2015). These modifications lead to the inhibition of Hdm2-p53 interaction. Further, ATM mediated phosphorylation of Hdmx leads to its ubiquitination by Hdm2 and destabilization of the heterodimer. Activated ATM kinase also phosphorylates and activates PPM1G phosphatase which in turn dephosphorylates

and downregulates USP7 (Khoronenkova et al. 2012). Loss of Hdmx, instability of USP7 and increase autoubiquitination of Hdm2 results in stability and transactivation of p53 (Chao 2015).

DAXX, the death domain associated protein, is another USP7 substrate involved in the p53-Hdm2 pathway. DAXX is a transcriptional co-repressor that localizes to the promyelocytic leukemia nuclear bodies (PML-NBs) (Hofmann et al., 2002). PML-NB components such as PML and DAXX are regulated by interferons and are involved in the antiviral response. It is well established that not only USP7 localizes to the PML-NBs, it also interacts with and stabilizes DAXX (Tang et al. 2006). In unstressed cells, DAXX interacts with USP7 and Hdm2 simultaneously and secures USP7 mediated stabilization of Hdm2. Also, this interaction leads to USP7 mediated stabilization of DAXX itself from Hdm2 ubiquitination (Tang et al. 2010). Upon DNA damage ATM dependent phosphorylation of DAXX leads to its separation from Hdm2 and promotes Hdm2 destabilization and p53 transactivation (Tang et al. 2013).

USP7 Regulation of Protein Localization:

Other than its crucial role in the regulation of the p53-Hdm2 pathway, USP7 is involved in many none p53 related cellular functions. For instance, the interaction of PTEN and FOXO4 tumor suppressor proteins with USP7 lead to their subcellular translocation. PTEN has a well-stablished role in downregulation of the highly oncogenic PI3K/AKT kinase pathway and plays an essential role in chronic myeloid leukemia (Morotti et al. 2015). PTEN is ubiquitinated on Lys289 which leads to its nuclear localization and activation of the apoptotic pathway (Song et al. 2008). In unstressed cells, USP7 deubiquitinates PTEN and leads to its nuclear exclusion. Upon stress signal PML nuclear bodies through adaptor protein DAXX oppose deubiquitination activity of USP7 on PTEN, which allows PTEN to enter the nucleus and activate its target genes (Song et al. 2008). Further, BCR-ABL, a chimeric oncogene and PTEN suppressor, was shown to physically interact with USP7 and upregulate its stability through phosphorylation (Morotti et al. 2015). Stabilized USP7 increases deubiquitination of PTEN and results in its nuclear exclusion. Constitutively active BCR-ABL tyrosine kinase has been identified in more than 90% of chronic myeloid leukemia cases (Morotti et al. 2015). Similar to PTEN nuclear localization of FOXO4 is induced by monoubiquitination. Upon oxidative stress c-Jun N-terminal kinase phosphorylates FOXO4 and leads to its multi-monoubiquitination and translocation to the nucleus (van der Horst et al. 2006). Hdm2 E3 ligase monoubiquitinates FOXO4 and mediates its nuclear localization, which in turn leads to transcription of the cyclin-dependent kinase inhibitors

p27 and p21 and cell cycle arrest (Coomans de Brachene & Demoulin 2016; Brenkman et al. 2008a). In unstressed cells, USP7 deubiquitinates FOXO4 and promotes its cytoplasmic sequestration.

USP7 Regulation of Genomic Stability and Cell Cycle Progression:

In response to DNA damage, the repair pathways activate cell cycle checkpoints to delay or arrest cell division. This provides enough time to repair DNA lesions and is essential for genomic stability. USP7 has a crucial role in the regulation of DNA damage response through stabilization or modulation of key proteins involved in the DNA break signaling pathways, such as Claspin, Chk1, Bub3, Rad18, ARF-BP1, PRC1, CHFR and Rb. DNA damage leads to ATR kinase dependent phosphorylation and activation of Chk1through Claspin, an adaptor protein, which itself is subject to ubiquitination and proteasomal degradation. USP7 through regulation of Claspin's half-life controls the duration of Chk1 phosphorylation and response to DNA damage (Alonso-de Vega et al. 2014; Faustrup et al. 2009). USP7 is also implicated in cell cycle regulation through stabilization of retinoblastoma-associated protein (Rb). Rb, a major checkpoint protein, is implicated in both cell cycle progression and cell cycle inhibition which is mostly mediated through its interaction with, and inhibition of E2F transcription factor (Bhattacharya & Ghosh 2014). Upon genotoxic stress phosphorylation of Rb by p38, mitogen-activated kinase, promotes its recognition and ubiquitination by Hdm2 E3 ligase, which leads to activation of E2F and apoptosis (Delston et al. 2011). In normal human cells, USP7 was shown to directly interact with Rb and stabilize it from Hdm2 mediated degradation (Bhattacharya & Ghosh 2014).

Further, USP7 depletion is correlated with mitotic abnormalities and genomic instability (Giovinazzi et al. 2014). Spindle assembly checkpoint monitors attachment of chromosomes to the mitotic spindle and prevents segregation errors. It's been shown that USP7 interacts with and stabilizes Bub3, a mitotic checkpoint protein and a subunit of the spindle assembly checkpoint. Depletion of USP7 decreases cellular levels of Bub3 and leads to genomic instability (Giovinazzi et al. 2014; Maresca & Salmon 2010). USP7 is also implicated in the regulation of CHFR, a RING domain E3 ligase and a mitotic stress checkpoint protein. CHFR activation upon mitotic stress signal leads to ubiquitination and proteasomal degradation of mitotic kinases such as Aurora A and Plk1 (polo-like kinase1) and therefore delays entry into metaphase. USP7 interacts with CHFR and stabilize it from autoubiquitination (Oh et al. 2007).

Furthermore, USP7 downregulation leads to impaired translesion synthesis (TLS) response and defective replication. Bulky DNA lesions block DNA polymerase and stall replication. Rad18, an E3 ligase enzyme and a substrate of USP7, along with Rad6 its cognate E2 conjugating enzyme monoubiquitinate PCNA which leads to recruitment of TLS DNA polymerases and activation of DNA replication through DNA lesions (Zlatanou et al. 2016). Upon DNA damage signal USP7 mediated deubiquitination of Rad18 protects it from degradation and leads to the activation of the TLS pathway (Zlatanou et al. 2016). USP7 is also implicated in the base excision repair (BER) pathway through regulation of ARF-BP1 (also known as Mule) E3 ligase enzyme. In unstressed cells, ARF-BP1 primary function is suppression of p53 and downregulation of the BER pathway by destabilizing DNA polymerase ß, the major BER polymerase (Parsons et al. 2009). Ser18 phosphorylated isoform of USP7 interacts with ARF-BP1 and inhibits its autoubiquitination and proteasomal degradation (Khoronenkova & Dianov 2013). Upon DNA damage USP7 is dephosphorylated and destabilized by PPM1G phosphatase. This leads to autoubiquitination of ARF-BP1 and its proteasomal degradation. Downregulation of ARF-BP1 is necessary for activation of p53 and cellular DNA damage response (Khoronenkova & Dianov 2013).

USP7 Regulation of Transcription and Epigenetics:

USP7 has been implicated in epigenetics through direct deubiquitination of histone H2B and regulation of proteins that are involved in DNA modification. The GMPS/USP7 complex opposes BRE1 E3 ligase monoubiquitination of histone H2B on Lys120 and promotes transcriptional silencing. Mutational analysis revealed that loss of GMPS or USP7 leads to increase in ubiquitinated histone H2B levels (van der Knaap et al. 2005). Further, GMPS/USP7 complex through stabilization of PRC1 promotes histone H2A ubiquitination on Lys119 and leads to transcriptional repression (de Bie et al. 2010). PRC1 is also implicated in the regulation of INK4b-ARF-INK4a tumor suppressor locus. USP7 and USP11 mediated stabilization of PRC1 subunits, RING1B, BMI1 and MEL18, represses tumor suppressors ARF and p16/INK4a expression, which suggests an oncogenic role for USP7 (Maertens et al. 2010; Lecona et al. 2015). USP7 is also involved in the regulation of DNA methylation through interaction with UHRF1 (Ub like with PHD and RING finger domains 1) and DNMT1 (maintenance DNA methyltransferase 1) proteins. UHRF1 is a RING domain E3 ligase enzyme that strongly associates with the heterochromatin and has been shown essential for maintaining genomic methylation (Zhang et al. 2015). UHRF1 recruits DNMT1 to heterochromatin to maintain DNA

methylation on the newly synthesized DNA strands. USP7 forms a heterodimer with DNMT1 which then associates with UHRF1 on the silenced methylated chromatin (Felle et al. 2011). USP7 interacts with DNMT1 through its C-terminal domain, stimulates DNMT1 enzymatic function and stabilizes it from UHRF1 negative regulation (Felle et al. 2011). UHRF1 interacts with the both N-terminal TRAF domain and C-terminal Ubl12 binding motif of USP7, which is important for is stabilization from autoubiquitination (Pfoh, Lacdao, Georges, et al. 2015). USP7 also allosterically promotes UHRF1 chromatin association (Zhang et al. 2015).

USP7 as a Target for Herpesviruses:

Human Herpesviruses (HHVs):

Herpesviruses are members of the *Herpesviridae*, a large family of double stranded DNA viruses, which can establish latent infection in their respective hosts (Edelman 2005). Out of more than 100 identified herpesviruses only eight species are known to routinely infect humans, including herpes simplex virus types 1 and 2 (HSV-1 & HSV-2), varicella-zoster virus (VZV/ HHV-3), Epstein-Barr virus (EBV/ HHV-4), human cytomegalovirus (HCMV/ HHV-5), human herpesvirus 6A & 6B (HHV-6A & HHV-6B), human herpesvirus 7 (HHV-7) and Kaposi's sarcoma associated herpesvirus (KSHV/ HHV-8) (Alibek et al. 2014). Mammalian herpesviruses are further classified into α, β or γ subfamilies mainly based on their genetic properties and evolutionary relatedness (Edelman 2005). The alphaherpesvirinae have an extremely short reproductive cycle in host cells (about one hour), infect a wide range of tissues and are able to stablish latent infection in sensory nerve ganglia. HSV-1, HSV-2 and VZV are alphaherpesviruses (Edelman 2005). The betaherpesvirinae, including HCMV, HHV-6 and HHV-7, share a long reproductive cycle. They have restricted host range and stablish latency mostly in lymphocytes and secretory glands (Edelman 2005). The gammaherpesvirinae also show very restricted host range and stablish latency in lymphoid tissue which is generally restricted to T or B cells. EBV and KSHV belong to this subfamily (Edelman 2005). HHVs are extremely widespread and more than 90% of adults have been infected with at least one type of these viruses (Alibek et al. 2014; Edelman 2005). In the majority of cases, treatment of the infection symptoms does not clear the virus and the latent form of the virus persists during the lifetime of the host (Chisholm & Lopez 2011). To stablish latency, herpesviruses have to suppress host immune responses and evade the immune system (Wen & Damania 2010). HHVs have evolved various mechanisms for host immune evasion including inhibition of cellular

senescence and apoptosis as well as promoting cell proliferation (Alibek et al. 2014; Wen & Damania 2010). Considering the crucial role of USP7 in regulating multiple tumor suppressor proteins and the DNA damage response pathways, it is not surprising that several proteins expressed by HHVs directly interact with USP7 and deregulate its function.

HHV Proteins Interaction with USP7:

Members of the herpesvirus family, such as HSV-1, EBV, KSHV and HCMV have evolved to interfere with the USP7 regulated pathways by competitively binding to USP7 and hindering its interaction with cellular substrates and binding proteins (Salsman et al. 2012; Lee et al. 2009; Saridakis et al. 2005; Everett et al. 1997). USP7, initially known as herpesvirus associated USP (HAUSP), was isolated as an interacting partner with HSV-1 ICP0 protein (Everett et al. 1997). ICP0 is a RING domain E3 ligase enzyme that promotes degradation of host PML-NBs associated proteins, such as PML and Sp100 (Lanfranca et al. 2014). PML proteins are primary components of PML-NBs which are mediators of crucial cellular functions such as p53 activation, DNA damage response, apoptosis and inhibition of viral genome replication in the nucleus (Lanfranca et al. 2014). The ICP0 C-terminal KXXXK sequence tightly interacts with the USP7 ^{758}DELMDGD^{764} motif on Ubl2. USP7 stabilizes ICP0 from autoubiquitination while ICP0 ubiquitinates USP7 and downregulates its cellular levels (Pfoh, Lacdao, Georges, et al. 2015). Further, ICP0 promotes translocation of USP7 to the cytoplasm where in complex with ICP0, USP7 deubiquitinates TRAF6 and NEMO Lys63-linked Ub chains and downregulates TLR mediated NF-κB activation and inflammatory cytokine response (Daubeuf et al. 2009)

Epstein-Barr virus, another USP7 interacting HHV, immortalizes B-lymphocytes during its latent infection and is implicated in multiple carcinomas and lymphomas. EBNA1, an EBV expressed latent protein, is involved in the maintenance of latent EBV genome, initiation of DNA replication and transcriptional activation of latent proteins (Frappier 2012; Pattle & Farrell 2006). Structural analysis revealed that EBNA1 binds the USP7 TRAF domain DWGF binding pocket with much higher affinity than USP7 cellular substrates, such as p53 and Hdm2 (Sarkari et al. 2010). It decreases cellular levels of p53 and subsequently suppresses DNA damage mediated apoptosis. In addition, EBNA1 induces degradation of PML, tumor suppressor protein, through simultaneous interaction with USP7 and CK2 kinase. EBNA1 recruits USP7 and CK2 to PML-NBs and induces CK2 mediated phosphorylation of PML protein. This leads to ubiquitination and degradation of PML. USP7 further downregulates PMLs independent of its

catalytic activity and p53 stabilization. EBNA1 mediated degradation of PMLs is linked to EBV-induced nasopharyngeal carcinoma (Sarkari et al. 2011; Sivachandran et al. 2010).

KSHV is the causative agent of Kaposi's sarcoma and primary effusion lymphoma. Multiple KSHV expressed proteins have shown interaction with USP7. Viral interferon regulatory factors 1 and 4 (vIRF1 & vIRF4), latency-associated nuclear antigen 1 (LANA) and ORF45 competitively bind USP7-NTD at the same region as USP7 cellular substrates (Chavoshi et al. 2016; Gillen et al. 2015; Jager et al. 2012; Lee et al. 2011; Sarkari et al. 2010; Lee et al. 2009; Saridakis et al. 2005). They block USP7-substrate interaction, cripple the cell's interferon and innate immune response and suppress p53 mediated apoptosis (Lee et al. 2009; Saridakis et al. 2005). Further, vIRF4 also directly interacts with Hdm2 and inhibits its autoubiquitination while vIRF1 interacts with p53 and inhibits its acetylation and transactivation by p300 (Nakamura et al. 2001). Therefore, multiple KSHV expressed proteins have evolved to target USP7 and other proteins in the p53-Hdm2 pathway to comprehensively suppress p53 activity.

UL35, an HCMV latent protein, is implicated in viral gene expression and replication. UL35 gene codes for two proteins: UL35 and UL35a, both of which were shown to interact with USP7. UL35 but not UL35a was reported to effect USP7 subcellular localization and inhibit USP7 nuclear body formation independent of their disruptive effect on PML-NBs (Salsman et al. 2012). The function of USP7 nuclear bodies is currently unknown, however they are associated with PML-NBs formation (Salsman et al. 2012).

X-ray Crystallography:

Three-dimensional structures of proteins can help identify common features, modes of regulation and protein interaction (Shapiro & Harris 2000). Atomic-level structural data provide crucial information, such as nature of the chemical bonds and chemical reaction mechanisms. In recent years, use of structural information has become an essential part of pharmaceutical drug discovery and optimization. Structural information on target proteins and their binding sites help optimize lead compounds and improve quality and selectivity of the drugs (Klebe 2000). To obtain the structure of a protein by crystallography, the initial steps include cloning, expression and purification of a soluble, highly pure and homogenous protein (Luna-Vargas et al. 2011). The subsequent step is a random and coarse screening using sparse matrix kits for conditions that would support crystal formation. In case of a successful hit, this step is followed by optimization

of the crystal quality. Crystals are then used for X-ray diffraction data collection and structure determination, which results in a three dimensional model of the protein (Blundell & Patel 2004).

Protein Crystallization:

In aqueous solutions and under non-denaturing conditions, pure and homogenous soluble proteins undergo slow precipitation which can promote protein crystallization. Slow precipitation allows the formation of a crystalline lattice consisting of organized repeats of protein units that are held together by noncovalent bonds (Rhodes 2006). The first stage in protein crystallization is nucleation which leads to the formation of thermodynamically stable protein aggregate also known as the critical nucleus. The crystal growth stage follows when macromolecules diffuse to the surface of the critical nucleus. Then growth ceases as protein concertation in the solution depletes or the growing faces of the crystal gets interrupted by impurities (Rupp 2010). Crystal growth can be visualized using a two-dimensional phase diagram depicting the change in the protein concentration versus concentration of the precipitating agent. Two major zones can be identified in the graph: unsaturated and supersaturated (Fig. 1-13). The unsaturated zone never supports crystal formation (Krauss et al. 2013). As the protein concentration increases beyond its solubility limits, solution becomes saturated and supersaturated. The supersaturated zone can be further divided into two zones. In the precipitation zone, very high concentration of protein leads to amorphous protein aggregation. In the nucleation zone or labile zone, intermediate supersaturation leads to the critical nucleus formation, while at metastable zone (lower supersaturation) only crystal growth is supported. In optimal cases, few critical nuclei form in the nucleation zone and as crystals grow, decreases in the protein concentration in the solution shift the system to the metastable zone where only crystal growth is supported and there is no more nucleation (Fig. 1-13) (Krauss et al. 2013; Boistelle 1986).

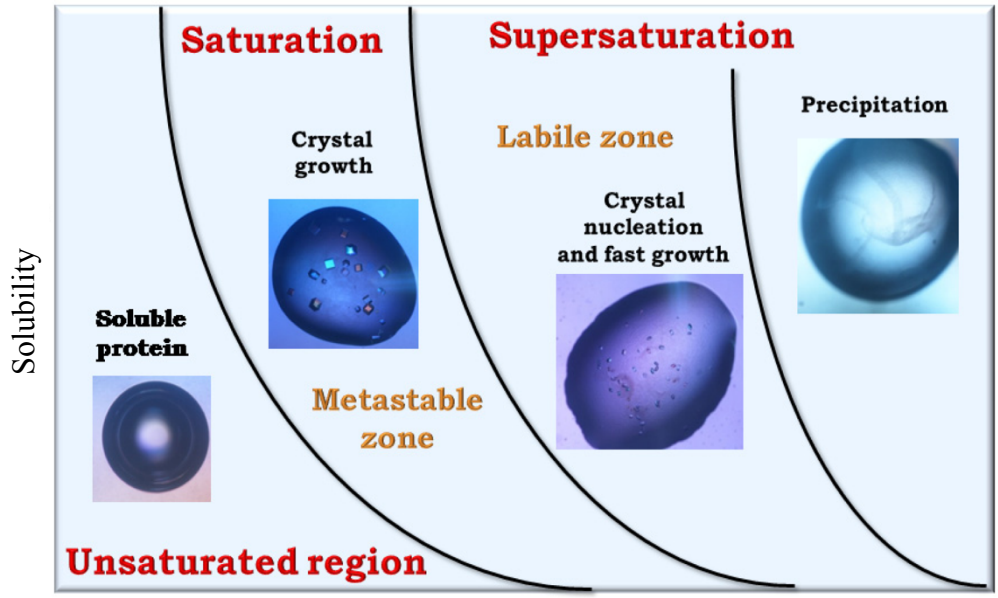

Fig. 1-13: Protein solubility phase diagram as a function of protein concentration. (Reprinted from MDPI: Journal of Biological Sciences, (Krauss et al. 2013), copyright 2013).

In practice, it is very difficult to find perfect conditions for crystal nucleation and growth and there are no systematic methods that would assure crystallization of macromolecules. Such conditions must be experimentally and individually developed for each protein. Furthermore, only 13-15% of soluble proteins that enter crystallization trials form crystals that are useful in structure determination (Wernimont & Edwards 2009).

Crystallization Screening Methods:

The most common protein crystallization screening methods include vapor diffusion and microbatch. In the vapor diffusion method, a few microliters of the protein in precipitation buffer is exposed to a reservoir containing the same precipitation buffer (100-500 μL) with slightly higher concentration than the protein droplet. Then the well is sealed to achieve equilibrium. As the equilibrium forms over the protein droplet, water molecules evaporate from the protein until the concentration of the protein droplet and the reservoir reaches equilibrium. The slow increase in the concentration of the protein and precipitant in the droplet can help shift the solution to supersaturation zone (Benvenuti & Mangani 2007). If all the other parameters such as temperature, pH, ionic strength, type of precipitant, etc. are appropriate, a critical nucleus can form and crystal growth will follow. Vapor diffusion screens can be set up as sitting drops where a protein droplet is placed on a pedestal above the reservoir level or hanging drops where a protein droplet is placed on an inverted lid or coverslip over the reservoir (Fig. 1-14A & B). In both methods, the environment is sealed to achieve equilibrium. In sandwich drop vapor diffusion technique protein droplet is placed between two coverslips over the buffer reservoir (Fig. 1-14C) (Krauss et al. 2013; Benvenuti & Mangani 2007). Another screening method is micro-batch where a small volume of the protein mixed with precipitant is placed on a well in a plate and is then covered with paraffin oil to prevent evaporation. In this method concentration of the precipitant and volume of the drop remains unchanged. However, the formation of protein aggregates or crystals can change protein concentration (Fig. 1-14D) (Krauss et al. 2013; Rupp 2010).

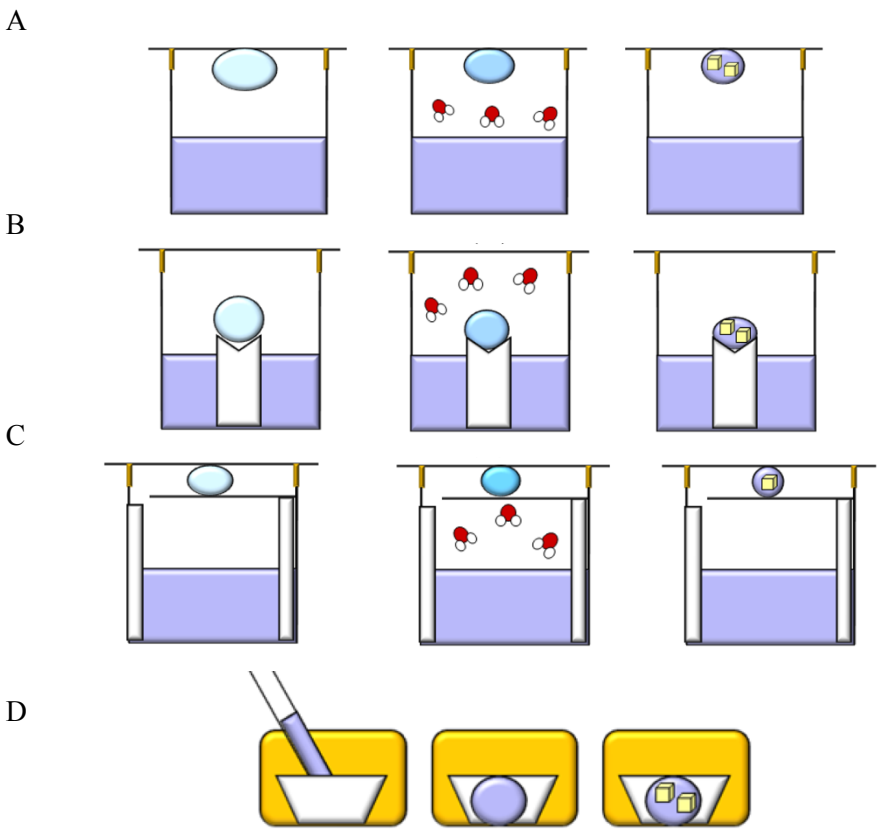

Fig. 1-14: Common crystallization screening methods. In vapor diffusion method, equilibrium is achieved in a sealed environment. Water molecules evaporate from less concentrated protein droplet and gradually increase protein concentration which can lead to crystal formation. A) Hanging drop vapor diffusion where protein droplet is placed on an inverted lid or coverslip over the reservoir. B) Sitting drop vapor diffusion where protein droplet is placed on a well above the reservoir level. C) Sandwich drop vapor diffusion technique where protein droplet is placed between two coverslips over the buffer reservoir. D) Microbatch method where a small volume of the protein mixed with precipitant is placed on a well in a plate and is then covered with paraffin oil to prevent evaporation. (Reprinted from MDPI: Journal of Biological Sciences, (Krauss et al. 2013), copyright 2013).

Substances known to precipitate proteins including salts, organic solvents and polymers, are typically used in crystallization solutions. Formation of a protein crystal has a very low success rate and depends on a variety of factors, such as protein concentration and purity, pH, temperature, ionic strength, pressure and types of precipitants and additives used (Krauss et al. 2013). Any substance that is added to the crystallization screen other than the compounds present in the precipitation buffer is considered an additive, such as cofactors, ligands, metal ions, salts, detergents, alcohols and amino acids (Krauss et al. 2013). Search for optimal conditions that can support nucleation and crystal growth is done through an initial random or coarse screening to identify crystalline conditions. These conditions are then optimized and refined using a systematic screening approach. The most common approach in screening is based on the sparse-matrix screens where varying precipitants are made according to the literature and based on the conditions that have previously led to the formation of quality crystals (Wooh et al. 2003).

X-ray Diffraction:

X-ray crystallography is a form of very high-resolution microscopy that is used to determine the three-dimensional structure of a protein. Chemical bonds between atoms in a molecule are about 1.5 angstrom (Å) apart; therefore, electromagnetic radiation such as X-rays with wavelengths in the angstrom range can be used to visualize them (Rhodes 2006). Ideally, the diffraction pattern from the crystal should be better than 4 Å resolution to distinguish secondary structure and better than 2.5 Å to distinguish hydrogen bonds (Munshi et al. 2012; Jeffrey 1997). Many ordered molecules in a crystal produce a strong and detectable diffraction pattern which appears as series of distinct spots referred to as reflections (Rupp 2010). The intensity of the spots, their amplitude and positions are measured by an optical scanner to produce an electron density map. Diffracted X-rays refer to the clouds of electrons and their distribution in the molecules, which is known as electron density. Using the protein's known amino acid sequence, the electron density map is fitted with a molecular model that must contain appropriate bond lengths, bond angles, conformational angles and distance between adjacent groups (Rupp 2010; Rhodes 2006).

Improvement of X-ray Diffraction Quality:

Techniques, such as microseeding with microcrystals are employed to promote either nucleation or formation of larger or better-quality crystals. Typically, a high level of

supersaturation is needed for nucleation to occur, which either is not achievable or can lead to a large number of nuclei formation and very small crystal growth (Oswald et al. 2008). A seed or nucleation agent provides a solid base for crystal growth by lowering the required energy for spontaneous nucleation (Oswald et al. 2008). Microseeding is done by transferring a microscopic crystal from a higher supersaturated solution to a lower supersaturated one (Oswald et al. 2008). Obtained crystals can be further soaked in ligands, inhibitors or heavy atoms to produce crystal ligand complex, or to improve crystalline lattice (Mizutani et al. 2014). Cross-linking reagents can be added to crystals to improve protein-protein docking, structural rigidity and handling of the crystals (Leitner et al. 2010). Annealing is another method used to increase the quality of X-ray diffraction which includes warming up flashed-cooled crystals to room temperature followed by reflash-freezing. Annealing has shown success in decreasing static disorder and mosaicity of the crystals (Harp et al. 1998). Further, optimization methods are employed to screen for best cryo conditions and improve quality of cryo-protectants for each protein. Cryo-protectants are used to avoid freezing of protein crystals and ice formation when crystals are exposed to liquid nitrogen stream during X-ray exposure (Rupp 2010). Another method to improve quality of crystals is the removal of highly flexible regions of proteins, such as loops or N-terminal or C-terminal unstructured regions. This is done by designing deletion mutant constructs or by partial proteolysis of the pure protein using proteolytic enzymes such as trypsin (Wernimont & Edwards 2009). If a protein contains flexible domains each domain can be expressed and crystallized separately. Further, point mutation can be used to alter surface residues that interfere with the formation of a well-ordered crystal lattice (Malawski et al. 2006).

Thesis Rationale and Outline:

Deubiquitinating enzymes negatively regulate ubiquitination and have crucial roles in many cellular processes such as regulation of protein stability, protein trafficking, cell cycle progression and DNA transcription and replication. Ubiquitin specific proteases, USPs in humans/ Ubps in yeast, are the largest family of deubiquitinating enzymes. USPs/Ubps involvement in many important pathways and cellular processes implicated in disease, disorder and cancer have made them an important subject of investigation. In the following chapters we have set out to investigate *S. cerevisiae* Ubp enzymes expression, function and structure and further shed light into the novel interaction of two human herpesviruses proteins with the human USP7 deubiquitinating enzyme.

S. cerevisiae Ubps have shown significant conservation of sequence and function with their human homologues. Lack of intron in *S. cerevisiae UBP* genes and less complicated post-translational modifications make them a much more convenient target for cloning, expression and purification and further functional studies compared to their human homologues. **In chapter 2,** we explored the possibility of expressing soluble recombinant *S. cerevisiae* Ubp enzymes in *E. coli* for the purpose of crystallography and structure determination. Multiple optimization methods were employed to express soluble proteins in *E. coli* and further purify these proteins for crystallization trials and screening. In chapter 2 we also provide the three-dimensional structure of yeast Ubp6 catalytic domain and further investigate yeast Ubp15, USP7 homologue, mechanism of substrate interaction.

In order to stablish latency human herpesviruses (HHVs) have evolved various mechanisms for host immune evasion, such as inhibition of cellular senescence and apoptosis and promoting cell proliferation. Deregulation of proteins involved in growth control has led to the recognition of some HHVs as underlying agents of human cancer. Proteins expressed by some members of the HHV family have evolved to interfere with the USP7-p53-Hdm2 pathway. They competitively bind to USP7 and hinder its interaction with cellular substrates or binding proteins. They block USP7-substrate interaction and cripple the cell's interferon and innate immune response and p53 mediated apoptosis. **In chapter 3,** we identified vIRF1 protein expressed by Kaposi's sarcoma-associated herpesvirus (KSHV) as a novel interacting protein with human USP7 and characterized this interaction using structural analysis of USP7-NTD and vIRF1 peptide complex and a series of *in vitro* pull-down assays. Further, we confirmed this interaction *in vivo* and investigated the effect of vIRF1 expression on proteins involved in the USP7-p53-Hdm2 pathway.

In chapter 4, we identified pp71 tegument transactivator protein expressed by human cytomegalovirus as a novel interacting protein with the human USP7 N-terminal domain and further characterized this interaction using complex crystal structure of the USP7 N-terminal domain with pp71 peptide and series of *in vitro* assays. The interaction was confirmed *in vivo* and effect of pp71 expression on the USP7-p53-Hdm2 pathway was analyzed.

Chapter 5 provides a summary of findings, future directions and concluding remarks.

Chapter 2: Investigating Expression and Purification of *S. cerevisiae* Ubps for Protein Crystallography; Crystal Structure of Ubp6 and Insight into the Interaction Mechanism of the Ubp15 N-Terminal Domain

In Fig. 2-4 (*S. cerevisiae* Ubp6 catalytic domain structure) Dr. Saridakis supervised the experiment and collected crystal diffraction data. Dr. Roland Pfoh refined the diffraction data. I set up and performed the experiments and produced the final figures. In Fig. 2-9 (Superimposed ^{15}N HSQC spectra of Ubp15-NTD before and after titration with (E/P/A)XXS containing peptides) Dr. Saridakis and Dr. Sheng supervised the experiment. Procedure was done with the help of Sahar Farhadi and I analyzed the data and produced the figures. I performed all other experiments in this chapter.

Introduction:

Ubiquitination:

Eukaryotic proteins undergo a variety of post-translational modifications, which help regulate and extend their functional diversity. One such modification is protein ubiquitination, where a multistep enzymatic process results in the addition of ubiquitin (Ub) moieties to specific substrate proteins. A covalent isopeptide bond forms between the carboxyl-terminal glycine of a ubiquitin molecule and either the amino-terminal or amino group of lysine residues of the specific substrate protein (Callis 2014; Varshavsky 2012; Hershko 2005). Up to 20% of yeast proteins under standard growth conditions have been found conjugated to ubiquitin (Peng et al. 2003). Ubiquitin itself possesses seven lysine residues including: Lys6, Lys11, Lys27, Lys29, Lys33, Lys48 and Lys63, which all can participate in the assembly of polyubiquitin chains. This leads to variety of modifications ranging from mono to poly ubiquitination of the substrate protein and results in varying Ub-Ub linkages, which dictate the fate of the tagged protein (Faggiano et al. 2016; Trempe 2011). Polyubiquitination of a substrate with Lys48 linked ubiquitins provides a strong signal for recognition and degradation by the 26S proteasome and forms the most abundant type of ubiquitination. Mono or multi-monoubiquitination in most cases is linked to protein trafficking and proteasomal independent degradation (Callis 2014; Kulathu & Komander 2012). Apart from protein degradation, ubiquitination is implicated in other cellular functions such as DNA repair, DNA transcription, cell cycle progression and signal transduction. For instance, Lys11-linked ubiquitin chains, the second most abundant Ub linkage in yeast, are involved in both cell cycle control and proteasomal degradation, while Lys63-linked Ub chains regulate the NF-κb and the DNA repair signaling pathways (Finley et al. 2012; Trempe 2011; Xu et al. 2009).

Deubiquitinating Enzymes:

The ubiquitination process is reversible. Deubiquitinating enzymes (DUBs) reverse ubiquitination by hydrolyzing the isopeptide bond between the C-terminal glycine (Gly76) of Ub and lysine residue of the substrate or another ubiquitin (Varshavsky 2012; Nijman et al. 2005). DUBs belong to the cysteine or metalloprotease families. Hydrolysis of the isopeptide bond by cysteine/thiol proteases relies on the function of three conserved cysteine, histidine and aspartate residues in their active site. A polarized aspartic acid assists histidine to deprotonate the thiol

group of the cysteine. Then deprotonated cysteine launches a nucleophilic attack on the substrate's carbonyl group carbon to form an intermediate thioester bond, which is then hydrolyzed to free the enzyme and form a carboxylic acid group on the remaining substrate (Eletr & Wilkinson 2014; Katz et al. 2010). Metalloproteases coordinate a Zn^{2+} ion in their active site typically with the help of two histidine residues, an aspartic acid and a water molecule, which is required for hydrolysis (Shrestha et al. 2014).

Cysteine protease DUBs are further divided into four subclasses based on the structure of their catalytic domain: ubiquitin-specific proteases (USP), ubiquitin C-terminal hydrolases (UCH), ovarian tumor domain proteases (OTU) and Machado Joseph disease proteases (MJD) (Sahtoe & Sixma 2015; Nijman et al. 2005). Recently a new family of cysteine proteases has been described, referred to as MINDY (motif interacting with Ub-containing novel DUB family), with members identified in yeast as well as mammals (Abdul Rehman et al. 2016).

Cellular Functions of DUBs:

DUBs are important regulators of the ubiquitin-proteasome system. Prior to degradation of substrate proteins by the 26S proteasome, DUBs remove polyubiquitin chains and assist in unfolding and translocation of proteins into the proteasome chamber (Finley 2009). Efficient removal of ubiquitin from substrate proteins prior to their rapid proteolysis inhibits inappropriate degradation of the ubiquitin tag along with the doomed protein and is crucial for maintaining available cellular ubiquitin pool for protein modifications (Eletr & Wilkinson 2014). Several DUBs have been found associated with the proteasome, such as yeast Ubp4, Ubp6 (USP14 in mammals) and Rpn11 (a metalloprotease) (Lee et al. 2011). In the absence of the proteasome associating Ubps, ubiquitin is very unstable and has a short half-life of 2 hours (Hanna et al. 2003). Furthermore, DUBs, through removal of the Lys63-linked Ub chains or single ubiquitin tags regulate cellular levels of proteins that are targeted for endocytosis and degradation in lysozymes (Piper et al. 2014; Dupre & Haguenauer-Tsapis 2001). Monoubiquitination of yeast endocytic and plasma membrane proteins were previously reported which suggests a role for DUBs in the regulation of membrane-bound proteins half-life (Clague et al. 2012; Polo et al. 2002). Deubiquitinating enzymes also remove ubiquitin tags from inappropriately tagged proteins involved in the ubiquitin-proteasome pathway and stabilize them, such as E3 ligases (Komander et al. 2009). Further, DUBs are involved in disassembly of the ubiquitin chains after their removal from tagged proteins. Excessive accumulation of ubiquitin chains competes with

the polyubiquitinated substrates for the 26S proteasome and inhibits proteasomal degradation. Deubiquitinating enzymes are also involved in non-proteolytic functions such as regulation of transcription and DNA damage response through deubiquitination of histone H2A and H2B (Cao & Yan 2012; Emre et al. 2005; Henry et al. 2003). Further, all ubiquitins are expressed with a C-terminal extension beyond the Gly76. These precursors are either expressed as ubiquitin fused to ribosomal proteins or as ubiquitin multimers linked through their first and last residues. Proper cleavage of Ub precursors is essential for generation of functional ubiquitins. Many DUBs in yeast have shown Ub precursor cleaving activity (Clague et al. 2012; Hochstrasser & Amerik 2004).

Yeast *S. cerevisiae* Ubp Enzymes:

A large number of DUBs belong to the USP subclass, which is known as Ubps in yeast. USPs/Ubps share well-conserved sequences known as His and Cys boxes that include the catalytic residues (Tencer et al. 2016; Nijman et al. 2005). The catalytic domains of Ubps vary greatly in size which indicates different modes of regulation, function and substrate interaction. Ubps have also shown substrate specificity. This is achieved through different extensions in their structure which modulates their cellular localization and protein-protein interaction. Ubps also gain specificity through recognition of specific Ub linkages, mono or poly Ub chains, free or bound polyubiquitin chains and affinity for certain substrates (Katz et al. 2010). Removal of Ub tags from specific substrates has crucial physiological impact on cellular processes. For instance, deletion of yeast Ubp3 leads to transcriptional silencing at the telomeres, whereas deletion of yeast Ubp10, which works in contrast to Ubp3, significantly reduces levels of Sir4, a protein involved in silencing of the heterochromatin (Emre et al. 2005; Kahana & Gottschling 1999).

Saccharomyces cerevisiae (*S. cerevisiae*) expresses 16 Ubp enzymes, which are involved in differentially regulating various cellular processes, such as protein degradation and transport and chromosomal modification. Under standard growth conditions deletion of *S. cerevisiae* Ubps indicated that they are non-essential for growth, suggesting overlapping functions (Reyes-Turcu et al. 2009).

Project Rationale:

Proteins function correlates with their three-dimensional fold. Structural studies can help identify common and evolutionary conserved features and provide clues to proteins specificity, function and interaction (Shapiro & Harris 2000). Generation of soluble proteins with high purity is essential for protein crystallography as well as assays, biochemical characterizations and industrial use (Hoi et al. 2015; Luna-Vargas et al. 2011). *S. cerevisiae* Ubps have shown significant conservation of sequence and function with their human homologues. Lack of introns in *S.c. UBP* genes and less complicated post-translational modifications make them much more convenient targets for cloning, expression and purification and further functional studies as compared to their human homologues. The first step towards structural studies is the production of soluble and pure proteins. The ability to express and purify large quantities of recombinant proteins from *Escherichia coli* and availability of a variety of molecular tools has made it an attractive choice for protein expression, despite its lack of post-translational modifications (Rosano & Ceccarelli 2014). To investigate expression of soluble *S. cerevisiae* Ubps from *E. coli* for protein crystallography and structure determination, 127 constructs encompassing full-length or selected domains of all 16 Ubps and Sad1 and Pan2 proteins (catalytically inactive Ubps) were designed.

Further, both *S. cerevisiae* Ubp15 and its well-studied human homologue, USP7, harbor a highly conserved DWGF motif in their N-terminal domains (NTD) (Bozza & Zhuang 2011; Sheng et al. 2006). The DWGF motif in USP7-NTD is efficiently recognized by its cellular substrates and interacting proteins through their (P/A/E)XXS sequence, where X stands for any amino acids (Sheng et al. 2006; Saridakis et al. 2005). To gain insight into the *S. cerevisiae* Ubp15 mode of protein interaction, we analyzed binding affinity of Ubp15-NTD for the (E/P/A)XXS motifs using fluorescence polarization binding assays and NMR titrations.

Material and Methods:

Primer Design and Construct Amplification:

Prior to primer design for polymerase chain reaction (PCR) amplification of the *S. cerevisiae* Ubp constructs, primary amino acid sequences and secondary predicted structures were analyzed by Phyre2 web portal for protein modeling (Kelley et al. 2015). Primers were designed for ligation independent infusion based cloning with p15TV-L vector (GenBank ID: EF456736.1). (5' TTG TAT TTC CAG GGC 3') and (5' CAA GCT TCG TCA TCA 3') inserts, which are required for homologous recombination with the vector, were added to the 5' ends of the forward and reverse primers respectively (Appendix A). To clone Ubp3 constructs into the pET-28b expression vector (Novagen #69865-3), restriction enzymes cut sites of NcoI (5' GCG CCC ATG GGC 3') and XhoI (5' GCG CTC GAG 3') were added to the 5' ends of the forward and reverse pET-28b primers respectively (Appendix A).

To amplify Ubp constructs, *S. cerevisiae* cells were grown overnight in yeast growth media (BioShop), followed by genomic DNA extraction using MasterPure™ yeast DNA purification kit (Epicentre, #MPY80200), according to the manufacturer's protocol. PCR reactions were set up in 50 µL reaction volumes using 0.1 µL *Pfu* high-fidelity DNA polymerase (gift from Dr. Dinesh Christendat, University of Toronto), 1x*Pfu* buffer (200 mM Tris-HCl pH 8.8, 100 mM $(NH_4)_2SO_4$, 100 mM KCl, 1 % (v/v) Triton X-100, 1 mg/mL BSA), 250 µM dNTP (Fermentas), 300 ng *S. cerevisiae* genomic DNA (measured using Thermo Scientific NanoDrop 2000), 1 µM of each forward and reverse primer and 250 µM $MgSO_4$. PCR reactions were set up using standard protocols at annealing temperatures 5-7ºC lower than primers melting point in a Hybaid Px2 Thermal Cycler (Thermo Scientific). Amplified fragments were purified using GFX™ PCR DNA purification kit (GE Healthcare) as outlined by the manufacturer.

Cloning of the Constructs:

All vectors were initially transformed into chemically competent DH5α *E. coli* following a standard chemical transformation protocol (Yoshida & Sato 2009). Plasmids were amplified and retrieved via a DNA plasmid miniprep kit (Qiagen). p15TV-L vector was linearized with BseRI restriction enzyme (New England BioLabs, #R0581S) for 1 hour at 37°C and purified with a GFX™ PCR DNA purification kit (GE Healthcare) according to the manufacturer's protocol and

eluted in 40 µL dH_2O to achieve DNA concentration of ~100 ng/ µL (measured using a Thermo Scientific NanoDrop). For ligation independent cloning 1 µL of vector and insert were annealed using an In-Fusion HD cloning kit (Clontech) in p15TV-L according to the manufacturers protocol. 1 µL of annealing reaction was transformed into 25 µL of electrocompetent DH5α *E. coli* cells following a standard electroporation protocol (Yoshida & Sato 2009). Cells were grown on Luria-Bertani (LB) agar (Bioshop) plates, supplemented 100 µg/mL ampicillin (for selection of p15TV-L vector), at 37°C overnight.

For cloning into pET-28b, the vector and the inserts were digested with NcoI and XhoI restriction enzymes (New England BioLabs) for 15 min at 37ºC and purified as mentioned above. Digested vector was further treated with calf intestinal alkaline phosphatase (New England BioLabs) for 15 min at 37ºC, purified and eluted in 40 µL dH_2O to achieve DNA concentration of ~100 ng/ µL. 1 µL of digested vector and insert were ligated with T4 DNA ligase (New England BioLabs) in 10 µL reaction volume at 16ºC overnight according to the manufacturer's protocol. 1 µL of the ligated mixture was electroporated into 25 µL electrocompetent DH5α *E. coli* and incubated on LB agar plates supplemented with 50 µg/mL kanamycin (for selection of pET-28b vector) at 37°C overnight. All positive transformants were validated by PCR and further screened by sequencing using T7 forward and reverse primers.

Protein Expression:

All positive recombinant p15TV-L vectors were heat shock transformed into *E. coli* BL21 (DE3) mgk cells, which harbor a Kanamycin resistant plasmid coding for 3 rare *E. coli* tRNAs including two arginines (AGG and AGA) and one Ile (ATA) (gift from Dr. Dinesh Christendat, University of Toronto). The recombinant pET-28b vectors were transformed into either BL21 DE3 or Rosetta Blue cells (Novagen, 71-059-3). Cells were grown in varying volumes of Terrific Broth (Bioshop) and the appropriate antibiotics at 37ºC. At OD_{600} nm of 1.2, expression was induced with 0.4 mM isopropyl β-D-1-thiogalactopyranoside (IPTG) and was carried out at 16ºC overnight. For co-expression with trigger factor (Tig) chaperone (TaKaRa Chaperone Plasmid Set), pg-Tf2 plasmid was transformed into BL21 mgk cells prior to re-transformation with p15TV-L plasmid. BL21 mgk cells were cultured in TB broth with 20 µg/mL chloramphenicol, along with 100 µg/mL ampicillin and 50 µg/mL kanamycin for the selection of the transformed clones. Expression of the Tig chaperone was induced by addition of 0.5 mg/ml of L-arabinose prior to the recombinant protein induction with IPTG. For NMR titration, uniformly labeled ^{15}N-

labeled 6xHis-tagged Ubp15-NTD (residues 1-204) was expressed from p15TV-L vector in BL21 mgk cells in M9 media enriched with 0.7 g/L $^{15}NH_4Cl$ as the sole nitrogen source.

Protein Purification:

Cells were harvested at 7,446 x g for 20 minutes at 4ºC and lysed by sonication at 30% amplitude in binding buffer (50 mM Tris pH 7.5, 150-500 mM NaCl, 5 mM Imidazole, 1x protease inhibitor cocktail [1 mM Benzamidine and 0.5 mM PMSF] and 1x Protease inhibitor tablet [Roche cOmplete ULTRA Tablets]). Lysates were clarified by centrifugation for 1 hour at 41,287 x g for 30 minutes at 4ºC. Supernatants were allowed to interact with nickel-nitrilotriacetic acid (Ni-NTA) beads (Qiagen) for 1 hour on a nutator at 4ºC. Beads were washed extensively with wash buffer (50 mM Tris pH 7.5, 150-500 mM NaCl and 20 mM Imidazole). Proteins were eluted by addition of elution buffer (50 mM Tris pH 7.5, 150-500 mM NaCl and 250 mM Imidazole). Protein expression was verified by resolving samples on 12% SDS-polyacrylamide gels followed by Coomassie blue staining or silver staining (Bio-Rad, Silver stain plus kit). All recombinant proteins were further purified by size exclusion chromatography using a HiLoad 16/60 Superdex 200 (GE Healthcare) on an ÄKTApurifier 10 UPC system (GE Healthcare) in 150, 300 or 500 mM NaCl and 20 mM Tris or Hepes pH 7.5. To remove fusion tags from the recombinant proteins expressed from p15TV-L or pET28-b vectors, proteins were incubated with tobacco etch virus (TEV) or thrombin proteases respectively, at 4ºC overnight, prior to size exclusion chromatography.

Protein Crystal Screening and Optimization:

Initial protein crystallization screening trials were set up using the vapor diffusion method in 96-well sitting drop plates (Axygem, CP-AXYGEM-96-10) with sparse matrix crystallization suites including: JCSG I-IV, JCSG +, PEGs II, PACT and Classics II (Qiagen). 1 µL of purified protein was mixed with 1 µL of precipitant buffer against 100 µL reservoir solution followed by incubation at either 4ºC or 22ºC. Positive hits were further optimized in 15-well hanging drop vapor diffusion crystallization plates (EasyXtal 15-well Tools, Qiagen) by mixing 1 µL of varying purified protein concentration with 1 µL of precipitant buffer against 500 µL reservoir solution containing varying pH or precipitant concentrations. Additive screens (Hampton) for positive hits were also set up in 15-well hanging drop plates by mixing 1 µL of purified protein with 0.8 µL of reservoir buffer and 0.2 µL of provided additive. Plates were incubated at either

4ºC or 22ºC. Positive hits were further optimized by crystal seeding using Seed Bead Kit (Hampton) following manufacturers protocol.

Partial proteolysis of recombinant proteins was performed by mixing trypsin (Sigma-Aldrich) and recombinant protein in a range of 1/100-1/10000 w/w ratio prior to crystallization screening according to (Wernimont & Edwards 2009).

X-ray Data Collection and Structure Determination:

X-ray data were collected at 100K on a Rigaku MicroMax007 rotating anode diffractometer with a 944+ charge-coupled device detector. Diffraction data were integrated and scaled using HKL2000 software. The Ubp6 structure was determined by molecular replacement method employing Ubp6 catalytic domain structure (Protein Data Bank ID 1VJV) as the search model using CNS 1.3 (Brunger 2007). The electron density was visualized and the Ubp6 protein model was built using Coot (Emsley & Cowtan 2004). REFMAC through PHENIX program suite was used for refinement and water picking at 2.5 Å resolution. The data collection and refinement statistics are shown in Table 2-2. Figures were prepared using PyMOL (Schrödinger 2010).

Peptide Synthesis and Preparation:

Peptides used in NMR studies, including wild-type (^{44}SPGEGPSGTG^{53}) and mutant (^{44}SPGEGP<u>A</u>GTG^{53}) vIRF1, wild-type (^{394}FLDLAHSSE^{402}) and mutant (^{394}FLDLAHS<u>A</u>E^{402}) HdmX, wild-type (^{152}RVSPSTSYT^{160}) and mutant (^{152}RVSPST<u>A</u>YT^{160}) MCMBP and wild-type (^{395}SQPSTSS^{401}) and mutant (^{395}SQPST<u>A</u>S^{401}) Hdm2, were synthesized by CanPeptide Inc. (Montreal, Canada) with both N-terminal acetylation and C-terminal amidation to mimic the native peptides. N-terminal fluorescein isothiocyanate (FITC) labeled wild-type (^{44}SPGEGPSGTG^{53}) and mutant (^{44}SPGEGP<u>A</u>GTG^{53}) vIRF1 and wild-type (^{400}GGLPSSSKLA^{409}) FOXO4 peptides used in fluorescent polarization assays were also synthesized by CanPeptide Inc. (Montreal, Canada).

Fluorescence Polarization Binding Assay:

N-terminal 6xHis-tagged USP7-NTD (residues 54-205) was expressed from the pET-15b vector and purified as described previously (Sheng et al. 2006). N-terminal 6xhis-tagged Ubp15-NTD and USP7-NTD were further purified by size-exclusion chromatography using a HiLoad 16/60

Superdex 200 (GE Healthcare) on an ÄKTApurifier 10 UPC system (GE Healthcare) in 150 mM NaCl and 50 mM Tris pH 8.0. FITC labeled wild-type (^{44}SPGEGPSGTG^{53}) and mutant (^{44}SPGEGP<u>A</u>GTG^{53}) vIRF1 and wild-type FOXO4 (^{400}GGLPSSSKLA^{409}) peptides were initially dissolved in dimethyl sulfoxide to a final concentration of 10 mM. Then 400 nM working stock of each peptide was prepared in assay buffer (150 mM salt, 50 mM Tris pH 8.0, 5% glycerol and 0.01% Triton X-100). 795 µM of Ubp15-NTD and 500 µM concentration of USP7-NTD were serially diluted and shortly incubated with 40 nM fixed concentration of each peptide. 10 µl of the above dilutions were transferred into a 384 well plate (Corning) and fluorescence polarization was measured on a Synergy H4 microplate reader (BioTek, USA) with λ_{ex} = 485 nm and λ_{em} = 520 nm. To obtain the equilibrium dissociation constant (K_d), polarization values were analyzed by Graphpad Prism 5.0 using a one-site binding model. Data were calculated based on three individual experiments and the standard deviation was calculated.

NMR Spectroscopy:

Uniformly ^{15}N-labeled 6xhis-tagged Ubp15-NTD was incubated with TEV protease to cleave the 6xHis fusion tag followed by dialysis into NMR buffer (200 mM NaCl, 25 mM Na phosphate pH 7.0 and 10 mM DTT). Interaction of Ubp15-NTD with wild-type (^{44}SPGEGPSGTG^{53}) and mutant (^{44}SPGEGPAGTG^{53}) vIRF1, wild-type (^{394}FLDLAHSSE^{402}) and mutant (^{394}FLDLAHS<u>A</u>E^{402}) HdmX, wild-type (^{152}RVSPSTSYT^{160}) and mutant (^{152}RVSPST<u>A</u>YT^{160}) MCMBP and wild-type (^{395}SQPSTSS^{401}) and mutant (^{395}SQPST<u>A</u>S^{401}) Hdm2 peptides was monitored by analyzing ^{1}H-^{15}N HSQC spectra. Briefly, up to 0.4 mM of each unlabeled peptide was titrated in 0.2 mM of ^{15}N-labeled Ubp15 (containing 10% D_2O) up to 2:1 peptide:Ubp15 molar ratio. NMR data were recorded at 25ºC using a triple resonance cryoprobe-equipped Bruker 700 MHz NMR spectrometer. Spectra were processed with Topspin 3.2 and analyzed with SPARKY program (Ye et al. 2012; Holowaty et al. 2003).

Results:

Construct Design and Recombinant Protein Expression for Crystallization Trials:

It is well established that differences of a few amino acids can significantly improve the solubility of recombinant proteins or their ability to crystallize (Malawski et al. 2006). To identify soluble and purifiable *S. cerevisiae* Ubp proteins, 127 constructs with varying N and C termini were designed, coding for 16 Ubps, Sad1 and Pan2 proteins or their domains (Table 2-1). 113 constructs that were successfully PCR amplified were inserted in p15TV-L vector via ligation independent cloning and expressed in *E. coli* BL21 (DE3) mgk cells as the first choice of expression vehicle. Expression of the Ubp3 constructs was also attempted from the pET-28b vector as shown in Table 2-1. Recombinant protein expression and solubility were screened by metal affinity chromatography via 6xHis fusion tags. All soluble recombinant proteins were further purified by size exclusion chromatography. Seventeen constructs failed to express any detectable levels of recombinant protein. Ten constructs expressed soluble proteins including Ubp1 (aa 92-741), Ubp3 (aa 1-912 and 189-912), Ubp3 catalytic domain (aa 449-912), Ubp6 (aa 1-499), Ubp12 N-terminal domain (aa 1-361, 90-361 and 98-345) and Ubp15 N-terminal and C-terminal domains (aa 1-204 and 538-1230).

Many optimizations and screening methods were routinely performed when attempting to crystallize soluble proteins. Initial protein crystallization screens were set up both at 4ºC and room temperature (22ºC) using recombinant proteins with the 6xHis fusion tag intact or cleaved. Also, partial *in situ* proteolysis of the purified proteins with trypsin was attempt to remove flexible surface loops that could interfere with protein crystallization (Wernimont & Edwards 2009).

Table 2-1: *S. cerevisiae* Ubp Constructs PCR Amplification, Cloning and Expression Outcome:

UBP	Domain	Residues	PCR	Expression
1	FL	1-809	–	–
	CD	92-741		**Soluble**
	CD	92-809	–	–
	CD	93-753		None
	CD	97-741		Insoluble
	CD	97-809	–	–
	CD	101-739		Insoluble
2	NTD	1-735		Insoluble
	NTD	434-832		Insoluble
	CD	724-1271		None
	CD	725-1271		Insoluble
	CD	725-1259		Insoluble
	CD	731-1271	–	–
	CD	731-1259		Insoluble
	CD	736-1259		None
Cloned in pET-28b vector	FL	1-912		**Soluble**
	NTD+CD	148-912		None
	NTD+CD	189-912		**Soluble**
3	FL	1-912		Insoluble
	NTD	1-459		Insoluble
	NTD+CD	50-912		None
	NTD+CD	104-912		None
	NTD+CD	148-912		None
	NTD+CD	189-912		Insoluble
	CD	412-912		Insoluble
	CD	426-909		Insoluble
	CD	426-912		Insoluble
	CD	429-909		None
	CD	429-912		Insoluble
	CD	445-909		Insoluble
	CD	445-912		Insoluble
	CD	447-909		Insoluble
	CD	447-912		Insoluble
	CD	449-909		Insoluble
	CD	449-912		**Soluble**
	CD	454-912		Insoluble
	CD	459-912		Insoluble

UBP	Domain	Residues	PCR	Expression
4	NTD	1-323		Insoluble
	NTD	1-330	–	–
	NTD	1-561		Insoluble
	NTD	2-315		Insoluble
	NTD	324-561		None
	CD	545-926		Insoluble
	CD	551-926		Insoluble
	CD	556-926		Insoluble
	CD	562-924		Insoluble
5	NTD	1-280		Insoluble
	NTD	1-289		None
	NTD	1-445		Insoluble
	NTD	3-270		Insoluble
	NTD	3-280		Insoluble
	NTD	281-445		Insoluble
	CD	431-805		Insoluble
	CD	434-805		Insoluble
	CD	440-805		Insoluble
	CD	446-805		Insoluble
6	FL	1-499		**Soluble**
	CD	109-488		Insoluble
7	NTD	1-460		Insoluble
	NTD	1-608		Insoluble
	CD	593-1071		Insoluble
	CD	598-1070		Insoluble
	CD	598-1071		Insoluble
	CD	603-1070		Insoluble
	CD	603-1071		Insoluble
	CD	608-1070		Insoluble
8	NTD	1-136		Insoluble
	CD	137-469		Insoluble

UBP	Domain	Residues	PCR	Expression
9	FL	1-754		None
	CD	122-671		Insoluble
	CD	122-707		None
	CD	124-674	–	–
	CD	128-671		Insoluble
	CD	128-707	–	–
	CD	134-668		Insoluble
	CD	311-668		Insoluble
10	NTD	1-361		Insoluble
	CD	336-746		**Soluble**
	CD	351-734		Insoluble
	CD	351-746		Insoluble
	CD	356-734	–	–
	CD	356-746	–	–
	CD	362-734		Insoluble
11	NTD	1-297		Insoluble
	NTD	1-135		Insoluble
	CD	297-710		Insoluble
	CD	283-713		Insoluble
	CD	287-717	–	–
	CD	291-717		Insoluble
12	FL	1-1123	–	–
	NTD	1-345		Insoluble
	NTD	1-361		**Soluble**
	NTD	1-367		None
	NTD	90-361		**Soluble**
	NTD	98-345		**Soluble**
	NTD	98-361		Insoluble
	NTD+CD	90-1123		Insoluble
	NTD+CD	98-1123		Insoluble
	NTD+CD	101-1119		None
	CD	353-1123		Insoluble
	CD	358-1123		Insoluble
	CD	362-1119	–	–

UBP	Domain	Residues	PCR	Expression
13	FL	1-747		Insoluble
	CD	139-669		Insoluble
	CD	129-673	–	–
	CD	129-682	–	–
	CD	134-673		Insoluble
	CD	134-682		Insoluble
	CD	329-669		Insoluble
14	FL	1-781		None
	NTD	1-322		**Soluble**
	NTD	40-277		Insoluble
	CD	312-781		None
	CD	316-781		None
	CD	317-781		Insoluble
	CD	322-781		**Soluble**
15	CD	215-537		Insoluble
	NTD	1-204		**Soluble**
	CTD	538-1230		**Soluble**
16	CD	41-497		Insoluble
	CD	46-499		Insoluble
	CD	47-497		Insoluble
	CD	53-499		Insoluble
SAD 1	NTD	1-149		Insoluble
	CD	44-448		Insoluble
	CD	150-448		Insoluble
PAN 2	NTD	1-504		Insoluble
	CD	493-826		Insoluble
	CD	505-846		Insoluble
	CTD	847-1115		Insoluble

FL: full-length, *CD*: catalytic domain, *NTD*: N-terminal domain, *CTD*: C-terminal domain, (-): failed PCR outcome.

Expression and Crystallization of *S. cerevisiae* Ubp1:

Ubp1, a 92 kDa protein, localizes to the ER membrane via an N-terminal transmembrane region, encompassing residues 34-51 (Wojtowicz et al. 2005). In efforts to express soluble Ubp1 from *E. coli,* we designed constructs to bypass the transmembrane region. Initial expression in BL21 mgk or Rosetta Blue *E. coli* strains did not lead to any detectable levels of soluble protein. However, expression and solubility were optimized through co-expression of Ubp1 (residues 92-741) with Tig chaperone in Bl21 mgk cells at 16ºC overnight, as opposed to an induction temperature of 25-37ºC reported previously (Wojtowicz et al. 2005) (Fig. 2-1A). Large quantities of soluble and stable Ubp1 was purified from *E. coli* in 500 mM NaCl and 20 mM Tris pH 7.5 via metal affinity chromatography and was subjected to further size exclusion chromatography (Fig. 2-1B). Purified protein was used to set up crystallization screening trials. Crystals appeared in Ubp1 concentrations ranging from 12 to 30 mg/ml in 0.2 M Na or K thiocyanate, 20% w/v PEG 3350 and pH 7.0-7.8. Additives including 0.1 M KCl, 0.1 M LiCl and 0.2 M NaCl helped obtain larger crystals with improved morphology (Fig. 2-1C & D). However, despite optimization of crystallization and cryo conditions and use of post-crystallization treatments, such as dehydration, annealing and cross-linking of protein crystals to improve diffraction quality, Ubp1 crystals diffracted poorly upon exposure to X rays.

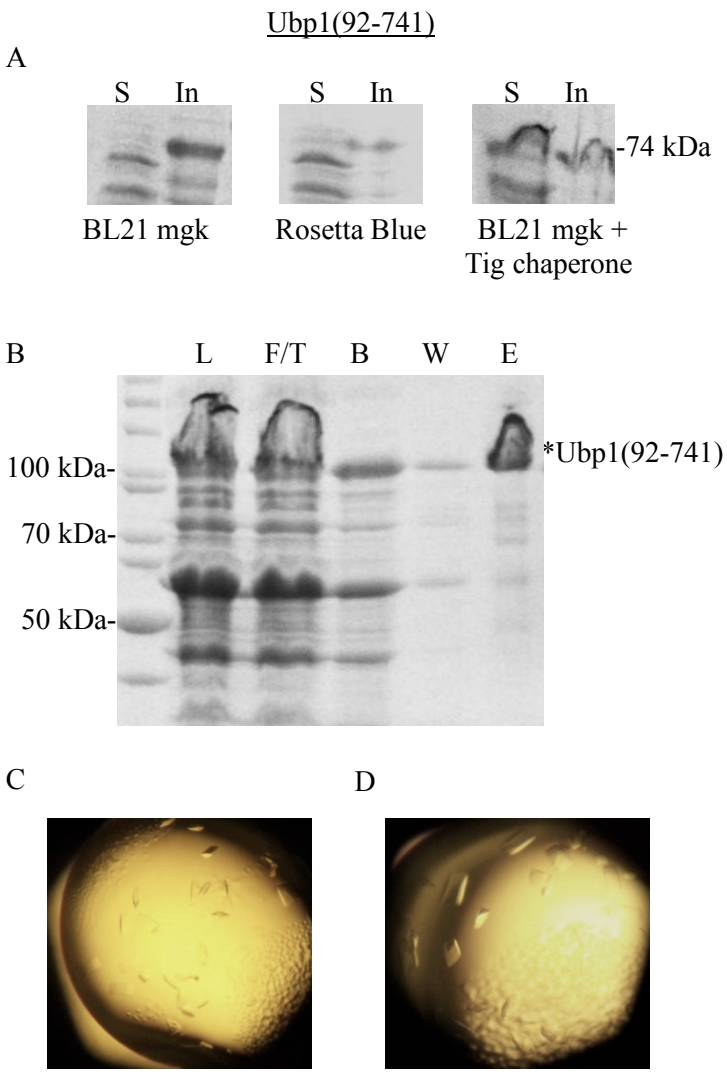

Fig. 2-1: Expression, purification and crystallization of *S. cerevisiae* Ubp1. A) Initially, Ubp1 (residues 92-741) did not express soluble in BL21 mgk or Rosetta Blue *E. coli* strains. Soluble expression in BL21 mgk *E. coli* was optimized through co-expression with trigger factor (Tig) chaperone. *S*, soluble lysate fraction; *In*, insoluble fraction. B) Soluble Ubp1 purification from BL21 mgk cells by metal affinity chromatography via 6xHis fusion tag on a Ni-NTA resin. *L,* lysate; *F/T,* resin flow through; *B,* binding buffer flow through; *W,* wash buffer flow through; *E, elution.* C) Ubp1 crystals appeared in 12 mg/ml protein concentration in 0.2 M Na or K thiocyanate, 20% PEG 3350 and pH 7.0. D) Optimized Ubp1 crystals, grown with either 0.1 M KCl or 0.1 M LiCl or 0.2 M NaCl additives, appeared in 30 mg/ml protein concentration and 0.2 M Na thiocyanate, 20% w/v PEG 3350, pH 7.4-7.8.

Expression of Soluble *S. cerevisiae* Ubp3:

S. cerevisiae Ubp3 (human USP10 homologue) is a 912-residue long protein with a C-terminal UCH catalytic domain. Ubp3 forms a heterotetramer complex with Bre5, its essential cofactor for DUB activity, via amino acids 186-272 (Li et al. 2007). In our efforts to express soluble Ubp3 catalytic domain, 13 constructs with varying N and C termini were cloned in p15TV-L vector and expressed in *E. coli* BL21 mgk. One construct coding for the catalytic domain residues 449-912 expressed a significant amount of soluble protein, which was stably purified in 500 mM NaCl and 20 mM Tris pH 7.5. (Fig. 2-2). Despite screening of numerous crystallization conditions at varying incubation temperatures, pH and protein and precipitant concentrations, crystalline condition were not identified. Considering that Ubp3 residues 186-272 are essential for interaction with Bre5, we designed constructs to include both the catalytic domain and the N-terminal region required for interaction with Bre5 (Table 2-1). Other than p15TV-L, constructs were also cloned into the pET-28b vector, which adds a 6xHis fusion tag to the C-terminus of the recombinant protein. Full-length Ubp3 residues 1-912 and 189-912 expressed soluble from pET-28b vector in Rosetta Blue (DE3) cells (Fig. 2-2); however, crystallization trials did not produce a crystalline outcome.

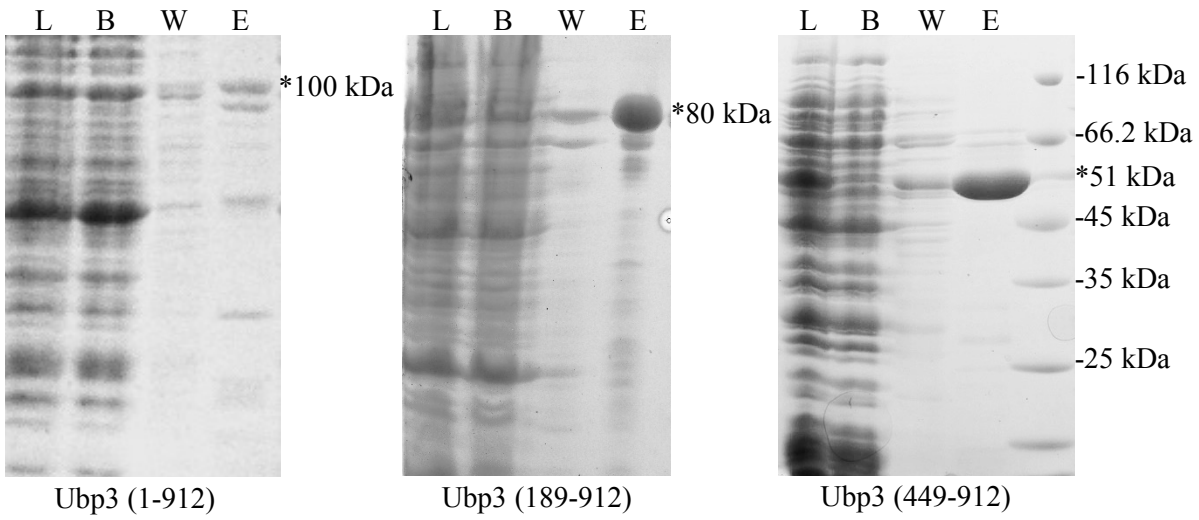

Fig. 2-2: Expression and purification of soluble Ubp3 constructs from *E. coli*. 6xhis-tagged Ubp3 catalytic domain (residues 449-912) expressed soluble from the p15TV-L vector in BL21 mgk *E. coli* cells. Ubp3 constructs containing residues 1-912 and 189-912 with a C-terminal 6xHis fusion tag expressed soluble from the pET-28b vector in Rosetta Blue *E. coli* cells. All proteins were purified by metal affinity chromatography via 6xHis fusion tag on a Ni-NTA resin. *L,* lysate; *B,* binding buffer flow through; *W,* wash buffer flow through; *E, elution.*

S. cerevisiae Ubp6 Expression and Crystallization:

S. cerevisiae Ubp6 consists of a ubiquitin-like domain (Ubl) at its N-terminus (residues 6-76) followed by a USP catalytic domain (residues 108-494) at its C-terminus (Wyndham et al. 1999). Ubp6 was shown to stably interact with the non-ATPase Rpn1 subunit of the proteasome 19S regulatory particle (RP) through its N-terminal Ubl domain (Bashore et al. 2016; Guterman & Glickman 2004; Park et al. 1997). Even though the Ubl domain is not essential for Ubp6 activity or its nuclear localization, it is involved in targeting Ubp6 to the proteasome (Crosas et al. 2006; Chernova et al. 2003). Interaction of the Ubp6 Ubl domain with the 19S RP Rpn1 subunit was shown to increase Ub-substrate hydrolysis activity by 300 fold (Hu et al. 2005; Leggett et al. 2002).

To date structural data available for Ubp6 or its human homologue, USP14, only represent the catalytic domain. In our efforts to obtain the crystal structure of the full-length Ubp6, residues 1-499 were expressed from the p15TV-L vector in BL21 mgk cells. 6xhis-tagged Ubp6 was purified to homogeneity using metal affinity chromatography on a Ni-NTA resin column followed by size exclusion chromatography (Fig. 2-3A). Protein purified in 150 mM NaCl and 20 mM Tris pH 7.5 crystallized at 4ºC in 20% w/v PEG 3350 and 0.2 M $MgCl_2.6H_2O$. Crystallization conditions were further refined by the addition of organic and inorganic additive compounds. Ubp6 crystals appeared at 60 mg/mL protein concentration and were optimized by the addition of 30% v/v 2-propanol as an additive. These crystals diffracted to 2.5 Å resolution and a complete data set was collected (Fig. 2-3B). The diffraction data was integrated, the structure was determined using molecular replacement and refined. A summary of data collection and refinement statistics is presented in (Table 2-2). The resulting model based on interpretation of the electron density only contained information for the Ubp6 catalytic domain; there was no density corresponding to the N-terminal Ubl domain. Examining the Ubp6 crystals by silver staining indicated that crystallized protein was indeed full-length Ubp6 (Fig. 2-3C). It seems that the Ubl domain is flexible and cannot produce an interpretable electron density. In an attempt to stabilize the Ubl domain, we tried co-crystallizing Ubp6 with single ubiquitin molecules in 1:1, 1:2 and 1:5 molar ratios however, crystals were never obtained.

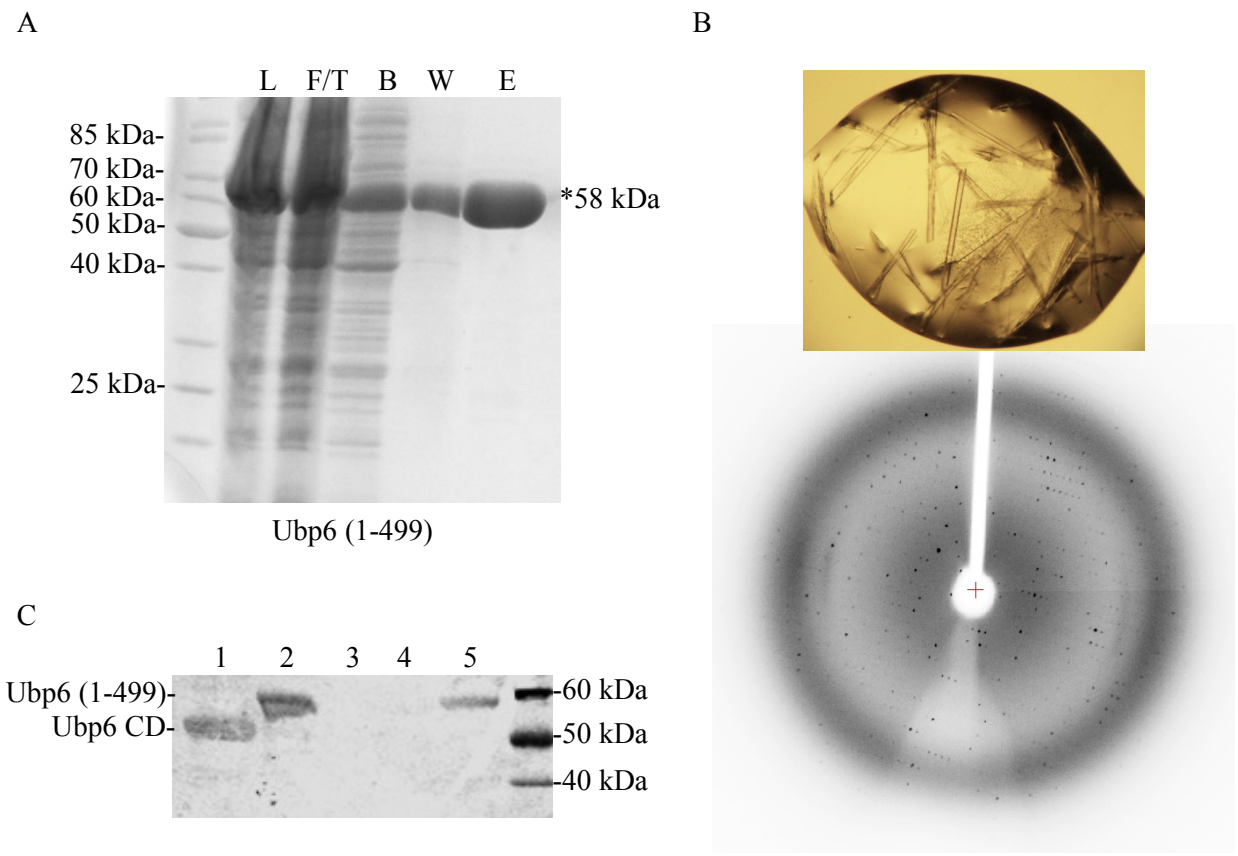

Fig. 2-3: Expression, purification and crystallization of Ubp6. A) 6xhis-tagged full-length Ubp6 was expressed from the p15TV-L vector in BL21 mgk cells. Proteins were purified by metal affinity chromatography via 6xHis fusion tag on a Ni-NTA resin. *L,* lysate; *F/T,* resin flow through; *B,* binding buffer flow through; *W,* wash buffer flow through; *E, elution.* B) Ubp6 native crystals and their diffraction pattern. Crystals appeared in 20% w/v PEG 3350 and 0.2 M $MgCl_2.6H_2O$ and 30% v/v 2-propanol additive at 4ºC, using 60 mg/mL of the protein. Ubp6 crystals diffracted to 2.5 Å resolution. C) Silver staining of the Ubp6 protein crystals. Prior to silver staining, Ubp6 crystals were washed in crystallization buffer and boiled in protein loading dye for 5 minutes. *Lanes 1&2*, positive controls for the Ubp6 catalytic domain (CD) (residues 109-499) and full-length respectively; *Lanes 3&4,* samples from the first and second wash of the crystals in crystallization buffer; *Lane 5*, Ubp6 crystals.

Table 2-2: Ubp6 X-Ray Data Collection and Refinement Parameters.

	Native Ubp6
X-Ray Data	
Space Group	C121
Resolution (Å)	27.64 – 2.50
Unit Cell Axes (Å^3, °)	a=220.94, b= 49.20, c=110.04 ß=114.45
Molecules / AU	2
Total Observations (#)	103736
Unique Reflections (#)	36144
Intensity (I/σ<I>)	4.1 (1.2)
Completeness (%)	95.9 (90.9)
[a]R_{merge}	0.152 (0.536)
Refinement	
R_{work}	0.261
R_{free}	0.297
Protein Atoms (#)	6395
Water Molecules (#)	112
rmsd bonds (Å)	0.014
rmsd angles (°)	1.60
rmsd dihedrals (°)	34.9
rmsd improper (°)	0.84
thermal factors (Å^2)	43.0
Ramachandran Plot	
Most Favoured	732 (94.33%)
Additionally Allowed	32 (4.12%)
Out Lier	12 (1.55%)

Numbers in brackets refer to the highest resolution shell, 2.59 Å to 2.5 Å. [a]$R_{sym} = \Sigma |I-<I>| / \Sigma I$ where I is the observed intensity and <I> is the average intensity from multiple observations of symmetry-related reflections.

Ubp6 Crystal Structure:

We were able to identify two Ubp6 molecules per asymmetric unit in the 2.5 Å electron density which were superimposable, therefore, only one of the molecules is used for results presentation. Three-dimensional structure of the Ubp6 catalytic domain, residues 103-499, similar to human USP14, is analogous to an extended right hand with the subdomains that represent thumb, fingers and palm (Fig. 2-4A) (Hu et al. 2005; Hu et al. 2002). The previous comparison of the known human USP catalytic domain structures suggested that the extended right-hand architecture is conserved among USPs (Hu et al. 2002). The hand-like structure produces a binding pocket with the catalytic residues in the palm subdomain and is suggested to fit the 8 kDa ubiquitin molecule between the fingers and the palm-thumb frameworks (Hu et al. 2002). Two larger alpha helices 4 and 5 and two smaller helices 3 and 6 form the thumb subdomain, while beta strands 1, 2, 4 and 5 form the fingers (Fig. 2-4B & C). Catalytic triad C118, H447 and N465 are located in the palm subdomain.

USP14, the human homologue of Ubp6, has 32% sequence similarity and high structural conservation with Ubp6 and can compensate for the loss of Ubp6 in knockout *S. cerevisiae* (Hu et al. 2005). As shown in Fig. 2-4D, the catalytic domain structures of USP14 and Ubp6 are superimposable and very similar (global and local RMSD= 1.285 Å) (Maiti et al. 2004). Further, USP14 blocking loops 1 and 2 (BL1 and BL2), which hover over the catalytic residues in the predicated ubiquitin binding pocket, are also conserved in *S. cerevisiae* Ubp6 and superimpose well (Hu et al. 2005). However, compared to USP14 α-helix 8, Ubp6 contains two extended α-helices 11 and 12 (Fig. 2-4D). In the case of USP14, it was observed that the catalytic Cys114 is about 3.3 Å away from the catalytic histidine (His435) and also the Asp451 forms a hydrogen bond with the His435, indicating that the catalytic site is in an active conformation (Hu et al. 2005). The Ubp6 catalytic domain structure also revealed that the catalytic triad is in an active conformation. Nitrogen δ atom of the catalytic His447 is within a hydrogen bond distance (3.1 Å) from the Cys118 thiol side chain and the Asn465 accepts a hydrogen bond from the nitrogen ε of the His447 and stabilize it (Fig. 2-4E).

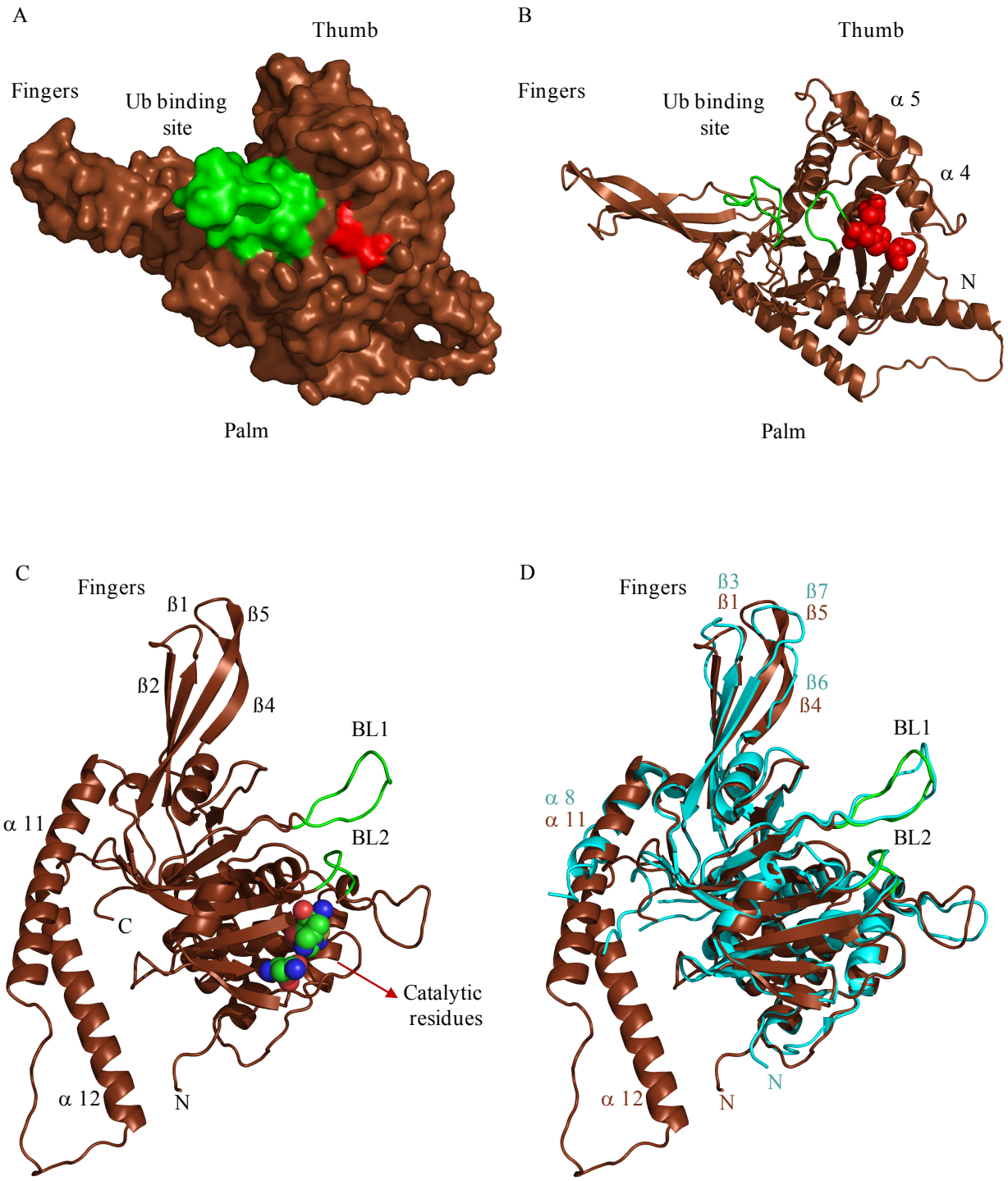
A
Thumb
Fingers
Ub binding site
Palm
B
Thumb
Fingers
Ub binding site
α 5
α 4
N
Palm
C
Fingers
ß1
ß5
ß2
ß4
BL1
α 11
BL2
C
Catalytic residues
α 12
N
D
Fingers
ß3
ß1
ß7
ß5
ß6
ß4
BL1
α 8
α 11
BL2
N
α 12
N

E

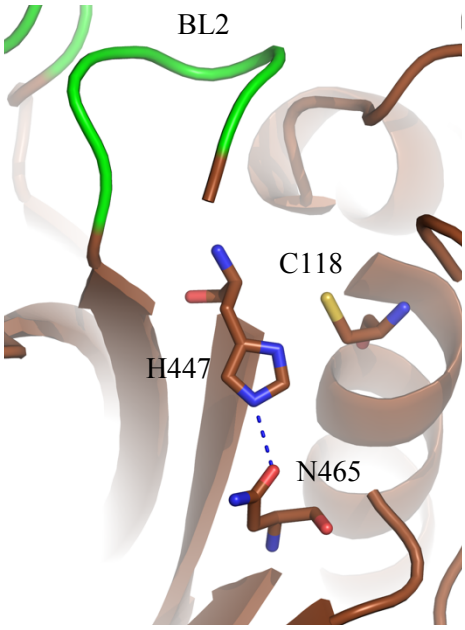

Fig. 2-4: Ubp6 catalytic domain structure. A&B) Catalytic domain of Ubp6 (residues 103-499) in surface and ribbon representation depicting the extended right-hand structure with the fingers, thumb and palm subdomains. Blocking loops 1 and 2 (BL1 and BL2) are shown in green and active site residues are shown in red. Predicted ubiquitin binding site is between the fingers and the palm-thumb structures. C) Ribbon representation of the Ubp6 catalytic domain showing BL1 and BL2 in green, hovering over the catalytic residues. D) Superimposition of the Ubp6 (in brown) and USP14 (in cyan) catalytic domains (global and local RMSD= 1.285 Å). E) The catalytic site of Ubp6. The catalytic triads, C118, H447 and N465, are oriented in an active conformation. The cysteine thiol side chain is shown in yellow, amino groups are shown in blue and carbonyl groups are shown in red. Blocking loop 2 is shown in green hovering closely over catalytic triad. Blue dashed-line represents hydrogen bond.

Expression and Crystallization of *S. cerevisiae* Ubp12-NTD:

S. cerevisiae Ubp12, a 143 kDa protein, contains a domain specific for USPs (DUSP) at its N-terminus (residues 97-199) and a USP catalytic domain at its C-terminus (residues 364-1110). The DUSP domain is conserved in Ubp12 orthologues in human USP4 and USP15 (Elliott et al. 2011). In attempts to obtain the Ubp12 DUSP domain structure, we designed 10 constructs for the Ubp12 N-terminal domain expression in *E. coli*. 6xhis-tagged constructs coding for residues 1-361, 90-361 and 98-345 expressed soluble from the p15TV-L vector in BL21 mgk *E. coli* cells. Proteins were purified by metal affinity chromatography on a Ni-NTA resin column via 6xHis fusion tag (Fig. 2-5A). Ubp12 (1-361) purified in 300 mM NaCl and 20 mM Hepes pH 7.5, crystallized at 4ºC at 12.5 mg/mL in 0.17 M NH_4OAc and 20% w/v PEG 3350 pH 7.5 (Fig. 2-5B). The diffraction resolution of the crystals were optimized from 5 Å to 3.4 Å using microseeding technique. However, despite extensive screening and optimization of the crystallization conditions, diffraction with a higher resolution was not achieved. Ubp12 (90-361), purified in 500 mM NaCl and 20 mM Tris pH 7.5, crystallized at room temperature in protein concentrations ranging from 30-40 mg/ml in three different conditions: 0.2 M $NH_4CH_3CO_2$, 20% w/v PEG 4000 pH 7.5; 0.2 M NH_4F, 20% w/v PEG 3350 pH 7.5 and 0.2 M $Mg(HCOO)_2$, 20% w/v PEG 3350 pH 7.5. Crystals formed in magnesium formate had the best diffraction resolution of 4-6 Å which was optimized to 3.5 Å (Fig. 2-5C). Ubp12 (98-345), purified in 500 mM NaCl and 20 mM Tris pH 7.5 at the concentration of 20 mg/ml, crystallized at 4ºC in 0.1 M NH_4OAc and 25% w/v PEG 3350 pH 7.5 crystallization buffer (Fig. 2-5D). Crystal size and morphology were significantly optimized by one round of microseeding using Ubp12 (98-345) crystals formed in the same condition. The best diffraction resolution obtained was 3.5 Å which is not adequate for detecting the amino acids side chains in the electron density map therefore structure determination was not pursued (Smyth 2000).

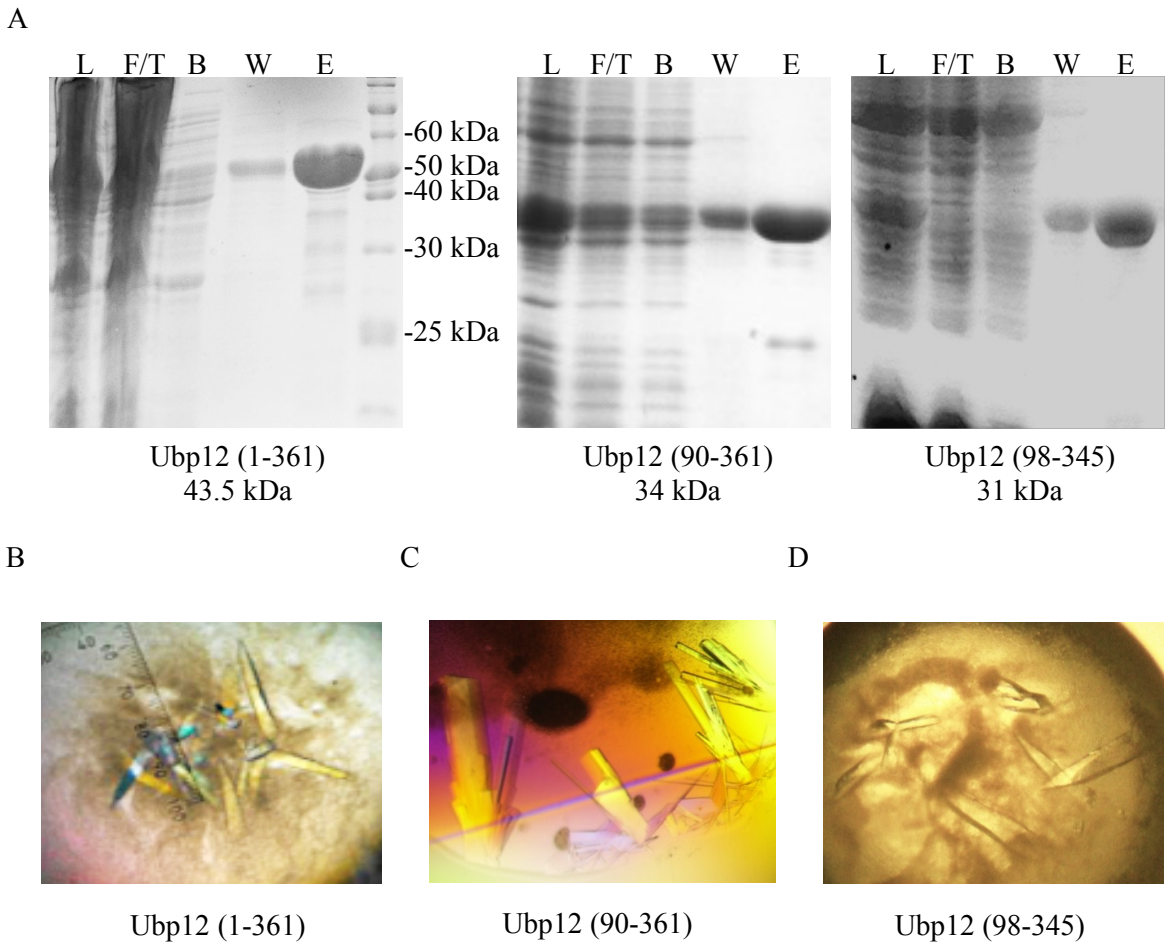

Fig. 2-5: Expression, purification and crystallization of the Ubp12 DUSP domain. A) Three constructs expressing 6xHis Ubp12 DUSP domain residues 1-361, 90-361 and 98-345 were expressed in soluble form in *E. coli* from the p15TV-L vector. Proteins were purified to homogeneity by metal affinity chromatography on a Ni-NTA resin column via 6xHis fusion tag. *L,* lysate; *F/T,* resin flow through; *B,* binding buffer flow through; *W,* wash buffer flow through; *E, elution.* B) Ubp12 (1-361) purified in 300 mM NaCl and 20 mM Hepes pH 7.5 crystallized at 4ºC at 12.5 mg/mL in 0.17 M NH_4OAc and 20% w/v PEG 3350 pH 7.5. C) Ubp12 (90-361) purified in 500 mM NaCl and 20 mM Tris pH 7.5 crystallized at room temperature at 30 mg/ml of protein concentration in 0.2 M $Mg(HCOO)_2$ and 20% w/v PEG 3350 pH 7.5. D) Ubp12 (98-345) purified in 500 mM NaCl and 20 mM Tris pH7.5 crystallized at 4ºC at 20 mg/ml in 0.1 M NH_4OAc and 25% w/v PEG 3350 pH 7.5.

Expression of *S. cerevisiae* Ubp15 N- and C-Terminal Domains:

The Ubp15-NTD residues 1-204 and C-terminal domain residues 538-1230 were expressed in soluble form from the p15TV-L vector in *E. coli* BL21 mgk cells. Proteins were purified by metal affinity chromatography on a Ni-NTA resin column via their 6xHis fusion tag (Fig. 2-6). 6xhis-tagged Ubp15-NTD despite many refinements and optimizations did not crystallize. 6xHis Ubp15-CTD purified in 500 mM NaCl and 20 mM Tris pH 7.5 formed microcrystals in 0.2 M $Mg(CH_3COO)_2$ and 20% w/v PEG 3350 (crystallized by Ira Lacdao). However, refinement of the crystallization conditions did not improve size and morphology of the protein crystals.

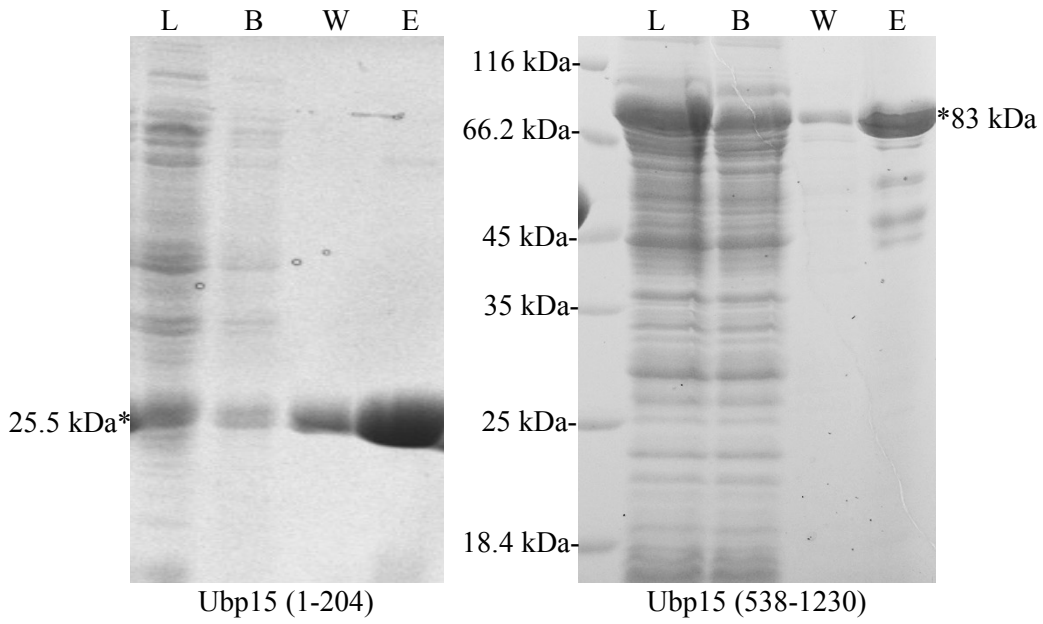

Fig. 2-6: Expression of the soluble Ubp15 N and C terminal domains in *E. coli*. 6xhis-tagged Ubp15-NTD residues 1-204 and Ubp15-CTD residues 538-1230 were expressed soluble from the p15TVL vector in BL21 mgk cells. Proteins were purified using metal affinity chromatography on a Ni-NTA resin column via 6xHis fusion tag. *L,* lysate; *B,* binding buffer flow through; *W,* wash buffer flow through; *E, elution.*

Binding Affinity of *S. cerevisiae* Ubp15-NTD for (E/P/A)XXS Motifs:

S. cerevisiae Ubp15 and its well-studied human homologue, USP7, contain a TRAF-like domain (Tumor necrosis factor receptor (TNFR) associated factors (TRAFs)) in their N-termini and five Ubl domains in their C-termini **(**Fig. 2-7A**)** (Bozza & Zhuang 2011; Sheng et al. 2006). Both USP7 and Ubp15 harbor a highly conserved DWGF motif within the binding pocket of their N-terminal TRAF-like domain. Aspartic acid and Trp residues have been found essential for USP7 substrate/protein interaction (Sheng et al. 2006). The DWGF motif in USP7-NTD is efficiently recognized by its cellular substrates and interacting proteins through their (P/A/E)XXS sequences, where X stands for any amino acid and S is essential for this interaction (Sheng et al. 2006; Saridakis et al. 2005). The N-terminal DWGF motif is conserved in all Ubp15/USP7 homologues (Fig. 2-7B).

A

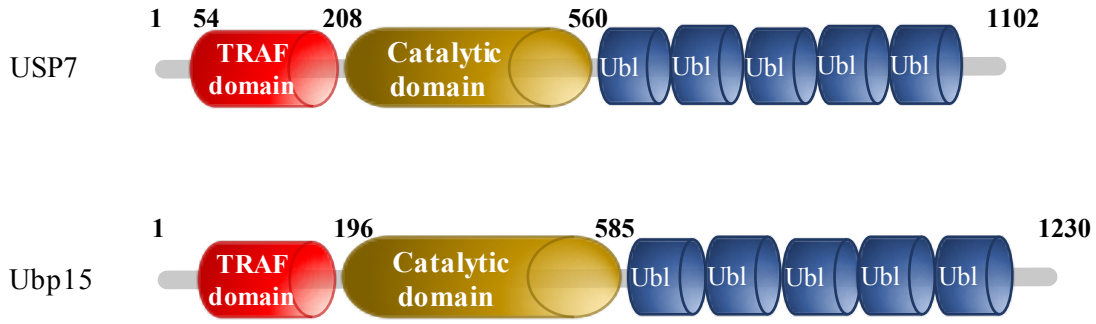

B

```
H. Sapiens      49  KSFSRRISHLFFHKENDWGFSNFMAWSEVTDPEKG----FIDDDKVTFEVFVQA-DAPHG  103
M. musculus     149 KSFSRRISHLFFHKENDWGFSNFMAWSEVTDPEKG----FIDDDKVTFEVFVQA-DAPHG  203
D. rerio        146 KSFSRRISHLFFHKENDWGFSNFMSWSDVTDPERG----FVEDDKVTFEVYVQA-DAPHG  200
G. gallus       148 KSFSRRISHLFFHKENDWGFSNFMAWSEVTDPEKG----FIEEDKVTFEVYVQA-DAPHG  202
X. laevis       150 KFFSRRISHLFFHKENDWGFSNFMAWSEVTDPEKG----FVEDDKVTFEVYVQA-DAPHG  204
A. gambiae      163 EPFIRRIRHTFCMQENDWGFSSFMNWQEILDPANG----FIENDTITLEVYVNA-EPPRG  217
A. thaliana     136 YSIRKETQHQFNARESDWGFTSFMPLSELYEPTRG----YLVNDTVLIEAEV--------  179
G. max          134 YSIRKDSQHQFNARESDWGFINFMPLAELYDPARG----YLVNDTCVVE-----------  180
C. elegans      259 PSIQKKIHHSFHNTEVDWGFSNYDQYDTLCNPKDG----YVVNDTIKLRCRFTA-DVPTG  309
S. cerevisiae   128 INLINKSHHRFNALDTDWGFANLIDLNNLKHPSKGRPLSFLNEGTLNITAYVRILKDPTG  187
                      : .   * *   : **** .      : .*  *    :: :..  .
```

Fig. 2-7: Schematic representation of human USP7 and *S. cerevisiae* Ubp15 domain structure. A) Both USP7 and Ubp15 harbor a TRAF-like domain in their N-termini and five Ubl domains in their C-termini. B) The N-terminal TRAF domain contains a DWGF motif which is highly conserved among all Ubp15/USP7 homologues. Asterisks represent conserved residues, and the period represents semi-conserved substitution. Sequence alignment employed the program ClustalW. Entries shown are from the National Center for Biotechnology Information Database (Resource 2016): USP7 sequence ID: (*H. Sapiens*, CAA96580.1); (*M. musculus*, NP_001003918.2); (*D. rerio*, XP_009297739.1); (*G. gallus*, NP_001334941.1); (*X. laevis*, NP_001121282.1); (*A. gambiae,* XP_316911.4); *(A. thaliana*, NP_001119179.1); (*G. max*, XP_006575589.1); (*C. elegans*, NP_001024012.1); (*S. cerevisiae,* ONH78017.1).

To investigate the interaction mechanism of Ubp15-NTD and its affinity for the (E/P/A)XXS motifs, we performed fluorescence polarization binding assays using FITC tagged EGPS containing vIRF1 (viral interferon regulatory factor 1, expressed by human Kaposi sarcoma herpesvirus; KSHV) and PSSS containing FOXO4 (human Forkhead box O transcription factor) peptides. Both proteins have previously shown high affinity for interaction with the human USP7 N-terminal domain (Chavoshi et al. 2016; van der Horst et al. 2006). 40 nM fixed concentration of FITC labeled vIRF1 wild-type (^{44}SPGEGPSGTG^{53}) and mutant (^{44}SPGEGP<u>A</u>GTG^{53}) peptides were titrated in increasing concentrations of Ubp15-NTD (0-795 μM). Complex formation was measured by detecting changes in the polarization values. A dissociation constant (K_d) of 757.1 ± 134 μM was obtained for wild-type vIRF1, while mutant vIRF1 peptide did not show any interaction (Fig. 2-8A). Mutation of serine to alanine of EGPS motif disrupts the binding, indicating the importance of the serine residue for this interaction. The experiment was repeated to test the interaction of PSSS containing (^{400}GGLPSSSKLA^{409}) human FOXO4 peptide with the Ubp15 N-terminal domain. A K_d of 48.2 ± 4.5 μM was obtained (Fig. 2-8B). In a similar experiment titration of 40 nM fixed concentration of FITC labeled FOXO4 peptide in increasing concentrations of USP7-NTD (0-500 μM) resulted in a K_d of 6.7 ± 0.6 μM (Fig. 2-8C). Our observations indicate that *S. cerevisiae* Ubp15-NTD has binding affinity for PSSS motif.

A

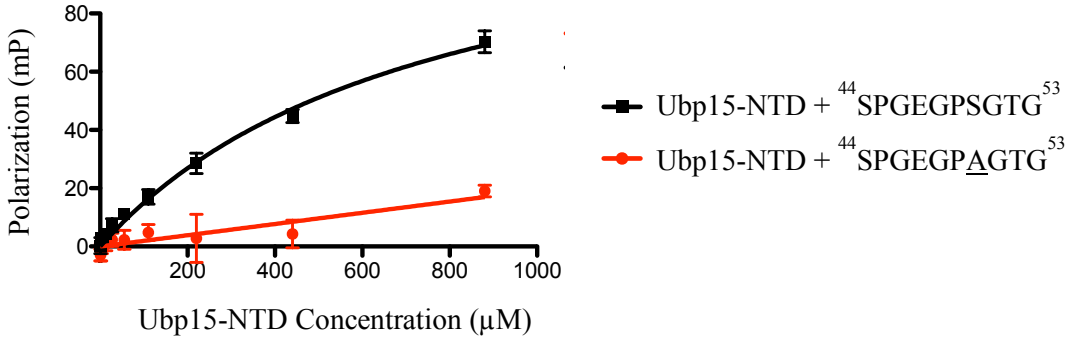

vIRF1 peptides	^{44}SPGEGPSGTG^{53}	^{44}SPGEGPAGTG^{53}
K_d (μM)	757.1	——
S.D.	134.5	——

B

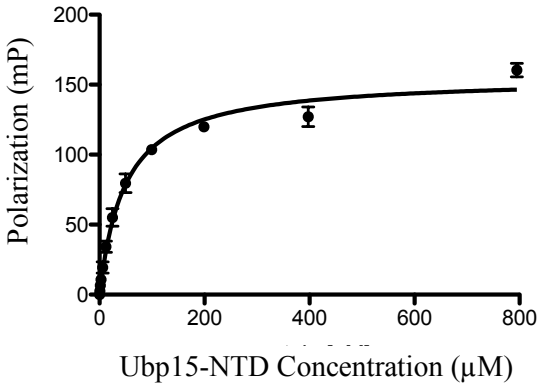

C

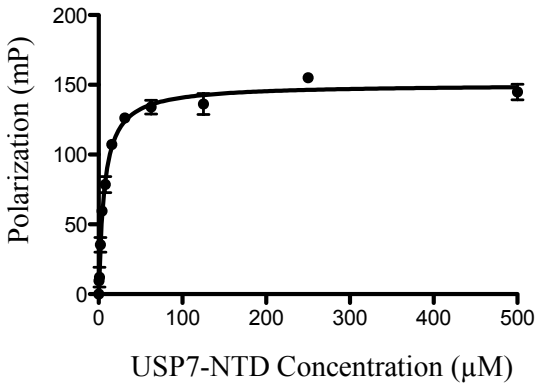

FOXO4 peptide ^{400}GGLPSSSKLA^{409}	Ubp15-NTD	USP7-NTD
K_d (μM)	48.2	6.66
S.D.	4.5	0.6

Fig. 2-8: Binding affinity of the Ubp15 N-terminal domain for (E/P/A)XXS motifs as determined by FITC fluorescence polarization assay. A) The assay was performed using FITC labeled EGPS containing vIRF1 wild-type (^{44}SPGEGPSGTG^{53} in black) or mutant (^{44}SPGEGP<u>A</u>GTG^{53} in red) peptides. The table represents dissociation constant (K_d) for Ubp15-NTD interaction with FITC labeled wild-type and mutant vIRF1 peptides. B&C) Fluorescence polarization assay was performed using FITC labeled PSSS containing FOXO4 peptide (^{400}GGLPSSSKLA^{409}) and increasing concentration of Ubp15-NTD or USP7-NTD respectively. The table represents dissociation constants (K_d) for Ubp15-NTD and USP7-NTD for interaction with FITC labeled FOXO4 peptide. *mP*, milipolarization. Error bars indicate standard error. Average values with standard deviation for three or more experiments are shown.

NMR 2D HSQC Detection of Ubp15-NTD Interaction with (E/P/A)XXS Motifs:

To investigate Ubp15-NTD interaction with (E/P/A)XXS motifs, we further monitored ^{1}H-^{15}N HSQC resonances of the uniformly ^{15}N-labeled Ubp15-NTD in the presence and absence of unlabeled protein peptides that have previously shown a strong affinity for the human USP7-NTD. 0.2 mM of the ^{15}N-labeled Ubp15-NTD was titrated with 0.4 mM of each peptide (2:1 peptide to Ubp15-NTD ratio). Fig. 2-9A represents superimposition of the ^{15}N-labeled Ubp15-NTD spectra before and after titration with the wild-type (^{44}SPGEGPSGTG^{53}) or mutant (^{44}SPGEGPAGTG^{53}) EGPS containing vIRF1 peptides. Strong disturbances were observed in the Ubp15-NTD chemical shift spectra after addition of the wild-type vIRF1 peptide. Mutation of Ser50 to alanine in the vIRF1 EGPS motif significantly reduced chemical shift disturbances of the Ubp15-NTD spectra, indicating the importance of serine residue for this interaction.

Further, the affinity of the Ubp15 N-terminal domain for AXXS motifs was analyzed. We monitored the effect of an AHSS containing HdmX peptide titration on the ^{15}N-labeled Ubp15-NTD 2D HSQC spectra (Meulmeester et al. 2005). The spectra were monitored before and after titration with the wild-type (^{394}FLDLAHSSE^{402}) or mutant (^{394}FLDLAHSAE^{402}) HdmX peptides. The Ubp15 N-terminal domain spectra showed disturbances upon titration with the HdmX peptide indicating that Ubp15 has binding affinity for AXXS motif (Fig. 2-9B) (Sarkari et al. 2010).

In addition, we tested the effect of PSTS containing peptides on the ^{15}N-labeled Ubp15-NTD spectra. 2D HSQC spectra of the Ubp15-NTD was analyzed before and after titration with wild-type (^{152}RVSPSTSYT^{160}) and mutant (^{152}RVSPSTAYT^{160}) MCMBP (minichromosome maintenance complex) and wild-type (^{395}SQPSTSS^{401}) and mutant (^{395}SQPSTAS^{401}) Hdm2 peptides (Fig. 2-9C & D). Both MCMBP and Hdm2 are substrates of USP7 and specifically interact with its N-terminal domain (Jagannathan et al. 2014; Sheng et al. 2006). Disturbances in the Ubp15-NTD chemical shift spectra indicated interaction of the Ubp15 N-terminal domain with MCMBP and Hdm2 peptides. Ser158 to alanine mutation of the PSTS motif in MCMBP peptide decreased disturbances in the Ubp15-NTD spectra, while Ser400 to alanine mutation of the PSTS motif in Hdm2 peptide did not have a strong effect. Our data suggest that Hdm2 peptide that contains two serine residues (PXXSS) still holds interaction with the Ubp15 N-terminal domain even after mutation of one of the serine residues to alanine.

A

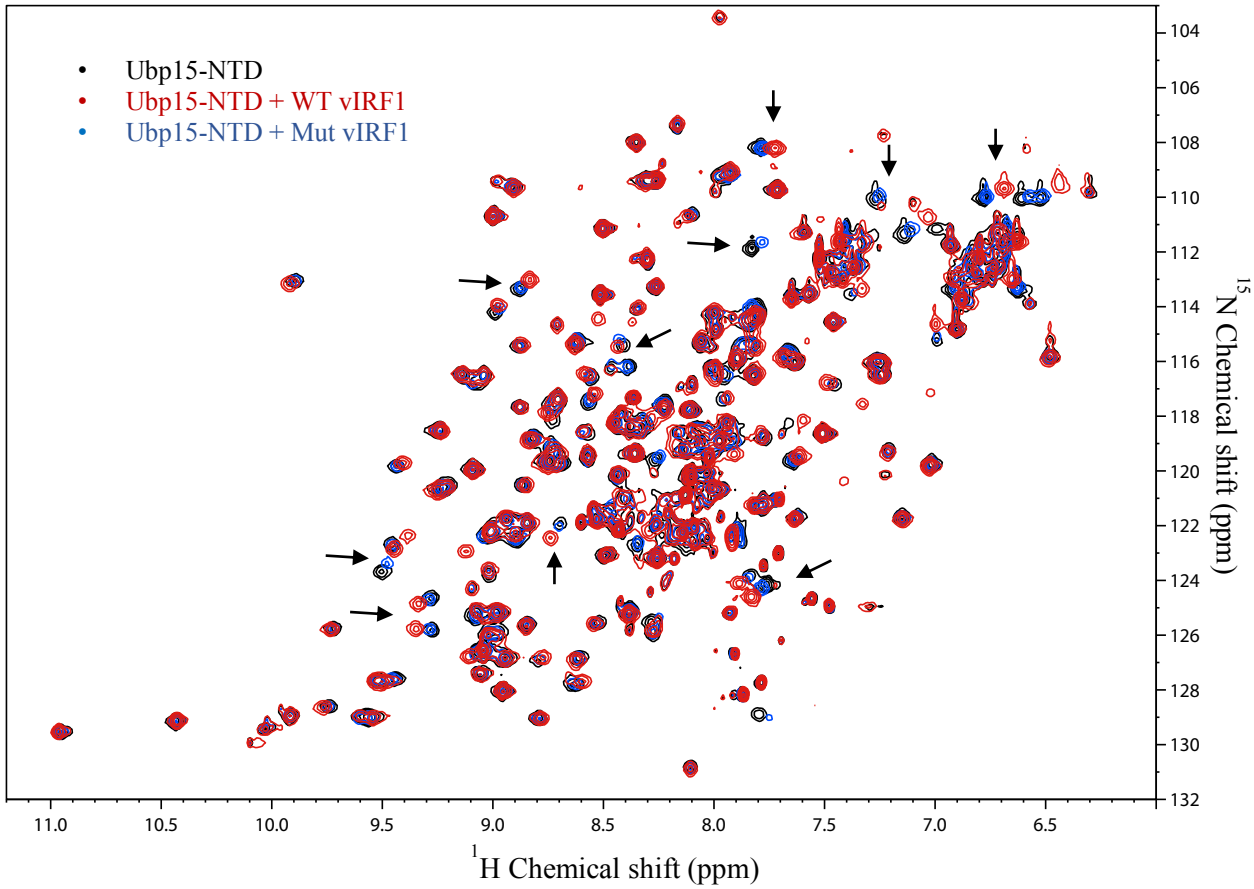
Ubp15-NTD
Ubp15-NTD + WT vIRF1
Ubp15-NTD + Mut vIRF1
11.0
10.5
10.0
9.5
9.0
8.5
8.0
7.5
7.0
6.5
1H Chemical shift (ppm)
104
106
108
110
112
114
116
118
120
122
124
126
128
130
132
15N Chemical shift (ppm)

B

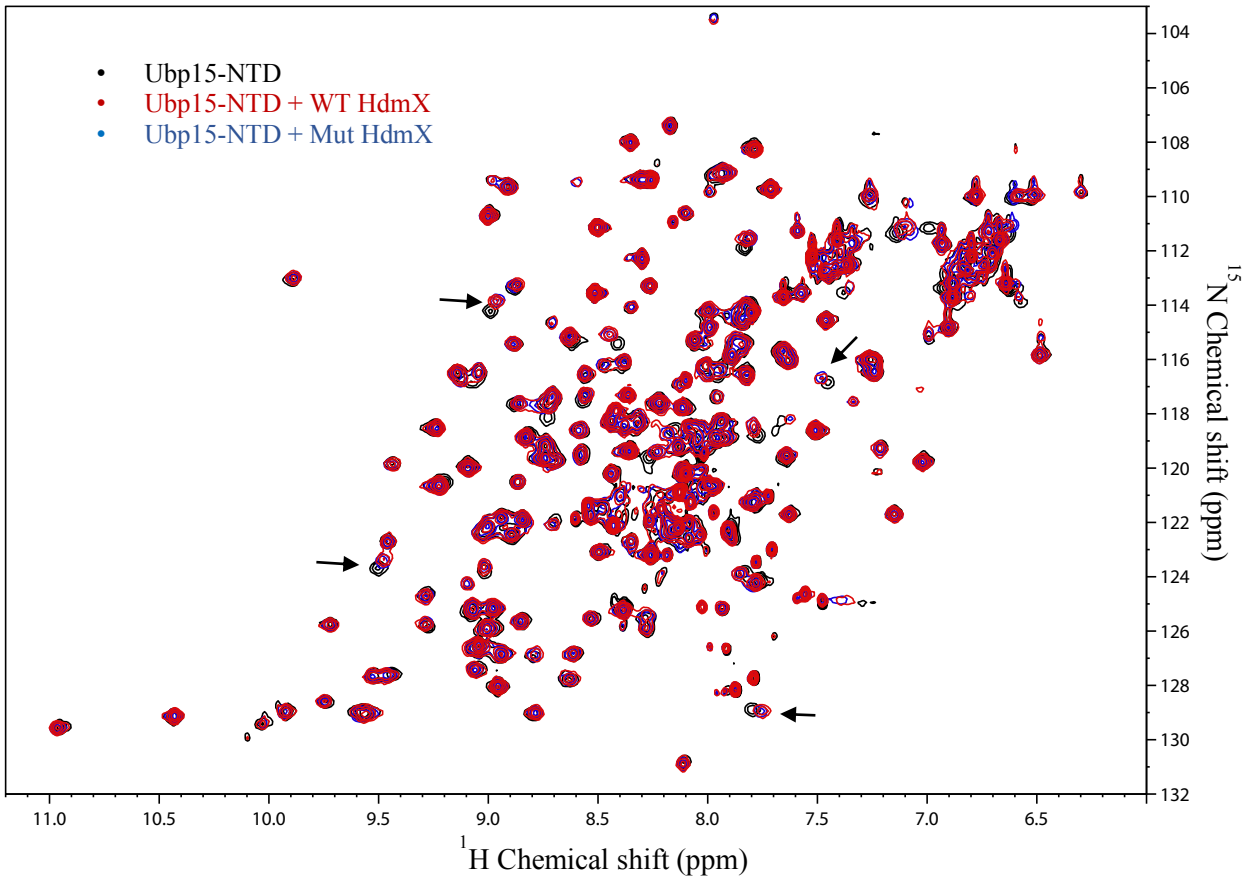
Ubp15-NTD
Ubp15-NTD + WT HdmX
Ubp15-NTD + Mut HdmX
11.0
10.5
10.0
9.5
9.0
8.5
8.0
7.5
7.0
6.5
1H Chemical shift (ppm)
104
106
108
110
112
114
116
118
120
122
124
126
128
130
132
15N Chemical shift (ppm)

C

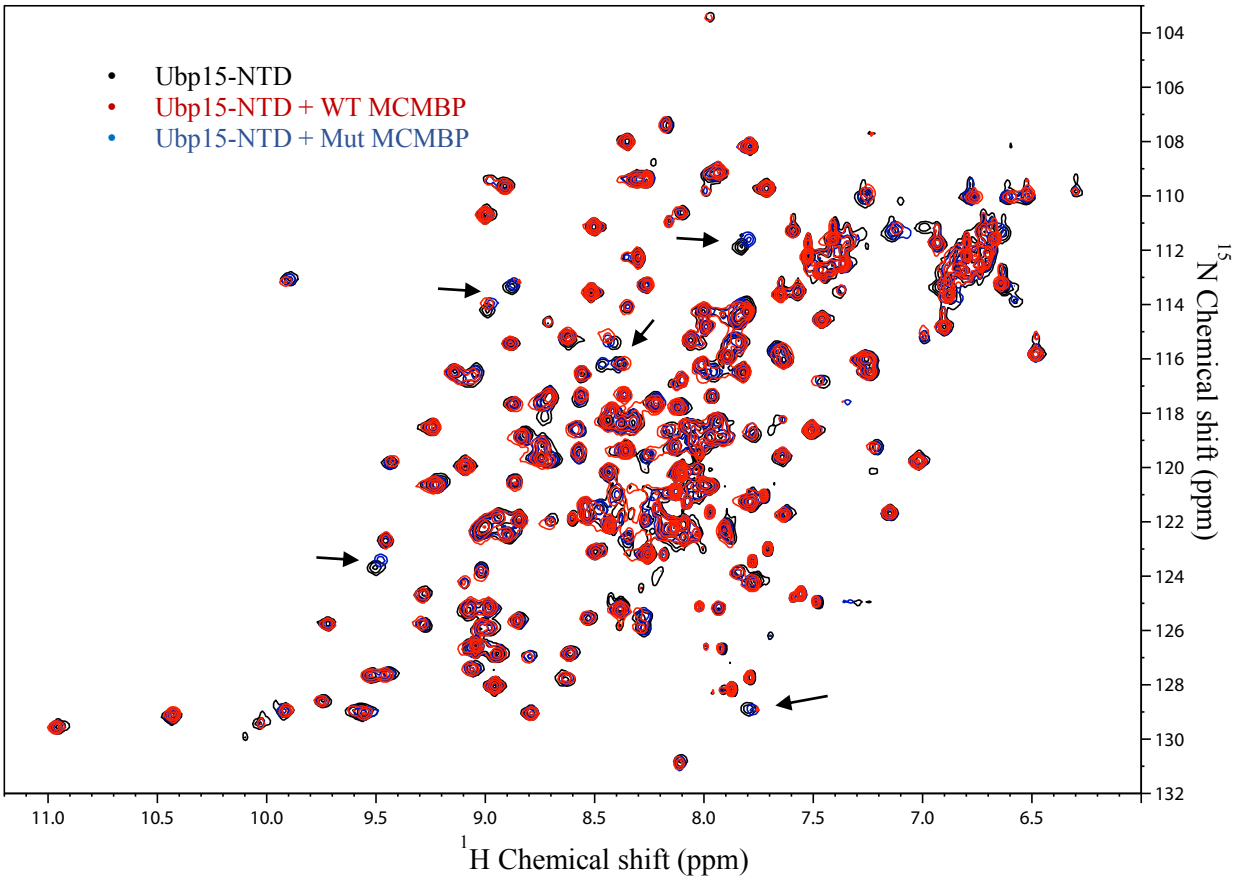
Ubp15-NTD
Ubp15-NTD + WT MCMBP
Ubp15-NTD + Mut MCMBP
104
106
108
110
112
114
116
118
120
122
124
126
128
130
132
15N Chemical shift (ppm)
11.0
10.5
10.0
9.5
9.0
8.5
8.0
7.5
7.0
6.5
1H Chemical shift (ppm)

D

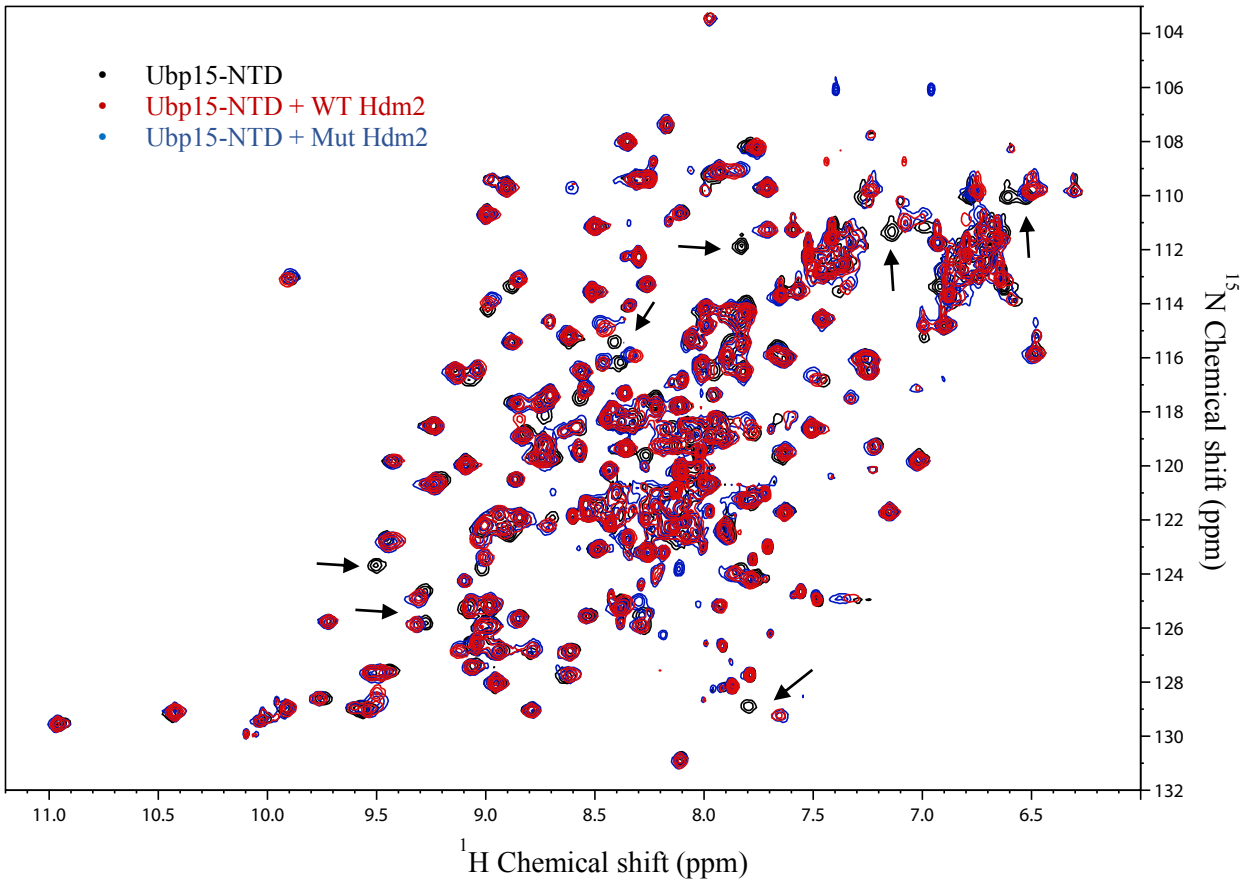

Fig. 2-9: Superimposed ^{15}N HSQC spectra of Ubp15-NTD before and after titration with (E/P/A)XXS containing peptides. For all NMR titration experiments the ^{15}N-labeled Ubp15-NTD was titrated with 2:1 molar ratio of wild-type (WT) or mutant (Mut) peptides. A): ^{15}N-labeled Ubp15-NTD spectra (in black) was titrated with EGPS containing wild-type (^{44}SPGEGPSGTG^{53} in red) or mutant (^{44}SPGEGPAGTG^{53} in blue) vIRF1 peptides. B): ^{15}N-labeled Ubp15-NTD spectra (in black) was titrated with AHSS containing HdmX wild-type (^{394}FLDLAHSSE^{402} in red) or mutant (^{394}FLDLAHSAE^{402} in blue) peptides. C) ^{15}N-labeled Ubp15-NTD spectra (in black) was titrated with PSTS motif containing MCMBP wild-type (^{152}RVSPSTSYT^{160} in red) or mutant (^{152}RVSPSTAYT^{160} in blue) peptides. D) ^{15}N-labeled Ubp15-NTD spectra (in black) was titrated with PSTS motif containing Hdm2 wild-type (^{395}SQPSTSS^{401} in red) or mutant (^{395}SQPSTAS^{401} in blue) peptides. Arrows indicate residues that were largely affected by the peptide interaction.

Discussion:

Conservation of the cellular pathways and genetic material from yeast to human has allowed a better understanding of the molecular mechanisms of different human diseases through research on yeast (Tencer et al. 2016; Botstein & Fink 2011). In most cases, human orthologues of yeast proteins have shown conservation in amino acid sequence, structure and function and can complement yeast deletion mutants (Mohammadi et al. 2015; Heinicke et al. 2007). The involvement of ubiquitin-specific proteases (USPs; Ubps in yeast) in various cellular pathways and processes, which are implicated in development and diseases such as cancer, have made them an important subject of investigation (D'Arcy et al. 2015; Kowalski & Juo 2012).

In this chapter, we have examined the expression of soluble *S. cerevisiae* Ubp enzymes in *E. coli* for protein crystallography. Generation of soluble and high purity proteins is essential for structural studies as well as biochemical characterization and industrial protein and enzyme expression (Luna-Vargas et al. 2011). Despite many advantages in using *E. coli* as an expression host for eukaryotic proteins, we had to face many setbacks. Lack of protein chaperones and post-translational modifications in *E. coli* contributes to incorrect protein folding and the formation of protein aggregates and inclusion bodies (Rosano & Ceccarelli 2014). In fact, it is reported that only about 10% of recombinant eukaryotic proteins expressed in *E. coli* are soluble and functional (Finley et al. 2004). There are many recommendations for optimal approaches to construct design, expression and purification of recombinant proteins in *E. coli,* however, since every protein has different characteristics, the success rate of such approaches should be tested experimentally. In our efforts to express *S. cerevisiae* Ubps or their domains in *E. coli,* 127 constructs for 16 Ubps and Sad1 and Pan2 (catalytically inactive Ubps) were designed and cloned in the p15TV-L vector. BL21 (DE3) mgk *E. coli* was used as the first choice of expression vehicle since it enhances the expression level by encoding for arginine (AGG and AGA) and Ile (ATA) tRNA codons that are rare in *E. coli* but common in eukaryotes (Rosano & Ceccarelli 2014). Further, we carried out the expression at 16ºC overnight as opposed to 37ºC. Expression at low temperature optimizes protein folding and decreases the rate of protein synthesis which helps reduce protein aggregation (Vera et al. 2007; Schellman 1997). Also, to improve yield or solubility of the recombinant proteins, we tried their co-expression with *E. coli* Tig chaperone (Martinez-Hackert & Hendrickson 2009). Extensive optimization of the constructs design and expression conditions, led to the successful expression of 10 soluble proteins including Ubp1 (aa 92-741), Ubp3 (aa 1-912 and 189-912), Ubp3 catalytic domain (aa

449-912), Ubp6 (aa 1-499), Ubp12 N-terminal domain (aa 1-361, 90-361 and 98-345) and Ubp15 N-terminal and C-terminal domains (aa 1-204 and 538-1230). *S. cerevisiae* Ubp1, Ubp6 and the Ubp12 N-terminal domain were successfully crystallized. Ubp6 protein crystal was used to determine the three-dimensional structure of its catalytic domain.

Despite the availability of bioinformatics techniques that aim to predict the secondary structures of proteins, it is not possible to predict which specific N and C-terminal boundaries have a higher potential for soluble protein expression. Therefore, the creation of multiple constructs of varying N or C-termini can increase the chance of generating a soluble recombinant protein (Graslund et al. 2008). For instance, after preparation of thirteen constructs for the Ubp3 catalytic domain, we were able to achieve soluble expression for one construct (residues 449-912) (Table 2-1). In case of Ubp12 DUSP domain, out of six constructs, three expressed in soluble form in *E. coli* which were all successfully crystallized (Fig. 2-5). Further, even though the N-terminal fusion tags have higher success rate for optimal protein expression, soluble expression of the full-length Ubp3 (residues 1-912) and Ubp3 residues 189-912 was only achieved from the pET-28b vector, which adds a 6xHis fusion tag to the C-terminus of the expressed protein (Fig. 2-2) (Anon 2008; Dyson et al. 2004). Recombinant Ubp1 construct (residues 92-741), which was designed to bypass a previously reported N-terminal transmembrane region, expressed in soluble form when co-expressed with *E. coli* Tig chaperone (Fig. 2-1A). Previously reported soluble expression of Ubp1 was achieved after extensive codon optimization of arginine and leucine residues and a point mutation of Glu754 to leucine (Wojtowicz et al. 2005). Here we showed that through co-expression with Tig chaperone it is possible to achieve efficient soluble expression of the yeast Ubp1 in *E. coli* without the need for codon optimization. Ubp1 (residues 92-741) successfully crystallized however, despite repeated optimization attempts, crystals diffracted very poorly. Crystal size, morphology and X-ray diffraction resolution of the Ubp12 DUSP domain, Ubp1 and Ubp6 proteins were significantly optimized by addition of organic or inorganic additives to the crystallization conditions and use of microseeding techniques. However, a diffraction resolution adequate for detecting the amino acids side chains in the electron density map was only achieved for the Ubp6 catalytic domain. This outcome indicates the benefit of microseeding and use of additive compounds in optimizing protein crystals, while at the same time reveals their limited potential.

Full-length Ubp6 successfully crystallized and diffracted at 2.5 Å resolution (Fig. 2-3). Even though the full-length protein was crystallized, the resulting electron density map only contained

information for the catalytic domain, suggesting that the Ubl domain is mobile and does not produce interpretable electron density. The model of Ubp6 was composed of residues 103-499 which was superimposable with the Ubp6 structure that was previously deposited in the protein data bank (accession code 1VJV). The Ubp6 catalytic domain revealed an extended right-hand architecture, which produces a binding pocket with the catalytic residues in the palm subdomain (Fig. 2-4). This binding pocket is suggested to fit the 8 kDa ubiquitin molecule between the fingers and the palm-thumb frameworks (Hu et al. 2002). Our structure indicated that the three catalytic residues are in an active conformation since the His447 is within hydrogen bond (3.1 Å) distance from the Cys118 thiol side chain and the Asn465 accepts a hydrogen bond from the His447 and stabilize it (Fig. 2-4E). Superimposition of human USP14 and yeast Ubp6 structures revealed that they are very similar and that the two blocking loops (BL1 and BL2) are also conserved in yeast and take similar positions (Fig. 2-4D). Even though catalytic triad of USP14/Ubp6 are aligned productively, the catalytic domain has a low binding affinity for Ub-substrate, possibly because BL1 and BL2 block Ub carboxyl terminal access to the active site's binding groove and decrease enzymatic activity (Hu et al. 2005). Previously it was shown that interaction of the Ubl domain of Ubp6 with the proteasome's 19S RP increases Ub-substrate hydrolysis activity by 300 folds (Leggett et al. 2002). Further, reconstruction of the Ubp6-proteasome complex using electron microscopy indicated that upon binding of the Ubp6 Ubl domain with Rpn1 subunit, Ubp6 surface loops make contact with the N-terminal domain of Rpt1, an ATPase subunit of the 19S RP (Bashore et al. 2016). This observation suggests that interaction of the Ubp6 Ubl domain with the 19S RP leads to BL1 and BL2 conformational change and makes active site residues accessible to the ubiquitin C-terminus. Superimposition of USP14 and Ubp6 also revealed that compared to USP14 α-helix 8, Ubp6 contains two extended α-helices 11 and 12 in the palm subdomain (Fig. 2-4D). The reconstructed model of Ubp6 bound to the 26S proteasome showed that interaction of the Ubl domain with Rpn1 subunit allows the two C-terminal helices of Ubp6 to contact the AAA+ domain of Rpt1 (Bashore et al. 2016). This suggests a function for the extended α-helices 11 and 12 in stabilizing and docking Ubp6 catalytic domain in the 19S RP.

Further, we were able to express Ubp15 N-terminal and C-terminal domains in soluble form in *E. coli* (Fig. 2-7). To gain insight into the Ubp15-NTD mode of protein interaction, we analyzed binding affinity of Ubp15-NTD for the (E/P/A)XXS motifs that have previously shown interaction with human USP7. Initially, using fluorescence polarization binding assay, we measured the affinity of the Ubp15 N-terminal domain for EGPS containing vIRF1 (of KSHV)

peptide. FITC labeled wild-type vIRF1 peptide (^{44}SPGEGPSGTG^{53}) revealed a K_d of 757.1 μM, while Ser50 to alanine mutant vIRF1 peptide did not show any interaction. Further, our ^{1}H-^{15}N HSQC 2D NMR titration of Ubp15-NTD with wild-type vIRF1 peptide revealed disturbances in Ubp15-NTD chemical shift spectra which decreased upon titration with the mutant vIRF1 peptide. This observation suggests that EGPS motif has a low binding affinity for Ubp15-NTD compared to that of USP7-NTD, which showed a K_d of 2 μM for interaction with vIRF1 peptide (Chavoshi et al. 2016). Also, mutation of serine to alanine of the EGPS motif disrupted this interaction, suggesting a similar mode of protein binding for Ubp15-NTD as compared to the USP7 N-terminal domain where serine residue is found essential for (E/P/A)XXS motifs interaction with USP7-NTD (Sarkari et al. 2010). Despite the high K_d of 757.1 μM, EGPS containing vIRF1peptide still led to strong disturbances of the Ubp15-NTD chemical shift spectra upon titration. It is important to note that for the FITC assay, a peptide concentration of 40 nM was used while for NMR titration, the peptide concentration was 200 nM. The higher concentration of vIRF1 peptide can be attributed to the strong disturbances observe in the Ubp15-NTD spectra. Further, observed data from NMR titration assays only confirm the binding affinity of the motifs for Ubp15-NTD and do not provide any quantitative information on the strength of these interactions.

We also measured the affinity of the Ubp15-NTD for PSSS containing FOXO4 peptide (^{400}GGLPSSSKLA^{409}) using FITC assay. Our data revealed a much stronger K_d of 48.2 μM, compared to that of EGPS motif, for interaction with the Ubp15 N-terminal domain. FITC analysis of human USP7-NTD interaction with FOXO4 peptide resulted in a K_d of 6.7 μM. These observations indicate that Ubp15 has binding affinity for PSSS sequence. It is interesting to note that Cdh1, *S. cerevisiae* protein that has shown strong binding with Ubp15-NTD, contains a PSSS motif at its N-terminus (residues 13-16), which is conserved among yeast (Bozza & Zhuang 2011).

Further, using NMR titration assays Ubp15-NTD interactions were monitored with peptides from human HdmX, Hdm2 and MCMBP proteins that have previously shown a strong affinity for the USP7 N-terminal domain (Jagannathan et al. 2014; Sheng et al. 2006; Meulmeester et al. 2005). Titration of the Ubp15 N-terminal domain with AHSS containing HdmX peptides led to disturbances of Ubp15-NTD spectra suggesting that Ubp15 interacts with AXXS sequences. Previously, Ecm30 was shown to interact with Ubp15 (Costanzo et al. 2010). Unpublished spot array analysis experiments from our lab indicated that AXXS motifs of Ecm30 including

(^{665}SYNAAMSLLY^{674}), (^{951}KLSALRSDIL^{960}) and (^{646}KKSASPSAAT^{655}) are involved in this interaction (Mandawe 2010, unpublished data). Furthermore, NMR ^{1}H–^{15}N HSQC resonances of ^{15}N-labeled Ubp15-NTD was monitored after titration with PSTS containing wild-type and mutant MCMBP and Hdm2 peptides. Addition of both peptides led to disturbances in the Ubp15-NTD spectra, indicating their interaction with the Ubp15 N-terminal domain. However, although mutation of serine to alanine in MCMBP peptide decreased the disturbances in the Ubp15-NTD spectra, mutant Hdm2 peptide still showed the same binding affinity as the wild-type Hdm2 peptide. The Hdm2 peptide contains two serine residues (PXXSS) which might hold interaction with the Ubp15 N-terminal domain even after mutation of one of the serine residues to alanine. In fact, intrinsic fluorescence assay had shown that PSTSSS containing Hdm2 peptide (^{394}YSQPSTSSSI^{476}) has the strongest affinity for the USP7 N-terminal domain as compared to other Hdm2 binding sites (Sarkari et al. 2010). Further, mutation of Hdm2 PSTSSS motif to PSTASS decreased its binding with the USP7 N-terminal domain but did not abolish the interaction (Sarkari et al. 2010). This observation suggests that PSTSS motif has a similar mode of interaction with the Ubp15 N-terminal domain as compared to that of the USP7 N-terminal domain.

In summary, we have examined the expression of 127 *Saccharomyces cerevisiae* constructs encompassing full-length or domains of Ubp enzymes in BL21 mgk *E. coli* cells. Despite optimizations of the constructs design and protein expression and purification conditions, only 10 constructs expressed in soluble form. Soluble proteins were purified to homogeneity and used in protein crystallization trials. Three proteins crystallized including Ubp1, Ubp6 and the Ubp12 N-terminal domain. Ubp6 crystals led to a three-dimensional structure determination of its catalytic domain. Further, to analyze the yeast Ubp15 N-terminal domain protein interaction mechanism, using FITC assay and NMR titration, we showed that Ubp15 similar to its human homologue, USP7, interacts with AXXS and PXXS motifs.

Chapter 3: Identification of Kaposi Sarcoma Herpesvirus (KSHV) vIRF1 Protein as a Novel Interaction Partner of Human Deubiquitinase USP7

This chapter has been reprinted or adapted from:

Chavoshi, S., Egorova, O., Lacdao, I.K., Farhadi, S., Sheng, Y., and Saridakis, V. 2016. Identification of KSHV vIRF1 as a novel interaction partner of human deubiquitinase USP7. *Journal of Biological Chemistry*. 291: 6281-6291

In Fig. 3-3, Fig. 3-4 and Fig. 3-5 Dr. Saridakis supervised the experiment and I performed the procedures, analyzed the data and produced the figures. In Fig. 3-6 (NMR titration of USP7-NTD with WT or mutant vIRF1 peptides) Dr. Saridakis and Dr. Sheng supervised the experiment. The procedure was done with the help of Sahar Farhadi and I analyzed the data and produced the figures. In Fig. 3-7 (Crystal structure of the UPS7-NTD:vIRF1 peptide complex) Dr. Sadridakis supervised the experiment, collected and refined the crystal diffraction data and prepared Table 3-1. I set up crystallization screening trials and produced the final figures. In Fig. 3-8 and Fig. 3-9 Dr. Saridakis supervised the experiments and Olga Egorova performed the initial tests and produced Fig. 3-8C. I set up and performed the experiments and produced the rest of the figures. Fig. 3-10, schematic representation, was prepared by Ira Lacdao.

Introduction:

Human Herpesviruses:

Human herpes viruses (HHV) are double-stranded DNA viruses, classified into α, β or γ subfamilies (Edelman 2005). To establish latency HHVs have to suppress host immune response and evade the immune system (Wen & Damania 2010). In the latent state, herpes viruses are dormant and remain in the nucleus by integrating their genome into the host chromosome and express only a small number of proteins essential for suppressing the host immune system (Wen & Damania 2010). HHVs have evolved various mechanisms for host immune evasion including inhibition of cellular senescence and apoptosis as well as promoting cell proliferation (Alibek et al. 2014). Another strategy to evade host immune surveillance is through expression of viral homologues of genes that are the host's first line of defense against viral infection, such as interferons and interferon regulatory factors (IRFs), and therefore sabotage the function and regulation of these cellular proteins (Jacobs & Damania 2011). Such deregulation of proteins involved in growth control has led to the recognition of some HHVs as underlying agents of human cancer (Alibek et al. 2014; Chang et al. 1994).

Karposi's Sarcoma Herpesvirus:

Karposi's sarcoma herpesvirus (KSHV), HHV-8, is the causative agent of Kaposi's sarcoma, primary effusion lymphoma and multicentric Castleman's disease which are especially prevalent in immunocompromised patients (Jacobs & Damania 2011; Angeletti et al. 2008). KSHV vIRF1 (viral interferon regulatory factor 1) protein is encoded by ORF K9 and is believed to have been acquired through molecular piracy (Moore & Chang 1998). vIRF1 contains two domains, an N-terminal DNA binding domain and a C-terminal IRF interaction domain (Fig. 3-1) (Hew et al. 2013). vIRF1 DNA binding domain has approximately 40% sequence similarity to the DBDs of human IRF3 and IRF7 and contains a helix-turn-helix motif which is common in IRFs and DNA binding proteins (Hew et al. 2013). vIRF1 mediated deregulation of IRF3 and IRF7 leads to disruption of cellular antiviral activity.

Fig. 3-1: Domain arrangement of KSHV vIRF1 protein. vIRF1 contains a DNA binding domain (DBD) and an interferon association domain (IAD).

vIRF1 is a potent inhibitor of the histone acetyltransferase activity of p300. It leads to hypoacetylation of histones and alteration of the chromatin structure, thereby reducing expression of IFNs (Li et al. 2000). vIRF1 also directly interacts with p53 and inhibits its acetylation by p300 (Nakamura et al. 2001). Furthermore, vIRF1 has shown an inhibitory effect on Ataxia Telangiectasia-Mutated (ATM) kinase (Shin et al. 2006). ATM activation leads to phosphorylation of Ser15 and Ser20 on p53 which are close to Hdm2 binding pocket. In addition, activated ATM phosphorylates Hdm2 on Ser395, which inhibits Hdm2 mediated nuclear export of p53 into the cytoplasm, where it is degraded. ATM function results in reduced Hdm2 affinity for p53, leading to p53 stabilization (Shin et al. 2006; Chehab et al. 1999). Also, phosphorylation of Ser15 is a signal for p300 acetylation of p53, which is important for its stability and activation (Lambert et al. 1998). Inhibition of ATM activity by vIRF1 increases ubiquitination and degradation of p53 by Hdm2 (Shin et al. 2006).

Human USP7:

Human Ubiquitin Specific Protease 7 (USP7) also known as Herpes Associated Ubiquitin Specific Protease (HAUSP) is a well characterized deubiquitinating enzyme (DUB) originally identified as an interacting protein with HSV-1 immediate early protein, ICP0 (Everett et al. 1997). USP7 harbors a TRAF-like domain in its N-terminus (USP7-NTD), a central catalytic domain and five Ubl folds in its C-terminus (Fig. 3-2) (Faesen et al. 2011; Sheng et al. 2006; Saridakis et al. 2005; Hu et al. 2002). The USP7-NTD recognizes and binds interacting proteins containing a (E/P/A)XXS motif (Sheng et al. 2006). All USP7 homologues harbor the highly conserved DWGF motif in their N-terminal domain, where the aspartic acid and Trp residues have been shown essential for protein interaction (Sarkari et al. 2010; Sheng et al. 2006).

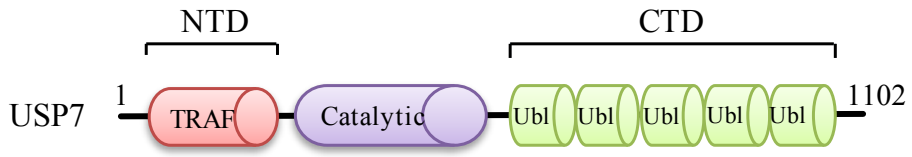

Fig. 3-2: Domain arrangement of human USP7. USP7 contains an N-terminal substrate binding TRAF domain, a catalytic domain and a C-terminal domain that is comprised of five ubiquitin-like (Ubl) sub-domains.

USP7 is involved in maintaining cellular levels of the p53 tumor suppressor protein which is essential for normal cellular stress response (Li et al. 2002). p53 and its negative regulator, the E3 ligase, Hdm2, interact with the ^{164}DWGF^{167} motif of USP7-NTD through their (P/A)XXS motifs, which leads to their deubiquitination and stabilization (Hu et al. 2006; Sheng et al. 2006). Since Hdm2 has a higher affinity for USP7 than p53, reduction in cellular levels of USP7 leads to instability of p53 while its removal results in destabilization of Hdm2, which in turn stabilizes p53 (Meulmeester et al. 2005; Cummins et al. 2004). USP7 also regulates the stability of Hdmx, a homolog of Hdm2. USP7 is an essential component of the p53-Hdm2-Hdmx pathway that maintains balance in the cellular levels of these proteins (Shadfan et al. 2012).

HHVs Interaction with USP7:

Members of the herpesviruses family such as Epstein-Barr virus (EBV), Kaposi's sarcoma associated herpesvirus (KSHV) and Herpes Simplex Virus type 1 (HSV-1) have evolved to interfere with the USP7-p53 pathway by competitively binding to USP7 and hindering its interaction with cellular substrates (Lee et al. 2009; Saridakis et al. 2005; Everett et al. 1997). ICP0 protein expressed by HSV-1 is an E3 ubiquitin ligase that ubiquitinates and destabilizes host proteins. Its interaction with USP7 leads to its rescue from self-ubiquitination and proteasomal degradation (Boutell et al. 2005). Epstein-Barr nuclear antigen 1 (EBNA1) expressed by EBV; viral interferon regulatory factor 4 (vIRF4), latency-associated nuclear antigen 1 (LANA) and ORF45 expressed by KSHV bind USP7-NTD at the same region as p53, Hdm2 and Hdmx (Gillen et al. 2015; Jager et al. 2012; Lee et al. 2011; Sarkari et al. 2010; Lee et al. 2009; Saridakis et al. 2005). They block USP7 substrate interaction and cripple the cell's interferon and innate immune response and p53 mediated apoptosis (Lee et al. 2009; Saridakis et al. 2005).

vIRF4 residues spanning Ser202-Met216 contain the well-conserved ASTS sequence which forms an extended interaction with the USP7 N-terminal domain resulting in a dissociation constant (K_d) significantly lower than those obtained for USP7 cellular substrates, such as p53 and Hdm2 (Lee et al. 2011). Furthermore, vIRF4 directly interacts with Hdm2 and inhibits its auto-ubiquitination which leads to Hdm2 survival and p53 instability (Lee et al. 2011). Likewise, LANA interacts with USP7-NTD through its ^{977}PGPS^{980} motif (Jager et al. 2012).

EBNA1 protein is involved in the initiation of DNA replication and transcriptional activation of EBV latent proteins (Pattle & Farrell 2006). Interaction of EBNA1 with the USP7 N-terminal DWGF motif occurs through EBNA1's EGPS sequence, which does not match the previously reported (P/A)XXS motif or other known sequences required for binding to TRAF domains (Saridakis et al. 2005). A newly identified KSHV protein, ORF45, also interacts with USP7-NTD through an EGPS motif (Gillen et al. 2015).

Project Rationale:

We identified a ^{45}PGEGPS^{50} consensus sequence in vIRF1 that is identical to the motif reported in EBNA1 and ORF45 (of KSHV) responsible for mediating their interaction with USP7-NTD (Gillen et al. 2015; Saridakis et al. 2005). It is already well established that HHVs target members of the USP7-p53-Hdm2 pathway. Multiple proteins expressed by KSHV, such as vIRF4, LANA and ORF45, have shown high-affinity binding with USP7, p53, Hdm2 and other proteins involved in regulation of p53 activity, such as ATM kinase and p300. vIRF1, expressed by KSHV, was previously reported to interact with p53 directly and inhibit its transactivity by blocking p300 acetylation of p53. This led us to investigate whether vIRF1 interacts with USP7. We characterized the interaction between USP7-NTD and KSHV vIRF1 using GST pull-down and fluorescence polarization assays, and further mapped the binding interface by 2D NMR HSQC. We also determined the crystal structure of a vIRF1 peptide with USP7-NTD. We confirmed that these two proteins interact *in vivo* and determined that expression of wild-type vIRF1 but not deletion mutant vIRF1 decreased cellular levels of p53 but not Hdm2 or ATM.

Material and Methods:

Protein Expression:

N-terminal 6xHis tagged wild-type (WT) and D164A/W165A mutant USP7-NTD were expressed from the pET15b vector as described previously (Sheng et al. 2006). His-tagged USP7-CTD was expressed from p15TV-L vector. Full-length His-USP7 in pFastBac was expressed in *Spodoptera frugiperda* (Sf9) cells as described previously (Pfoh et al. 2015). Full-length vIRF1 was synthesized by GenScript (NJ, USA). ΔvIRF1 (deletion of residues ^{45}PGEGPS^{50}) was made by ACGT Corporation (Toronto, Canada). The N-terminal GST fusion constructs were generated by PCR amplification corresponding to residues 1-90 of WT or ΔvIRF1 and inserted between the BamHI and NdeI sites of the pGEX2-TK vector.

Protein Purification:

For NMR titrations, uniformly labeled ^{15}N 6xHis N-terminal tagged USP7-NTD was expressed in M9 media enriched with 0.7 g/L $^{15}NH_4Cl$ as the sole nitrogen source. All constructs were expressed in *E. coli* BL21 mgk cells in TB (Terrific broth, Bioshop) (except ^{15}N His-USP7 which was expressed in M9 media) with overnight 0.4 mM Isopropyl β-D-1-thiogalactopyranoside induction at 16°C. The cells were harvested, resuspended in 50 mM Tris pH7.5, 500 or 150 mM NaCl, 5 mM Imidazole, 1x protease inhibitor cocktail (1mM Benzamidine and 0.5 mM PMSF) and 1x protease inhibitor tablet (Roche cOmplete ULTRA Tablets) and lysed using sonication. The lysate was cleared and allowed to interact with nickel-NTA beads (Qiagen) for 1 hour. Beads were washed extensively with 50 mM Tris pH 7.5, 500 or 150 mM NaCl and 20 mM imidazole. Proteins were eluted with the addition of 50 mM Tris pH7.5, 500 or 150 mM NaCl and 250 mM imidazole.

Peptide Synthesis:

Wild-type (^{44}SPGEGPSGTG^{53}) and mutant (^{44}SPGEGPAGTG^{53}) vIRF1 peptides were synthesized by CanPeptide Inc. (Montreal, Canada) with both N-terminal acetylation and C-terminal amidation to mimic the native peptides. FITC labeled WT (FITC-Acp-SPGEGPSGTG-NH_2) and mutant (FITC-Acp-SPGEGPAGTG-NH_2) vIRF1 peptides were also synthesized by CanPeptide Inc. (Montreal, Canada).

Fluorescence Polarization Binding Assay:

Both wild-type and mutant USP7-NTD were further purified by size-exclusion chromatography using a HiLoad 16/60 Superdex 200 (GE Healthcare) on an ÄKTApurifier 10 UPC system (GE Healthcare) in 150 mM NaCl and 50 mM Tris pH 8.0. FITC labeled WT (FITC-Acp-SPGEGPSGTG-NH_2) and mutant (FITC-Acp-SPGEGPAGTG-NH_2) vIRF1 peptides were initially dissolved in dimethyl sulfoxide to a final concentration of 10 mM. A 400 nM working stock of each peptide was prepared in assay buffer (50 mM Tris pH 8.0, 150 mM NaCl and 0.01% Triton X-100). 500 µM of each protein was serially diluted and incubated with 40 nM of each peptide. 10µl of the above mixtures were transferred into a 384 well plate (Corning) and fluorescence polarization was measured on a Synergy H4 microplate reader (BioTek, USA) with λ_{ex}=485nm and λ_{em}=520nm. Polarization values were analyzed by Graphpad Prism 5.0 using a one-site binding model to obtain the equilibrium dissociation constant (K_d). Data were calculated based on four individual experiments and the standard deviation was calculated.

NMR Spectroscopy:

NMR spectra were acquired at 25˚C on a Bruker 700 MHz NMR spectrometer equipped with a triple resonance cryo probe. Interaction of USP7-NTD with WT (^{44}SPGEGPSGTG^{53}) and mutant (^{44}SPGEGPAGTG^{53}) vIRF1 peptides was monitored by analyzing ^{1}H-^{15}N HSQC spectra. Briefly, ^{15}N-labeled USP7-NTD was incubated with thrombin to cleave the 6xHis fusion tag followed by dialysis into NMR buffer (200 mM NaCl, 25 mM Na phosphate pH 7.0 and 10 mM DTT). Up to 0.4 mM unlabeled wild-type or mutant vIRF1 peptide was titrated in 0.2 mM of ^{15}N-labeled USP7 (containing 10% D_2O) up to 2:1 peptide:USP7 molar ratio. Spectra were processed with Topspin 3.2 and analyzed with SPARKY program (Ye et al. 2012; Holowaty et al. 2003).

GST Pull-Down Assay:

Cells expressing GST fusion tagged proteins were lysed using sonication in 50 mM Tris pH 7.5, 150 mM NaCl, 1x protease inhibitor cocktail (1 mM benzamidine and 0.5 mM PMSF) and 1x protease inhibitor tablet (Roche cOmplete ULTRA Tablets). Lysate was cleared and allowed to interact with glutathione-sepharose beads (GE Healthcare) for 1 hour. The beads were washed extensively with 50 mM Tris pH7.5 and 150 mM NaCl. GST tagged WT and deletion mutant

vIRF1$_{1-90}$ were kept bound to the glutathione-sepharose beads. Prior to the GST pull-down assays, USP7 proteins were dialyzed against 100 mM NaCl, 50 mM Tris pH 8.0, 5% glycerol, 5 mM β-ME and 1x Protease inhibitor tablet. 30 µl of GST-tagged wild-type and deletion mutant vIRF1$_{1-90}$ bound to glutathione-sepharose resin were incubated with 150 µg of purified full-length USP7, wild-type and mutant USP7-NTD and USP7-CTD for 2 hours at 4˚C. 1 nmole of GST alone bound to glutathione-sepharose beads was used as a negative control. The mixtures were then transferred to micro columns and washed extensively with assay buffer. The bound proteins were eluted with 20 mM reduced glutathione and detected by Coomassie Blue staining following sodium dodecyl sulfate-polyacrylamide gel electrophoresis.

Crystallization:

Prior to setting up crystal trials purified USP7-NTD was incubated with thrombin to remove the 6xHis N-terminal fusion tag. USP7-NTD was further purified by size-exclusion chromatography using a HiLoad 26/60 Superdex 75 (GE Healthcare) on an ÄKTApurifier 10 UPC (GE Healthcare) in 500 mM NaCl and 20 mM Hepes pH 7.5. USP7-NTD (100 mg/ml) was co-crystallized with at least five-fold molar excess of vIRF1 (^{44}SPGEGPSGTG^{53}) peptide at 4˚C using the hanging-drop vapor-diffusion method. Rod shape crystals appeared after 4 days following one round of micro-seeding using USP7-NTD:CHFR peptide crystal seeds in 30% PEG 4000, 0.1 M Tris pH 8.5 and 0.2 M $LiSO_4$.

X-ray Data Collection and Structure Determination:

X-ray data was collected at the Advanced Photon Source. Diffraction data was integrated and scaled using autoPROC software (Monleon et al. 2002). The structure was determined by molecular replacement employing USP7-NTD (Protein Data Bank ID 1YY6) as search model without the EBNA1 peptide using CNS (version 1.3) and was refined also using CNS at 1.5 Å resolution (Sarkari et al. 2013). The electron density was visualized and the vIRF1 peptide model was built using Coot (Vonrhein et al. 2011). CNS 1.3 was used for refinement and $2F_o$-F_c and F_o-F_c maps were inspected for further refinement and model rebuilding in Coot. Water molecules were picked using CNS 1.3. Figure 3-7 was prepared using Pymol (Schrödinger 2010).

Structure Deposition:

Coordinates and structure factors for USP7-NTD:vIRF1 have been deposited in the RCSB under

Protein Data Bank ID 4YSI.

Cell Culture and Antibodies:

Human osteosarcoma U2OS cells were grown in McCoy's medium supplemented with 10% FBS and 1 mg/ml Penicillin-Streptomycin. The antibodies were rabbit polyclonal against USP7 (Bethyl Laboratories, A300-033A), mouse monoclonal against USP7 (Millipore, 05-1946), mouse monoclonal against Myc (Millipore 05-724), rabbit polyclonal against FLAG tag (Bethyl Laboratories, A190-102A), mouse monoclonal against FLAG tag (Sigma, F3165), mouse monoclonal against p53 (Santa Cruz, sc-126), rabbit polyclonal against phospho-p53 (Ser15) (Cell Signaling, #9284), rabbit monoclonal against ATM (#2873), rabbit monoclonal against phospho-ATM (Ser1981) (Cell Signaling, #5883), mouse monoclonal against MDM2 (Santa Cruz, sc-965), rabbit polyclonal against phospho-MDM2 (Ser166) (#3521) and mouse monoclonal against GAPDH (Santa Cruz, sc-47724). To detect proteins of interest HRP-conjugated anti-mouse IgG (Jackson ImmunoResearch 115-035-166) and anti-rabbit IgG (Jackson ImmunoResearch 111-035-003) antibodies were used.

Co-immunoprecipitation:

Cells were transfected with pCMV/N-Myc USP7 and pcDNA3.1/FLAG vIRF1 (wild-type or EGPS deletion mutant) vectors (total of 10 μg of DNA per 15 cm tissue culture plate) using PolyJet transfection reagent according to the manufacturer's protocol (SignaGen Laboratories). Cells were harvested 48 hours post-transfection and lysed in radioimmunoprecipitation buffer (50 mM Tris-HCl pH 8.0, 150 mM NaCl, 0.5% Nonidet P-40, 20% glycerol, 1X protease inhibitor cocktail (Roche)) followed by 2 sec sonication at 10% amplitude. Cell lysates were incubated with either mouse monoclonal anti-Myc primary antibody or rabbit polyclonal anti-FLAG primary antibody overnight at 4 ˚C followed by the addition of pre-cleared protein A/G Plus-Agarose beads (Santa Cruz, sc-2003) for 1 hour. Immunoprecipitates were washed with radioimmunoprecipitation buffer five times and then boiled in SDS sample buffer for 5 minutes at 95 ˚C. Samples were resolved on 10% SDS-polyacrylamide gels and immunoblotted using antibodies described above. Co-immunoprecipitation experiment for endogenous USP7 was carried out following the same protocol using rabbit polyclonal anti-USP7 antibody.

Results:

Identification of an EGPS Sequence in KSHV vIRF1:

It is well established that many USP7 substrates including Hdm2, p53 and Hdmx contain (P/A)XXS motifs for interaction with USP7-NTD through the highly conserved ^{164}DWGF^{167} motif with dissociation constant (K_d) values ranging from 10-45 μM (Sarkari et al. 2010; Hu et al. 2006; Sheng et al. 2006). KSHV proteins including vIRF4 and LANA interact with the USP7-NTD ^{164}DWGF^{167} motif through (P/A)XXS sequences (Jager et al. 2012; Lee et al. 2011). EBV EBNA1 also interacts with USP7-NTD however, with an unusual motif, EGPS, instead of (P/A)XXS (Saridakis et al. 2005). A recent study revealed that ORF45, a KSHV immediate early protein, also interacts with USP7-NTD through an EGPS sequence (Gillen et al. 2015).

We utilized SCAN Prosite to search for viral proteins containing the DPGEGPST sequence of EBNA1 and identified ^{44}SPGEGPSG^{51} from KSHV vIRF1 (de Castro et al. 2006). Alignment of EBV EBNA1, KSHV ORF45 and KSHV vIRF1 proteins showed conservation of the EGPS interaction motif, and therefore we hypothesized that vIRF1 may interact with USP7-NTD (Fig. 3-3).

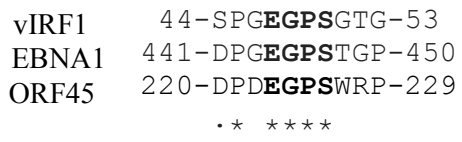

Fig. 3-3: Alignment of the USP7 binding motif of vIRF1 with the previously identified USP7 binding motifs of EBV EBNA1 and KSHV ORF45. "*" represents conserved residues and "." represents semi-conserved substitution.

USP7-NTD and vIRF1 Interact *in Vitro*:

To test the binary interaction between vIRF1 and USP7, a series of GST pull-down assays were performed using GST-tagged vIRF1$^{1-90}$. GST-vIRF1$^{1-90}$ interacted with both full-length USP7 and USP7-NTD but not USP7-CTD confirming that vIRF1 binding is mediated through USP7-NTD (Fig. 3-4). Neither full-length USP7 nor USP7-NTD were retained by GST alone, indicating that the interaction with GST- vIRF1$^{1-90}$ was specific. Deletion of residues ^{45}PGEGPS^{50} (GST-ΔvIRF1$^{1-90}$) abolished its interaction with both full-length USP7 and USP7-NTD confirming that vIRF1 interacts with USP7-NTD through its EGPS sequence, which is similar to the USP7 binding motif found in EBNA1. We also performed GST pull-downs using USP7-NTD^{DW}, a double mutant containing alanine mutations at residues D164 and W165 within the ^{164}DWGF^{167} motif. As expected, USP7-NTD^{DW} did not interact with vIRF1. These pull-down assays demonstrated that USP7-NTD interacts specifically with vIRF1 *in vitro*.

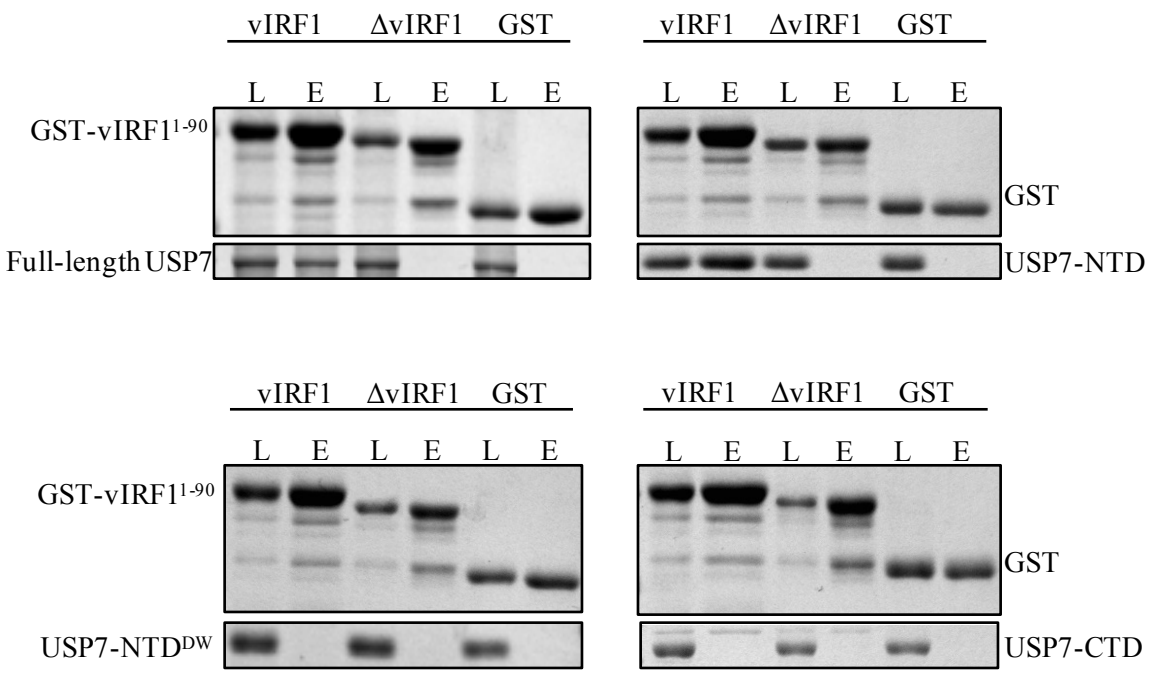

Fig. 3-4: USP7 and vIRF1 GST pull-down assay. GST pull-down assay with GST-vIRF1$^{1-90}$, GST-ΔvIRF1$^{1-90}$ (deletion of ^{45}PGEGPS^{50}) or GST alone as negative control. Full-length USP7, USP7-NTD, USP7-CTD and USP7-NTD^{DW} were used as prey. *L*, load; *E*, elution.

Binding Affinity of vIRF1 and USP7-NTD:

Fluorescence polarization was used to determine the dissociation constant between USP7-NTD and vIRF1. FITC labeled wild-type (WT) (^{44}SPGEGPSGTG^{53}) and mutant (Mut) (^{44}SPGEGPAGTG^{53}) vIRF1 peptides containing the potential USP7 interaction site were used in these assays. A fixed concentration of 40 nM FITC labeled vIRF1 peptide was titrated with increasing concentrations of USP7-NTD (up to 500 μM) to detect the fluorescence polarization changes during formation of the protein-peptide complex. The dissociation constant of WT vIRF1 peptide was calculated to be 2.0 ± 0.1 μM while K_d for the mutant peptide was calculated to be 46.1 ± 4 μM (Fig. 3-5A & B). Interaction was not observed between USP7-NTD^{DW} and either WT or mutant vIRF1 peptides. The K_d value of 2μM for the interaction between vIRF1 and USP7 compares well with that of EBNA1 and implies that KSHV vIRF1 interacts with USP7-NTD.

A

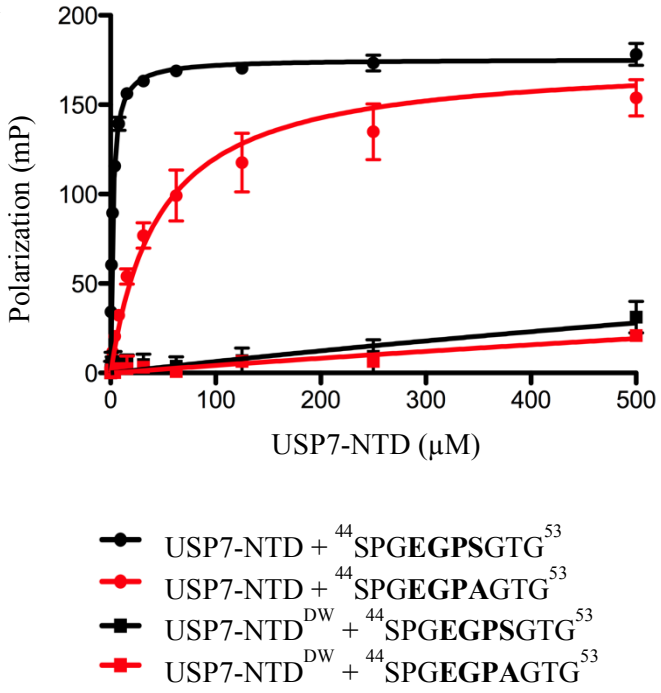

B

USP7-NTD	K_d (μM)	S.D.
^{44}SPG**EGPS**GTG^{53}	2.04	0.11
^{44}SPG**EGPA**GTG^{53}	46.1	4.3
USP7-NTD^{DW}		
^{44}SPG**EGPS**GTG^{53}	-	-
^{44}SPG**EGPA**GTG^{53}	-	-

Fig. 3-5: Binding curve of vIRF1 and USP7. A) Fluorescence polarization of FITC labeled wild-type (^{44}SPGEGPSGTG^{53} in black) or mutant (^{44}SPGEGPAGTG^{53} in red) vIRF1 peptides with USP7-NTD and USP7-NTD^{DW}. B) Dissociation constants (K_d values) for the USP7-NTD interaction with FITC-labeled vIRF1 peptides. *mP*, milliPolarization. Error bars indicate means ± S.D. Average values with standard deviation for three or more experiments are shown.

NMR Analysis of the USP7-NTD and vIRF1 Peptide Interaction:

To further investigate the interaction between USP7-NTD and the vIRF1 peptide, 2D NMR HSQC spectra of ^{15}N labeled USP7-NTD was analyzed in the presence of unlabeled WT (^{44}SPGEGPSGTG^{53}) or mutant (^{44}SPGEGPAGTG^{53}) vIRF1 peptides. Figure 3-6A displays the overlay of USP7-NTD ^{1}H-^{15}N HSQC spectra for USP7-NTD alone (in black) and USP7-NTD titrated with 0.4 mM of wild-type (in red) or mutant (in blue) vIRF1 peptides (2:1 peptide:USP7-NTD ratio). Strong perturbations were observed in the USP7-NTD resonances in the presence of WT vIRF1 peptide while these disturbances were notably decreased in the presence of mutant vIRF1 peptide. Using previously assigned USP7-NTD spectra (Saridakis et al. 2005) (Biological Magnetic Resonance Data Bank Entry 6939) we were able to observe that upon vIRF1 binding, disturbances in USP7-NTD spectra were mostly in β-strand 7 residues such as D164, W165 (shift was observed in indole side chain), G166, F167, S168 and Met171 (Fig. 3-6B). Resonances of a few residues from β3, β4 and β6 were also affected including Met100, F118 and S155. These observations are very similar to those of EBNA1/USP7-NTD interaction. However, in contrast to EBNA1, spectra of residues such as N169 and F170 from β7 and residues Met102 and F117 did not show any change upon addition of vIRF1 peptide suggesting slightly different mode of interaction with USP7-NTD.

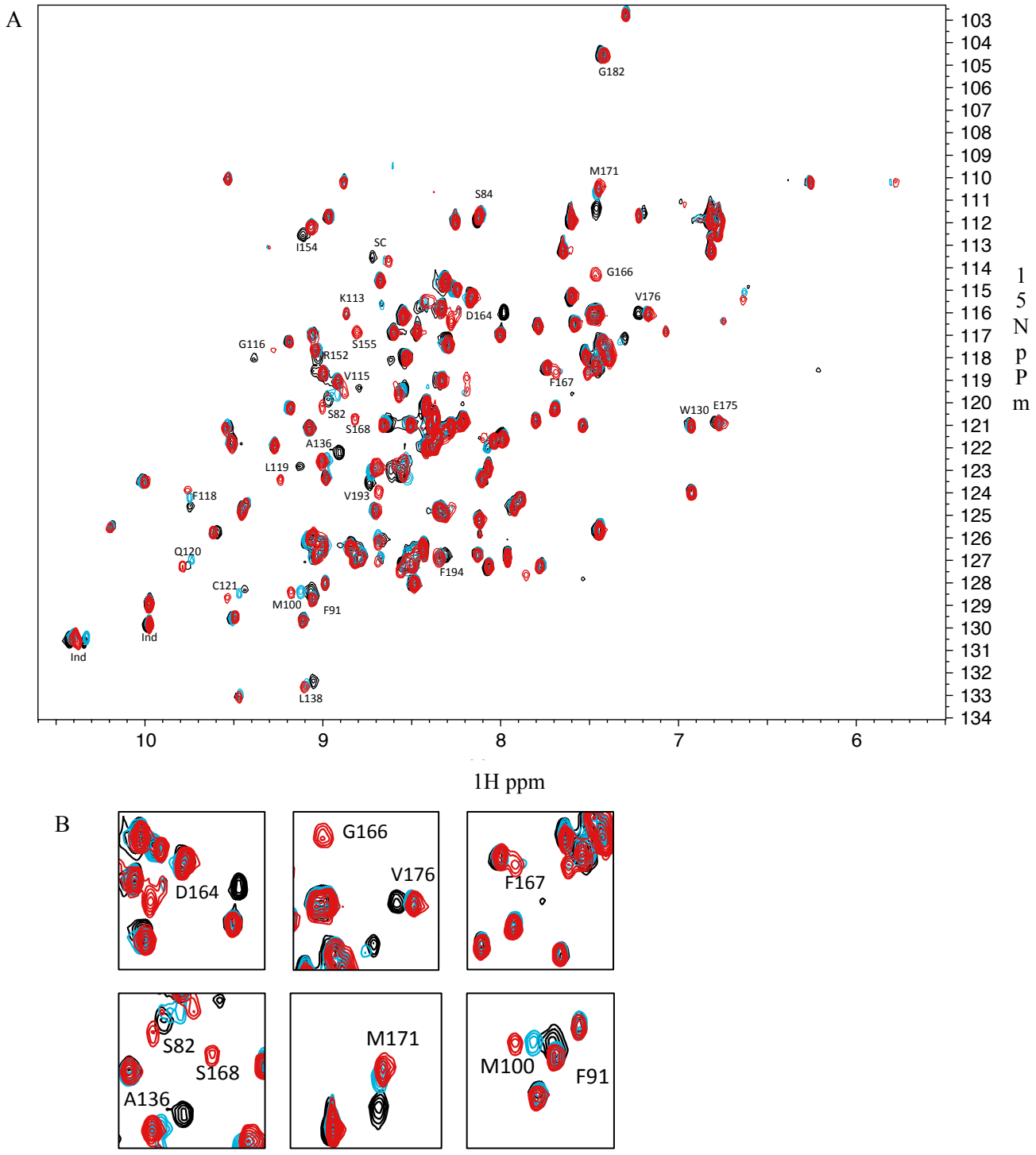

Fig. 3-6: NMR titration of USP7-NTD with WT or mutant vIRF1 peptides. Overlay of 2D ^{1}H-^{15}N HSQC correlation spectra of ^{15}N labeled USP7-NTD (black) titrated with 1:2 molar ratio of unlabeled wild-type (^{44}SPGEGPSGTG^{53} in red) or mutant (^{44}SPGEGP<u>A</u>GTG^{53} in cyan) vIRF1 peptides. (D) Individual residues from USP7-NTD ß strand 7 and M100 from ß strand 3 that showed the largest shifts are identified.

Crystal Structure of the USP7-NTD and vIRF1 Peptide Complex:

To elucidate the molecular basis of this interaction *in vitro* we co-crystallized USP7-NTD with the following vIRF1 peptide (^{44}SPGEGPSGTG^{53}). The structure of the USP7-NTD:vIRF1 peptide complex was determined using molecular replacement and refined to 1.5Å resolution. X-ray data collection and refinement parameters are provided in (Table 3-1). USP7-NTD residues 54–62 and 106–111 are disordered and were not built in the final model.

As previously shown, USP7-NTD forms a TRAF domain similar to that of tumor necrosis factor receptor associated factor (TRAF) 2, which consists of an eight-stranded antiparallel β-sandwich fold with a shallow groove on the surface (Fig. 3-7A & B) (Park et al. 1999). The conserved ^{164}DWGF^{167} motif is found in β-strand 7 which also contains a beta-bulge essential for its interaction with binding partners. The electron density allowed building of vIRF1 residues 44-51 (SPGEGPSG) in the binding site of USP7-NTD (Fig. 3-7C). Residues 52 and 53 of the vIRF1 peptide did not have interpretable electron density suggesting that they do not make contact with USP7-NTD. There are several polar and non-polar interactions that occur between USP7-NTD and the vIRF1 peptide (Fig. 3-7E). Ser50 of vIRF1 forms H-bonds through its side chain hydroxyl and backbone amide group with Asp164 of USP7-NTD β-strand 7. It also forms a hydrogen bond with ine104 of β-strand 3. The Glu47 side chain of vIRF1 forms a water-mediated H-bond with Trp165 of USP7. Comparison between the EBNA1 and the vIRF1 peptides revealed that they are superimposable and make very similar contacts with USP7-NTD (Fig. 3-7D).

Table 3-1: USP7-NTD:vIRF1 Peptide X-Ray Data Collection and Refinement Parameters.

	USP7-NTD:vIRF1 peptide
X-Ray Data	
Space Group	$P4_1$
Resolution (Å)	50.0 – 1.02
Unit Cell Axes (Å^3)	70.0 x 70.0 x 45.4
Molecules / AU	1
Total Observations (#)	684942
Unique Reflections (#)	111563
Intensity (I/σ<I>)	20.6 (2.0)
Completeness (%)	99.9 (98.2)
Multiplicity	6.1 (5.5)
[a]R_{merge}	0.039 (0.776)
Refinement	
R_{work}	0.171
R_{free}	0.176
Protein Atoms (#)	1186
Water Molecules (#)	268
rmsd bonds (Å)	0.008
rmsd angles (°)	1.29
rmsd dihedrals (°)	25.2
rmsd improper (°)	0.86
thermal factors (Å^2)	13.5
Ramachandran Plot	
Most Favoured	0.95
Additionally Allowed	0.05

Numbers in brackets refer to the highest resolution shell, 1.023 Å to 1.02 Å. [a]$R_{sym} = \Sigma |I-\langle I\rangle| / \Sigma I$ where I is the observed intensity and <I> is the average intensity from multiple observations of symmetry-related reflections.

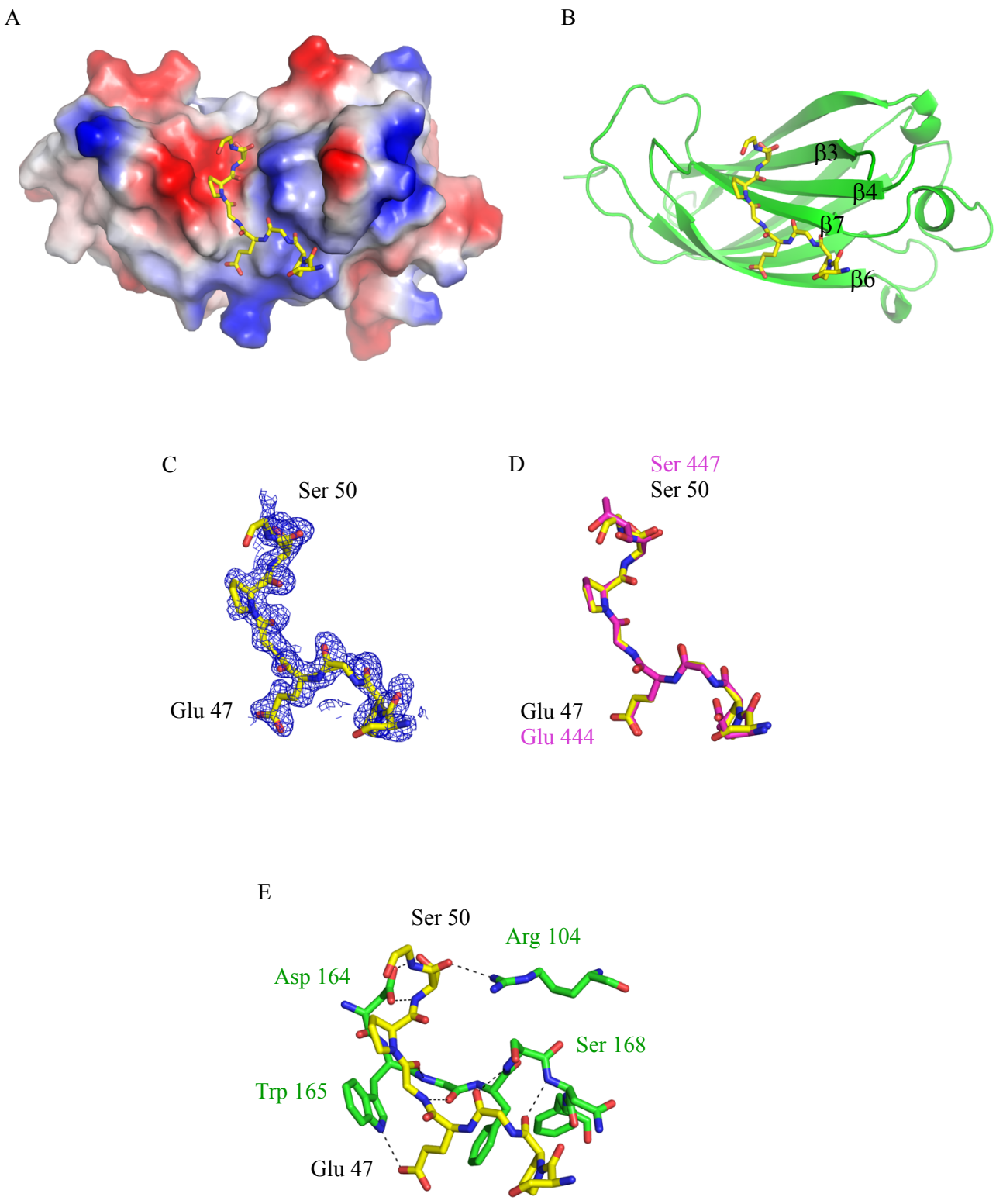
A
B
β3
β4
β7
β6
C
Ser 50
Glu 47
D
Ser 447
Ser 50
Glu 47
Glu 444
E
Ser 50
Arg 104
Asp 164
Ser 168
Trp 165
Glu 47

Fig. 3-7: Crystal structure of the UPS7-NTD:vIRF1 peptide complex. A) Electrostatic surface representation of USP7-NTD showing the vIRF1 peptide ^{44}SPGEGPSGTG^{53} in stick form (yellow). B) Ribbon diagram of USP7-NTD (green) showing the vIRF1 peptide in stick form (yellow). C) Electron density prior to the addition of peptide with the final peptide model (yellow) contoured at 1 σ. D) Superposition of the vIRF1 (^{44}SPGEGPSGTG^{53}, yellow) and EBNA1 (^{441}DPGEGPSTGP^{450}, fuchsia) peptides. E) Interactions formed between USP7-NTD (green) and the vIRF1 peptide (yellow).

USP7 and vIRF1 Interact *in Vivo*:

We investigated the vIRF1 interaction with USP7 *in vivo*. The ability of vIRF1 to interact with USP7 was examined by transfecting U2OS cells with Myc-tagged USP7 and FLAG-tagged WT vIRF1. After immunoprecipitation of the lysate with a USP7 antibody, immunoblotting with anti-FLAG led to the identification of FLAG-tagged vIRF1 (Fig. 3-8A). Lysate incubated with rabbit IgG served as a negative control and did not show any interaction. We also examined whether the PGEGPS vIRF1 deletion mutant (ΔvIRF1) could be co-immunoprecipitated with USP7. U2OS cells were transfected with Myc-tagged USP7 and FLAG-tagged ΔvIRF1. The lysate was immunoprecipitated with a USP7 antibody and immunoblotted with anti-FLAG, however, ΔvIRF1 could not be detected (Fig. 3-8A). These results indicated that USP7 was interacting with vIRF1 but not ΔvIRF1 in U2OS cells. We also performed the reciprocal experiments in which immunoprecipitation of the lysate with anti- FLAG rather than anti-USP7 readily identified USP7 in complex with vIRF1 while ΔvIRF1 was not able to pull-down USP7 (Fig. 3-8B). Combined, these results confirmed that the EGPS residues in vIRF1 are essential for interaction with USP7 *in vivo*.

Further, we examined the interaction of vIRF1 with endogenously expressed USP7 (performed by Olga Egorova). After transfection of U2OS cells with FLAG-tagged vIRF1, USP7 was immunoprecipitated with anti-USP7. Blotting for anti-FLAG readily identified vIRF1 (Fig. 3-8C). In a reciprocal experiment, immunoprecipitation of FLAG-tagged vIRF1 from transfected U2OS lysate also successfully led to the detection of endogenous USP7. In each case lysate incubated with rabbit IgG served as negative control which did not show any interaction.

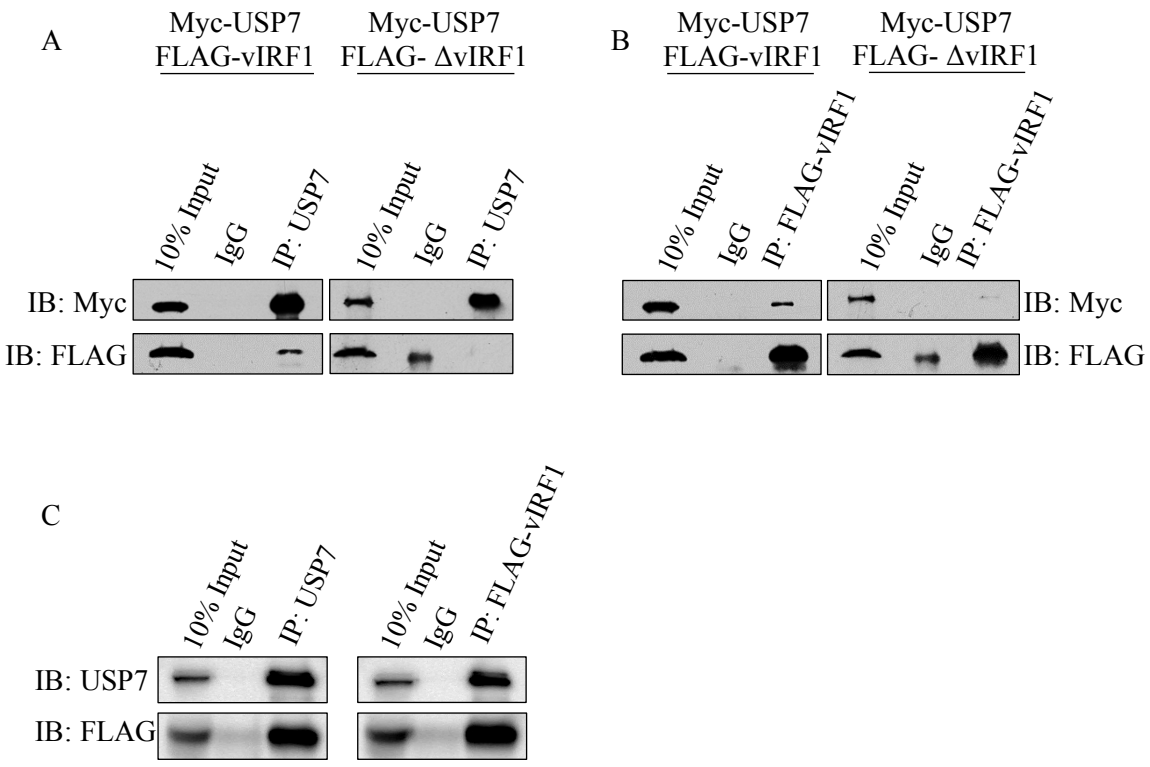

Fig. 3-8: vIRF1 and USP7 interaction *in vivo*. Overexpressed USP7 interacts with ectopically expressed vIRF1 but not EGPS deletion mutant vIRF1 (ΔvIRF1). U2OS cells were transfected with Myc-USP7 and FLAG-vIRF1 or FLAG-ΔvIRF1. Immunoprecipitation (IP) was carried out by incubating the lysate with (A) USP7 or (B) FLAG antibodies using rabbit IgG as the negative control. Immunoblotting (IB) was performed with antibodies against Myc and FLAG tags. (C) Endogenous USP7 interacts with vIRF1 *in vivo*. U2OS cells were transfected with FLAG-vIRF1. IP was performed using USP7 or FLAG antibodies followed by IB using antibodies against USP7 and FLAG (Figure C was prepared by Olga Egorova).

Effect of vIRF1 on p53, Hdm2 and ATM Stability:

USP7 stabilizes cellular levels of the tumor suppressor p53 and its negative regulator, Hdm2, through deubiquitination. Reduction in cellular levels of USP7 leads to instability of p53 whereas deletion of USP7 leads to degradation of Hdm2 resulting in stabilization of p53 (Cummins et al. 2004; Li et al. 2002). We hypothesized that interaction between vIRF1 and USP7-NTD at the same binding site that is known to interact with p53 and Hdm2 should decrease the availability of USP7 and therefore lead to instability of p53. To test the effect of vIRF1 on p53, U2OS cells were transfected with expression vectors for FLAG-tagged vIRF1 or ΔvIRF1. Endogenous levels of p53, Ser15 phosphorylated p53 and USP7 were detected by immunoblotting after transfection. As shown in (Fig. 3-9A and C), transfection of cells with vIRF1 resulted in significant decrease in the level of p53 (about 50%) compared to levels in cells transfected with empty vector ($p<0.01$) or ΔvIRF1.

Considering that USP7 deubiquitinates and stabilizes Hdm2, we monitored Hdm2 as well as phospho-Hdm2 (Ser166) in cells transfected with vIRF1 or ΔvIRF1 to assure that changes in the levels of p53 were not a result of change in stability of Hdm2. Phosphorylation at Ser166 stabilizes Hdm2 and stimulates p53 ubiquitination (Feng et al. 2004). To test our hypothesis, U2OS cells were transfected with expression vectors for FLAG-tagged vIRF1 or ΔvIRF1. As shown in (Fig. 3-9B and D), expression of vIRF1 or ΔvIRF1 had no effect on the endogenous levels of USP7, Hdm2 or Ser166 phosphorylated Hdm2 compared to control. This observation suggests that change in the stability of p53 is not caused by changes in the stability of Hdm2 or USP7.

It was previously reported that vIRF1 expression inhibits auto-phosphorylation of ATM on Ser1981 which is important for ATM activation. Decreased ATM activity resulted in reduced Ser15 phosphorylation of p53 (Shin et al. 2006). This p53 phosphorylation decreases the Hdm2 affinity for p53 and leads to stability of p53 (Nakagawa et al. 1999). As shown in (Fig. 3-9A), we observed decreased levels of Ser1981 phosphorylated ATM as well as Ser15 phosphorylated p53 in cells transfected with vIRF1 or ΔvIRF1, suggesting that under our experimental conditions, ΔvIRF1, which is incapable of binding to USP7, is still able to exert an inhibitory effect on ATM activation and Ser15 phosphorylation of p53. This indicates that the reduced p53 levels observed with ΔvIRF1 compared to vIRF1 are mainly due to the interaction between vIRF1 and USP7. Therefore, we show that interaction of vIRF1 with USP7 leads to destabilization of p5

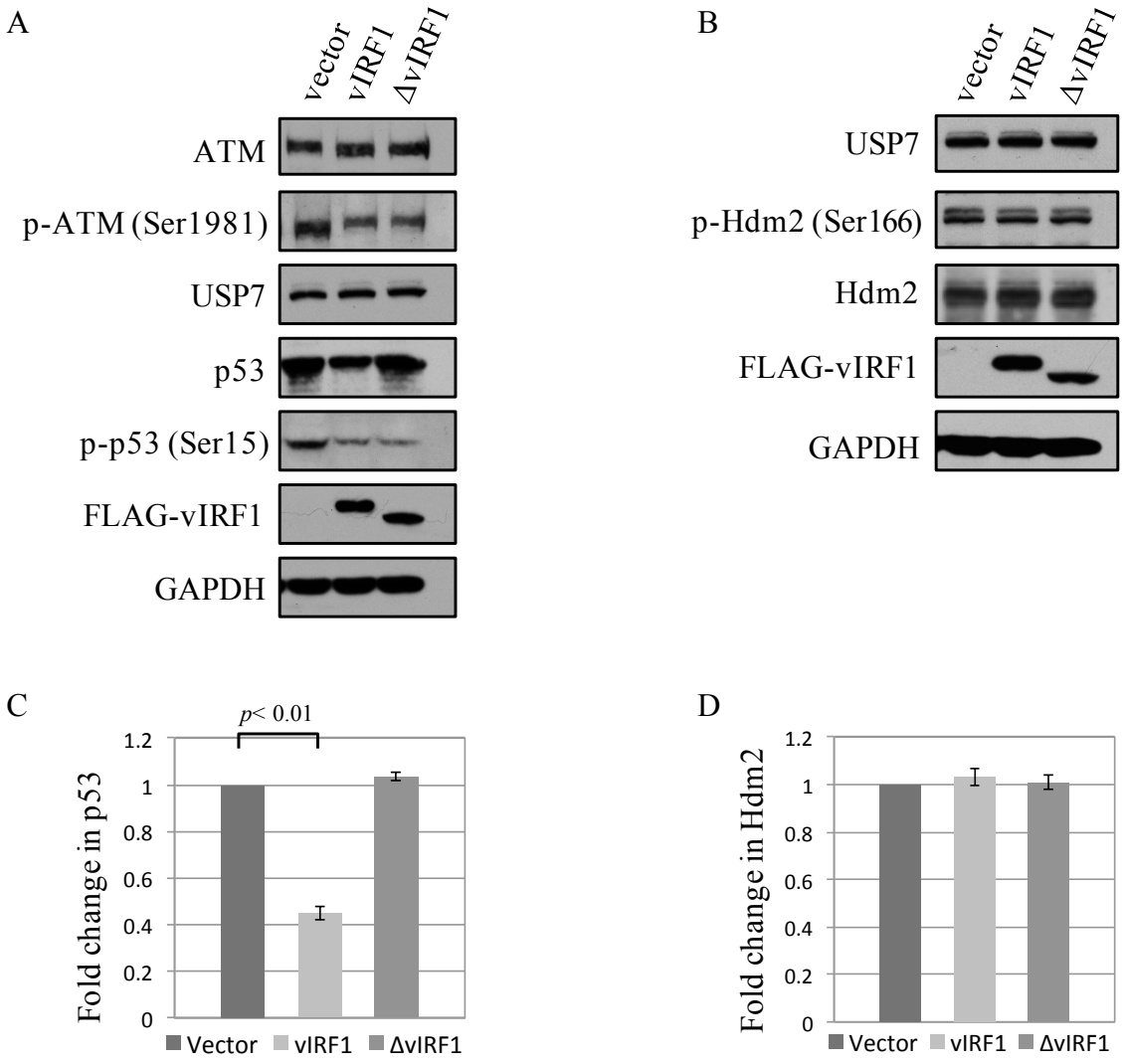

Fig. 3-9: Effect of vIRF1 on p53, Hdm2 and ATM stability. A) Effect of vIRF1 expression on p53 and ATM. U2OS cells were transfected with FLAG-vIRF1 or FLAG-ΔvIRF1. After 24hrs, IB was performed using antibodies against ATM, phospho-ATM (Ser1981), USP7, p53, phospho-p53 (Ser15) and FLAG tag. Cells transfected with empty vector were used as negative control. GAPDH levels were detected as control for equal loading. B) Effect of vIRF1 on Hdm2. The levels of USP7, Hdm2 and Ser166 phosphorylated Hdm2 were monitored after expression of vIRF1 or ΔvIRF1 in U2OS cells. Cells were incubated for 24 hours following transfection with FLAG-tagged vIRF1 and ΔvIRF1. IB was performed on whole cell lysates using USP7, Hdm2, phospho-Hdm2 (Ser166) and FLAG tag antibodies. C&D) Fold change was determined by normalizing p53 and Hdm2 ratios to the vector control ratio. A paired t-test was performed to evaluate the statistical significance of the changes in p53 and Hdm2 levels after the introduction of vIRF1 or ΔvIRF1. Error bars indicate S.E.M. and are from 3 independently transfected U2OS lysates.

Discussion:

Members of the herpesvirus family such as herpes simplex virus type 1 (HSV-1), Epstein-Barr virus (EBV), Kaposi's sarcoma-associated herpesvirus (KSHV) and human cytomegalovirus (HCMV) have evolved to interfere with the USP7-p53-Hdm2 pathway by competitively binding to USP7 and hindering its interaction with cellular substrates or binding proteins (Jager et al. 2012; Lee et al. 2011; Saridakis et al. 2005; Emsley & Cowtan 2004; Meredith et al. 1994). For instance, HSV-1 expressed ICP0 protein is an E3 ubiquitin ligase that ubiquitinates and causes degradation of host proteins (Boutell & Everett 2003). ICP0 interaction with USP7 leads to its rescue from self-ubiquitination and proteasomal degradation (Boutell et al. 2005). UL35, a HCMV latent protein, interacts with USP7 and alters its subcellular localization (Salsman et al. 2012). EBNA1 expressed by EBV and vIRF4, LANA and ORF45 expressed by KSHV interact with the USP7 N-terminal domain, block USP7 substrate interaction and cripple the cell's interferon and innate immune response (Lee et al. 2009; Saridakis et al. 2005). Further, USP7 interacting viral proteins such as ICP0, UL35 and EBNA1 also co-localize with and disrupt promyelocytic leukemia (PML) nuclear bodies and induce degradation of PML proteins (Sivachandran et al. 2008; Maul & Everett 1994). PML nuclear bodies (PML-NB), primarily composed of PML protein, are important mediators of critical cellular processes including apoptosis, DNA repair and intrinsic response to viral infection (Salsman et al. 2012; Salsman et al. 2008; Bernardi & Pandolfi 2007). Further, PML nuclear bodies recruit proteins such as p53 and p300 (Seo et al. 2001; Li et al. 2000). USP7 is also known to associate with PML-NBs (Sarkari et al. 2011). vIRF1 protein expressed by KSHV was shown to interact with both p53 and p300. In addition, in KSHV infected BCBL-1 cells, vIRF1 was shown to localize with PMLs during both lytic and latent cycles (Pozharskaya et al. 2004).

Through analysis of viral protein sequences followed by biochemical, structural and *in vivo* studies, we identified KSHV vIRF1 as a novel USP7 binding protein. Fluorescence polarization indicated that the vIRF1 peptide, ^{44}SPGEGPSGTG^{53}, interacts with USP7-NTD with a K_d value of 2.0 μM compared to substrates such as Hdm2 and p53 that bind with K_d values varying between 10 μM and 45 μM respectively. A single point mutation of serine to alanine in the vIRF1 peptide decreased the dissociation constant approximately 25-fold indicating the importance of Ser50 in mediating interaction with the USP7-NTD binding site. The interaction between USP7-NTD^{DW} and the vIRF1 peptide was completely abolished confirming that the vIRF1 ^{47}EGPS^{50} sequence interacts with the USP7-NTD ^{164}DWGF^{167} motif.

The vIRF1 peptide binds to a groove on the surface of USP7-NTD, forming identical interactions with USP7-NTD as those seen with the USP7-NTD:EBNA1 peptide complex structure. The HSQC NMR analysis revealed perturbations in USP7-NTD residues from β-strands 3, 4, 6 and 7 upon addition of the vIRF1 peptide. These residues correlate well with the residues seen in the crystal structure analysis especially those found in β-strand 7. The side chains of residues from β-strands 3 and 7 form polar contacts with the vIRF1 peptide whereas the remaining residue side chains, from β-strands 4 and 6, are in close proximity to the vIRF1 peptide but do not make any polar contacts. Along with EBNA1 and ORF45, vIRF1 contains a negatively charged glutamic acid residue at the position of P/A in the (P/A)XXS USP7 binding motif. Glutamic acid rather than proline or alanine in that position is thought to increase the affinity of EBNA1 for USP7-NTD therefore, allowing it to effectively compete with USP7 cellular substrates (Sheng et al. 2006). Comparing the interaction with USP7-NTD made by glutamic acid rather than proline or alanine shows an increased number of H-bonds formed with glutamic acid to USP7-NTD. This unique mode of interaction achieved through substitution of a glutamic acid residue for alanine or proline is advantageous for vIRF1, ORF45 and EBNA1 in that it provides them with a higher binding affinity. This empowers the virus to sufficiently disrupt USP7 deubiquitination of cellular substrates such as p53. Identification of yet another USP7-NTD interacting herpesvirus protein suggests that these viruses target USP7 at least in part because it is a critical cellular regulator of p53.

Our *in vivo* data in U2OS cells indicates that vIRF1, but not ΔvIRF1, leads to a decrease in the levels of cellular p53. Therefore, vIRF1 binds USP7-NTD through its EGPS sequence and decreases availability of USP7 for binding and deubiquitinating p53. vIRF1 was previously reported to directly interact with p53 through its central region (residues 152-360), prevent p53 acetylation by p300 and thus inhibit p53 transcriptional activation (Shin et al. 2006; Seo et al. 2001). It was also reported that vIRF1 led to increased ubiquitination and degradation of p53 (Shin et al. 2006). Our data suggests that increased ubiquitination and degradation of p53 can in part be attributed to vIRF1 hijacking USP7, thus decreasing USP7's ability to deubiquitinate and stabilize p53. Since Hdm2, a p53 negative regulator, is also a substrate of USP7 and interacts through its ^{164}DWGF^{167} motif, we monitored cellular levels of Hdm2 to investigate whether the vIRF1-mediated decrease in availability of USP7 also destabilized Hdm2. We were never able to detect any significant changes in the level of Hdm2 suggesting that the USP7:vIRF1 interaction preferably disrupted USP7 deubiquitination and stabilization of p53.

It was previously reported that vIRF1 inhibits Ser1981 auto-phosphorylation (activation) of ATM which prevents ATM mediated Ser15 phosphorylation of p53 and leads to p53 degradation (Shin et al. 2006). We monitored ATM and Ser1981 phosphorylated ATM but did not observe any changes in their levels between vIRF1 and ΔvIRF1 transfected cells, however both showed lower levels compared to mock transfected cells, indicating that vIRF1 and ΔvIRF1 are still able to interact with ATM and inhibit its activity. As it was previously reported that vIRF1 interacts with ATM through its CTD while the USP7 binding motif that we identified is located N-terminal to its DNA binding domain, we were not expecting changes in ATM levels (Shin et al. 2006).

High levels of vIRF1 expression in KSHV infected BCBL-1 cells were only observed transiently during lytic infection. Whereas, low levels of vIRF1, localized with PML nuclear bodies, were reported during latency (Pozharskaya et al. 2004). In KSHV infected cells, p53 was only detectable in PML nuclear bodies during the lytic cycle while latently infected cells did not show detectable levels of p53 (Pozharskaya et al. 2004). These observations suggest that vIRF1 may prevent USP7 deubiquitination of p53 during latency as all three proteins are localized to PML nuclear bodies. However, it is also important that vIRF1-mediated disruption of USP7 regulation of p53 is only one of the many mechanisms used by vIRF1 and other KSHV expressed proteins to weaken the cellular anti-viral response (Jacobs & Damania 2011).

KSHV vIRF4, ORF45 and LANA interact with and inhibit multiple members of the USP7-p53-Hdm2 pathway indicating the importance of p53 degradation for KSHV to establish and maintain life-long latency in host cells (Jager et al. 2012; Lee et al. 2011; Chen et al. 2010; Shin et al. 2006). vIRF1 also uses multiple redundant mechanisms to combat the cell's anti-viral response by inhibiting multiple targets of the USP7-p53-Hdm2 pathway. Under normal (unstressed) cellular conditions, USP7 predominantly stabilizes Hdm2 which permits p53 ubiquitination and degradation as low levels of p53 are required for normal cellular homeostasis (Fig. 3-10A). Upon cellular stress (DNA damage or viral entry into the nucleus) ATM kinase is activated which leads to phosphorylation of p53, Hdm2 and Hdmx. ATM-mediated Hdm2 phosphorylation leads to p53 stabilization. ATM-mediated phosphorylation of p53 decreases its affinity for Hdm2, signals its acetylation and transactivation by p300 as well as its stabilization by USP7 (Fig. 3-10B). vIRF1 is a potent inhibitor of ATM kinase activity, p300 acetyltransferase activity and p53 transcriptional activity (Fig. 3-10C). We've shown that vIRF1 interaction with USP7 decreases p53 levels suggesting that it also blocks USP7 deubiquitination

and stabilization of p53. Our novel finding that vIRF1 also targets USP7 fits well with the mechanism that KSHV must destroy p53 for a successful lifelong infection.

A

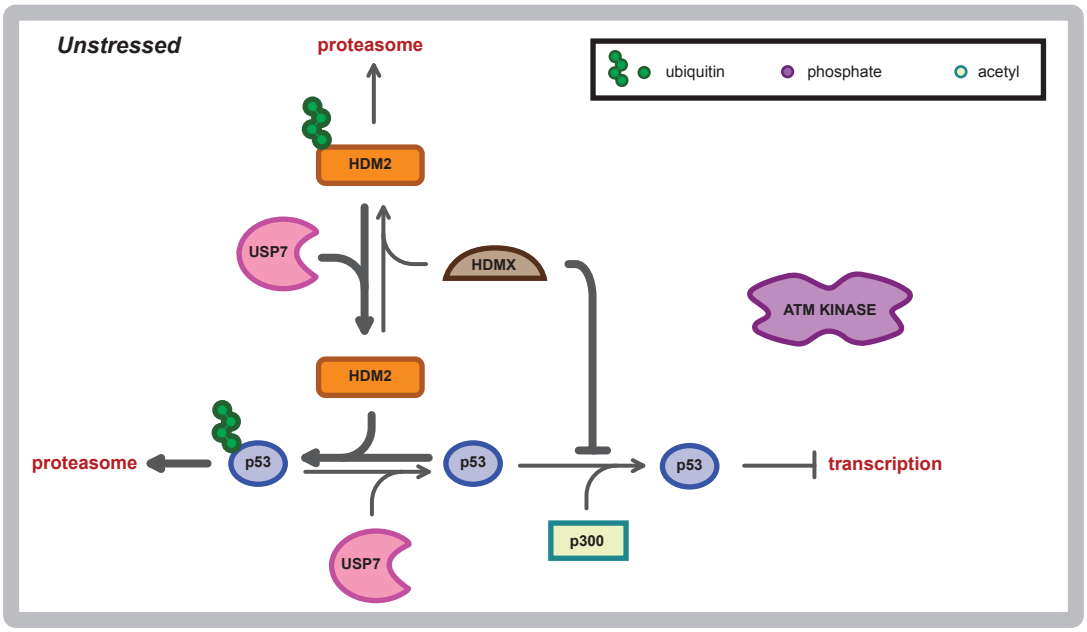

B

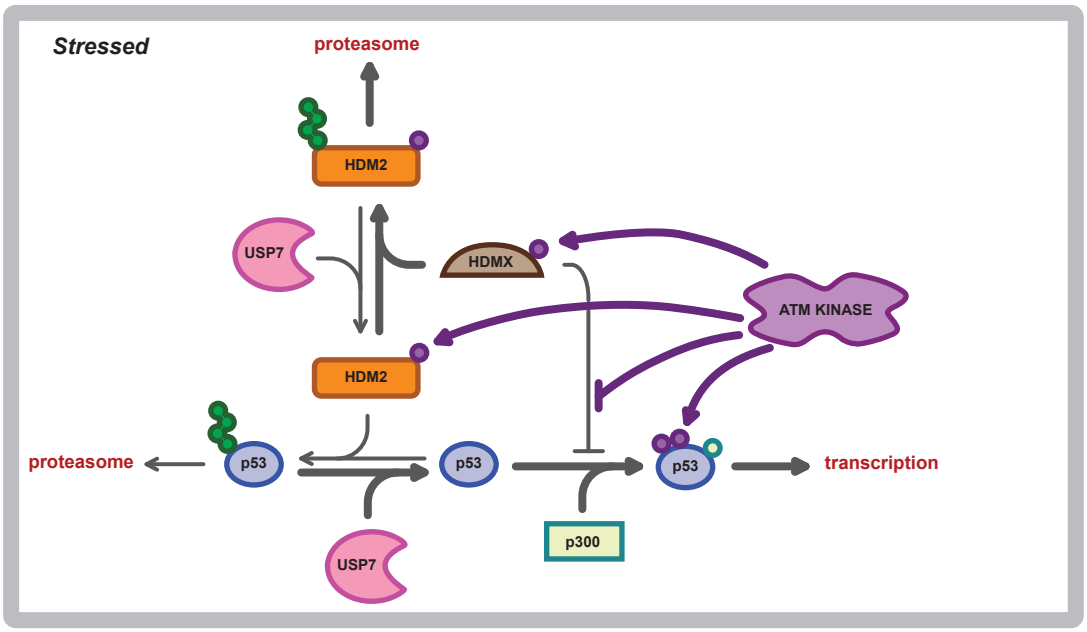

C

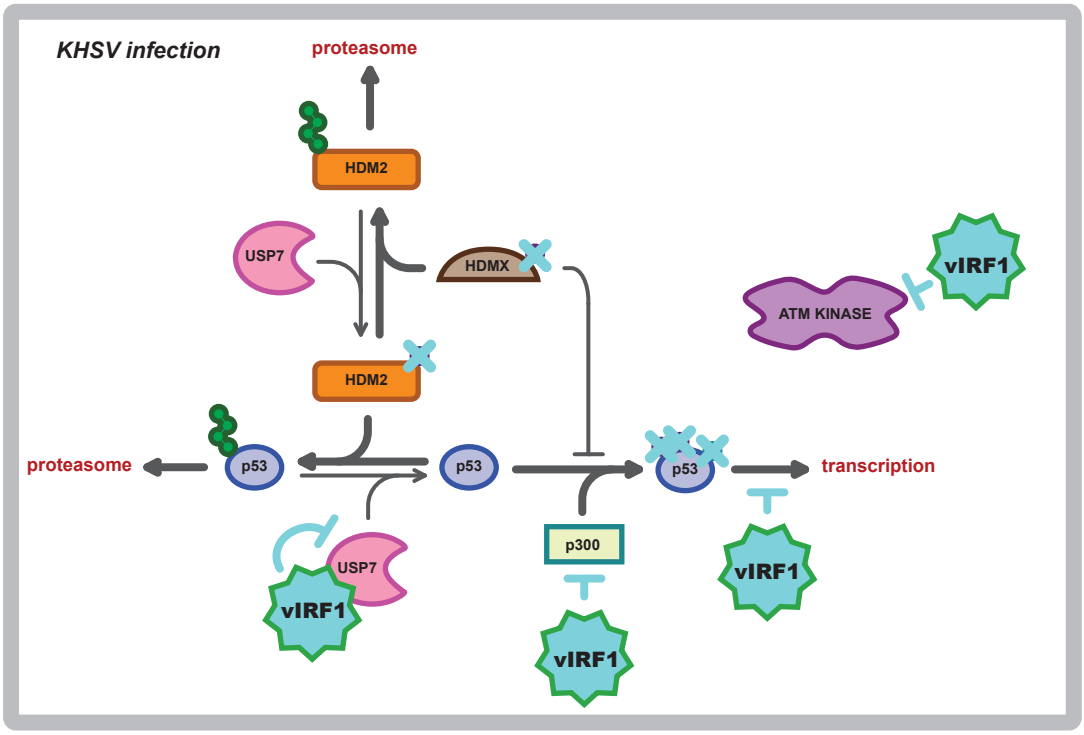

Fig. 3-10: A new role for vIRF1 in hijacking USP7 and degrading p53. A-B) depicting USP7, Hdm2 and ATM effect on p53 signaling pathway under normal and stressed cellular conditions. C) vIRF1 disrupts the p53 signaling pathway during viral infection by (1) inhibiting ATM phosphorylation (2) inhibiting p53 transcription activation and (3) inhibiting p300 acetylation of p53. Our results suggest that vIRF1 also binds USP7 and decreases availability of USP7 for deubiquitinating and stabilizing p53 (Schematic representation was prepared by Ira Lacdao).

Chapter 4: Human Cytomegalovirus Tegument Transactivator pp71 Interacts with Human Deubiquitinating Enzyme USP7

In Fig. 4-5 (Superimposed ^{15}N HSQC spectra of USP7-NTD before and after titration with pp71 peptide) Dr. Saridakis and Dr. Sheng supervised the experiment. The procedure was done with the help of Dr. Howard Hunter. I analyzed the data and produced the figures. In Fig. 4-8 (Complex crystal structure of USP7-NTD and pp71 peptide) Dr. Sadridakis supervised the experiment, collected and refined crystal diffraction data and prepared Table 4-1. I set up and performed the experiments and produced the final figures.

Introduction:

Human Cytomegalovirus:

Human cytomegalovirus (HCMV, also known as HHV-5) is a member of the human herpesvirus (HHV) family that has acquired the ability to evade the immune system and persist in latent form in healthy individuals throughout their life time. Disease symptoms and mortality occur in infants infected in the womb, newborns infected shortly after birth and in individuals with weakened immune system, such as organ transplant patients or older individuals (Griffiths et al. 2015; Penkert & Kalejta 2012). Similar to other members of the human herpesviruses, HCMV is very common. A recent survey revealed that by age 50 about 50% of Americans are positive for HCMV while for South America and parts of Europe this number reaches about 90% (Boeckh & Geballe 2011). HCMV is one the dominant causative agents behind congenital hearing loss and mental retardation in children and less commonly results in CMV mononucleosis (Goderis et al. 2016; Grosse et al. 2008).

HCMV is a β herpesvirus, a sub-family of *Herpesviridae,* with a linear double stranded DNA. Its genome is incased in an icosahedral protein capsid which is further enveloped by a lipid bilayer (Tomtishen III 2012). Between the capsid and the lipid envelope there is a layer known as tegument. The tegument contains about 38 viral & some cellular proteins along with some viral and cellular mRNAs (Smith et al. 2014; Varnum et al. 2004). Upon diffusion of the lipid envelope with the host cell membrane, components of the tegument are released into the cytoplasm and become active (Tomtishen III 2012). Tegument proteins, of which many are phosphorylated, play a crucial rule in preparation of the cellular environment for viral infection prior to viral gene expression (Rieder et al. 2017) . They are involved in immune repression, control of cell cycle, initiation of viral immediate early gene expression, transfer of capsid to the nucleus and virion assembly and exit from the host cell (Smith et al. 2014). For their crucial rule in initiation of the viral infection, tegument proteins have been studied as targets for HCMV infection treatment, therapeutic design and vaccine development (Xia et al. 2017; Kalejta 2008).

HCMV pp71 Tegument Protein:

Upon release of the tegument proteins into the cytoplasm, pp71 (71-kDa phosphoprotein), the main HCMV tegument transactivator, is immediately transported to the nucleus. It activates

expression of viral immediate early (IE) genes from the major immediate early promoter. This leads to expression of the IE1 and IE2 proteins, necessary for initiation of lytic infection, and other IE genes that are important for efficient HCMV gene expression and replication (Bresnahan & Shenk 2000). pp71 translocation back to the cytoplasm during late infection leads to silencing of the majority of viral genes, which is important for establishment of a latent state (Penkert & Kalejta 2012). pp71 expression and its RNA have not been detected during latency. In addition, expression of pp71 mRNA does not lead to activation of lytic cycle in latently infected cells (Reeves & Sinclair 2010). It is reported that pp71 deletion mutant CMVs that lack pp71 in their tegument have 100 fold decrease in growth and show severe defect in expression of the IE genes (Bresnahan & Shenk 2000). The ability of pp71 to activate gene expression goes beyond the HCMV genome since it can also activate the herpes simplex virus type 1 (HSV-1) genome lacking functional proteins, such as the IE protein ICP0. pp71 disrupts the quiescent state of HSV-1 and resumes viral gene expression suggesting a similar function as HSV-1 ICP0 protein in suppression of the host innate antiviral defense (Everett et al. 2013).

The HCMV genome is divided into two regions known as the unique long region (UL) and the unique short region (US). pp71 is the product of the 82nd open reading frame on the UL region and therefore it is also referred to as ppUL82 (phosphoprotein expressed from UL82) (Chee et al. 1990). Primary amino acid sequence of pp71 analysis revealed sequence similarity to 2′-deoxyuridine 5′-triphosphate pyrophosphatase (dUTPase) however, it lacks some of the conserved residues required for enzymatic activity and its dUTPase function has not been confirmed (Davison & Stow 2005). The pp71 mid-region (MR), amino acids 94-300, have been identified as necessary for its localization to the nucleus (Fig. 4-1) (Shen et al. 2008). Nine phosphorylation sites have been identified on pp71 with one on threonine 223 within the MR, which has been proposed to be involved in pp71 cytoplasmic export (Fig. 4-1) (Shen et al. 2008). Since pp71 Thr223 is phosphorylated in the tegument, it is proposed that this phosphorylation occurs during late infection to promote pp71 transport to the cytoplasm where it can be packaged into virions (Shen et al. 2008).

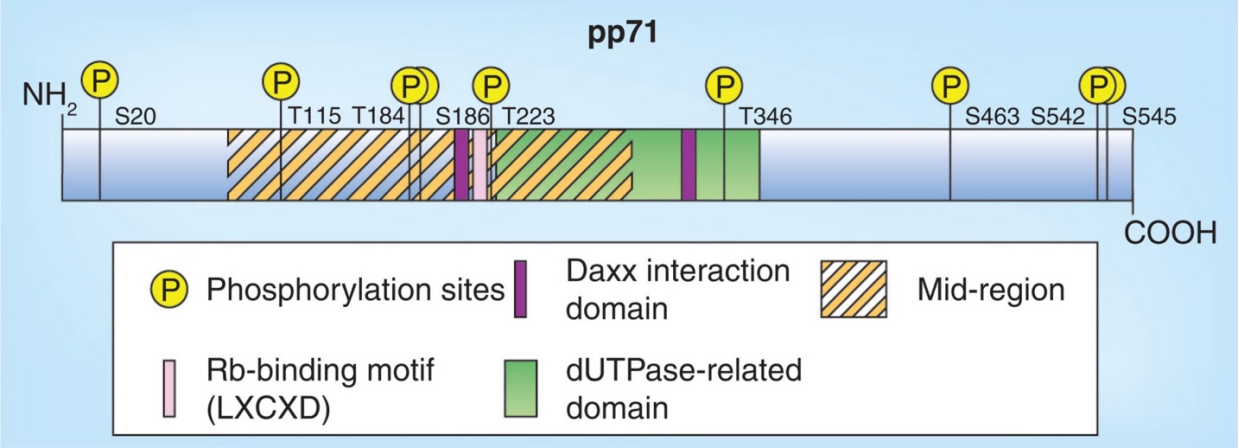

Fig. 4-1: Schematic representation of pp71 sequence and domains. Known phosphorylation sites are indicated. Mid-region (residues 94-300) important for nuclear localization, two DAXX interaction sites (residues 206-213 and 324-331) and Rb family binding motif (residues 216-220) have been identified. *S*: Serine; *T*: Threonine. (Reprinted by permission from Future Medicine: Future Virology, (Penkert & Kalejta 2012), copyright 2012).

Nuclear localization of pp71 upon viral entry into the cell depends on the differentiation status of the host cells. It has been observed that when HCMV infects fully differentiated cells, such as fibroblasts, it is immediately delivered to the nucleus where it localizes to promyelocytic leukemia nuclear bodies (PML-NBs) and initiates lytic infection (Penkert & Kalejta 2010; Hensel et al. 1996). However, infection of poorly differentiated cells, such as $CD34^+$, leads to the cytoplasmic accumulation of pp71 and establishment of the latent state (Penkert & Kalejta 2010). It has been shown that compared to specialized cells, incompletely differentiated cells lack factors that are important for nuclear translocation of pp71 (Penkert & Kalejta 2010).

In the nucleus pp71 interacts with or disrupts function of the PML-NB components including PML, DAXX and ATRX (Hensel et al. 1996). PML and DAXX are regulated by interferons and are involved in antiviral response. PML-NBs are the sites of DNA synthesis for DNA viruses and their components in many cases are recruited by these viruses (Maul 1998). Further, PML-NBs are important sites for p53 tumor suppressor protein acetylation, which is indispensable for its transactivation and induction of cell cycle arrest (Reed & Quelle 2015; Pearson et al. 2000). pp71 localization to PML-NBs and the stimulation of IE gene expression depend on its interaction with the cellular DAXX protein, which subsequently leads to degradation of DAXX (Saffert & Kalejta 2007; Ishov et al. 2002). Investigation of the pp71 interaction with cellular proteins has proven challenging due to the observation that pp71 leads to degradation and decrease in the half-life of proteins it binds to. Since proteasome inhibitors have been able to restore levels of pp71 interacting proteins, their degradation is considered proteasome dependent (Winkler et al., 2013).

pp71 Interaction with Cellular Proteins:

DAXX, death domain associated protein, is a transcriptional co-repressor that localizes to PML-NBs (Hofmann et al., 2002). It forms a complex with ATRX (chromatin remodeling protein) and acts as a histone chaperon for H3.3, a histone variant. The DAXX/ATRX complex formation is essential for H3.3 deposition into heterochromatin, maintenance of heterochromatin H3K9me3 modification and suppression of transcription at telomeres (He et al. 2016; Voon & Wong 2016). DAXX in complex with ATRX recruits histone deacetylases to the histones around the HCMV major IE promoter at PML-NBs and silences IE gene expression (Reeves & Sinclair 2013; McFarlane & Preston 2011). Localization of the ATRX to PML-NBs entirely depends on its interaction with DAXX. Shortly after HCMV infection (~2 h) ATRX is displaced from PML-

NBs and spreads evenly in the nucleus (Lukashchuk et al., 2008). pp71 mutants unable to interact with DAXX and UL82-null HCMV mutants were not able to relocate ATRX and could not support IE gene expression (Lukashchuk et al., 2008). In human osteosarcoma cell line (U2OS), where DAXX is present in normal levels while ATRX is undetectable, UL-82 null HCMV mutants were able to activate IE gene expression to levels comparable to that of wild-type HCMV infected fibroblast cells. This indicates that ATRX alone acts as a repressor of the major immediate early promoter and DAXX's role is to localize ATRX to the accumulated viral genome at PML-NBs (McFarlane & Preston 2011). Two regions on DAXX interact with two short motifs on pp71 N-terminal and central regions (Fig. 4-1) (Hofmann et al. 2002). Deletion of any one of these interaction sites abolishes pp71/DAXX interaction (Hofmann et al. 2002). pp71 interrupts DAXX/ATRX complex formation and leads to ubiquitin independent-proteasome dependent degradation of DAXX (Winkler et al., 2013). In latently infected cells, such as $CD34^{+}$, and during the late stage of viral infection DAXX remains stable since pp71 accumulates in the cytoplasm where it is packaged into new viral particles (Shen et al. 2008).

Shortly after discovery of the pp71 and DAXX interaction, identification of a retinoblastoma (Rb) binding motif (LXCXD, where X stands for any amino acid) in pp71 revealed that it interacts with all three members of the Rb family of tumor suppressor proteins including Rb, p107 and p130 (Fig. 4-1) (Kalejta et al., 2003). pp71 leads to the proteasomal dependent degradation of hypophosphorylated Rb proteins which results in induction of DNA synthesis in quiescent cells and cell cycle progression into S phase (Kalejta et al. 2003). Mutation of the pp71 Rb binding motif inhibited DNA synthesis activation in quiescent cells however, still allowed acceleration of the cell cycle through G1 phase. This observation indicated that aside from inhibition of the Rb proteins, pp71 should have other means of accelerating cell cycle progression (Kalejta & Shenk 2003).

Human USP7:

Human ubiquitin specific protease 7 (USP7) plays crucial roles in regulating cellular levels of the p53 tumor suppressor and other proteins involved in the p53 pathway, such as Hdm2, an E3 ligase and p53 negative regulator (Brooks et al. 2007). A highly conserved DWGF motif in the USP7 N-terminal tumor necrosis factor receptor-associated factor (TRAF) domain is efficiently recognized by its cellular substrates and interacting proteins through their (P/A/E)XXS sequence, where X stands for any amino acids and S is essential for this interaction (Sheng et al. 2006;

Saridakis et al. 2005). It's been shown in multiple cases that human herpesviruses (HHVs) have evolved to exploit this interaction site and hijack USP7 to deregulate p53 and promote cell cycle progression, which in some cases leads to tumor formation and cancer (Lee et al. 2009; Saridakis et al. 2005; Everett et al. 1997). Epstein-Barr nuclear antigen 1 (EBNA1) expressed by Epstein-Barr virus (EBV/HHV-4); viral interferon regulatory factor 1 and 4 (vIRF1 and vIRF4), latency-associated nuclear antigen 1 (LANA) and ORF45 expressed by Kaposi's sarcoma-associated herpesvirus (KSHV/HHV-8) interact with the USP7 N-terminal domain (NTD) at the same region as its cellular substrates and therefore block USP7-substrate interaction (Chavoshi et al. 2016; Gillen et al. 2015; Jager et al. 2012; Lee et al. 2011; Sarkari et al. 2010; Saridakis et al. 2005).

Project Rationale:

Amino acid sequence analysis of HCMV pp71 protein revealed three possible interaction sites with USP7-NTD. Two N-terminal motifs: ^{4}ASSS^{7} and ^{10}EGPS^{13} and one C-terminal sequence: ^{547}ASTS^{550} (Fig. 4-2). The amino acid sequence ^{10}EGPS^{13} in pp71 N-terminal region is identical to that of EBNA1, vIRF1 and ORF45 (of KSHV), which mediate interaction with the USP7 N-terminal DWGF motif (Fig. 4-3) (Chavoshi et al. 2016; Gillen et al. 2015; Saridakis et al. 2005). In addition, similar to pp71, human USP7 is also found to associate with PML-NBs and negatively regulate PMLs through recruitment of other cellular proteins (Sarkari et al., 2011). HHV proteins such as ICP0 (expressed by HSV-1) and EBNA1 (expressed by EBV), which both are known to disrupt PML-NBs and cause degradation of the PML proteins also interact with USP7 with high affinity (Sivachandran et al. 2008; Boutell et al. 2003). Interaction with USP7 was shown important for ICP0 and EBNA1 mediated disruption of PML-NB components (Sivachandran et al. 2008; Parkinson & Everett 2000). Furthermore, DAXX, which itself is a substrate of USP7, was shown to interact with Hdm2 and USP7 simultaneously and secure USP7 mediated stabilization of Hdm2 (Tang et al. 2013; Tang et al. 2006). siRNA knockdown of USP7 significantly decreased half-life and cellular levels of DAXX, indicating the important role of USP7 in stabilizing DAXX (Tang et al., 2010). Considering pp71's disruptive effect on PML-NBs, its strong interaction with and downregulation of DAXX and its effect on cell cycle progression, it proved to be a good candidate for interaction with USP7. Therefore, we investigated the possible pp71 interaction with the USP7 N-terminal domain.

```
         10          20          30          40          50          60
MSQASSSPGE GPSSEAAAIS EAEAASGSFG RLHCQVLRLI TNVEGGSLEA GRLRLLDLRT

         70          80          90         100         110         120
NIEVSRPSVL CCFQENKSPH DTVDLTDLNI KGRCVVGEQD RLLVDLNNFG PRRLTPGSEN

        130         140         150         160         170         180
NTVSVLAFAL PLDRVPVSGL HLFQSQRRGG EENRPRMEAR AIIRRTAHHW AVRLTVTPNW

        190         200         210         220         230         240
RRRTDSSLEA GQIFVSQFAF RAGAIPLTLV DALEQLACSD PNTYIHKTET DERGQWIMLF

        250         260         270         280         290         300
LHHDSPHPPT SVFLHFSVYT HRAEVVARHN PYPHLRRLPD NGFQLLIPKS FTLTRIHPEY

        310         320         330         340         350         360
IVQIQNAFET NQTHDTIFFP ENIPGVSIEA GPLPDRVRIT LRVTLTGDQA VHLEHRQPLG

        370         380         390         400         410         420
RIHFFRRGFW TLTPGKPDKI KRPQVQLRAG LFPRSNVMRG AVSEFLPQSP GLPPTEEEEE

        430         440         450         460         470         480
EEEEDDEDDL SSTPTPTPLS EAMFAGFEEA SGDEDSDTQA GLSRALILTG QRRRSGNNGA

        490         500         510         520         530         540
LTLVIPSWHV FASLDDLVPL TVSVQHAALR PTSYLRSDMD GDVRTAADIS STLRSVPAPR

        550
PSPISTASTS STPRSRPRI
```

Fig. 4-2: Human cytomegalovirus primary amino acid sequence. Identification of possible USP7 N-terminal domain interaction sites in pp71 sequence.

Material and Methods:

Plasmids and Expression of Recombinant Proteins:

N-terminal 6xHis fusion tagged USP7 residues 54-205 (USP7-NTD), USP7 residues 62-205 (USP7-NTD$^{62-205}$) and mutant D164A/W165A USP7 residues 62-205 (USP7-NTD^{DW}) were expressed from pET15b vector as described previously (Holowaty et al. 2003). 6xHis tagged USP7 amino acids 535-1102 (USP7-CTD) were expressed from p15TVL vector as described previously (Pfoh et al. 2015). Full-length 6xHis tagged USP7 was expressed in *Spodoptera frugiperda* (Sf9) cells from pFastBac vector, kindly provided by Dr. Lori Frappier (Holowaty et al., 2003). N-terminal GST fusion tagged USP7 amino acids 1-205 (GST-USP7-NTD) was expressed from pGEX-2TK plasmid vector as described previously (Jagannathan et al. 2014). HA-tagged full-length pp71 (Ul-82 gene) was expressed from pcGN71 plasmid (kindly provided by Dr. Tom Shenk). FLAG-tagged full-length or deletion mutant pp71 constructs were generated by PCR amplification and insertion of residues 1-559, 8-559, 16-559, 1-538, 8-538, 16-538 between the BamHI and XbaI sites of pcDNA3.1/FLAG vector (Invitrogen, V790-20).

Protein Purification:

All USP7 constructs were expressed in *E. coli* BL21 mgk cells in TB (Terrific broth, Bioshop) (except ^{15}N 6xHis tagged USP7 which was expressed in M9 media) with overnight 0.4 mM isopropyl β-D-1-thiogalactopyranoside induction at 16ºC. For NMR titration, uniformly labeled 6xHis tagged N-terminal USP7 residues 54-205 (USP7-NTD) was expressed in M9 media enriched with 0.7 g/L $^{15}NH_4Cl$ as the sole nitrogen source. Cells expressing 6xHis tagged recombinant proteins were harvested at 7,446 x g for 20 minutes at 4ºC followed by sonication at 30% amplitude in 50 mM Tris pH 7.5, 500 or 150 mM NaCl, 5 mM Imidazole, 1x protease inhibitor cocktail (1 mM Benzamidine and 0.5 mM PMSF) and 1x Protease inhibitor tablet (Roche cOmplete ULTRA Tablets). Lysates were clarified by centrifugation for 1 hour at 41,287 x g for 30 minutes at 4ºC. Supernatants were allowed to interact with nickel-nitrilotriacetic acid beads (Qiagen) for 1 hour on a nutator at 4ºC. Beads were washed extensively with 50 mM Tris pH 7.5, 500 or 150 mM NaCl and 20 mM Imidazole. Proteins were eluted with addition of 50 mM Tris pH 7.5, 500 or 150 mM NaCl and 250 mM Imidazole. Cells expressing GST fusion tagged proteins were sonicated at 30% amplitude in 50 mM Tris pH 7.5, 150 mM NaCl, 1x protease inhibitor cocktail (1mM Benzamidine and 0.5 mM PMSF) and 1x Protease inhibitor

tablet (Roche cOmplete ULTRA Tablets). The lysates were cleared by centrifugation and allowed to interact with glutathione-Sepharose resin (GE Healthcare) for 1 hour on a nutator at 4ºC. After extensive washing with 50 mM Tris pH 7.5 and 150 mM NaCl, proteins were eluted with addition of 20 mM reduced glutathione (GSH).

Peptide Synthesis and Preparation:

Wild-type pp71 peptide co-crystallized with USP7 and used in NMR studies (^{7}SPGEGPSSEA^{16}) and the mutant pp71 peptide with point mutation in Ser50 to alanine (^{7}SPGEGP<u>A</u>SEA^{16}) were synthesized with both N-terminal acetylation and C-terminal amidation to mimic the native peptides (CanPeptide Inc., Montreal, Canada). N-terminal FITC labeled wild-type (^{7}SPG<u>EGPS</u>SEA^{16}), (^{2}SQ<u>ASSS</u>PGE^{10}), (^{545}ST<u>ASTS</u>STP^{553}) and Ser50 to alanine mutant (^{7}SPGEGP<u>A</u>SEA^{16}) pp71 peptides used in fluorescence polarization assays were also synthesized with both N-terminal acetylation and C-terminal amidation by CanPeptide Inc. (Montreal, Canada).

Fluorescence Polarization Binding Assay:

USP7-NTD was further purified by size-exclusion chromatography using a HiLoad 16/60 Superdex 200 (GE Healthcare) on an ÄKTApurifier 10 UPC system (GE Healthcare) in 150 mM NaCl and 50 mM Tris pH 8.0. FITC labeled pp71 wild-type (^{7}SPG<u>EGPS</u>SEA^{16}), (^{2}SQ<u>ASSS</u>PGE^{10}), (^{545}ST<u>ASTS</u>STP^{553}) and mutant (^{7}SPG<u>EGPA</u>SEA^{16}) peptides were initially dissolved in dimethyl sulfoxide dimethyl sulfoxide to a final concentration of 10 mM. Then 400 nM working stock of each peptide was prepared in assay buffer (150 mM salt, 50 mM Tris pH 8.0, 5% glycerol and 0.01% Triton X-100). 518 µM of USP7-NTD was serially diluted and incubated with 40 nM of each peptide. 10 µl of the above dilutions were transferred into a 384 well plate (Corning) and fluorescence polarization was measured on a Synergy H4 microplate reader (BioTek, USA) with λex = 485 nm and λem = 520 nm. To obtain the equilibrium dissociation constant (K_d), polarization values were analyzed by Graphpad Prism 5.0 using a one-site binding model. K_ds were calculated based on three individual experiments and used to calculate the standard deviation.

NMR Spectroscopy:

To prepare samples for NMR, uniformly labeled ^{15}N-USP7-NTD was incubated with thrombin to cleave the 6xHis fusion tag followed by dialysis into NMR buffer (200 mM NaCl, 25 mM sodium phosphate pH 7.0 and 10 mM DTT). Interaction of USP7-NTD with wild-type pp71 peptide (^{7}SPGEGPSSEA^{16}) and mutant pp71 peptide (^{7}SPGEGPASEA^{16}) was monitored by analyzing ^{1}H-^{15}N HSQC spectra. Up to 0.4 mM unlabeled wild-type or mutant pp71 peptide was titrated in 0.2 mM of ^{15}N-USP7-NTD (containing 10% D_2O) up to 2:1 peptide:USP7 molar ratio. NMR data were recorded at 25ºC using a triple resonance cryoprobe-equipped Bruker 700 MHz NMR spectrometer. Spectra were processed with Topspin 3.2 and analyzed with SPARKY program (Ye et al. 2012; Monleon et al. 2002).

GST Pull-Down Assay:

Full-length FLAG-tagged pp71 and its deletion mutant constructs were transfected into U2OS cells and lysate was collected 24 hours post transfection. Prior to GST pull-down assays, purified GST-tagged USP7-NTD was dialyzed against assay buffer (100 mM NaCl, 50 mM Tris pH 8.0, 5% glycerol, 5 mM β-Mercaptoethanol and 1x Protease inhibitor tablet (Roche cOmplete ULTRA Tablets). 2.5 nmoles of GST-USP7-NTD or GST alone (as negative control) were incubated with 20 µl of pre-equilibrated glutathione-Sepharose resin for 1 hour. The resin was then briefly washed with assay buffer and incubated with 100 µg of U2OS lysate containing each of the FLAG-tagged pp71 constructs in assay buffer for 2 hours at 4ºC. Mixtures were then transferred to a micro column and after extensive wash with assay buffer, bound proteins were eluted with 20mM reduced glutathione. Samples were resolved on 12% SDS-polyacrylamide gels. USP7-NTD and GST were detected by Coomassie Blue staining, while FLAG-tagged pp71 proteins were detected by immunoblotting using a FLAG antibody.

FLAG Pull-Down Assay:

Prior to FLAG pull-down assay, purified His-tagged full-length USP7, USP7-NTD$^{62-205}$, USP7-NTD^{DW} and USP7-CTD were dialyzed against assay buffer (100 mM NaCl, 50 mM Tris pH 8.0, 5% glycerol, 5 mM β-Mercaptoethanol and 1x Protease inhibitor tablet (Roche cOmplete ULTRA Tablets)). U2OS cells were transfected with FLAG-tagged wild-type pp71$^{1-559}$ or empty pcDNA3.1/FLAG vector as negative control. Lysates were collected 24 hours post transfection. Anti-FLAG M2 affinity resin (Sigma) was pre-equilibrated with assay buffer. 500 µg of U2OS cell lysate, transfected with either FLAG-pp71 or empty pcDNA3.1/FLAG, was incubated with

anti-FLAG resin for 1 hour at 4ºC. Following a brief wash, anti-FLAG resin was incubated with 5 nmoles of each of the USP7 constructs in assay buffer for 2 hours at 4ºC. Samples were washed extensively with assay buffer and then boiled in SDS sample loading dye. Interacting proteins were resolved on 12% SDS-polyacrylamide gels and immunoblotted using His and FLAG antibodies.

Crystallization, X-ray Data Collection and Structure Determination:

Prior to setting up crystal trials, purified USP7-NTD was incubated with thrombin to remove the 6xHis N-terminal fusion tag. USP7 was further purified by size-exclusion chromatography using a HiLoad 26/60 Superdex 75 (GE Healthcare) on an ÄKTApurifier 10 UPC (GE Healthcare) in 500 mM NaCl and 20 mM Hepes pH 7.5. USP7-NTD (100 mg/ml) was co-crystalized with at least 5-fold molar excess of pp71 peptide (^{7}SPGEGPSSEA^{16}) at 4ºC using hanging-drop vapor-diffusion method. Rod-shaped crystals appeared after 4 days following one round of micro-seeding using USP7-NTD:UbE2E1 peptide crystals as seed in 30% PEG 4000, 0.1 M Tris pH 8.5 and 0.2 M $LiSO_4$ (Sarkari et al., 2013).

X-ray data were collected at 100K on a Rigaku MicroMax007 rotating anode diffractometer with a 944+ charge-coupled device detector. Diffraction data were integrated and scaled using HKL2000 software. The structure was determined by molecular replacement method employing USP7-NTD (Protein Data Bank identifier [ID] 1YY6, without the EBNA1 peptide) structure as the search model using CNS 1.3 (Brunger 2007). The electron density was visualized and the pp71 peptide model was built using Coot (Emsley & Cowtan 2004). CNS was used for refinement and water picking at 2.0 Å resolution. The data collection and refinement statistics are shown in Table 4-1. Fig. 4-8 was prepared using PyMOL (Schrödinger 2010).

Cell Culture and Antibodies:

Human osteosarcoma U2OS cells and human colon cancer HCT116 cells were grown in McCoy's medium. BJ human foreskin fibroblast cells (kindly provided by Dr. Sam Benchimol) were grown in Dulbecco's Modified Eagle's medium medium. All media were supplemented with 10% FBS and 1 mg/ml Penicillin-Streptomycin. The antibodies were rabbit polyclonal against USP7 (Bethyl Laboratories, A300-033A), mouse monoclonal against USP7 (Millipore, 05-1946), rabbit polyclonal against FLAG tag (Bethyl Laboratories, A190-102A), mouse

monoclonal against FLAG tag (Sigma, F3165), mouse monoclonal against p53 (Santa Cruz, sc-126), Rabbit polyclonal against DAXX (Upstate Biotechnology, 07-741), mouse monoclonal against Penta-His (Qiagen, 34660), Rabbit polyclonal against p21 (Santa Cruz, sc-397), rabbit polyclonal against phospho-p53 (Ser15) (Cell Signaling, 9284), rabbit monoclonal against ATM (Cell Signaling, 2873), rabbit mono- clonal against phospho-ATM (Ser1981) (Cell Signaling, 5883), mouse monoclonal against MDM2 (Santa Cruz, sc-965), rabbit polyclonal against phospho-MDM2 (Ser166) (Cell Signaling, 3521) and mouse monoclonal against GAPDH (Santa Cruz, sc-47724). To detect proteins of interest HRP-conjugated anti-mouse IgG (Jackson ImmunoResearch 115-035-166) and anti-rabbit IgG (Jackson ImmunoResearch 111-035-003) antibodies were used.

Co-immunoprecipitation:

U2OS cells were transfected with 9 μg pCMV/N-Myc-USP7 and 1 μg pcDNA3.1/FLAG-pp71 (wild-type or triple deletion mutant) vectors (total of 10 μg of DNA per 15 cm tissue culture plate) using PolyJet transfection reagent according to the manufacturer's protocol (SignaGen Laboratories). The cells were washed 6 hours post transfection and incubated with 10 μM MG132 proteasome inhibitor overnight. Cells were harvested 24 hours post-transfection and lysed in radioimmunoprecipitation buffer (50 mM Tris-HCl pH 8.0, 150 mM NaCl, 0.5% Nonidet P-40, 20% glycerol, 1X protease inhibitor cocktail (Roche)) followed by 2 sec sonication at 10% amplitude. Cell lysates were incubated with either rabbit polyclonal anti-USP7 primary antibody or rabbit polyclonal anti-FLAG primary antibody overnight at 4ºC followed by the addition of pre-cleared protein A/G Plus-Agarose beads (Santa Cruz, sc-2003) for 1 hour. Immunoprecipitates were washed with radioimmunoprecipitation buffer five times and then boiled in SDS sample buffer for 5 minutes at 95ºC. Samples were resolved on 12% SDS-polyacrylamide gels and immunoblotted using antibodies described above.

Immunoblotting:

All cells were transfected with pcDNA3.1/FLAG empty vector and pcDNA3.1/FLAG $pp71^{1-559}$ (wild-type) or $pp71^{16-538}$ (triple deletion mutant) vectors (4 μg of DNA per 15 cm tissue culture plate) using PolyJet transfection reagent according to the manufacturer's protocol (SignaGen Laboratories). U2OS cells were also co-transfected with 5 μg pCMV/N-Myc USP7 vector. Cells were harvested 24 hours post-transfection and lysed in radioimmunoprecipitation buffer (50 mM

Tris-HCl pH 8.0, 150 mM NaCl, 0.5% Nonidet P-40, 1X protease inhibitor cocktail (Roche)) followed by 1 sec sonication at 10% amplitude. Supernatants were boiled in SDS sample buffer for 5 minutes at 95ºC and resolved on 12% SDS-polyacrylamide gels. Immunoblotting was performed using antibodies described above.

Results:

pp71 Sequence Analysis for the USP7 N-Terminus Interaction Motifs:

To initiate viral IE gene expression, most immediate role of pp71 post HCMV infection is to translocate to the nucleus, interact with DAXX and disrupt the DAXX/ATRX complex (Ishov et al. 2002). USP7 interaction with DAXX is important for DAXX stability (Tang et al. 2010). Considering the interaction of DAXX with Hdm2 (a well-studied USP7 substrate) and its involvement in Hdm2 stability and p53 regulation, we believed pp71 would be a good candidate for interaction with USP7 (Tang et al. 2013; Tang et al. 2006). Such interaction would further disrupt the USP7/DAXX complex and lead to instability of DAXX. USP7 substrates, such as Hdm2, p53 and Hdmx, interact with the highly conserved ^{164}DWGF^{167} region in its N-terminal domain through their (P/A)XXS motifs with K_ds ranging from 8-45 μM (Sarkari et al. 2010; Sheng et al. 2006). While HHV proteins, such as EBNA1, ORF45 and vIRF1, bind the USP7 DWGF motif through an EGPS sequence (Chavoshi et al. 2016; Gillen et al. 2015; Saridakis et al. 2005). In case of EBNA1 and vIRF1, K_d ranges from 0.9-2 μM which is much lower than that of USP7 cellular substrates (Chavoshi et al. 2016; Sheng et al. 2006). Other USP7 interacting KSHV proteins, vIRF4 and LANA, bind the NTD domain through their ^{211}ASTS^{214} and ^{977}PGPS^{980} motifs (Lee et al. 2014; Jager et al. 2012).

We analyzed the pp71 sequence for possible interaction sites with USP7-NTD. Three candidate interaction motifs were identified in the pp71 sequence including two N-terminal ^{4}ASSS^{7} and ^{10}EGPS^{13} motifs and one C-terminal ^{547}ASTS^{550} sequence (Fig. 4-2). The ^{10}EGPS^{13} sequence in pp71 aligns with that of EBNA1, vIRF1 and ORF45 (Fig. 4-3). We examined the possibility of this interaction.

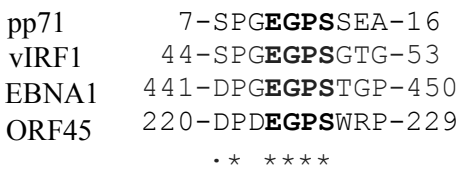

Fig. 4-3: Alignment of the pp71 EGPS motif with those of vIRF1, EBNA1 and ORF45 proteins. Asterisks represent conserved residues, and the period represents semi-conserved substitution.

Binding Analysis of pp71 Peptide and USP7-NTD:

To investigate interaction of the pp71 (^{7}SPGEGPSSEA^{16}) peptide with USP7-NTD, we first performed a fluorescence polarization binding assay. Fluorescein isothiocyanate (FITC) tagged pp71 peptide with the potential USP7 binding motif (^{7}SPGEGPSSEA^{16}) and mutant pp71 peptide with an alanine substitution for serine (^{7}SPGEGP<u>A</u>SEA^{16}) were titrated with increasing concentration of USP7-NTD to obtain the dissociation constant. 40nM fixed concentration of FITC labeled pp71 wild-type (^{7}SPGEGPSSEA^{16}) and mutant (^{7}SPGEGP<u>A</u>SEA^{16}) peptides were titrated in increasing concentrations of USP7-NTD of 0-518 μM. Complex formation was measured by detecting changes in the polarization values. A dissociation constant (K_d) of 4.6 ± 0.3 μM was obtained for wild-type peptide while K_d of mutant peptide increased to 126.4 ± 9 μM (Fig. 4-4A). This K_d value indicates higher affinity for USP7-NTD than its cellular substrates such as Hdm2 and p53 and compares well with that of vIRF1 and EBNA1.

The experiment was repeated to investigate potential binding of ASTS and ASSS motifs of pp71 with USP7-NTD. FITC tagged pp71 peptides, ^{2}SQ<u>ASSS</u>PGE^{10} and ^{545}ST<u>ASTS</u>STP^{553}, were titrated with increasing concentration of USP7-NTD of 0-664 μM. Dissociation constants of 2.0 ± 0.2 μM and 18.7 ± 2.0 μM were obtained for ^{545}ST<u>ASTS</u>STP^{553} and ^{2}SQ<u>ASSS</u>PGE^{10} respectively compared to K_d of 3.4 ± 0.2 μM for the EGPS containing peptide ^{7}SPG<u>EGPS</u>SEA^{16} (Fig. 4-4B). These data suggest that all three pp71 binding sites can potentially interact with USP7-NTD.

A

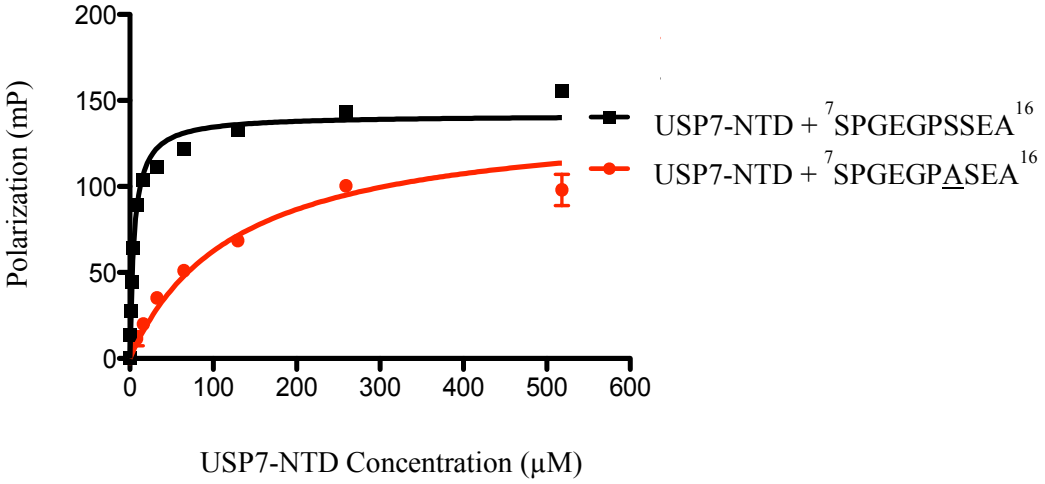

pp71 peptides	^{7}SPGEGPSSEA^{16}	^{7}SPGEGPASEA^{16}
K_d (μM)	4.6	126.4
S.D.	0.3	9

B

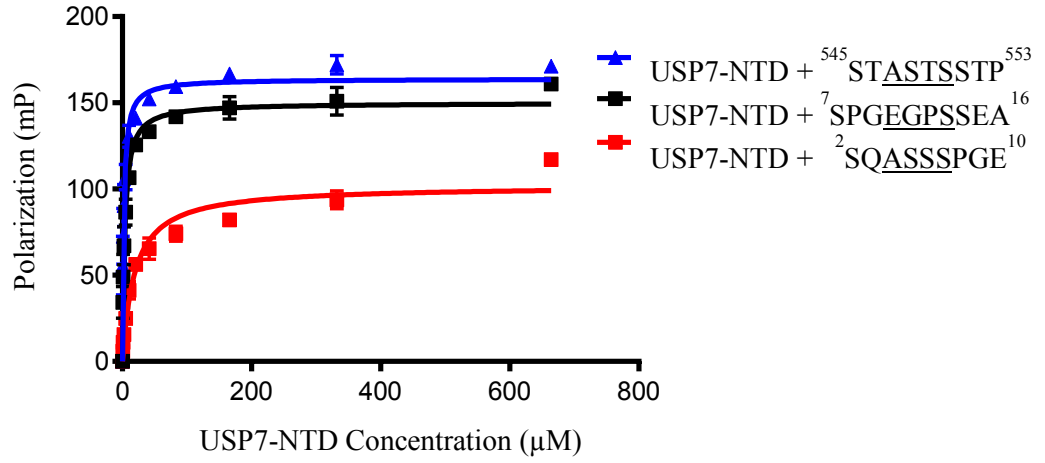

pp71 peptides	^{2}SQASSSPGE^{10}	^{7}SPGEGPSSEA^{16}	^{545}STASTSSTP^{553}
K_d (μM)	18.7	3.4	2.0
S.D.	2.0	0.2	0.2

Fig. 4-4: Binding analysis of USP7-NTD and pp71 peptides via fluorescence polarization assay. A) The assay was performed using FITC labeled wild-type pp71 peptide (^{7}SPGEGPSSEA^{16} in black) or mutant pp71 peptide (^{7}SPGEGP<u>A</u>SEA^{16} in red). Table represents dissociation constant (K_d) for the USP7-NTD interaction with FITC labeled wild-type and mutant pp71 peptides. B) Fluorescence polarization assay was performed using FITC labeled pp71 peptides (^{2}SQ<u>ASSS</u>PGE^{10} in red), (^{7}SPG<u>EGPS</u>SEA^{16} in black) and (^{545}ST<u>ASTS</u>STP^{553} in blue). Table represents dissociation constant (K_d) for the USP7-NTD interaction with FITC labeled pp71 peptides. *mP*, milipolarization. Error bars indicate standard error. Average values with standard deviation for four or more experiments are shown.

NMR Evidence for pp71 EGPS Motif Interaction with USP7-NTD:

After obtaining a K_d of 4.6 μM, we further monitored $^{1}H–^{15}N$ HSQC resonances of uniformly ^{15}N-labeled USP7-NTD in the presence and absence of unlabeled pp71 (^{7}SPGEGPSSEA^{16}) peptide. 0.2 mM concentration of ^{15}N-USP7-NTD was titrated with 0.4 mM of wild-type pp71 peptides (2:1 peptide to USP7-NTD ratio). Figure 4-5 represents the USP7-NTD ^{1}H-^{15}N HSQC spectra (in black) over-laid by USP7-NTD titrated with 0.4 mM of wild-type pp71 peptide (^{7}SPGEGPSSEA^{16} in blue). Strong disturbances were observed in the USP7-NTD chemical shift spectra after addition of pp71 peptide. Using the previously assigned USP7-NTD spectra (deposited in Biological Magnetic Resonance Data Bank Entry 6939), we were able to identify residues that were most disturbed by this interaction and compare the affected residues with that of EBNA1 and vIRF1 involved in binding with USP7-NTD (Chavoshi et al. 2016; Saridakis et al. 2005). Similar to that of EBNA1 and vIRF1, interaction of pp71 peptide with the USP7 N-terminal domain mostly affected residues from ß-strand 7 specially the conserved ^{164}DWGF^{167} motif such as Asp164, Trp165 (shift was observed in indole side chain), Gly166, Phe167, Ser168, and Met171 (Fig. 4-5 A&B). Residues from ß-strands 3, 4 and 6 such as Met100, Phe118 and Ser155 were also affected.

A

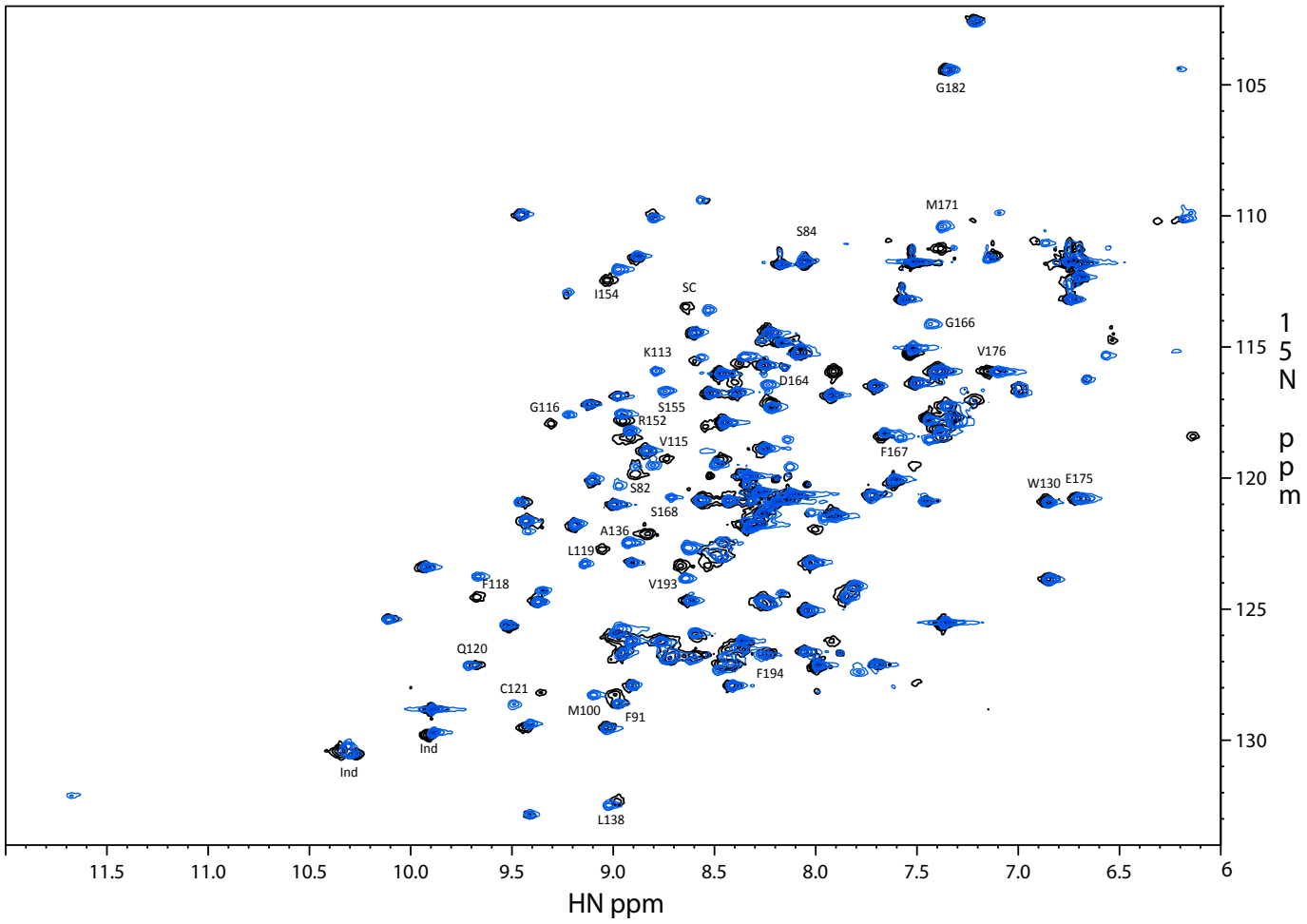
G182
M171
S84
I154
SC
G166
K113
V176
D164
G116
S155
R152
V115
F167
S82
W130
E175
S168
A136
L119
V193
F118
Q120
F194
C121
M100
F91
Ind
Ind
L138
105
110
115
120
125
130
15N ppm
11.5
11.0
10.5
10.0
9.5
9.0
8.5
8.0
7.5
7.0
6.5
6
HN ppm

B

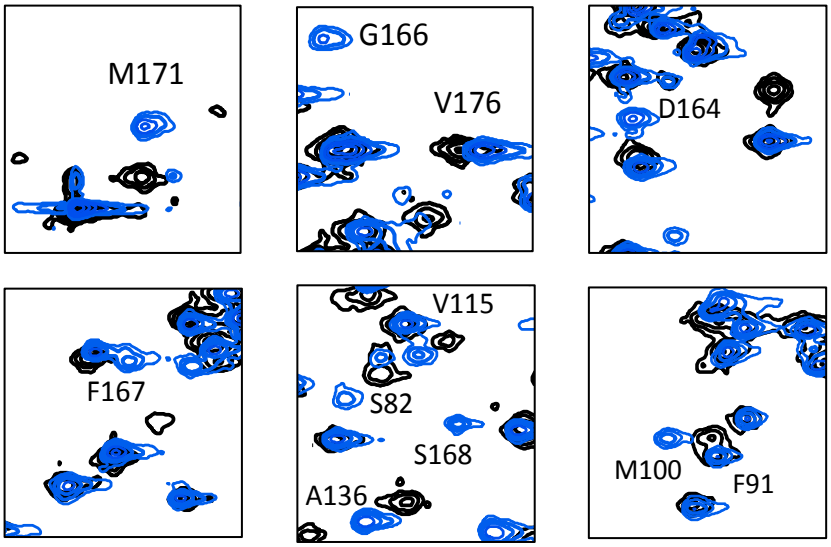
M171
G166
V176
D164
F167
V115
S82
S168
A136
M100
F91

Fig. 4-5: Superimposed ^{15}N HSQC spectra of USP7-NTD before and after titration with pp71 peptide. A) ^{15}N-labeled USP7-NTD spectra (in black) was titrated with 2:1 molar ratio of wild-type pp71 peptide ^{7}SPGEGPSSEA^{16} (in blue). B) Residues from USP7-NTD ß-strand 7 and M100 from ß-strand 3 that were largely affected by pp71 peptide interaction are shown.

pp71 Specifically Interacts with the USP7 N-Terminal Domain:

To further examine pp71 interaction with USP7 we performed an *in vitro* FLAG tag pull-down assay using anti-FLAG affinity resin. FLAG and His antibodies were used to detect pp71 and USP7 constructs respectively. U2OS cell lysate transfected with full-length FLAG-tagged pp71 or empty pcDNA3.1/FLAG vector, as negative control, were first incubated with anti-FLAG affinity resin and later with either full-length USP7, USP7 N-terminal or USP7 C-terminal domains. Both full-length USP7 and USP7-NTD were retained by the FLAG-tagged pp71, while U2OS lysate expressing empty pcDNA3.1/FLAG vector was not able to pull-down any of the USP7 constructs. Also, the C-terminal domain of USP7 did not show any interaction with pp71, indicating that pp71 exclusively recognizes the USP7 N-terminal domain (Fig. 4-6A). We then tested interaction of FLAG-tagged pp71 with double mutant USP7-NTD^{DW} containing alanine substitution for Asp164 and Trp165 within the ^{164}DWGF^{167} motif. USP7-NTD with mutations in the DWGF motif lost its interaction with pp71, indicating the importance of ^{164}DWGF^{167} for pp71 recognition and binding with the USP7 N-terminus (Fig. 4-6B).

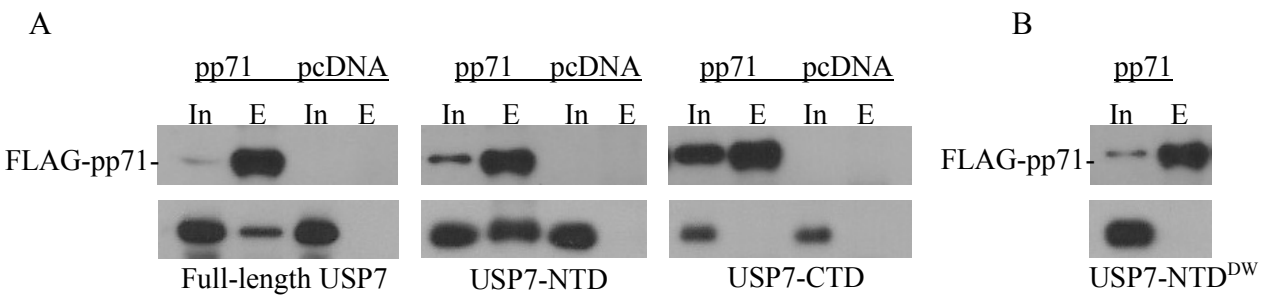

Fig. 4-6: pp71 interacts with the USP7 N-terminal domain *in vitro*. A) FLAG-tag pull-down experiments showed that U2OS cell lysate expressing FLAG-pp71 was able to pull-down full-length USP7 and USP7-NTD but not USP7-CTD. U2OS lysate expressing empty pcDNA3.1/FLAG vector was used as control. B) pp71 did not pull-down double mutant USP7-NTD^{DW} with alanine substitution for DW in the ^{164}DWGF^{167} motif. *In*, input; *E*, elution.

Investigating Interaction of the Three USP7-NTD Binding Sites of pp71:

As previously shown, other than ^{7}SPGEGPSSEA^{16} sequence two more possible USP7 N-terminal domain interaction motifs were identified in pp71 (Fig. 4-2). Binding affinity of ^{2}SQASSSPGE^{10}, ^{7}SPGEGPSSEA^{16} and ^{545}STASTSSTP^{553} peptides were initially investigated through FITC polarization assay. To further study the interaction of USP7 binding sites of pp71: ^{4}ASSS^{7}, ^{10}EGPS^{13} and ^{547}ASTS^{550}, we designed and engineered five pcDNA3.1/FLAG vectors expressing FLAG-tagged pp71 deletion mutant constructs lacking one, two or all three possible interaction sites as follows: pp71$^{8-559}$ with deletion in the ^{4}ASSS^{7} motif, pp71$^{16-599}$ with deletion in both ^{4}ASSS^{7} and ^{10}EGPS^{13} motifs, pp71$^{1-538}$ missing the C-terminus ^{547}ASTS^{550} sequence, pp71$^{8-538}$ with deletions in the ^{4}ASSS^{7} and ^{547}ASTS^{550} motifs and pp71$^{16-538}$ missing all three potential interaction sites.

A series of GST pull-down assays were set up to test interaction of the FLAG-tagged pp71 constructs with the GST-tagged USP7 N-terminal domain. 2.5 nmoles of GST-USP7-NTD, was allowed to interact with GST beads. Later beads were incubated with 100 µg of U2OS cell lysate expressing either full-length or one of the deletion mutant pp71 constructs. GST-USP7-NTD was detected by Coomassie Blue staining, while the FLAG-tagged pp71 constructs were detected by western blot, using FLAG antibody. All pp71 constructs retained binding with GST-USP7-NTD except the triple mutant pp71, FLAG-pp71$^{16-538}$, lacking all three binding sites. These observations revealed that all three USP7 N-terminal domain interaction sites of pp71 are able to recognize and bind USP7, indicating a strong evolutionary pressure for interaction of pp71 with USP7.

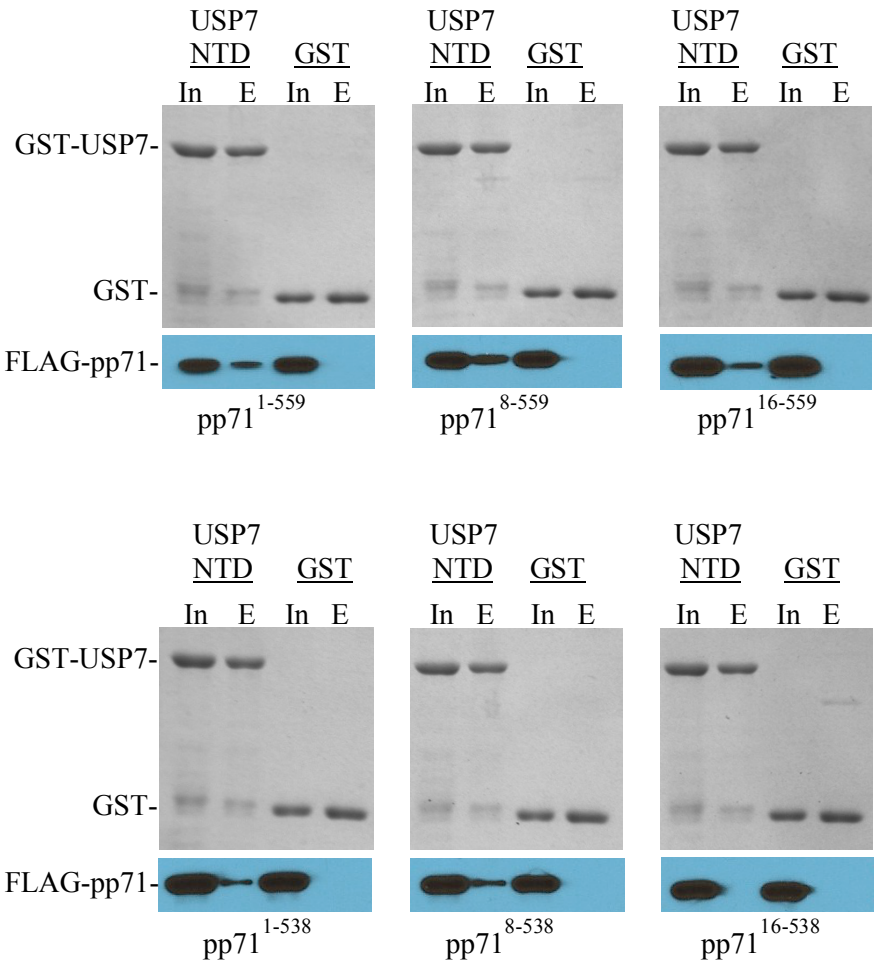

Fig. 4-7: All three USP7-NTD interaction motifs of pp71 bind the USP7 N-terminal domain. GST pull-down assay was performed using GST-tagged USP7-NTD and either full-length or one of the deletion mutant pp71 constructs. FLAG-tagged full-length pp71 (residues 1-559) and deletion mutant constructs missing either one, two or three of the ^{4}ASSS^{7}, ^{10}EGPS^{13} and ^{547}ASTS^{550} motifs were expressed in U2OS cells. All of the FLAG-tagged pp71 constructs retained binding with USP7-NTD except pp71$^{16-538}$ with deletion mutation of all three binding sites.

Co-crystal Structure of the USP7-NTD and pp71 Peptide:

To gain further insight into the molecular basis of this interaction, we setup trials to obtain a complex crystal of USP7-NTD and pp71 ^{7}SPGEGPSSEA^{16} peptide. Crystals were resolved to 2.0 Å resolution and the complex structure was determined using molecular replacement. There was no visible electron density for residues 54-62 and 106-111 and we could not fit them in the final model, suggesting that they are disordered. A summary of data collection and refinement statistics is presented in Table 4-1.

The structure of USP7-NTD has been previously well characterized (Saridakis et al. 2005). Briefly, the USP7-NTD forms an eight-stranded antiparallel beta sandwich similar to all MATH domain containing proteins (Fig. 4-8, A & B). The pp71 peptide ^{7}SPGEGPSSEA^{16} was found on the surface of USP7 and interacts with residues in β-strand 7 of the USP7 N-terminal domain, which contains the conserved ^{164}DWGF^{167} motif. Electron density only allowed building of pp71 residues ^{7}SPGEGPSS^{14} into the map and there was no visible density for residues Glu15 and Ala16 (Fig. 4-8C). A closer look at the site of interaction reveled that pp71 Ser13, which is essential for the ^{7}SPGEGPSSEA^{16} interaction with the USP7 N-terminal domain, makes the most extensive contact (Fig. 4-8D). Ser13 interacts with Asp164 of β-strand 7 by forming two hydrogen bonds, one through its hydroxyl side chain and one through its backbone amide group. The Ser13 carbonyl group also forms a hydrogen bond with Arg104 of β-strand 3. Glu10 of pp71 forms H-bond with Trp165 of β-strand 7 through its side chain carboxylic acid. Also, the carbonyl group of pp71 Ser7 forms a H-bond with side chain amide of Asn169 of β-strand 7. There are 4 hydrogen bonds formed through backbone interactions between pp71 peptide and USP7 β-strand 7. A comparison between pp71 ^{7}SPGEGPSSEA^{16} peptide and that of EBNA1 and vIRF1 revealed that they are superimposable and have similar mode of interaction with the USP7 N-terminal binding pocket (Fig. 4-8, E-H).

Table 4-1: USP7-NTD:pp71 Peptide X-Ray Data Collection and Refinement Parameters.

	USP7-NTD:pp71 peptide
X-Ray Data	
Space Group	$P4_1$
Resolution (Å)	50.0 – 2.01
Unit Cell Axes ($Å^3$)	70.0 x 70.0 x 45.5
Molecules / AU	1
Total Observations (#)	70748
Unique Reflections (#)	14708
Intensity ($I/\sigma<I>$)	32.4 (9.6)
Completeness (%)	99.1 (100)
[a]R_{sym}	0.087 (0.188)
Refinement	
R_{work}	0.157
R_{free}	0.195
Protein Atoms (#)	1298
Water Molecules (#)	135
rmsd bonds (Å)	0.010
rmsd angles (°)	1.25
rmsd dihedrals (°)	25.3
rmsd improper (°)	0.87
thermal factors ($Å^2$)	22.20
Ramachandran Plot	
Most Favoured	0.97

Numbers in brackets refer to the highest resolution shell, 2.04 Å to 2.01 Å. [a]$R_{sym} = \Sigma |I-<I>| / \Sigma I$ where I is the observed intensity and <I> is the average intensity from multiple observations of symmetry-related reflections.

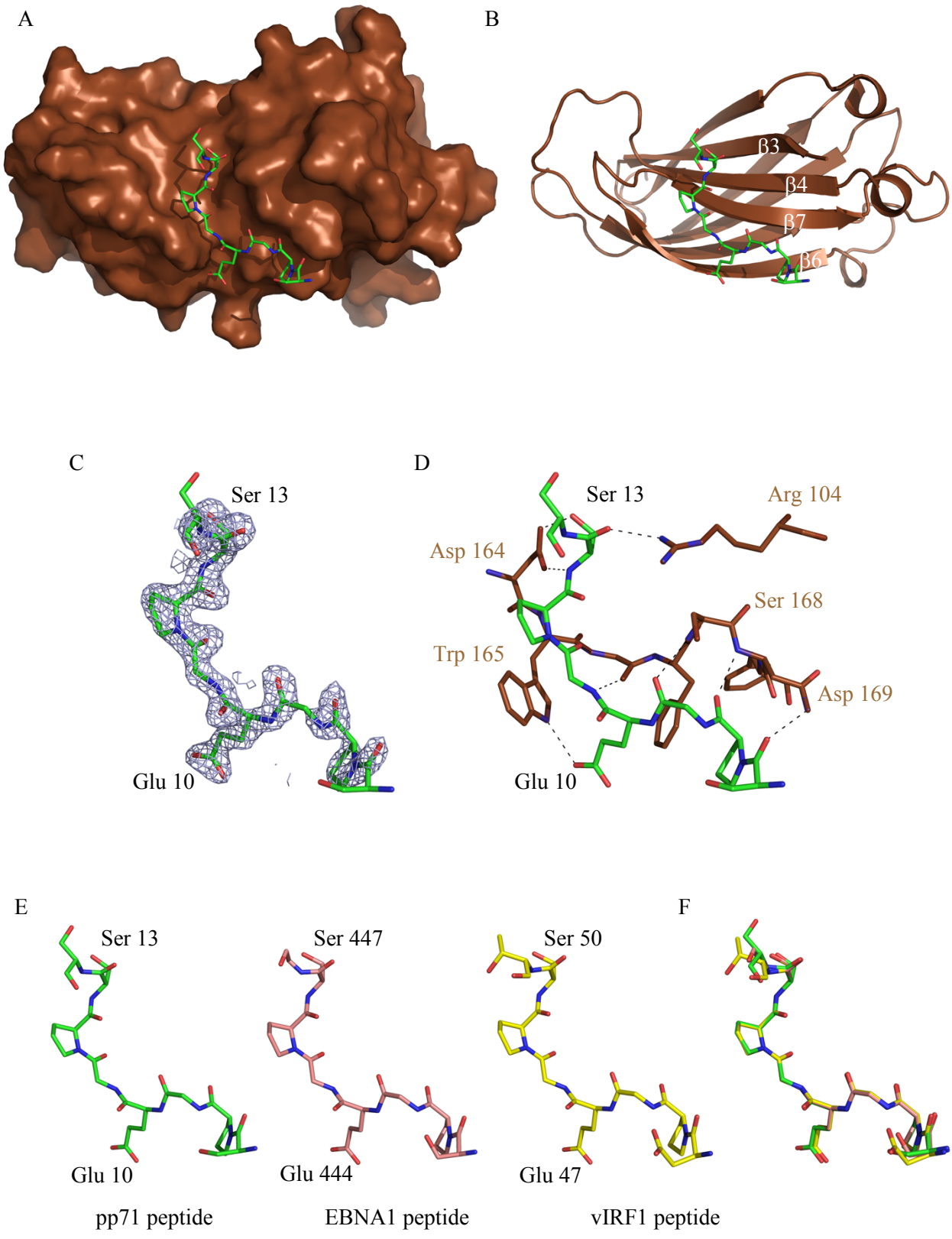
A
B
β3
β4
β7
β6
C
Ser 13
Glu 10
D
Ser 13
Arg 104
Asp 164
Ser 168
Trp 165
Asp 169
Glu 10
E
Ser 13
Glu 10
pp71 peptide
Ser 447
Glu 444
EBNA1 peptide
Ser 50
Glu 47
vIRF1 peptide
F

Fig. 4-8: Complex crystal structure of USP7-NTD and pp71 peptide. A) Surface representation of the USP7 N-terminal domain (brown) bound to pp71 peptide ^{7}SPGEGPSSEA^{16} in stick form (green). B) Ribbon diagram representation of USP7-NTD (brown) and pp71 peptide in stick form (green). C) Electron density of the pp71 peptide. D) Detailed interactions between USP7-NTD (brown) and pp71 peptide (green). Dashed lines indicate hydrogen bonds. E) Comparison between pp71 peptide (^{7}SPGEGPSSEA^{16}, green) with that of EBNA1 (^{441}DPGEGPSTGP^{450}, pink) and vIRF1(^{44}SPGEGPSGTG^{53}, yellow). F) Superimposition of the three peptides.

Effect of pp71 on the Cellular Levels of USP7:

Previously it was reported that pp71 decreases cellular levels of proteins it interacts with, such as DAXX and the Rb family (Rb, p107 and p130), in a ubiquitin independent but proteasome dependent manner (Winkler et al. 2013; Kalejta et al. 2003). Thus, we investigated the effect of pp71 on USP7. Experiment was performed in three cell lines: human fibroblast cells, human osteosarcoma cells (U2OS) and human colon cancer cells (HCT116). FLAG and USP7 antibodies were used to detect pp71 and USP7 levels respectively. First U2OS cells transfected with wild-type FLAG-pp71$^{1\text{-}559}$ and Myc-USP7 were incubated for 24 or 48 hours (Fig. 4-9A). Within 24 hours post transfection, a significant decrease in the level of USP7 was observed as compared to cells that were transfected with empty pcDNA3.1/FLAG vector. U2OS, BJ fibroblast and HCT116 cells were transfected for 24 hours with wild-type pp71$^{1\text{-}559}$ or triple mutant pp71$^{16\text{-}538}$ (Fig. 4-9B-D). It was interesting to observe that even though triple mutant pp71$^{16\text{-}538}$ lost its binding with USP7-NTD (Fig. 4-7) it was still able to decrease cellular levels of USP7. This observation suggest that decreases in the levels of USP7 might not be caused by direct interaction with pp71 but through pp71 effect on another cellular factor. Fold change analysis revealed that in U2OS cells both wild-type and mutant pp71 ($p<0.01$) significantly reduced levels of USP7 by about 30% when compared with control (Fig. 4-9E). In fibroblast cells, wild-type and mutant pp71 decreased levels of USP7 by about 40 and 60% respectively ($p<0.05$) (Fig. 4-9F).

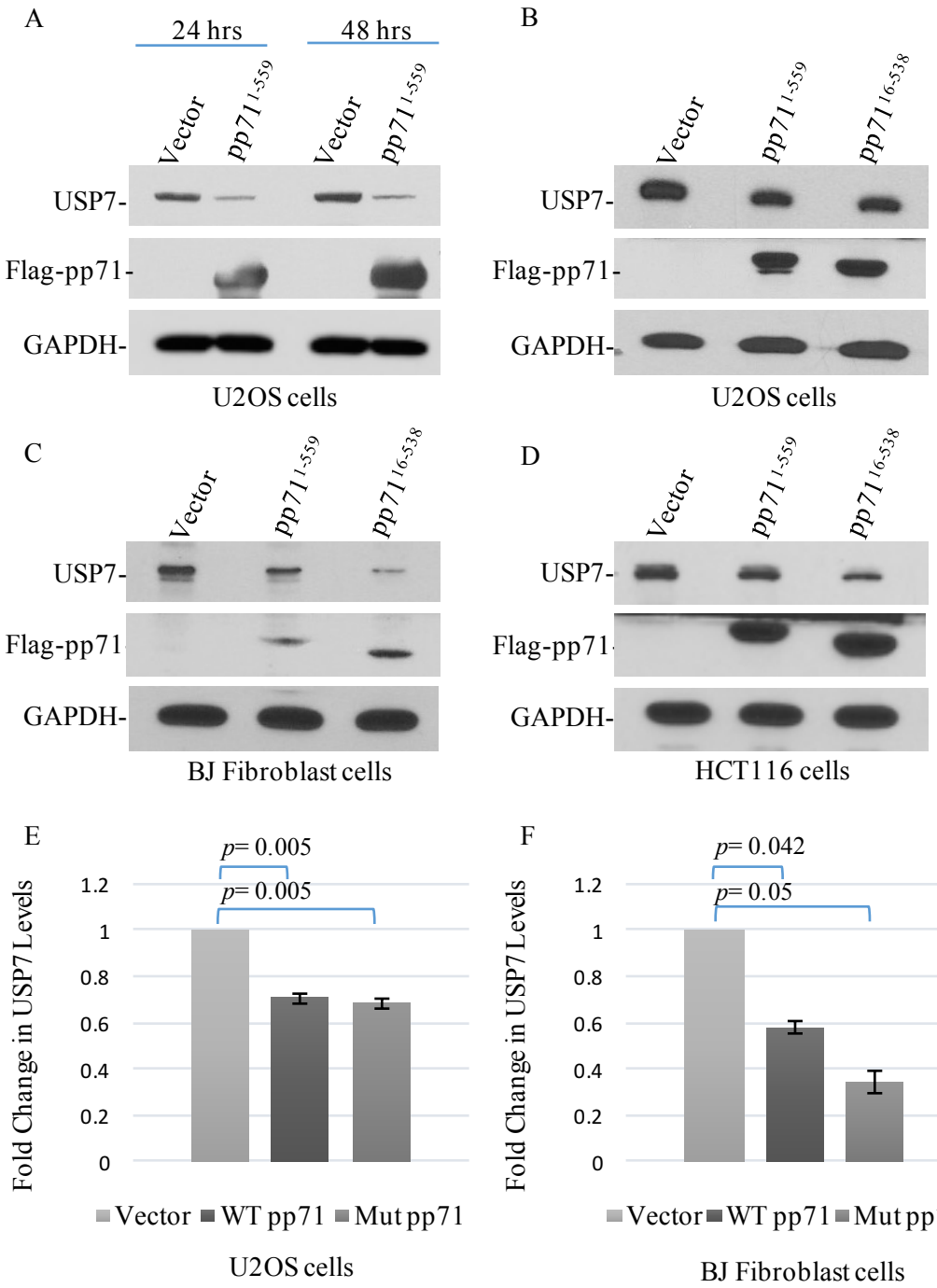
A
24 hrs
48 hrs
Vector
pp71 1-559
Vector
pp71 1-559
USP7-
Flag-pp71-
GAPDH-
U2OS cells
B
Vector
pp71 1-559
pp71 16-538
USP7-
Flag-pp71-
GAPDH-
U2OS cells
C
Vector
pp71 1-559
pp71 16-538
USP7-
Flag-pp71
GAPDH-
BJ Fibroblast cells
D
Vector
pp71 1-559
pp71 16-538
USP7-
Flag-pp71
GAPDH-
HCT116 cells
E
p= 0.005
p= 0.005
Fold Change in USP7 Levels
1.2
1
0.8
0.6
0.4
0.2
0
Vector
WT pp71
Mut pp71
U2OS cells
F
p= 0.042
p= 0.05
Fold Change in USP7 Levels
1.2
1
0.8
0.6
0.4
0.2
0
Vector
WT pp71
Mut pp71
BJ Fibroblast cells

Fig. 4-9: pp71 decreases cellular levels of USP7. A) U2OS cells were transfected with Myc-USP7 and FLAG-pp71 and further incubated for 24 or 48 hours post transfection. FLAG and USP7 antibodies were used to identify pp71 and USP7 respectively. B-D) U2OS, BJ fibroblast and HCT116 cells were transfected with either wild-type $pp71^{1-559}$, triple mutant $pp71^{16-538}$ or empty pcDNA3.1/FLAG vector as negative control. Cells were incubated for 24 hours post transfection. E&F) Fold change in USP7 was calculated by normalizing USP7 levels and comparing them to the vector ratio in U2OS and BJ fibroblast cells. A paired *t* test was used to calculate the statistical significance of the changes in USP7 levels after expression of wild-type (WT) or triple mutant (Mut) pp71. Error bars indicate standard error and are from three independently transfected U2OS or fibroblast cell lysates.

pp71 and USP7 Interaction *in vivo*:

To test *in vivo* interaction of pp71 with USP7, U2OS cells were transfected with Myc-USP7 and FLAG-tagged pp71. Previously we observed that pp71 significantly decreases USP7 levels therefore, *in vivo* immunoprecipitation assay was optimized to allow pull-down and detection of USP7. U2OS cells were transfected with only 1/5 of the recommended pp71 expression vector (based on manufacturer's protocol) and MG132 was used to inhibit proteasomal degradation. Also, cells were co-transfected with Myc-USP7 to increase the levels of available USP7 for immunoprecipitation.

U2OS lysate was incubated with USP7 antibody to immunoprecipitate USP7 followed by immunoblotting with FLAG antibody, which led to identification of FLAG-tagged pp71 (Fig. 4-10A). In a reciprocal experiment, lysate was incubated with FLAG antibody followed by immunoblotting with anti-USP7 which led to identification of USP7. Lysate incubated with rabbit IgG served as negative control which did not show any interaction. Further, we tested the effect of deletion mutations of pp71 ^{4}ASSS^{7}, ^{10}EGPS^{13} and ^{547}ASTS^{550} sequences on its binding with USP7. U2OS lysate transfected with Myc-USP7 and triple mutant pp71$^{16\text{-}538}$ was immunoprecipitated with anti-USP7 followed by immunoblotting with FLAG antibody (Fig. 4-10B). In a reciprocal experiment lysate was immunoprecipitated with FLAG antibody followed by immunoblotting using anti-USP7. In both cases USP7 did not co-immunoprecipitate with triple mutant pp71$^{16\text{-}538}$. Lysate immunoprecipitated with rabbit IgG served as negative control. Results indicate that wild-type pp71 but not the triple mutant pp71$^{16\text{-}538}$ interacts with USP7 *in vivo*.

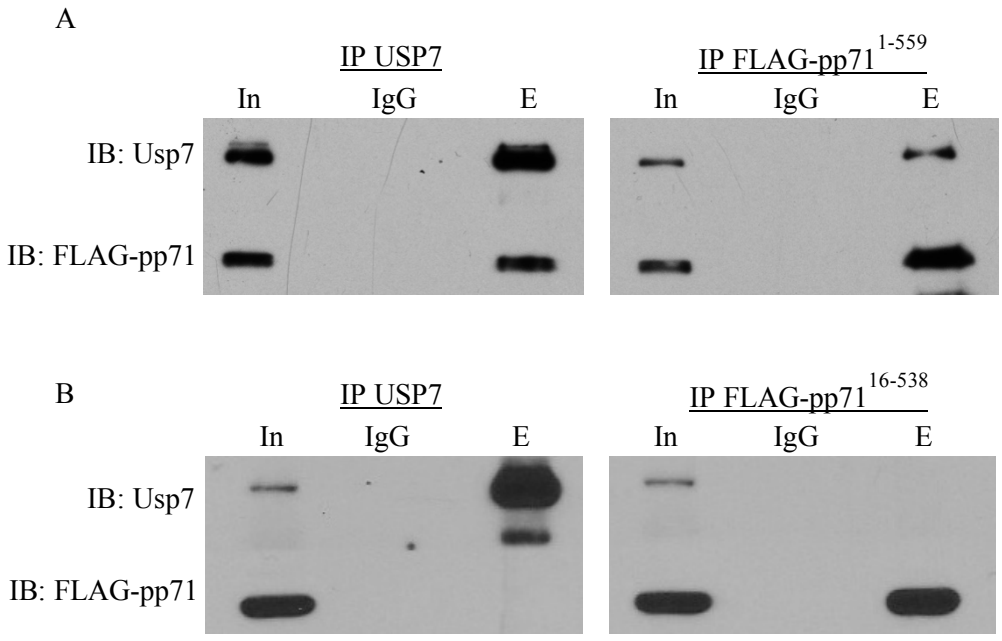

Fig. 4-10: Wild-type pp71 but not triple mutant pp71 interacts with USP7 *in vivo*. A) U2OS cells were transfected with wild-type FLAG-pp71 and Myc-USP7 followed by proteasome inhibition using MG132. Lysate was incubated with either USP7or FLAG antibodies to immunoprecipitated USP7 or pp71 respectively. In both cases USP7 and pp71 were successfully co-immunoprecipitated. Lysate incubated with rabbit IgG served as negative control. B) U2OS cells were transfected with deletion mutant FLAG-pp71$^{16\text{-}538}$ and Myc-USP7 followed by proteasome inhibition. Lysate was incubated with either USP7 or FLAG antibodies for immunoprecipitation. Mutant pp71$^{16\text{-}538}$ was not able to co-immunoprecipitate with USP7. *In*, input; *E*, elution.

pp71 Expression Effect on Hdm2 and p53 Levels in U2OS Cells:

USP7 is a critical regulator of p53 and Hdm2 stability and an important component of the USP7-Hdm2-p53 pathway. While both p53 and Hdm2 are deubiquitinated and stabilized through interaction with the USP7 N-terminal DWGF motif, Hdm2 is the preferred substrate and shows higher affinity (Brooks et al. 2007; Li et al. 2002). Considering that pp71 also interacts with the USP7-NTD DWGF motif and further decreases USP7 levels, we set out to investigate the effect of pp71 expression on p53 and Hdm2 stability. In addition, we monitored levels of Ser15 phosphorylated p53 and Ser166 phosphorylated Hdm2 post pp71 transfection. Ser15 phosphorylation is important for p53 stability and transactivation while Ser166 phosphorylation stabilizes Hdm2, by inhibiting its self-ubiquitination, and promotes its translocation to the nucleus, where it can target p53 (Reed & Quelle 2015; Feng et al. 2004). Further, we analyzed levels of p21, a cyclin-dependent kinase inhibitor and one of the major targets of p53 transactivation, to monitor p53 transcriptional activity (Cazzalini et al. 2010; Sun 2006). Cellular levels of DAXX were detected as a positive control for pp71 activity (Cantrell & Bresnahan 2006).

U2OS cells were transfected with FLAG-tagged wild-type $pp71^{1-559}$ and triple mutant $pp71^{16-538}$. In addition, all cells were transfected with Myc-USP7 to compensate for pp71 induced loss of USP7. Endogenous levels of p53 and Ser15 phosphorylated p53 as well as Hdm2 and Ser166 phosphorylated Hdm2 were detected. As shown in figure 11A, and shown previously in figure 9, both wild-type pp71 and triple mutant $pp71^{16-538}$ were able to decrease cellular levels of USP7. Wild-type $pp71^{1-559}$ was able to decrease Hdm2 (by 50%, $p=0.019$) and Ser166 phosphorylated Hdm2 in U2OS cells (Fig. 4-11 A&B), while mutant $pp71^{16-538}$ did not show any significant effect. We also observed a significant decrease of about 40% in the levels of p53 ($p=0.01$) and Ser15 p53 in U2OS cells within 24 hours post transfection with wild-type pp71 (Fig. 4-11 A&E). Mutant pp71 did not have a significant effect on Ser15 phosphorylated p53 however, p53 levels decreased by about 15% ($p=0.05$). Instability of p53 was followed by a drop in p21 levels, indicating decrease in p53 transcriptional activity. As reported previously, we also noticed decline in the levels of cellular DAXX post pp71 transfection (Ishov et al. 2002). These observations imply that in U2OS cells pp71 mediated downregulation of USP7 and DAXX destabilizes Hdm2 however, it seems the remaining Hdm2 and possibly the activity of other p53 negative regulators are potent enough to downregulate p53 when USP7 is compromised (Wang et al. 2011).

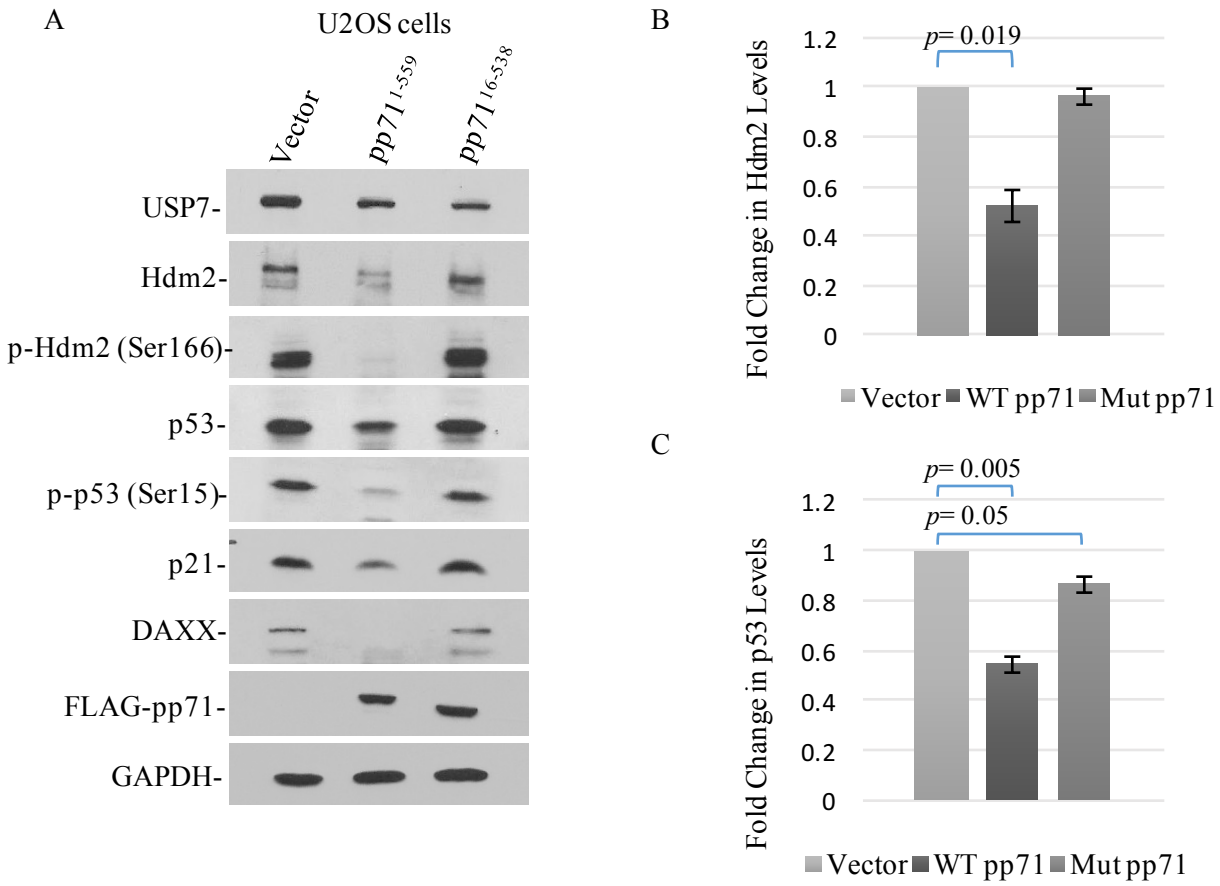

Fig. 4-11: The effect of pp71 expression on Hdm2 and p53 stability in U2OS cells. Cellular levels of p53, Ser15 phosphorylated p53 (p-p53), Hdm2 and Ser166 phosphorylated Hdm2 (p-Hdm2) were monitored in U2OS cells after transfection with Myc-USP7 and cotransfection with either wild-type pp71$^{1-559}$, mutant pp71$^{16-538}$ or empty pcDNA3.1/FLAG vector as control. Cells were collected 24 hours post transfection. DAXX and p21 levels were monitored as control for pp71 and p53 activity respectively. GAPDH levels were detected as loading control. B) Fold change in Hdm2 was determined by normalizing Hdm2 levels and comparing them to that of vector ratio in U2OS cells. C) Fold change differences in p53 were calculated by normalizing p53 levels and comparing them to that of vector ratio in U2OS cells. A paired *t* test statistical analysis was used to calculate the significance of changes in the Hdm2 and p53 levels after expression of wild-type (WT) pp71$^{1-559}$ and triple mutant (Mut) pp71$^{16-538}$. Error bars indicate standard error (n=3).

pp71 Expression Effect on Hdm2 and p53 Levels in BJ Fibroblast Cells:

We further investigated expression effect of pp71 on endogenous levels of p53, Ser15 phosphorylated p53, Hdm2 and Ser166 phosphorylated Hdm2 in human fibroblast cells. Cellular levels of DAXX and p21 were monitored as positive control for pp71 and p53 activity respectively. Fibroblast cells were transfected with FLAG-tagged wild-type $pp71^{1-559}$ or triple mutant $pp71^{16-538}$. As shown in figure 12A, and shown previously in figure 9, both wild-type $pp71^{1-559}$ and triple mutant $pp71^{16-538}$ were able to destabilize USP7. However, in contrast to what was observed in U2OS cells, in fibroblast cells both wild-type $pp71^{1-559}$ and mutant $pp71^{16-538}$ decreased Hdm2 (by 40%, $p<0.05$) and Ser166 Hdm2 levels (Fig. 4-12 A&B). Further, both wild-type and mutant pp71 also decreased cellular levels of p53 (by 40-50%, $p<0.05$) and Ser15 phosphorylated p53 within 24 hours post transfection (Fig. 4-12 A&C). Instability of p53 was followed by a drop in p21 level, indicating decrease in p53 transcriptional activity. We also noticed significant decrease in the levels of cellular DAXX in the presence of both wild-type and mutant pp71. Our results in figure 12 indicate that in fibroblast cells, the primary cells infected by HCMV, although triple deletion mutation in pp71 disrupts its interaction with USP7, it does not affect pp71 mediated downregulation of USP7 and DAXX, which is followed by decline in Hdm2 and p53 concentrations.

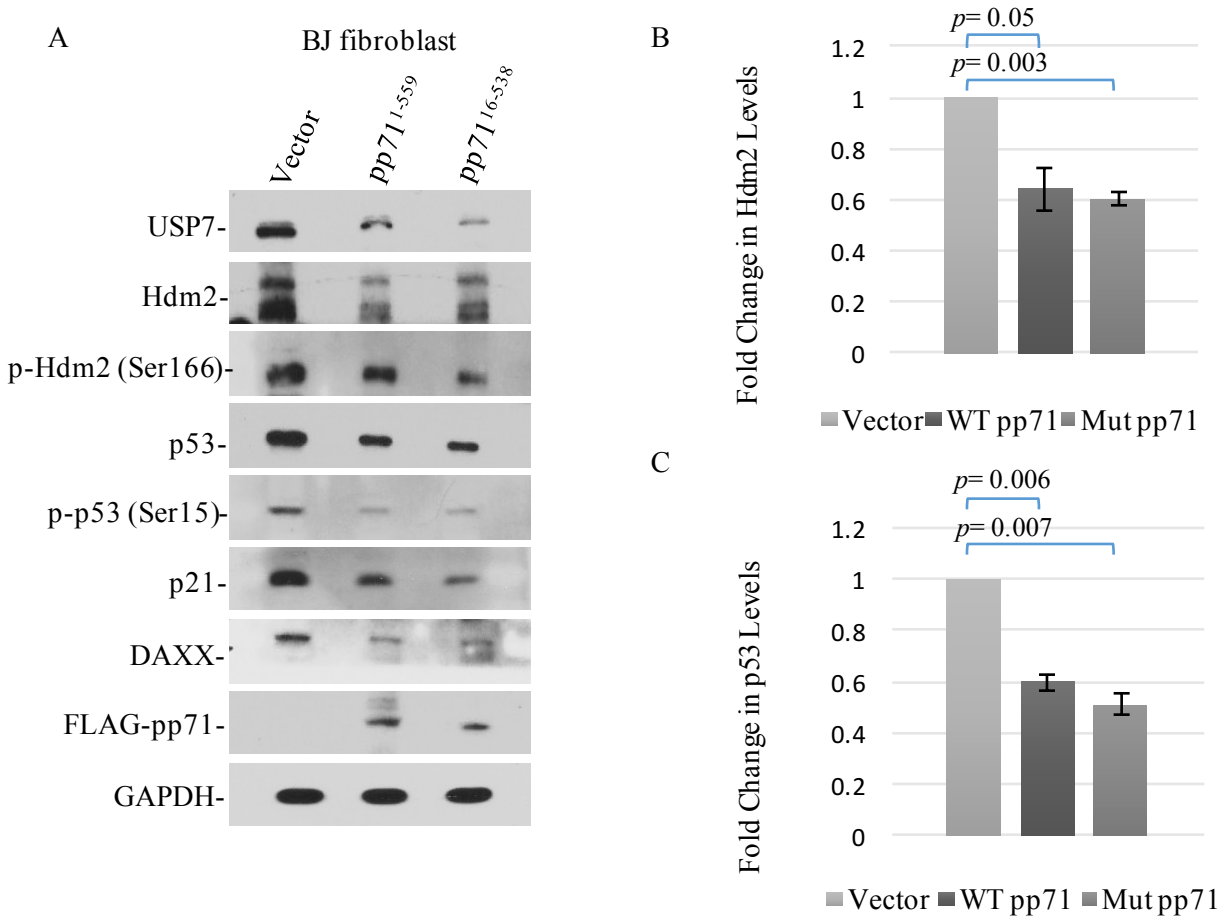

Fig. 4-12: The effect of pp71 expression on Hdm2 and p53 levels in BJ fibroblast cells. Cellular levels of p53, Ser15 phosphorylated p53 (p-p53), Hdm2 and Ser166 phosphorylated Hdm2 (p-Hdm2) were monitored in BJ fibroblast cells 24 hours post transfection with wild-type pp71$^{1-559}$, mutant pp71$^{16-538}$ or empty pcDNA3.1/FLAG vector as negative control. Levels of DAXX and p21 were monitored as control for pp71 and p53 activity respectively. GAPDH levels were detected as loading control. B) Fold change in Hdm2 was determined by normalizing Hdm2 levels and comparing them to that of vector ratio in fibroblast cells. C) Fold change differences in p53 were calculated by normalizing p53 levels and comparing them to that of vector ratio in fibroblast cells. A paired *t* test statistical analysis was used to calculate the significance of changes in Hdm2 and p53 levels after expression of wild-type (WT) pp71$^{1-559}$ and triple mutant (Mut) pp71$^{16-538}$. Error bars indicate standard error (n=3).

pp71 Expression Effect on ATM Kinase Stability:

Double stranded DNA (ds-DNA) breaks initiate kinase activity of ataxia telangiectasia mutated (ATM) serine-protein kinase through intermolecular autophosphorylation of serine 1981 (Bakkenist & Kastan 2003). DNA replication of some viruses, such as KSHV and HCMV, inside the nucleus exposes the ends of the viral genomes, which are recognized as ds-DNA breaks, and activate the ATM mediated ds-DNA damage response (Gaspar & Shenk 2006; Shin et al. 2006). It was observed that post HCMV transfection, several checkpoint proteins, including ATM kinase, instead of accumulating in the nucleus were mislocalized to the cytoplasm, resulting in suppression of the cellular DNA damage response (Gaspar & Shenk 2006). Considering that pp71 expression decreased Ser15 phosphorylated p53 levels and since ATM is responsible for Ser15 phosphorylation and stabilization of p53, we investigated ATM stability and its autophosphorylation on Ser1981 post pp71 transfection.

U2OS cells were transfected with Myc-USP7 followed by cotransfection with either wild-type $pp71^{1-559}$, triple mutant $pp71^{16-538}$ or empty vector as control. BJ fibroblast cells were transfected with wild-type $pp71^{1-559}$, triple mutant $pp71^{16-538}$ or empty vector. Levels of ATM and Ser1981 phosphorylated ATM were detected by western blotting using ATM and Ser1981-ATM antibodies. As shown in figure 13, wild-type pp71 transfection decreased cellular levels of ATM by about 40% in U2OS cells and 30% in BJ fibroblasts. Ser1981 phosphorylated ATM levels were also decreased in both cell lines within 24 hours post transfection (Fig. 4-13). In U2OS cells triple mutant $pp71^{16-538}$ lost its effect on ATM and Ser1981 phosphorylated ATM, while in fibroblast cells triple mutant $pp71^{16-538}$ still was able to significantly reduce ATM levels (p=0.015). These observations suggest that pp71, either directly or through indirect interactions, significantly destabilizes ATM (p=0.016 & 0.0002) and inhibits its autophosphorylation with in 24 hours post transfection.

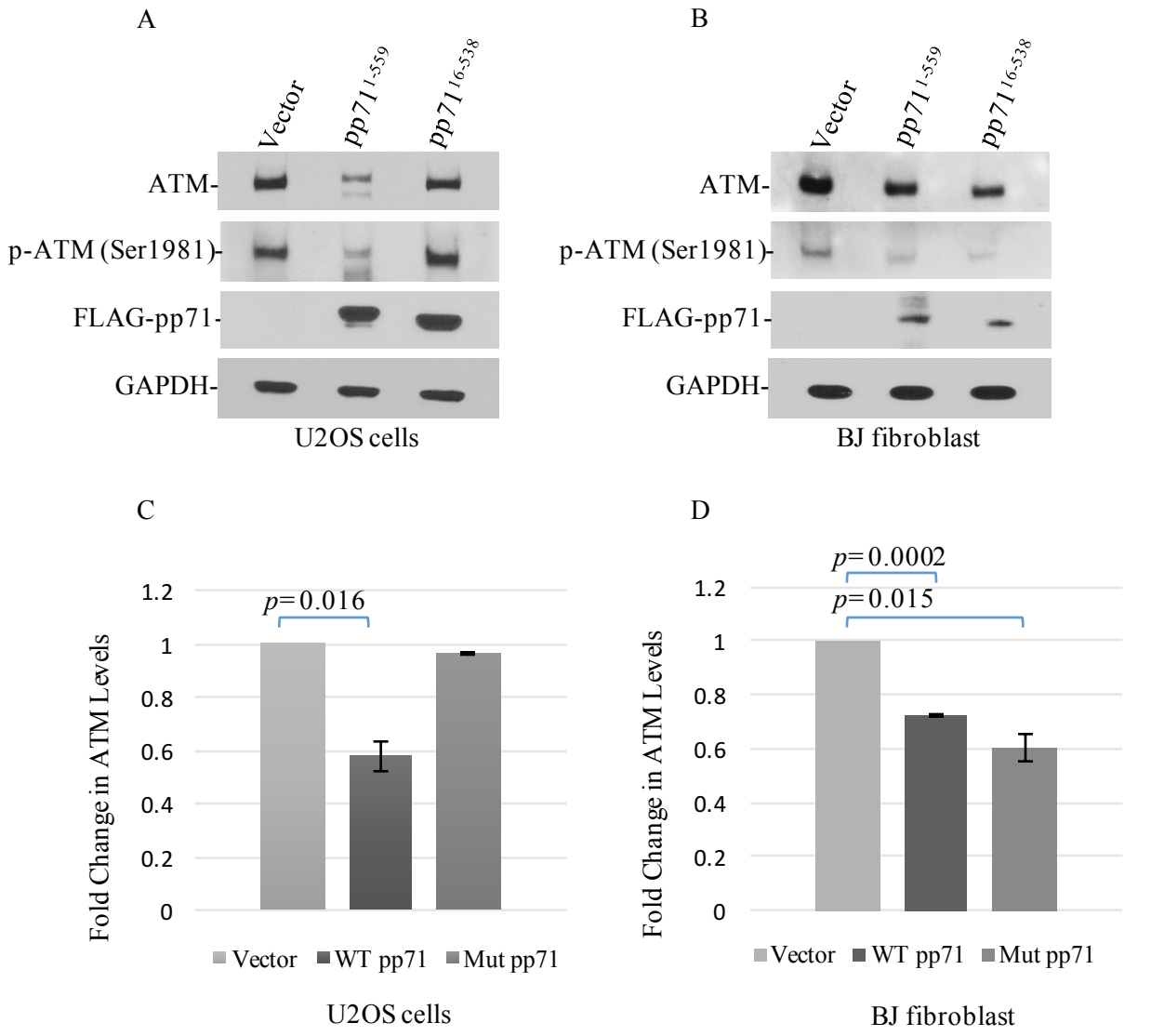

Fig. 4-13: The effect of pp71 expression on ATM kinase. (A) U2OS cells were transfected with Myc-USP7 followed by cotransfection with either wild-type pp71$^{1-559}$, triple mutant pp71$^{1-538}$ or empty pcDNA3.1/FLAG vector as negative control. (B) BJ fibroblast cells were transfected with wild-type pp71$^{1-559}$, triple mutant pp71$^{1-538}$ or empty pcDNA3.1/FLAG vector. 24 h post transfection whole cell lysates were collected and immunoblotting was performed using ATM, Ser1981 phosphorylated ATM and FLAG antibodies. GAPDH levels were monitored as loading control. C & D) Fold change differences in ATM was calculated by normalizing ATM levels and comparing them to that of vector ratio in U2OS (C) and fibroblast cells (D). A paired *t* test statistical analysis was used to calculate the significance of changes in ATM levels after expression of wild-type pp71$^{1-559}$ (WT) and triple mutant pp71$^{16-538}$ (Mut). Error bars indicate standard error (n=3).

Discussion

Human cytomegalovirus (HHV-5), similar to other members of the HHV family, has evolved to suppress the immune system and establish a latent state in the host. One of the mechanisms that HHVs employ to suppress the intrinsic cellular antiviral response is inhibition of the tumor suppression pathways and disruption of proteins that regulate cell cycle progression, such as p53 (Alibek et al. 2014). Proteins expressed by HSV-1, EBV, KSHV and HCMV interfere with the USP7-p53-Hdm2 pathway by either competitively interacting with or disrupting function of its components (Chavoshi et al. 2016; Pfoh et al. 2015; Salsman et al. 2012; Lee et al. 2011; Saridakis et al. 2005; Meredith et al. 1994). Loss of the p53 or inhibition of its transactivity is strongly correlated with cell transformation and oncogenesis (Kawauchi & Wolf 2014). In addition, HHVs disrupt PML nuclear bodies, sites of the cellular factors that inhibit initiation of the viral gene expression (Frappier 2011). They code for proteins that localize to PML-NBs and specifically target their components, such as PML, DAXX, Sp100 and ATRX (Tavalai & Stamminger 2011; Everett 2001). For instance, ICP0, expressed by HSV-1, is an E3 ligase involved in degradation of the host proteins. It destabilizes p53 through direct ubiquitination and by hijacking USP7 for self-stabilization (Boutell et al. 2005; Boutell & Everett 2003). Further, ICP0 induces degradation of PML proteins (Maul & Everett 1994). Similarly, EBNA1 expressed by EBV strongly binds the USP7 N-terminal domain and blocks USP7 interaction with its cellular substrates (Saridakis et al. 2005). EBNA1 also disrupts PML-NBs and decreases levels of PML through interaction with USP7 (Sivachandran et al. 2008). Likewise, vIRF1, vIRF4, LANA and ORF45 expressed by KSHV have been shown to interact with the USP7 N-terminal domain at the same site as its cellular substrates (Chavoshi et al. 2016; Jager et al. 2012; Gillen et al. 2015; Lee et al. 2011). They block USP7 substrate interaction, destabilize p53 and suppress p53 mediated apoptosis (Lee et al. 2009; Saridakis et al. 2005). vIRF1 and LANA also directly interact with p53 and inhibit its acetylation and transactivation, while vIRF4 destabilizes p53 by interacting with Hdm2 and inhibiting its autoubiquitination (Lee et al. 2009; Seo et al. 2001; Li et al. 2000; Friborg et al. 1999).

pp71, HCMV main tegument transactivator, has a crucial role in preparing the cellular environment for lytic infection and activation of IE gene expression (Torres & Tang 2015; Bresnahan & Shenk 2000). Upon release to the host cell cytoplasm, pp71 is immediately translocated to the nucleus and localizes to PML-NBs through interaction with DAXX, which subsequently leads to DAXX degradation and disruption of the DAXX/ATRX complex

(Lukashchuk et al. 2008; Ishov et al. 2002). Primary amino acid sequence analysis of pp71 revealed three potential interaction sites with the USP7 N-terminal domain including: ^{4}ASSS^{7}, ^{10}EGPS^{13} and ^{547}ASTS^{550}. Considering that USP7 localizes to PML-NBs and it is also known to interact with and stabilize DAXX, we investigated the possibility of pp71 interacting with USP7. The pp71/USP7 interaction was confirmed through *in vitro* biochemical, structural and functional studies. FITC polarization binding assays revealed that pp71 ^{2}SQ<u>ASSS</u>PGE^{10}, ^{7}SPG<u>EGPS</u>SEA^{16} and ^{545}ST<u>ASTS</u>STP^{553} peptides interact with the USP7 N-terminal domain with K_ds of 18.7 µM, 3.4 µM and 2.0 µM respectively. Binding affinities of ^{7}SPG<u>EGPS</u>SEA^{16} and ^{545}ST<u>ASTS</u>STP^{553} peptides are much higher than that of USP7 cellular substrates, such as Hdm2, p53 and Hdmx, that bind USP7-NTD with K_ds ranging from 8 to 45 µM (Sarkari et al. 2010; Sheng et al. 2006). A single point mutation of Ser13 to alanine in ^{7}SPG<u>EGPS</u>SEA^{16} peptide increased the K_d to 126.4 µM, indicating the importance of this residue in interaction with the USP7 N-terminal binding site.

In vitro pull-down experiments revealed that pp71 exclusively interacts with the USP7 N-terminal domain. Substitution mutations of Asp164 and Trp165 of the USP7 ^{164}DWGF^{167} motif to alanine abolished full-length pp71 interaction with USP7, indicating that pp71 (including all three USP7 interaction sites) recognizes and interacts with the DWGF motif of the USP7 N-terminal domain. In addition, we generated 5 deletion-mutant pp71 constructs missing one, two or all three potential USP7 N-terminal domain interaction sites of pp71. Only the pp71 construct with deletion mutation of all three potential USP7-NTD binding sites lost interaction, indicating that all three USP7 interaction sites of pp71 bind the USP7 N-terminal domain.

Further, we monitored the USP7-NTD ^{1}H-^{15}N HSQC spectra after titration with pp71 ^{7}SPGEGPSSEA^{16} peptide. Strong disturbances were observed mostly in the USP7-NTD ß-strand 7 residues comprising the conserved ^{164}DWGF^{167} motif and residues from ß-strands 3, 4 and 6. Observed disturbances in the USP7-NTD chemical shift closely correlated with residues that were affected by pp71 peptide interaction seen in our complex crystal structure of the USP7-NTD and pp71 ^{7}SPGEGPSSEA^{16} peptide. The pp71 peptide forms hydrogen bonds with Asp164, Trp165 and Asn169 of β-strand 7 and Arg104 of β-strand 3. Residues from β-strand 4 and 6 are affected due to close proximity to pp71 peptide but do not make polar contact. The pp71 peptide (^{7}SPGEGPSSEA^{16}), similar to that of EBNA1, vIRF1 and ORF45, instead of the more commonly identified USP7-NTD binding sequence of (P/A)XXS, contains a negatively charged glutamic acid residue and interacts with the DWGF motif of USP7-NTD through an EGPS

sequence. The glutamic acid residue in EGPS makes more H-bonds with the USP7 N-terminal domain DWGF motif and therefore increases the affinity of the EGPS containing proteins for USP7 compared to its cellular substrates or other viral proteins that incorporate a (P/A)XXS motif in their binding site. Identification of another USP7-NTD interacting herpesvirus protein suggests that these viruses target USP7 for its role in regulating stability of tumor suppressor proteins, such as p53.

Our functional analysis showed that pp71 not only interacts with USP7, it also significantly decreases its cellular levels. Even though triple deletion mutant $pp71^{16\text{-}538}$ loses its interaction with USP7, it was still able to reduce USP7 levels. Our findings suggest that direct interaction is not the only mechanism by which pp71 destabilizes USP7 and other cellular factors might be involved. In fibroblast cells both wild-type and mutant pp71 were still able to destabilize DAXX. This was expected as pp71 residues 206-213 and 324-331, that are involved in interaction with DAXX, are not altered in our deletion mutant pp71 construct (Hofmann et al. 2002). Further, USP7 was previously shown to interact with and stabilize DAXX (Tang et al. 2006). Deletion mutant pp71, that has lost its interaction sites with USP7-NTD, can potentially effect USP7 through simultaneous interaction with DAXX, which can bring pp71 and USP7 in close proximity. However, this hypothesis must be further investigated since in U2OS cell line triple mutant pp71 lost its reducing effect on DAXX but it was still able to destabilize USP7. This observation puts forward the possibility that pp71 recruits or regulates another cellular factor to exert its effect on USP7.

We noticed that in fibroblast cells, the primary cells infected by HCMV, wild-type $pp71^{1\text{-}559}$ and triple mutant $pp71^{16\text{-}538}$ were able to significantly decrease both p53 and Hdm2 levels. Downregulation of USP7 was expected to mainly effect p53 stability, since Hdm2 has higher affinity for USP7. Considering that simultaneous interaction of DAXX with USP7 and Hdm2 allows for efficient deubiquitination and stabilization of Hdm2 and since DAXX also enhances Hdm2 E3 ligase activity, it can be suggested that significant decrease in the levels of DAXX and USP7, under pp71 influence, compromises Hdm2 stability (Tang et al. 2006). This is supported by our *in vivo* data from U2OS cell line where triple mutant pp71 that was not able to alter DAXX levels had also no effect Hdm2, even though it was still able to decrease cellular levels of USP7. We further investigated the cellular levels of Ser166 phosphorylated Hdm2. Ser166 phosphorylation stabilizes Hdm2 by inhibiting its self-ubiquitination and promotes its shuttling to the nucleus, where it can target p53 (Feng et al. 2004; Mayo & Donner 2001; Lambert et al.

1998). In addition, Ser166/186 phosphorylated Hdm2 cannot interact with ARF, its negative regulator, and is more stable (Weber et al. 2000). Our results indicated decreases in the levels of Ser166 phosphorylated Hdm2, suggesting that post pp71 transfection, Hdm2 is mostly cytoplasmic and cannot affect p53. Also, decrease in Ser166 phosphorylation correlates with self-ubiquitination and instability of Hdm2, which further explains the observed decrease in Hdm2 levels. Ser166 and 186 phosphorylation of Hdm2 is mediated through PI3-kinase and its downstream targets, Akt/PKB kinases (Feng et al. 2004). Human herpesviruses such as HSV-1 and KSHV have already been shown to interact with PI3-kinase & deregulate the Akt/PKB signaling pathway (Wagner & Smiley 2011; Uddin et al. 2005).

Despite downregulation of Hdm2, p53 negative regulator, p53 levels showed significant decrease after transfection with pp71. In part instability of p53 can be correlated with downregulation of USP7. To further explain the concurrent decrease in the levels of p53 and Hdm2, we investigated Ser15 phosphorylated p53 levels. Ser15 is located in the Hdm2/p53 binding pocket and its phosphorylation inhibits p53 interaction with Hdm2 and stabilizes p53 (Moll & Petrenko 2003). Also, this phosphorylation is important for p300/CBT mediated acetylation and transcriptional activation of p53 (Iyer et al. 2004; Lambert et al. 1998). Our data indicated decreases in Ser15 phosphorylated p53 after pp71 transfection, which suggest increase in p53/H2m2 interaction. Further, we investigated cellular levels of p21, an essential mediator of the cell cycle arrest at G1/S and G2 phase and one of the major targets of p53 transactivation (Cazzalini et al., 2010). Reduced p53 levels post pp71 transfection was followed by decrease in p21 expression, indicating suppression of the p53 transcriptional activity.

It was previously reported that HCMV leads to the mislocalization of ATM, DNA damage check point protein, from the nucleus to the cytoplasm and inhibits its activation upon viral DNA replication (Gaspar & Shenk 2006). Observing a decrease in the levels of Ser15 phosphorylated p53 led us to investigate stability and auto-activation of ATM by monitoring ATM and Ser1981 phosphorylated ATM levels post pp71 transfection. ATM is a key kinase involved in the regulation of the USP7-p53-Hdm2 pathway components. Activated ATM phosphorylates Ser15 on p53 and thereby leads to its acetylation by p300 and transactivation (Shiloh & Ziv 2013). Further, ATM phosphorylates and activates cycle checkpoint kinase 2 (Chk2), which results in Chk2 mediated phosphorylation of p53 on Ser20 and interruption of the p53/Hdm2 interaction (Sancar et al., 2004). Consequently, Ser15/Ser20 phosphorylated p53 induces expression of its downstream targets such as p21 and leads to cell cycle arrest or apoptosis (Chehab et al. 2000;

Craig et al. 1999). In addition, activated ATM phosphorylates Hdm2 on Ser395 and inhibits Hdm2 mediated shuttling of p53 to the cytoplasm (Maya 2001). Furthermore, upon DNA break signal ATM mediated phosphorylation of DAXX on Ser564 disrupts DAXX/Hdm2 interaction and results in Hdm2 autoubiquitination and p53 stabilization (Tang et al. 2013). Indeed, we noted significant decrease in the levels of ATM and Ser1981 phosphorylated ATM, indicating that under pp71 influence not only ATM is destabilized, its auto-activation is also reduced. In fibroblast cells both wild-type and triple mutant pp71 were able to decrease levels of ATM which correlated with the observed decrease in the levels of p53 and p21. In U2OS cells, triple mutant pp71 that had lost its effect on ATM kinase was also unable to reduce p53 and p21 levels. Therefore, p53 destabilization despite downregulation of Hdm2 can be in part due to inhibition of ATM mediated phosphorylating of p53 on Ser15 and Ser20 (indirectly). In addition, decrease in p53 acetylation by p300/CBT further downregulates p53 and inhibits its transactivation.

It was noted that pp71 degradation of the Rb proteins results in the induction of DNA synthesis in quiescent cells and cell cycle progression into the S phase (Kalejta et al. 2003). However, mutation of the pp71 Rb binding motif still allowed cell cycle progression through the G1 phase, indicating that apart from inhibiting the Rb proteins pp71 should have other means of accelerating the cell cycle (Kalejta et al. 2003). In addition, it has been shown that activated ATM blocks the G1/S cycle progression by phosphorylating and activating Chk2 kinase and stabilizing p53, which together mediate arrest at the G1/S phase through expression of p21 (Sancar et al. 2004; Chehab et al. 2000). Our data shows significant decrease in the levels of ATM, activated Ser1981 phosphorylated ATM and p21 24 hours post pp71 transfection. Here we suggest that pp71, other than mislocalization of ATM kinase, inhibits cell cycle arrest through downregulation of ATM and p53.

In summary, we have identified that tegument transactivator pp71, expressed by human cytomegalovirus, as a novel interactor of USP7. Further, we have shown that pp71 targets USP7 and ATM to downregulate p53 induced cell cycle arrest upon entering the host cell. This correlates well with the function of pp71, which is preparing the cellular environment for HCMV immediate early gene activation and lytic infection.

Chapter 5: Thesis Summary, General Discussion and Future Directions

Summary:

Ubiquitin mediated degradation was first described by Hershko, Ciechanover and Rose in the 1990s which led to the 2004 Nobel Prize in Chemistry. Their discovery revealed that the system involved in proteolysis in eukaryotes is more complex than lysosomal degradation. Since then, extensive research and investigations have demonstrated that the process of protein ubiquitination and deubiquitination is far more sophisticated than was originally expected. To date, it is well appreciated that deubiquitinating enzymes, other than their essential role in protein stabilization, are implicated in many non-proteolytic cellular functions, such as protein trafficking, cell cycle progression, DNA repair and regulation of transcription (He et al. 2016; Hanpude et al. 2015).

Chapter 2: Investigating Expression and Purification of Yeast *S. cerevisiae* Ubps from *E. coli* for Protein Crystallography.

When I started my project, there were many ongoing investigations on the structure and function of human USP deubiquitinating enzymes; however, the roles in regulating cellular processes and the structures of budding yeast *S. cerevisiae* Ubps were not well characterized. *S. cerevisiae* Ubps have shown significant conservation of sequence, function and structure with their human homologues. Lack of introns in *UBP* genes and less complicated post-translational modifications make them more convenient targets for cloning, expression and purification and further functional studies compared to their human homologues. The availability of the *S. cerevisiae* complete genome sequence and the convenience of working with yeast proteins rather than more complicated eukaryotic orthologues persuaded us to start an investigation into yeast *S. cerevisiae* Ubp enzymes and examine the possibility of obtaining soluble Ubp constructs from *E. coli* (Heinicke et al. 2007). In chapter 2, I described my efforts in obtaining soluble recombinant *S. cerevisiae* Ubps from *E. coli*. I examined various optimization methods such as employing different expression vectors and designing multiple constructs per protein or per domains of each protein as recommended by previous publications (Luna-Vargas et al. 2011; Dyson et al. 2004). Out of 127 constructs that were designed to express 16 *S. cerevisiae* Ubps and their domains in *E. coli*, 10 soluble proteins were purified including Ubp1 (aa 92-741), Ubp3 catalytic domain (aa 449-912), Ubp6 full-length (aa 1-499), Ubp12 N-terminal domain (aa 1-361, 90-361 and 98-345) and Ubp15 N-terminal and C-terminal domains (aa 1-204 and 538-1230). I was able to obtain

protein crystals for *S. cerevisiae* Ubp1, Ubp6 and Ubp12 N-terminal DUSP domain. X-ray diffraction data obtained from Ubp6 protein crystal was used to determine the three-dimensional structure of its catalytic domain.

Despite designing 127 constructs for 16 *S. cerevisiae* Ubp enzymes (including Sad1 and Pan2 which are catalytically inactive Ubps) and extensive optimizations based on the previously tested methods (Dyson et al. 2004), we were able to obtain only 10% soluble expression of the recombinant proteins in *E. coli*. As was expected, expression in *E. coli,* even though convenient and less costly, is inefficient for eukaryotic proteins or their domains. Methods examined by other research groups to increase the efficiency of soluble recombinant protein expression in *E. coli*, such as expression of the same construct from a collection of vectors at once, have produced encouraging results (Luna-Vargas et al. 2011). If handling a large number of proteins, however, one would end up dealing with an overwhelming number of constructs. Another option is to use a yeast expression system. Even though much smaller amounts of recombinant protein are expressed in yeast, purification is more cumbersome and laboratory procedure is costly, expressed protein is potentially soluble and properly folded. Many research groups have explored the efficiency of different expression systems in yeast and have attempted to optimize them for high-level production of secreted as well as soluble cytosolic fusion proteins (Liu et al. 2012; Rasmussen et al. 2011; Mitchell et al. 1993; Romanos et al. 1992). Certain Ubps of interest can be expressed and purified from yeast using large multi-liters of culture to hopefully obtain enough protein for crystal trials. Full-length or domains of *S. cerevisiae* Ubps can be cloned in yeast expression vectors such as pEGH (based on pEG(KG) vector under the control of GAL1/10 promoter) for expression in *S. cerevisiae* (Zhu et al. 2001; Mitchell et al. 1993). Further, *S. cerevisiae* open reading frames (ORFs) collections, cloned into yeast expression plasmids, are commercially available. They code for more than 5000 yeast proteins with a C-terminal fusion tag (Gelperin et al. 2005). However, expression in *S. cerevisiae* results in much lower yield as compared to expression in *E. coli,* which makes protein purification for crystallization trials quite cumbersome. Therefore, to date expression of proteins in *E. coli* remains the easiest, quickest and cheapest method.

Automation of Protein Expression, Detection and Crystal Screening:

For future experiments, automation of steps involved in recombinant protein purification from *E. coli* cells that are interlinked, such as cell lysis, affinity binding and elution of the recombinant

proteins can speed up the experimental process. Also, automation of protein expression detection and solubility testing using methods such as 96-well microplate array sodium dodecyl sulfate-polyacrylamide gel electrophoresis and fusion tag interacting biarsenical fluorescein derivatives, which allow detection of small quantities of tagged proteins, will save a considerable amount of time when handling a large number of samples (Pomorski & Krezel 2011; Feldman et al. 2004).

Recently an automated droplet robot has been described which allows set up of crystallization screens using 4-8 nL droplets combined with microfluidic techniques, that involve preparation of nanoliters of protein samples in microchannels, valves or chambers (Zhu et al. 2014; Zhu & Fang 2013). The proposed automation method decreases required purified protein amounts by 50-500 fold as compared to the current 96 well crystal trial set ups (Zhu et al. 2014). Currently, available automated protein crystallization setups, such as Phoenix (Art Robbins Instruments, Inc.), Mosquito (TTP Labtech, Ltd.), and OryxNano (Douglas Instruments, Ltd.), allow preparation of trials with droplets in the range of 25-100 nLs. More advanced robotics techniques will make set up of crystal trials using small amounts of purified proteins from yeast expression system much more feasible. However, despite the high potential of the automated robotics for protein expression detection and crystallization screening, employing these techniques requires set up and operation of microfluidic devices and specific equipment and robotics which are not readily available in many structural biology labs.

Chapter 2: Crystal Structure of *S. cerevisiae* Ubp6.

I was able to express and purify the full-length Ubp6 protein (aa 1-499) from the p15TV-L vector in BL21 *E. coli* cells. Ubp6 protein crystals diffracted to 2.5 Å resolution. Even though full-length protein was crystallized, the electron density map only contained information for the Ubp6 catalytic domain, indicating the flexibility of the Ubp6 N-terminal Ubl domain. Superimposition of the Ubp6 catalytic domain residues 103-499 with that of USP14, its human homologue, revealed the conserved extended right-hand architecture (similar to that of the USP7 catalytic domain) with structures representing the thumb, fingers and palm subdomains (Hu et al. 2005). Further, the blocking loops 1 and 2 (BL1 and BL2), which are located in the predicated ubiquitin binding pocket and hover over the catalytic residues, are also conserved in *S. cerevisiae* Ubp6 and superimpose well with that of USP14. My structure revealed that the catalytic triad residues are arranged in an active conformation. Further, superimposition of the USP14 and Ubp6 catalytic domain structures revealed that compared to the USP14 α-helix 8, Ubp6 contains

two extended α-helices 11 and 12. In the reconstructed model of Ubp6 bound to the 26S proteasome, it was shown that interaction of the Ubl domain with 19S RP Rpn1 subunit allows the two C-terminal helices of Ubp6 to contact the AAA+ domain of Rpt1 (Bashore et al. 2016). This suggests a function for extended α-helices 11 and 12 in stabilizing and docking Ubp6 catalytic domain in the 19S RP.

Future high resolution full-length Ubp6 structure is required to examine how the Ubl domain interacts with the catalytic domain and effects its catalytic activity or function. It is shown through yeast-two-hybrid experiment that the 19S RP Rpn1 subunit residues 391-642 are necessary and sufficient for interaction with the Ubl domain of Ubp6 and proteasome shuttling receptors in *S. cerevisiae* (Gomez et al. 2011). The Ubp6 Ubl domain is stabilized through interaction with the 19S Rpn1 subunit (Bashore et al. 2016; Gomez et al. 2011). Therefore, the cocrystal structure of Ubp6 and Rpn1 (residues 391-642) can help stabilize the Ubl domain and allow obtaining the full-length Ubp6 structure. Such structure will further help clarify the mechanism involved in stimulation of Ubp6 deubiquitination activity through the Ubl-Rpn1 interaction.

Chapter 2: An Insight into the *S. cerevisiae* Ubp15 N-Terminal Domain Protein Interaction Mechanism.

The USP7 N-terminal DWGF motif is highly conserved among all Ubp15/USP7 homologs, indicating its essential functional importance. Considering the significant conservation of domains and sequence between the well-characterized human USP7 and less studied *S. cerevisiae* Ubp15, I investigated the mechanism of the Ubp15 N-terminal domain (NTD) protein interaction compared with that of USP7. Using fluorescence polarization assay (FITC) and NMR titration, I showed that Ubp15-NTD, similar to its human homologue USP7, interacts with EGPS, AXXS and PXXS motifs of proteins that previously have shown interaction with human USP7, including the EGPS containing vIRF1 peptide, the PSTS containing MCMBP peptide and the PSTSS containing Hdm2 peptide. Ubp15 showed higher affinity for PSSS, PSTS and PXXSS sequences. Interestingly, Yeast Cdh1 that has previously shown strong binding with Ubp15-NTD (Bozza & Zhuang 2011) contains a PSSS motif at its N-terminus (residues 13-16), which is highly conserved among fungi. The possibility of this motif involvement in Cdh1 interaction with Ubp15-NTD can be further investigated.

To further identify *S. cerevisiae* Ubp15 potential substrates or the N-terminal domain interacting proteins, yeast-2-hybrid experiment using Ubp15-NTD as a bait or tandem affinity purification (TAP) using TAP-tagged Ubp15-NTD can be employed. C-terminal fusion TAP-tagged Ubp15 full-length protein has previously shown strong interaction with *S. cerevisiae* Ecm30, Trr1 and Sdd1 proteins (Lam 2010, Unpublished doctoral dissertation). Both Ecm30 and Trr1 possess a PSSS motif, while Sdd1 protein contains a PGSS motif. These proteins may interact with Ubp15 using these motifs and should be further investigated.

Ubp15 Involvement in the DNA Damage Response and Cell Cycle Progression:

The main components of the DNA damage checkpoints, such as Tel1 (ATM homologue), Rad3 (ATR homologue), Cds1 (CHK1 homologue) and Chk2, are also conserved in yeast. However, p53 protein has not been identified in yeast and is considered an additional response to DNA damage that has evolved in multicellular eukaryotes (Lane & Verma 2012; Wahl & Carr 2001). Despite the absence of the most notable USP7 homologues, p53 and Hdm2, in yeast, it was shown that Ubp15, similar to USP7, is involved in regulation of the cell cycle progression. It interacts with Cdh1, the APC complex activator, and stabilize Clb5, a type-B cyclin involved in DNA replication (Ostapenko et al. 2015).

Human USP7 is also implicated in activation of the DNA damage response through stabilization of RAD18 E3 ligase (also Rad18 in yeast), which along with its cognate E2 enzyme RAD6 (also Rad6 in yeast) mono-ubiquitinates PCNA and leads to initiation of the post-replication repair (PRR) (Zlatanou et al. 2015). RAD18 interacts with USP7-NTD through ^{179}PDPS^{183} and ^{190}PSTS^{194} consensus sequences (Zlatanou et al. 2015). Preliminary examination of the yeast Rad18 sequence also revealed three possible USP7 interaction sites: ^{114}PENSS^{118} and ^{159}PLSS^{162}, which are located between the Rad18 RING domain (residues 28-65) and the Zinc-binding motif (residues 190-210), and a ^{346}PQNSS^{350} sequence that is located C-terminus of the Zinc-binding motif. The possibility of Ubp15 involvement in the stabilization of Rad18 needs to be investigated.

Chapter 3: Identification of Kaposi Sarcoma Herpesvirus (KSHV) vIRF1 Protein Interaction with Human Deubiquitinating Enzyme USP7.

In Chapters 3 and 4 I focused my research on the interaction of human herpesvirus (HHV) proteins with the USP7-NTD. Through these investigations, I was able to identify two novel HHV proteins that interacted with USP7-NTD. When I started my research, a few HHV proteins had already been identified as USP7 binding partners. The strong interaction of HSV-1 ICP0 protein with USP7-CTD was previously described (Meredith et al. 1994). EBNA1, an Epstein-Barr virus (EBV) expressed latent protein and its functional homologue, LANA, expressed by KSHV had also shown a strong affinity for USP7-NTD (Jager et al. 2012; Saridakis et al. 2005). UL35, an HCMV latent protein, had shown binding with USP7 affecting its cellular localization (Salsman et al. 2012). And more recently vIRF4 and ORF45, expressed by KSHV, showed binding with the USP7-NTD at the same region as its cellular substrates, including p53, Hdm2 and HdmX (Gillen et al. 2015; Lee et al. 2011). It was becoming apparent that HHVs tend to aim for destruction and deregulation of the USP7-p53-Hdm2 pathway by competitively binding to USP7. They block USP7 substrate interaction and cripple the cell's interferon and innate immune response and p53 mediated apoptosis. Since mutations and loss of function in p53 are responsible for greater than half of all human tumors, it is not surprising that KSHV and HCMV are linked to multiple human malignancies (Olivier et al. 2010; Hainaut et al. 1997). To date, KSHV is recognized as the causative agent of three human malignancies: Kaposi's sarcoma, primary effusion lymphoma and multicentric Castleman's disease (Wen & Damania 2010).

KSHV vIRF1 Protein Interaction with USP7:

KSHV expresses a large number of oncogenes and immunomodulatory proteins with homology to the host cell cycle regulatory proteins and inflammatory cytokines, such as viral IRFs (vIRFs). KSHV expressed vIRF1, a lytic protein, inhibits IRF1 and IRF3 transcription activation and blocks IFNα/β and IFNγ induced gene transcription (Baresova et al. 2013). Further, vIRF1 was previously reported to directly interact with the p53 central DNA binding region (residues 152-360) and hinder its DNA binding ability. At the same time, vIRF1 is a potent inhibitor of the transcriptional coactivator p300/CREB and inhibits p53 acetylation by p300, which is essential for its transcriptional activation (Shin et al. 2006; Seo et al. 2001).We

identified a ^{45}PGEGPS^{50} consensus sequence in vIRF1 that is identical to the motifs reported in EBNA1 and ORF45 (of KSHV) responsible for mediating their interaction with USP7-NTD (Gillen et al. 2015; Saridakis et al. 2005). I showed that vIRF1 interacts with the ^{164}DWGF^{167} motif of USP7-NTD with high affinity and that this interaction leads to a decrease in the cellular levels of tumor suppressor protein p53. Further, my cellular data revealed that vIRF1 also hinders ATM function by inhibiting its autophosphorylation, but does not destabilize USP7, ATM or Hdm2. Therefore, vIRF1 not only inhibits p53 activity through direct binding, but it also destabilizes it by blocking the p53-USP7 interaction and inhibiting ATM autophosphorylation.

KSHV Expressed vIRF Proteins Inhibitory Effect on USP7 and p53:

Multiple interferon-modulating proteins and known oncogenes in KSHV have been identified as USP7-NTD interacting proteins including vIRF1, vIRF4 and ORF45. It is interesting to find out why KSHV has evolved to express various USP7 inhibitors. It is possible that these proteins work together and their effect is up or downregulated by other viral proteins. However, since KSHV proteins are expressed in a timely manner during lytic infection and latent state, it is more likely that these proteins exert their effect independently at different time points and therefore evoke distinct mechanisms of IFN and p53 pathway invasion. For future directions, localization of vIRFs, their expression levels and their effect on p53 pathway components during different stages of infection should be compared to gain a better understanding of their specific role in KSHV infection. Subcellular localization of vIRFs can be examined in tetracycline-inducible TRExBJAB and TRExBCBL-1 cells, a B-cell-tumor-derived cell line infected with KSHV, which allows the efficient introduction of test genes into the latently infected BCBL-1 primary effusion lymphoma cell line (Nakamura et al. 2003). After induction of lytic infection, localization of vIRFs can be investigated by immunofluorescence using confocal microscopy.

Other than stabilization of p53 and Hdm2, USP7 has also been implicated in the IFN pathway. It stabilizes RAUL, a HECT domain E3 ligase enzyme, which negatively regulates IFN transcription by ubiquitinating IRF3 and IRF7 (Yu & Hayward 2010). It was shown that RTA, an immediate-early gene encoded by KSHV ORF50 and a critical switch for initiating lytic replication, recruits USP7 and RAUL to form a complex and further induces USP7 mediated stabilization of RAUL (Ashizawa et al. 2012; Deng et al. 2007). Recently it was reported that USP7 upregulates the IFNα pathway through direct interaction and deubiquitination of IFNα-2 receptors. USP7 knock-down downregulates cellular levels of signal transducer and

transcriptional activator proteins, STAT-1 and STAT-2, and selected IFN inducible genes (Yu et al. 2017). In a recent doctoral dissertation (Fowotade 2017), it was shown that USP7 further upregulates the IFNα pathway through stabilization of STAT2. Considering the involvement of USP7 in IFN signaling and the p53 pathway it is not surprising that so many KSHV proteins have evolved to deregulate USP7 as they hit two birds with one stone. It would be interesting to examine if transfection with vIRFs affects the stability of IFNα-2 receptors and STAT2 proteins as compared with USP7 binding mutant vIRFs. Further, cellular levels of IFNα-2 receptors and STAT2 proteins can be examined in tetracycline-inducible TRExBJAB and TRExBCBL-1 cells after induction of lytic infection.

vIRF1 Effect on the Host Cell as an Oncogene and Immunosuppressor:

Upon viral infection, interferons are activated as part of the immune response and trigger tumor suppression and apoptosis by regulating the cell cycle. vIRF1, by interfering with various interferon and apoptotic signaling pathways, greatly influences tumorigenicity of KSHV and is recognized as a viral oncogene (Mesri et al. 2014). It inhibits IRF transactivation, cyclic GMP-AMP synthase (cGAS) and STING signaling, Toll-like receptors 3 (TLR3) activation and p300 function, which further inhibits expression of type I IFNs and IFN-induced proteins (Dittmer & Damania 2016). Also, vIRF1 directly interacts with GRIM19 and pro-apoptotic BIM and inhibits GRIM19 induced IFN mediated apoptosis (Choi & Nicholas 2010; Seo et al. 2002; Lin et al. 2001). In addition, vIRF1 modulates apoptosis by inhibiting ATM autophosphorylation and p53 transactivation (Chavoshi et al. 2016; Shin et al. 2006).

vIRF1 expression was shown to significantly reduce p53 mediated apoptosis through down-regulation of cyclin-dependent kinase inhibitor p21 and apoptotic activator Bax genes (Nakamura et al. 2001). My data further indicated that vIRF1 destabilizes p53 through disruption of the USP7-p53 interaction, based on the observation that mutant vIRF1 that cannot bind USP7-NTD was unable to decrease the cellular levels of p53. The Ser50Ala mutant vIRF1 that has lost its ability to bind USP7 and destabilize p53 should still be able to directly interact with p53 and p300 as it hasn't lost its p53 and p300 binding sites. For future investigations, I would like to test whether USP7 binding mutant vIRF1 can still inhibit p53 mediated apoptosis as that would clarify if the interaction of vIRF1 with USP7 only leads to destabilization of p53 without affecting its transactivation. Also, expression levels of the well-known downstream p53 targets such as p21 and BAX should be studied in the presence of wild-type and mutant vIRF1. Further,

using reporter gene assays ability of p53 to activate transcription should be analyzed in the presence of mutant vIRF1 compared to wild-type vIRF1. To do so, p53 null cells can be transfected with vectors expressing p53, vIRF1 and a vector coding for a reporter gene followed by a p53 DNA binding site such as PG13-Lu plasmid (with a Luciferase reporter gene) (el-Deiry et al. 1993).

It is proposed that targeting LANA, a latent KSHV protein that also inhibits IFN-β and IFN- γ activity, can potentially help cure latent KSHV infection (Dittmer & Damania 2016). Also, it was shown that knock-down of vIRF1 in KSHV infected cells significantly increased IFN-β production, suppressed viral gene transcription and attenuated KSHV lytic replication (Ma et al. 2015). Since vIRF1 is a lytic protein and a potent oncogene, targeting vIRF1 can help cripple KSHV during lytic infection. vIRF1 interacts with USP7-NTD through an EGPS sequence, as opposed to (P/A)XXS sequence, which is used by the majority of the USP7 cellular substrates. Therefore, identifying and optimizing a compound that targets vIRF1, especially its USP7 interaction motif, can potentially weaken vIRF1, decrease KSHV tumorigenicity and increase p53 induced apoptosis without effecting USP7 cellular substrates. To identify small molecule inhibitors, high throughput high content screening methods can be employed (Nickischer et al. 2018; Evensen et al. 2010). Promising hits can be further validated using techniques such as surface plasmon resonance. In addition, immunotherapy can be used to target KSHV vIRF1 protein as an intracellular target for anti-tumor therapy. It has been shown that monoclonal antibodies can enter human cells, for instance through Fc receptor-mediated endocytosis, and provide an effective antiviral immunity (Hong & Zeng 2014; Mallery et al. 2010).

USP7 as a Therapeutic Target for KSHV Related Malignancies:

Understanding the mechanism through which KSHV deregulates and exploits the USP7-p53-Hdm2 pathway provides the basis for the development of therapeutics against KSHV related cancers. Currently, there are no standard guidelines for KSHV related malignancies and treatment based on the tumor location, the severity of the symptoms and immune competence is in most cases surgical excision, chemotherapy or radiotherapy (Mariggiò et al. 2017; Coen et al. 2014). To date, therapeutic interventions mostly focus on blocking Hdm2-p53 interaction by employing Hdm2 inhibitors, such as Nutlin-3A small molecule inhibitor, that has shown strong stabilization effect on p53 (Vu & Vassilev 2011). Considering that USP7 is a strong stabilizer of both Hdm2 and HdmX, blocking the function of this enzyme would effectively inhibit both

proteins and yield a more potent p53 response (Turnbull et al. 2017). Since USP7 seems to be a common host target for HHVs and its deregulation is necessary to support their life cycle and pathogenesis, it is considered to be a potential target for HHV derived tumor therapy. For instance, as shown by (Lee et al. 2011) two vIRF4 derived USP7 interacting peptides successfully blocked USP7-substrate interaction and induced apoptosis in KSHV-induced primary effusion lymphoma tumor cell lines (carrying wild-type p53) and led to marked tumor regression in primary effusion lymphoma tumor-bearing mice. However, since targeting USP7 causes severe cytotoxicity, localized delivery of anti USP7 therapeutic agents can help reduce side the effects.

Chapter 4: Identification of Human Cytomegalovirus (HCMV) Tegument Transactivator pp71 Interaction with USP7.

Amino acid sequence analysis of HCMV pp71 protein revealed three possible interaction sites with USP7-NTD. Two N-terminal motifs: ^{4}ASSS^{7} and ^{8}PGEGPS^{13} and one C-terminal sequence: ^{547}ASTS^{550}. Considering the involvement of pp71 with PML-NBs, its strong interaction with and down-regulation of DAXX, a known USP7 substrate, and its effect on the cell cycle progression, it proved to be a good candidate for interaction with USP7. My initial analysis of the EGPS containing pp71 peptide revealed a high-affinity interaction with USP7-NTD ^{164}DWGF^{167} motif. Later my data revealed that all three pp71 peptides are able to interact with USP7 with affinities ranging from 2.0 to 18.7 μM. pp71 ^{7}SPGEGPSSEA^{16} and ^{545}STASTSSTP^{553} peptides interacted with USP7-NTD with K_ds of 3.4 μM and 2.0 μM respectively, which are much lower than that of USP7 cellular substrates (Sarkari et al. 2010; Sheng et al. 2006). My work further strengthens the idea that HHVs have evolved to specifically interact with USP7 to destabilize p53 and inhibit cellular antiviral responses.

pp71 Expression Effect on the p53 Pathway Components:

My data suggest that within 24 to 48 hours post-transfection of U2OS and human fibroblast cells pp71 reduces cellular levels of USP7, p53, Hdm2 and ATM kinase. The decrease in the levels of Hdm2 can be correlated with the degradation of DAXX and USP7, its known stabilizers. Also, downregulation of USP7 destabilizes HdmX, Hdm2 homologue, which is a substrate of USP7 and a binding partner and stabilizer of Hdm2 (Sarkari et al. 2010).

Investigating cellular levels of HdmX upon pp71 transfection can further explain the instability of Hdm2. In addition, upon pp71 transfection, my *in vivo* data indicated a decrease in the levels of cellular p53. Considering the destabilization of Hdm2, we expected to see an increase in p53 levels, even though USP7 was also downregulated. Such discrepancy has been previously observed. For instance, transfection of cells with EBV EBNA1 protein, which is known to inhibit USP7 strongly, has shown a significant decrease in the levels of both p53 and Hdm2 (Sarkari 2010, Doctoral dissertation, Chapter 3). It seems the remaining amounts of Hdm2 and further activity of the other p53 negative regulators, such as Cop1 and Pirh2, are potent enough to downregulate p53 (Wang et al. 2011). Also, considering that ATM kinase phosphorylates p53 on Ser15 and Ser20 (indirectly) and stabilize it upon DNA damage signal, instability of ATM post pp71 transfection can further explain downregulation of p53. Since HHVs proteins, such as vIRF1 and vIRF4 of KSHV, each tend to interact with multiple components of the USP7-p53-Hdm2 pathway, it won't be surprising to find out that pp71 also exerts it downregulating effect on p53 through direct interaction (Chavoshi et al. 2016; Lee et al. 2011; Shin et al. 2006; Seo et al. 2001).

pp71 has already shown downregulating effect on cellular proteins it interacts with, such as Rb family of tumor suppressors and DAXX (Kalejta & Shenk 2003; Ishov et al. 2002). In my functional analysis, pp71 significantly decreased cellular levels of ATM kinase and its autophosphorylation on Ser1981. In addition, previously it was reported that upon HCMV infection ATM is mislocalized to the cytoplasm (Gaspar & Shenk 2006). ATM kinase is a critical regulator of the USP7-p53-Hdm2 pathway and is involved in inhibition of the G1/S cell cycle progression; therefore, destabilization of ATM will give HCMV virus power to cripple intrinsic antiviral defense mechanism (Sancar et al., 2004). Since pp71 downregulates proteins it interacts with, the possible binary interaction of pp71 with ATM kinase should be further investigated.

Suppressing and Targeting pp71 for Therapeutic Drug Design:

Similar to the other members of human herpesviruses, HCMV is very common, infecting as much as 88-96% of adults especially in Europe and South America (Boeckh & Geballe 2011). Further, it is the leading viral cause of congenital hearing loss and mental retardation in newborns (Cohen et al. 2014; Grosse et al. 2008). To date, lack of suitable treatments exposes infected fetuses to serious side effects (Torres & Tang 2015). Upon HCMV entrance into the

host cell, activation of the immediate early (IE) genes expression followed by activation of the early genes by IE proteins is critical for acute infection. Accordingly, targeting IE proteins activation has proven effective in inhibiting viral replication and blocking lytic infection (Stinski & Isomura 2008). To date, there are multiple vaccine candidates that are proposed to protect developing fetuses and organ transplant recipient, such as ones designed to elicit immune reaction against tegument proteins and phospholipid envelope glycoproteins (Xia et al. 2017; Smith et al. 2013). HCMV tegument transactivator pp71 is responsible for immediate early activation of IE genes transcription from the major immediate early promoter and hence it is essential for successful lytic infection (Bresnahan & Shenk 2000). pp71 deletion mutant HCMV has limited growth and inefficient productive replication (Bresnahan & Shenk 2000). Therefore, identifying small molecule inhibitors that target pp71 can help inhibit IE gene transcription and lytic infection in infected individuals.

USP7 is considered a potential target for HHV derived tumor therapies. However, targeting host USP7 to inhibit HCMV multiplication in infected fetuses causes severe cytotoxicity and is not an option. Therefore, considering the pp71 critical role in activation of viral gene transcription and its downregulating effect on cell cycle regulating proteins, such as USP7 and p53, targeting pp71 to suppress HCMV lytic infection is quite promising. To inhibit pp71 suppression of p53 mediated apoptosis, identifying pp71 amino acid sequence responsible for the destabilization of USP7 is important. Deletion mutation of small sequences within pp71 and analyzing the effect of mutants on USP7 post transfection can help identify amino acids that are implicated in USP7 downregulation. Using mutational studies and structural data I have been able to pinpoint the exact interaction sites between pp71 and USP7. Identifying blocking agents that target USP7 interaction motifs of pp71 can help upregulate p53 and DAXX levels in infected cells and potentially lead to silencing of the viral genome and induction of the cell cycle arrest.

Also, to suppress downregulating effect of pp71 on USP7, DAXX and Rb proteins it is necessary to find out how pp71 destabilizes its binding partners. Previously it was reported that pp71 decreases cellular levels DAXX and Rb proteins (Rb, p107 and p130) in a ubiquitin-independent but proteasome-dependent manner (Winkler et al. 2013; Kalejta et al. 2003). Further, it was shown that the 19S RP is necessary for pp71 imposed degradation of Rb and DAXX and that 19S RP subunits Rpn1was critical for pp71-mediated DAXX degradation (Winkler et al. 2013). For future investigations, it is important to initially examine whether

proteasome inhibition results in accumulation of USP7 post pp71 transfection. Furthermore, proteins known as proteasome shuttling receptors, such as Rad23 in yeast (hHR23B in human), specifically recognize Lys48-linked Ub chains as well as proteasome subunits, such as Rpn1 and Rpn13, and shuttle tagged proteins to the proteasome (Shi et al. 2016). Possible direct interaction of pp71 with proteasome subunits, such as Rpn1 and Rpn13, should be investigated.

Concluding Remarks:

In this thesis, I have examined the soluble expression of the yeast *Saccharomyces cerevisiae* ubiquitin processing enzymes, Ubps, in *E. coli* for protein crystallography. I have employed multiple optimization methods which some have proven to be beneficial. Since *E. coli* remains the preferred microbial cell factory for recombinant protein expression, hopefully, the current advances in robotics and automation of the protein purification and expression methods can help facilitate large-scale protein expression from *E. coli*. Also, I was able to obtain the three-dimensional structure of the *S. cerevisiae* Ubp6 catalytic domain which helped clarify its catalytic active site arrangement. In addition, my work on the Ubp15 N-terminal domain revealed its similar mode of substrate interaction as compared to human USP7 and provided important clues for identification of Ubp15 cellular substrates in future investigations. Furthermore, my research on KSHV expressed vIRF1 protein and HCMV expressed pp71 protein has shown novel interactions between these viral oncogenes and human USP7. My findings in part have helped clarify these viral proteins mechanism of p53 pathway suppression.

References:

Chapter 1:

Abdouh, M. et al., 2016. The Polycomb Repressive Complex 1 Protein BMI1 Is Required for Constitutive Heterochromatin Formation and Silencing in Mammalian Somatic Cells. *The Journal of biological chemistry*, 291(1), pp.182–197.

Abdul Rehman, S.A. et al., 2016. MINDY-1 Is a Member of an Evolutionarily Conserved and Structurally Distinct New Family of Deubiquitinating Enzymes. *Molecular cell*, 63(1), pp.146–155.

Abukhdeir, A.M. & Park, B.H., 2008. P21 and p27: roles in carcinogenesis and drug resistance. *Expert reviews in molecular medicine*, 10, p.e19.

Aggarwal, K. & Massague, J., 2012. Ubiquitin removal in the TGF-beta pathway. *Nat Cell Biol*, 14(7), pp.656–657.

Al-Shami, A. et al., 2010. Regulators of the proteasome pathway, Uch37 and Rpn13, play distinct roles in mouse development. *PloS one*, 5(10), p.e13654.

Alibek, K. et al., 2014. Implication of human herpesviruses in oncogenesis through immune evasion and supression. *Infectious agents and cancer*, 9(1), p.3.

Alonso-de Vega, I., Martin, Y. & Smits, V.A.J., 2014. USP7 controls Chk1 protein stability by direct deubiquitination. *Cell cycle (Georgetown, Tex.)*, 13(24), pp.3921–3926.

Atanassov, B.S., Koutelou, E. & Dent, S.Y., 2011. The role of deubiquitinating enzymes in chromatin regulation. *FEBS letters*, 585(13), pp.2016–2023.

Aviram, S. & Kornitzer, D., 2010. The ubiquitin ligase Hul5 promotes proteasomal processivity. *Molecular and cellular biology*, 30(4), pp.985–994.

Avvakumov, G. V et al., 2012. Two ZnF-UBP domains in isopeptidase T (USP5). *Biochemistry*, 51(6), pp.1188–1198.

Balakirev, M.Y. et al., 2003. Otubains: a new family of cysteine proteases in the ubiquitin pathway. *EMBO reports*, 4(5), pp.517–522.

Baldi, L. et al., 1996. Critical role for lysines 21 and 22 in signal-induced, ubiquitin-mediated proteolysis of I kappa B-alpha. *The Journal of biological chemistry*, 271(1), pp.376–379.

Bartel, D.P., 2009. MicroRNAs: target recognition and regulatory functions. *Cell*, 136(2), pp.215–233.

Bashore, C. et al., 2016. Ubp6 deubiquitinase controls conformational dynamics and substrate degradation of the 26S proteasome. *Nat Struct Mol Biol.*, 22(9), pp.712–719.

Bassermann, F. et al., 2008. The Cdc14B-Cdh1-Plk1 axis controls the G2 DNA-damage-response checkpoint. *Cell*, 134(2), pp.256–267.

Bekker-Jensen, S. & Mailand, N., 2011. The ubiquitin- and SUMO-dependent signaling response to DNA double-strand breaks. *FEBS letters*, 585(18), pp.2914–2919.

Ben-Saadon, R. et al., 2004. The tumor suppressor protein p16(INK4a) and the human papillomavirus oncoprotein-58 E7 are naturally occurring lysine-less proteins that are degraded by the ubiquitin system. Direct evidence for ubiquitination at the N-terminal residue. *The Journal of biological chemistry*, 279(40), pp.41414–41421.

Benvenuti, M. & Mangani, S., 2007. Crystallization of soluble proteins in vapor diffusion for x-ray crystallography. *Nature protocols*, 2(7), pp.1633–1651.

Bhattacharya, S. & Ghosh, M.K., 2014. HAUSP, a novel deubiquitinase for Rb - MDM2 the critical regulator. *The FEBS journal*, 281(13), pp.3061–78.

Bianchi, M. et al., 2015. Dynamic transcription of ubiquitin genes under basal and stressful conditions and new insights into the multiple UBC transcript variants. *Gene*, 573(1),

pp.100–109.
de Bie, P. & Ciechanover, A., 2011. Ubiquitination of E3 ligases: self-regulation of the ubiquitin system via proteolytic and non-proteolytic mechanisms. *Cell death and differentiation*, 18(9), pp.1393–1402.
de Bie, P., Zaaroor-Regev, D. & Ciechanover, A., 2010. Regulation of the Polycomb protein RING1B ubiquitination by USP7. *Biochemical and biophysical research communications*, 400(3), pp.389–395.
Birol, M. & Echalier, A., 2014. Structure and function of MPN (Mpr1/Pad1 N-terminal) domain-containing proteins. *Current protein & peptide science*, 15(5), pp.504–517.
Bishop, P., Rocca, D. & Henley, J.M., 2016. Ubiquitin C-terminal hydrolase L1 (UCH-L1): structure, distribution and roles in brain function and dysfunction. *Biochemical Journal*, 473(16), pp.2453–2462.
Blot, V. et al., 2004. Nedd4.1-mediated ubiquitination and subsequent recruitment of Tsg101 ensure HTLV-1 Gag trafficking towards the multivesicular body pathway prior to virus budding. *Journal of cell science*, 117(Pt 11), pp.2357–2367.
Blundell, T.L. & Patel, S., 2004. High-throughput X-ray crystallography for drug discovery. *Current opinion in pharmacology*, 4(5), pp.490–496.
Boban, M., Ljungdahl, P.O. & Foisner, R., 2015. Atypical ubiquitylation in yeast targets lysine-less Asi2 for proteasomal degradation. *The Journal of biological chemistry*, 290(4), pp.2489–2495.
Boistelle, R., 1986. The concepts of crystal growth from solution. *Advances in nephrology from the Necker Hospital*, 15, pp.173–217.
Boisvert, R.A. & Howlett, N.G., 2014. The Fanconi anemia ID2 complex: dueling saxes at the crossroads. *Cell cycle (Georgetown, Tex.)*, 13(19), pp.2999–3015.
Boudreaux, D.A. et al., 2010. Ubiquitin vinyl methyl ester binding orients the misaligned active site of the ubiquitin hydrolase UCHL1 into productive conformation. *Proceedings of the National Academy of Sciences of the United States of America*, 107(20), pp.9117–9122.
Boutet, S.C. et al., 2010. Taf1 regulates Pax3 protein by monoubiquitination in skeletal muscle progenitors. *Molecular cell*, 40(5), pp.749–761.
Brenkman, A.B., de Keizer, P.L.J., van den Broek, N.J.F., Jochemsen, A.G., et al., 2008. Mdm2 induces mono-ubiquitination of FOXO4. *PloS one*, 3(7), p.e2819.
Brenkman, A.B., de Keizer, P.L.J., van den Broek, N.J.F., van der Groep, P., et al., 2008. The peptidyl-isomerase Pin1 regulates p27kip1 expression through inhibition of Forkhead box O tumor suppressors. *Cancer research*, 68(18), pp.7597–7605.
Brooks, C.L. et al., 2007. The p53--Mdm2--HAUSP complex is involved in p53 stabilization by HAUSP. *Oncogene*, 26(51), pp.7262–6.
Bueno, A.N. et al., 2015. Dynamics of an Active-Site Flap Contributes to Catalysis in a JAMM Family Metallo Deubiquitinase. *Biochemistry*, 54(39), pp.6038–6051.
Burroughs, A.M., Iyer, L.M. & Aravind, L., 2012. The natural history of ubiquitin and ubiquitin-related domains. *Frontiers in bioscience (Landmark edition)*, 17, pp.1433–1460.
Callis, J., 2014. The ubiquitination machinery of the ubiquitin system. *The Arabidopsis book / American Society of Plant Biologists*, 12, p.e0174.
Campbell, S.J. et al., 2012. Molecular insights into the function of RING finger (RNF)-containing proteins hRNF8 and hRNF168 in Ubc13/Mms2-dependent ubiquitylation. *The Journal of biological chemistry*, 287(28), pp.23900–23910.
Carlton, J., 2010. The ESCRT machinery: a cellular apparatus for sorting and scission.

Biochemical Society transactions, 38(6), pp.1397–1412.
Carvallo, L. et al., 2010. Non-canonical Wnt signaling induces ubiquitination and degradation of Syndecan4. *The Journal of biological chemistry*, 285(38), pp.29546–29555.
De Ceuninck, L. et al., 2013. Reciprocal cross-regulation between RNF41 and USP8 controls cytokine receptor sorting and processing. *Journal of cell science*, 126(Pt 16), pp.3770–3781.
Chao, C.C.-K., 2015. Mechanisms of p53 degradation. *Clinica chimica acta; international journal of clinical chemistry*, 438, pp.139–147.
Chavoshi, S. et al., 2016. Identification of KSHV vIRF1 as a novel interaction partner of human deubiquitinase USP7. *Journal of Biological Chemistry*, 291(12), pp.6281–6291.
Chen, C. & Matesic, L.E., 2007. The Nedd4-like family of E3 ubiquitin ligases and cancer. *Cancer metastasis reviews*, 26(3-4), pp.587–604.
Chen, L. & Madura, K., 2006. Evidence for distinct functions for human DNA repair factors hHR23A and hHR23B. *FEBS letters*, 580(14), pp.3401–3408.
Chen, Z.J., 2012. Ubiquitination in signaling to and activation of IKK. *Immunological reviews*, 246(1), pp.95–106.
Chicooree, N. et al., 2013. Enhanced detection of ubiquitin isopeptides using reductive methylation. *Journal of the American Society for Mass Spectrometry*, 24(3), pp.421–430.
Chisholm, C. & Lopez, L., 2011. Cutaneous infections caused by herpesviridae: A review. *Archives of Pathology and Laboratory Medicine*, 135, pp.1357–1362.
Ciechanover, A., 2003. The ubiquitin proteolytic system and pathogenesis of human diseases: a novel platform for mechanism-based drug targeting. *Biochemical Society transactions*, 31(2), pp.474–481.
Clague, M.J. et al., 2013. Deubiquitylases from genes to organism. *Physiological reviews*, 93(3), pp.1289–315.
Cocklin, R. et al., 2011. New insight into the role of the Cdc34 ubiquitin-conjugating enzyme in cell cycle regulation via Ace2 and Sic1. *Genetics*, 187(3), pp.701–715.
Cohn, M.A. et al., 2007. A UAF1-containing multisubunit protein complex regulates the Fanconi anemia pathway. *Molecular cell*, 28(5), pp.786–797.
Cole, A.J., Clifton-Bligh, R. & Marsh, D.J., 2015. Histone H2B monoubiquitination: roles to play in human malignancy. *Endocrine-related cancer*, 22(1), pp.T19–33.
Coomans de Brachene, A. & Demoulin, J.-B., 2016. FOXO transcription factors in cancer development and therapy. *Cellular and molecular life sciences : CMLS*, 73(6), pp.1159–1172.
Cope, G.A. et al., 2002. Role of predicted metalloprotease motif of Jab1/Csn5 in cleavage of Nedd8 from Cul1. *Science (New York, N.Y.)*, 298(5593), pp.608–611.
Costa, M. do C. & Paulson, H.L., 2012. Toward understanding Machado-Joseph disease. *Progress in neurobiology*, 97(2), pp.239–257.
Coulombe, P. et al., 2004. N-Terminal ubiquitination of extracellular signal-regulated kinase 3 and p21 directs their degradation by the proteasome. *Molecular and cellular biology*, 24(14), pp.6140–6150.
Coyne, E.S. & Wing, S.S., 2016. The business of deubiquitination - location, location, location. *F1000Research*, 5, pp.1–9.
Crosas, B. et al., 2006. Ubiquitin Chains Are Remodeled at the Proteasome by Opposing Ubiquitin Ligase and Deubiquitinating Activities. *Cell*, 127(7), pp.1401–1413.
Das, R. et al., 2013. Allosteric regulation of E2:E3 interactions promote a processive ubiquitination machine. *The EMBO journal*, 32(18), pp.2504–2516.

Daubeuf, S. et al., 2009. HSV ICP0 recruits USP7 to modulate TLR-mediated innate response. *Blood*, 113(14), pp.3264–3275.
Davies, C.W., Paul, L.N. & Das, C., 2013. Mechanism of recruitment and activation of the endosome-associated deubiquitinase AMSH. *Biochemistry*, 52(44), pp.7818–7829.
Davis, M.I. & Simeonov, A., 2015. Ubiquitin-Specific Proteases as Druggable Targets. *Drug target review*, 2(3), pp.60–64.
Dayal, S. et al., 2009. Suppression of the deubiquitinating enzyme USP5 causes the accumulation of unanchored polyubiquitin and the activation of p53. *The Journal of biological chemistry*, 284(8), pp.5030–5041.
Delston, R.B. et al., 2011. p38 phosphorylates Rb on Ser567 by a novel, cell cycle-independent mechanism that triggers Rb-Hdm2 interaction and apoptosis. *Oncogene*, 30(5), pp.588–599.
Deng, H.-X. et al., 2011. Mutations in UBQLN2 cause dominant X-linked juvenile and adult-onset ALS and ALS/dementia. *Nature*, 477(7363), pp.211–215.
Deshaies, R.J. & Joazeiro, C.A.P., 2009. RING domain E3 ubiquitin ligases. *Annual review of biochemistry*, 78, pp.399–434.
Dikic, I., Wakatsuki, S. & Walters, K.J., 2009. Ubiquitin-binding domains - from structures to functions. *Nature reviews. Molecular cell biology*, 10(10), pp.659–671.
Dimova, N. V et al., 2012. APC/C-mediated multiple monoubiquitylation provides an alternative degradation signal for cyclin B1. *Nature cell biology*, 14(2), pp.168–176.
Diouf, B. et al., 2011. Somatic deletions of genes regulating MSH2 protein stability cause DNA mismatch repair deficiency and drug resistance in human leukemia cells. *Nature medicine*, 17(10), pp.1298–1303.
Dove, K.K. et al., 2016. Molecular insights into RBR E3 ligase ubiquitin transfer mechanisms. *EMBO reports*, 17(8), pp.1221–1235.
Draker, R., Sarcinella, E. & Cheung, P., 2011. USP10 deubiquitylates the histone variant H2A.Z and both are required for androgen receptor-mediated gene activation. *Nucleic acids research*, 39(9), pp.3529–3542.
Du, H.-N., 2012. Transcription, DNA damage and beyond: the roles of histone ubiquitination and deubiquitination. *Current protein & peptide science*, 13(5), pp.447–466.
Du, M.-Q., 2011. MALT lymphoma: many roads lead to nuclear factor-kappab activation. *Histopathology*, 58(1), pp.26–38.
Dupont, S. et al., 2009. FAM/USP9x, a deubiquitinating enzyme essential for TGFbeta signaling, controls Smad4 monoubiquitination. *Cell*, 136(1), pp.123–135.
Dupre, S. & Haguenauer-Tsapis, R., 2001. Deubiquitination Step in the Endocytic Pathway of Yeast Plasma Membrane Proteins : Crucial Role of Doa4p Ubiquitin Isopeptidase. *Molecular and cellular biology*, 21(14), pp.4482–4494.
Durcan, T.M. et al., 2012. Ataxin-3 deubiquitination is coupled to Parkin ubiquitination via E2 ubiquitin-conjugating enzyme. *The Journal of biological chemistry*, 287(1), pp.531–541.
Edelman, D.C., 2005. Human herpesvirus 8--a novel human pathogen. *Virology journal*, 2, p.78.
Eletr, Z.M. & Wilkinson, K.D., 2014. Regulation of Proteolysis by Human Deubiquitinating Enzymes. *Biochim Biophys Acta.*, 1843(1).
Elia, A.E.H. et al., 2015. Quantitative Proteomic Atlas of Ubiquitination and Acetylation in the DNA Damage Response. *Molecular cell*, 59(5), pp.867–881.
Elliott, P.R. & Komander, D., 2016. Regulation of Met1-linked polyubiquitin signalling by the deubiquitinase OTULIN. *The FEBS journal*, 283(1), pp.39–53.
Emmerich, C.H. et al., 2013. Activation of the canonical IKK complex by K63/M1-linked hybrid

ubiquitin chains. *Proceedings of the National Academy of Sciences of the United States of America*, 110(38), pp.15247–15252.
Emre, N.C.T. et al., 2005. Maintenance of low histone ubiquitylation by Ubp10 correlates with telomere-proximal Sir2 association and gene silencing. *Molecular cell*, 17(4), pp.585–594.
Enchev, R.I. et al., 2012. Structural basis for a reciprocal regulation between SCF and CSN. *Cell reports*, 2(3), pp.616–627.
Enesa, K. et al., 2008. NF-kappaB suppression by the deubiquitinating enzyme Cezanne: a novel negative feedback loop in pro-inflammatory signaling. *The Journal of biological chemistry*, 283(11), pp.7036–7045.
Epping, M.T. et al., 2011. TSPYL5 suppresses p53 levels and function by physical interaction with USP7. *Nature cell biology*, 13(1), pp.102–108.
Everett, R.D. et al., 1997. A novel ubiquitin-specific protease is dynamically associated with the PML nuclear domain and binds to a herpesvirus regulatory protein. *The EMBO journal*, 16(7), pp.1519–1530.
Faesen, A.C. et al., 2011. Mechanism of USP7 / HAUSP Activation by Its C-Terminal Ubiquitin-like Domain and Allosteric Regulation by GMP-Synthetase. *Molecular Cell*, 44(1), pp.147–159.
Faesen, A.C., Luna-Vargas, M.P.A. & Sixma, T.K., 2012. The role of UBL domains in ubiquitin-specific proteases. *Biochemical Society transactions*, 40(3), pp.539–545.
Faustrup, H. et al., 2009. USP7 counteracts SCFbetaTrCP- but not APCCdh1-mediated proteolysis of Claspin. *The Journal of cell biology*, 184(1), pp.13–19.
Felle, M. et al., 2011. The USP7/Dnmt1 complex stimulates the DNA methylation activity of Dnmt1 and regulates the stability of UHRF1. *Nucleic acids research*, 39(19), pp.8355–8365.
Feng, L., Wang, J. & Chen, J., 2010. The Lys63-specific deubiquitinating enzyme BRCC36 is regulated by two scaffold proteins localizing in different subcellular compartments. *The Journal of biological chemistry*, 285(40), pp.30982–30988.
Finley, D., 2009. Recognition and processing of ubiquitin-protein conjugates by the proteasome. *Annual review of biochemistry*, 78, pp.477–513.
Finley, D. et al., 2012. The ubiquitin-proteasome system of *Saccharomyces cerevisiae*. *Genetics*, 192(2), pp.319–360.
Fong, C.S. et al., 2016. 53BP1 and USP28 mediate p53-dependent cell cycle arrest in response to centrosome loss and prolonged mitosis. *eLife*, 5.
Frangini, A. et al., 2013. The aurora B kinase and the polycomb protein ring1B combine to regulate active promoters in quiescent lymphocytes. *Molecular cell*, 51(5), pp.647–661.
Frappier, L., 2012. Contributions of Epstein-Barr nuclear antigen 1 (EBNA1) to cell immortalization and survival. *Viruses*, 4(9), pp.1537–1547.
Fu, Q.-S., Song, A.-X. & Hu, H.-Y., 2012. Structural aspects of ubiquitin binding specificities. *Current protein & peptide science*, 13(5), pp.482–489.
Fuchs, G. et al., 2012. RNF20 and USP44 regulate stem cell differentiation by modulating H2B monoubiquitylation. *Molecular cell*, 46(5), pp.662–673.
Fujita, H. et al., 2014. Mechanism underlying IkappaB kinase activation mediated by the linear ubiquitin chain assembly complex. *Molecular and cellular biology*, 34(7), pp.1322–1335.
Gatti, M. et al., 2015. RNF168 promotes noncanonical K27 ubiquitination to signal DNA damage. *Cell reports*, 10(2), pp.226–238.
Gatzka, M. et al., 2015. Interplay of H2A deubiquitinase 2A-DUB/Mysm1 and the

p19(ARF)/p53 axis in hematopoiesis, early T-cell development and tissue differentiation. *Cell death and differentiation*, 22(9), pp.1451–1462.
Ghaboosi, N. & Deshaies, R.J., 2007. A conditional yeast E1 mutant blocks the ubiquitin-proteasome pathway and reveals a role for ubiquitin conjugates in targeting Rad23 to the proteasome. *Molecular biology of the cell*, 18(5), pp.1953–1963.
Gillen, J. et al., 2015. A Survey of the Interactome of Kaposi's Sarcoma-Associated Herpesvirus ORF45 Revealed Its Binding to Viral ORF33 and Cellular USP7, Resulting in Stabilization of ORF33 That Is Required for Production of Progeny Viruses K. Frueh, ed. *Journal of Virology*, 89(9), pp.4918–4931.
Giovinazzi, S. et al., 2014. Usp7 protects genomic stability by regulating Bub3. *Oncotarget*, 5(11), pp.3728–3742.
Glickman, M.H. & Ciechanover, A., 2002. The ubiquitin-proteasome proteolytic pathway: destruction for the sake of construction. *Physiological reviews*, 82(2), pp.373–428.
Gorelik, M. et al., 2016. Inhibition of SCF ubiquitin ligases by engineered ubiquitin variants that target the Cul1 binding site on the Skp1-F-box interface. *Proceedings of the National Academy of Sciences of the United States of America*, 113(13), pp.3527–3532.
Grice, G.L. & Nathan, J.A., 2016. The recognition of ubiquitinated proteins by the proteasome. *Cellular and Molecular Life Sciences*, 73, pp.3497–3506.
Grigoreva, T.A. et al., 2015. The 26S proteasome is a multifaceted target for anti-cancer therapies. *Oncotarget*, 6(28), pp.24733–24749.
Groen, E.J.N. & Gillingwater, T.H., 2015. UBA1: At the Crossroads of Ubiquitin Homeostasis and Neurodegeneration. *Trends in Molecular Medicine*, 21(10), pp.622–632.
Grou, C.P. et al., 2015. The de novo synthesis of ubiquitin: identification of deubiquitinases acting on ubiquitin precursors. *Scientific reports*, 5, p.12836.
Le Guen, T. et al., 2015. An in vivo genetic reversion highlights the crucial role of Myb-Like, SWIRM, and MPN domains 1 (MYSM1) in human hematopoiesis and lymphocyte differentiation. *The Journal of allergy and clinical immunology*, 136(6), pp.1615–1619.
Gupta, A. et al., 2014. Role of 53BP1 in the regulation of DNA double-strand break repair pathway choice. *Radiation research*, 181(1), pp.1–8.
Ham, S.J. et al., 2016. Interaction between RING1 (R1) and the Ubiquitin-like (UBL) Domains Is Critical for the Regulation of Parkin Activity. *The Journal of biological chemistry*, 291(4), pp.1803–1816.
Hamazaki, J., Hirayama, S. & Murata, S., 2015. Redundant Roles of Rpn10 and Rpn13 in Recognition of Ubiquitinated Proteins and Cellular Homeostasis. *PLoS genetics*, 11(7), p.e1005401.
Hanpude, P. et al., 2015. Deubiquitinating enzymes in cellular signaling and disease regulation. *IUBMB life*, 67(7), pp.544–555.
Hao, Y.H. et al., 2015. USP7 Acts as a Molecular Rheostat to Promote WASH-Dependent Endosomal Protein Recycling and Is Mutated in a Human Neurodevelopmental Disorder. *Molecular Cell*, 59(6), pp.956–969.
Haririnia, A. et al., 2008. Mutations in the Hydrophobic Core of Ubiquitin Differentially Affect its Recognition by Receptor Proteins. *Journal of molecular biology*, 375(4), pp.979–996.
Harp, J.M., Timm, D.E. & Bunick, G.J., 1998. Macromolecular crystal annealing: overcoming increased mosaicity associated with cryocrystallography. *Acta crystallographica. Section D, Biological crystallography*, 54(Pt 4), pp.622–628.
He, J. et al., 2013. Insights into degron recognition by APC/C coactivators from the structure of

an Acm1-Cdh1 complex. *Molecular cell*, 50(5), pp.649–660.
He, M. et al., 2016. The emerging role of deubiquitinating enzymes in genomic integrity, diseases, and therapeutics. *Cell & bioscience*, 6, p.62.
Hellmuth, S. et al., 2015. Positive and Negative Regulation of Vertebrate Separase by Cdk1-Cyclin B1 May Explain Why Securin Is Dispensable. *The Journal of Biological Chemistry*, 290(12), pp.8002–8010.
Hendriks, I.A. et al., 2014. Uncovering global SUMOylation signaling networks in a site-specific manner. *Nature structural & molecular biology*, 21(10), pp.927–936.
Henry, K.W. et al., 2003. Transcriptional activation via sequential histone H2B ubiquitylation and deubiquitylation, mediated by SAGA-associated Ubp8. *Genes and Development*, 17(21), pp.2648–2663.
Hershko, A., 2005. The ubiquitin system for protein degradation and some of its roles in the control of the cell division cycle. *Cell death and differentiation*, 12(9), pp.1191–7.
Hershko, A. & Ciechanover, A., 1992. The ubiquitin system for protein degradation. *Annual review of biochemistry*, 61, pp.761–807.
Heyninck, K. & Beyaert, R., 2005. A20 inhibits NF-kappaB activation by dual ubiquitin-editing functions. *Trends in biochemical sciences*, 30(1), pp.1–4.
Hochrainer, K. et al., 2005. The human HERC family of ubiquitin ligases: novel members, genomic organization, expression profiling, and evolutionary aspects. *Genomics*, 85(2), pp.153–164.
Hochstrasser, M. & Amerik, A.Y., 2004. Mechanism and function of deubiquitinating enzymes. *Biochimica et Biophysica Acta (BBA) - Molecular Cell Research*, 1695(1-3), pp.189–207.
Hoesel, B. & Schmid, J.A., 2013. The complexity of NF-kappaB signaling in inflammation and cancer. *Molecular cancer*, 12, p.86.
Hofmann, H., Sindre, H. & Stamminger, T., 2002. Functional interaction between the pp71 protein of human cytomegalovirus and the PML-interacting protein human Daxx. *Journal of virology*, 76(11), pp.5769–5783.
Holowaty, M.N. et al., 2003. Protein Interaction Domains of the Ubiquitin-specific Protease, USP7/HAUSP. *Journal of Biological Chemistry*, 278(48), pp.47753–47761.
van der Horst, A. et al., 2006. FOXO4 transcriptional activity is regulated by monoubiquitination and USP7/HAUSP. *Nature cell biology*, 8(10), pp.1064–1073.
Hou, D. et al., 1994. Activation-dependent ubiquitination of a T cell antigen receptor subunit on multiple intracellular lysines. *The Journal of biological chemistry*, 269(19), pp.14244–14247.
Hu, M. et al., 2002. Crystal structure of a UBP-family deubiquitinating enzyme in isolation and in complex with ubiquitin aldehyde. *Cell*, 111(7), pp.1041–1054.
Hu, M. et al., 2005. Structure and mechanisms of the proteasome-associated deubiquitinating enzyme USP14. *The EMBO Journal*, 24(21), pp.3747–3756.
Huang, D. et al., 2015. BRCC3 mutations in myeloid neoplasms. *Haematologica*, 100(8), pp.1051–1057.
Huang, T.T. et al., 2006. Regulation of monoubiquitinated PCNA by DUB autocleavage. *Nature cell biology*, 8(4), pp.339–347.
Husnjak, K. & Dikic, I., 2012. Ubiquitin-binding proteins: decoders of ubiquitin-mediated cellular functions. *Annual review of biochemistry*, 81, pp.291–322.
Hutti, J.E. et al., 2009. Phosphorylation of the tumor suppressor CYLD by the breast cancer oncogene IKKepsilon promotes cell transformation. *Molecular cell*, 34(4), pp.461–472.

Ikeda, F. & Dikic, I., 2008. Atypical ubiquitin chains: new molecular signals. "Protein Modifications: Beyond the Usual Suspects" review series. *EMBO reports*, 9(6), pp.536–42.
Imura, Y. et al., 2015. Cellular Ubc2/Rad6 E2 ubiquitin-conjugating enzyme facilitates tombusvirus replication in yeast and plants. *Virology*, 484, pp.265–275.
Iwai, K., 2011. Linear polyubiquitin chains: A new modifier involved in NFκB activation and chronic inflammation including dermatitis. *Cell Cycle*, 10(18), pp.3095–3104.
Iwai, K., Fujita, H. & Sasaki, Y., 2014. Linear ubiquitin chains: NF-kappaB signalling, cell death and beyond. *Nature reviews. Molecular cell biology*, 15(8), pp.503–508.
Jager, W. et al., 2012. The Ubiquitin-Specific Protease USP7 Modulates the Replication of Kaposi's Sarcoma-Associated Herpesvirus Latent Episomal DNA. *Journal of Virology*, 86(12), pp.6745–6757.
Jasin, M. & Haber, J.E., 2016. The democratization of gene editing: Insights from site-specific cleavage and double-strand break repair. *DNA repair*.
Jeffrey, G.A., 1997. *An Introduction to Hydrogen Bonding*, Oxford: Oxford University Press.
Jiao, L. et al., 2014. Mechanism of the Rpn13-induced activation of Uch37. *Protein & cell*, 5(8), pp.616–630.
Katz, E.J., Isasa, M. & Crosas, B., 2010. A new map to understand deubiquitination. *Biochemical Society transactions*, 38(Pt 1), pp.21–28.
Keusekotten, K. et al., 2013. OTULIN antagonizes LUBAC signaling by specifically hydrolyzing Met1-linked polyubiquitin. *Cell*, 153(6), pp.1312–1326.
Khoronenkova, S. V & Dianov, G.L., 2013. USP7S-dependent inactivation of Mule regulates DNA damage signalling and repair. *Nucleic acids research*, 41(3), pp.1750–1756.
Khoronenkova, S. V. et al., 2012. ATM-Dependent Downregulation of USP7/HAUSP by PPM1G Activates p53 Response to DNA Damage. *Molecular Cell*, 45(6), pp.801–813.
Kim, H.C. & Huibregtse, J.M., 2009. Polyubiquitination by HECT E3s and the determinants of chain type specificity. *Molecular and cellular biology*, 29(12), pp.3307–3318.
Kim, W. et al., 2011. Systematic and quantitative assessment of the ubiquitin-modified proteome. *Molecular cell*, 44(2), pp.325–340.
Klebe, G., 2000. Recent developments in structure-based drug design. *Journal of molecular medicine (Berlin, Germany)*, 78(5), pp.269–281.
Kleijnen, M.F. et al., 2000. The hPLIC proteins may provide a link between the ubiquitination machinery and the proteasome. *Molecular cell*, 6(2), pp.409–419.
van der Knaap, J.A. et al., 2010. Biosynthetic enzyme GMP synthetase cooperates with ubiquitin-specific protease 7 in transcriptional regulation of ecdysteroid target genes. *Molecular and cellular biology*, 30(3), pp.736–744.
van der Knaap, J.A. et al., 2005. GMP synthetase stimulates histone H2B deubiquitylation by the epigenetic silencer USP7. *Molecular cell*, 17(5), pp.695–707.
Kobayashi, T., Masoumi, K.C. & Massoumi, R., 2015. Deubiquitinating activity of CYLD is impaired by SUMOylation in neuroblastoma cells. *Oncogene*, 34(17), pp.2251–2260.
Koulich, E., Li, X. & DeMartino, G.N., 2008. Relative structural and functional roles of multiple deubiquitylating proteins associated with mammalian 26S proteasome. *Molecular biology of the cell*, 19(3), pp.1072–1082.
Krauss, I.R. et al., 2013. An overview of biological macromolecule crystallization. *International Journal of Molecular Sciences*, 14(6), pp.11643–11691.
Kravtsova-Ivantsiv, Y. & Ciechanover, A., 2012. Non-canonical ubiquitin-based signals for proteasomal degradation. *Journal of cell science*, 125(Pt 3), pp.539–548.

Kristariyanto, Y.A., Choi, S.-Y., et al., 2015. Assembly and structure of Lys33-linked polyubiquitin reveals distinct conformations. *The Biochemical journal*, 467(2), pp.345–352.
Kristariyanto, Y.A., Abdul Rehman, S.A., et al., 2015. K29-selective ubiquitin binding domain reveals structural basis of specificity and heterotypic nature of k29 polyubiquitin. *Molecular cell*, 58(1), pp.83–94.
Kulathu, Y. et al., 2013. Regulation of A20 and other OTU deubiquitinases by reversible oxidation. *Nature communications*, 4, p.1569.
Kulathu, Y. & Komander, D., 2012. Atypical ubiquitylation — the unexplored world of polyubiquitin beyond Lys48 and Lys63 linkages. *Nature Reviews Molecular Cell Biology*, 13(8), pp.508–523.
Kumar, B. et al., 2010. Ser(120) of Ubc2/Rad6 regulates ubiquitin-dependent N-end rule targeting by E3{alpha}/Ubr1. *The Journal of biological chemistry*, 285(53), pp.41300–41309.
Lanfranca, M.P., Mostafa, H.H. & Davido, D.J., 2014. HSV-1 ICP0: An E3 Ubiquitin Ligase That Counteracts Host Intrinsic and Innate Immunity. *Cells*, 3(2), pp.438–454.
Lecona, E., Narendra, V. & Reinberg, D., 2015. USP7 cooperates with SCML2 to regulate the activity of PRC1. *Molecular and cellular biology*, 35(7), pp.1157–1168.
Lee, H.-R. et al., 2011. Bilateral inhibition of HAUSP deubiquitinase by a viral interferon regulatory factor protein. *Nature structural & molecular biology*, 18(12), pp.1336–44.
Lee, H.-R. et al., 2009. Kaposi's sarcoma-associated herpesvirus viral interferon regulatory factor 4 targets MDM2 to deregulate the p53 tumor suppressor pathway. *Journal of virology*, 83(13), pp.6739–47.
Lee, J.-G. et al., 2013. Reversible inactivation of deubiquitinases by reactive oxygen species in vitro and in cells. *Nature communications*, 4, p.1568.
Lee, M.J. et al., 2011. Trimming of ubiquitin chains by proteasome-associated deubiquitinating enzymes. *Molecular & cellular proteomics : MCP*, 10(5), p.R110.003871.
Leitner, A. et al., 2010. Probing native protein structures by chemical cross-linking, mass spectrometry, and bioinformatics. *Molecular & cellular proteomics : MCP*, 9(8), pp.1634–1649.
Lenk, U. et al., 2002. A role for mammalian Ubc6 homologues in ER-associated protein degradation. *Journal of cell science*, 115(Pt 14), pp.3007–3014.
Li, H. et al., 2009. Lysine-independent turnover of cyclin G1 can be stabilized by B'alpha subunits of protein phosphatase 2A. *Molecular and cellular biology*, 29(3), pp.919–928.
Li, J. et al., 2008. Differential display identifies overexpression of the USP36 gene, encoding a deubiquitinating enzyme, in ovarian cancer. *International journal of medical sciences*, 5(3), pp.133–142.
Li, J. et al., 2015. NEDD8 Ultimate Buster 1 Long (NUB1L) Protein Suppresses Atypical Neddylation and Promotes the Proteasomal Degradation of Misfolded Proteins. *The Journal of biological chemistry*, 290(39), pp.23850–23862.
Li, J. & Xu, X., 2016. DNA double-strand break repair: a tale of pathway choices. *Acta biochimica et biophysica Sinica*, 48(7), pp.665–670.
Li, M. et al., 2003. Mono- versus polyubiquitination: differential control of p53 fate by Mdm2. *Science (New York, N.Y.)*, 302(5652), pp.1972–1975.
Li, T. et al., 2014. HSCARG downregulates NF-kappaB signaling by interacting with USP7 and inhibiting NEMO ubiquitination. *Cell death & disease*, 5, p.e1229.
Li, W. et al., 2008. Genome-wide and functional annotation of human E3 ubiquitin ligases

identifies MULAN, a mitochondrial E3 that regulates the organelle's dynamics and signaling. *PloS one*, 3(1), p.e1487.
Lin, X. et al., 2015. A Novel Aspect of Tumorigenesis-BMI1 Functions in Regulating DNA Damage Response. *Biomolecules*, 5(4), pp.3396–3415.
Ling, R. et al., 2000. Histidine-tagged ubiquitin substitutes for wild-type ubiquitin in *Saccharomyces cerevisiae* and facilitates isolation and identification of in vivo substrates of the ubiquitin pathway. *Analytical biochemistry*, 282(1), pp.54–64.
Lingaraju, G.M. et al., 2014. Crystal structure of the human COP9 signalosome. *Nature*, 512(7513), pp.161–165.
Liu, J. et al., 2011. Beclin1 controls the levels of p53 by regulating the deubiquitination activity of USP10 and USP13. *Cell*, 147(1), pp.223–234.
Liu, W., Shang, Y. & Li, W., 2014. gp78 elongates of polyubiquitin chains from the distal end through the cooperation of its G2BR and CUE domains. *Scientific reports*, 4, p.7138.
Long, L. et al., 2014. The U4/U6 recycling factor SART3 has histone chaperone activity and associates with USP15 to regulate H2B deubiquitination. *The Journal of biological chemistry*, 289(13), pp.8916–8930.
Lopez-Martinez, D., Liang, C.-C. & Cohn, M.A., 2016. Cellular response to DNA interstrand crosslinks: the Fanconi anemia pathway. *Cellular and molecular life sciences*, 73(16), pp.3097–114.
Lub, S. et al., 2016. Novel strategies to target the ubiquitin proteasome system in multiple myeloma. *Oncotarget*, 7(6), pp.6521–6537.
Lui, T.T.H. et al., 2011. The ubiquitin-specific protease USP34 regulates axin stability and Wnt/beta-catenin signaling. *Molecular and cellular biology*, 31(10), pp.2053–2065.
Luna-Vargas, M.P. a et al., 2011. Enabling high-throughput ligation-independent cloning and protein expression for the family of ubiquitin specific proteases. *Journal of Structural Biology*, 175(2), pp.113–119.
Ma, J. et al., 2010. C-terminal region of USP7/HAUSP is critical for deubiquitination activity and contains a second mdm2/p53 binding site. *Archives of biochemistry and biophysics*, 503(2), pp.207–212.
MacDonald, E., Urbe, S. & Clague, M.J., 2014. USP8 controls the trafficking and sorting of lysosomal enzymes. *Traffic (Copenhagen, Denmark)*, 15(8), pp.879–888.
Maertens, G.N. et al., 2010. Ubiquitin-specific proteases 7 and 11 modulate Polycomb regulation of the INK4a tumour suppressor. *The EMBO journal*, 29(15), pp.2553–2565.
Malawski, G.A. et al., 2006. Identifying protein construct variants with increased crystallization propensity--a case study. *Protein science : a publication of the Protein Society*, 15(12), pp.2718–28.
Maresca, T.J. & Salmon, E.D., 2010. Welcome to a new kind of tension: translating kinetochore mechanics into a wait-anaphase signal. *Journal of cell science*, 123(Pt 6), pp.825–835.
Margolis, S.S. et al., 2015. Angelman Syndrome. *Neurotherapeutics : the journal of the American Society for Experimental NeuroTherapeutics*, 12(3), pp.641–650.
Martinez-Climent, J.A., 2014. The origin and targeting of mucosa-associated lymphoid tissue lymphomas. *Current opinion in hematology*, 21(4), pp.309–319.
Mashtalir, N. et al., 2014. Autodeubiquitination protects the tumor suppressor BAP1 from cytoplasmic sequestration mediated by the atypical ubiquitin ligase UBE2O. *Molecular cell*, 54(3), pp.392–406.
Matsuda, N., 2016. Phospho-ubiquitin: upending the PINK-Parkin-ubiquitin cascade. *Journal of*

biochemistry, 159(4), pp.379–385.
Mattiroli, F. et al., 2012. RNF168 ubiquitinates K13-15 on H2A/H2AX to drive DNA damage signaling. *Cell*, 150(6), pp.1182–1195.
McDowell, G.S. & Philpott, A., 2013. Non-canonical ubiquitylation: Mechanisms and consequences. *International Journal of Biochemistry and Cell Biology*, 45(8), pp.1833–1842.
McGinty, R.K., Henrici, R.C. & Tan, S., 2014. Crystal structure of the PRC1 ubiquitylation module bound to the nucleosome. *Nature*, 514(7524), pp.591–596.
McKnight, N.C. & Zhenyu, Y., 2013. Beclin 1, an Essential Component and Master Regulator of PI3K-III in Health and Disease. *Current pathobiology reports*, 1(4), pp.231–238.
Melo-Cardenas, J. et al., 2016. Ubiquitin-specific peptidase 22 functions and its involvement in disease. *Oncotarget*, 7(28), pp.44848–44856.
Messick, T.E. et al., 2008. Structural basis for ubiquitin recognition by the Otu1 ovarian tumor domain protein. *The Journal of biological chemistry*, 283(16), pp.11038–11049.
Metzger, M.B., Hristova, V.A. & Weissman, A.M., 2012. HECT and RING finger families of E3 ubiquitin ligases at a glance. *Journal of Cell Science*, 125(3), pp.531–537.
Meulmeester, E. et al., 2005. Loss of HAUSP-mediated deubiquitination contributes to DNA damage-induced destabilization of Hdmx and Hdm2. *Molecular cell*, 18(5), pp.565–576.
Mevissen, T.E.T. et al., 2013. OTU deubiquitinases reveal mechanisms of linkage specificity and enable ubiquitin chain restriction analysis. *Cell*, 154(1), pp.169–184.
Micel, L.N. et al., 2013. Role of ubiquitin ligases and the proteasome in oncogenesis: Novel targets for anticancer therapies. *Journal of Clinical Oncology*, 31(9), pp.1231–1238.
Min, M. & Lindon, C., 2012. Substrate targeting by the ubiquitin-proteasome system in mitosis. *Seminars in cell & developmental biology*, 23(5), pp.482–491.
Misaghi, S. et al., 2009. Association of C-terminal ubiquitin hydrolase BRCA1-associated protein 1 with cell cycle regulator host cell factor 1. *Molecular and cellular biology*, 29(8), pp.2181–2192.
Misaghi, S. et al., 2005. Structure of the ubiquitin hydrolase UCH-L3 complexed with a suicide substrate. *The Journal of biological chemistry*, 280(2), pp.1512–1520.
Mizutani, R. et al., 2014. Spatiotemporal development of soaked protein crystal. *Scientific reports*, 4, p.5731.
Morotti, A. et al., 2015. HAUSP compartmentalization in chronic myeloid leukemia. *European journal of haematology*, 94(4), pp.318–321.
Morrow, M.E. et al., 2013. Stabilization of an unusual salt bridge in ubiquitin by the extra C-terminal domain of the proteasome-associated deubiquitinase UCH37 as a mechanism of its exo specificity. *Biochemistry*, 52(20), pp.3564–3578.
Mortensen, F. et al., 2015. Role of ubiquitin and the HPV E6 oncoprotein in E6AP-mediated ubiquitination. *Proceedings of the National Academy of Sciences of the United States of America*, 112(32), pp.9872–9877.
Mosadeghi, R. et al., 2016. Structural and kinetic analysis of the COP9-Signalosome activation and the cullin-RING ubiquitin ligase deneddylation cycle. *eLife*, 5, p.e12102.
Mukai, A. et al., 2010. Balanced ubiquitylation and deubiquitylation of Frizzled regulate cellular responsiveness to Wg/Wnt. *The EMBO journal*, 29(13), pp.2114–2125.
Mulder, K.W. et al., 2007. Modulation of Ubc4p/Ubc5p-mediated stress responses by the RING-finger-dependent ubiquitin-protein ligase Not4p in *Saccharomyces cerevisiae*. *Genetics*, 176(1), pp.181–192.

Munshi, P. et al., 2012. Rapid visualization of hydrogen positions in protein neutron crystallographic structures. *Acta crystallographica. Section D, Biological crystallography*, 68(Pt 1), pp.35–41.
Murai, J. et al., 2011. The USP1/UAF1 complex promotes double-strand break repair through homologous recombination. *Molecular and cellular biology*, 31(12), pp.2462–2469.
Murali, R., Wiesner, T. & Scolyer, R.A., 2013. Tumours associated with BAP1 mutations. *Pathology*, 45(2), pp.116–126.
Nakada, S. et al., 2010. Non-canonical inhibition of DNA damage-dependent ubiquitination by OTUB1. *Nature*, 466(7309), pp.941–946.
Nakamura, H. et al., 2001. Inhibition of p53 tumor suppressor by viral interferon regulatory factor. *Journal of virology*, 75(16), pp.7572–7582.
Nathan, J.A. et al., 2013. Why do cellular proteins linked to K63-polyubiquitin chains not associate with proteasomes? *The EMBO journal*, 32(4), pp.552–565.
Nicassio, F. et al., 2007. Human USP3 is a chromatin modifier required for S phase progression and genome stability. *Current biology : CB*, 17(22), pp.1972–1977.
Nicholson, B. & Suresh Kumar, K.G., 2011. The Multifaceted Roles of USP7: New Therapeutic Opportunities. *Cell Biochemistry and Biophysics*, 60(1-2), pp.61–68.
Nijman, S.M.B. et al., 2005. A genomic and functional inventory of deubiquitinating enzymes. *Cell*, 123(5), pp.773–86.
Noy, T. et al., 2012. HUWE1 ubiquitinates MyoD and targets it for proteasomal degradation. *Biochemical and biophysical research communications*, 418(2), pp.408–413.
Oh, Y.M., Yoo, S.J. & Seol, J.H., 2007. Deubiquitination of Chfr, a checkpoint protein, by USP7/HAUSP regulates its stability and activity. *Biochemical and biophysical research communications*, 357(3), pp.615–619.
Ohtake, F. et al., 2015. Ubiquitin acetylation inhibits polyubiquitin chain elongation. *EMBO reports*, 16(2), pp.192–201.
Olmos, Y. & Carlton, J.G., 2016. The ESCRT machinery: new roles at new holes. *Current opinion in cell biology*, 38, pp.1–11.
Ordureau, A. et al., 2015. Defining roles of PARKIN and ubiquitin phosphorylation by PINK1 in mitochondrial quality control using a ubiquitin replacement strategy. *Proceedings of the National Academy of Sciences of the United States of America*, 112(21), pp.6637–6642.
Oswald, C. et al., 2008. Microseeding – A Powerful Tool for Crystallizing Proteins Complexed with Hydrolyzable Substrates. *International Journal of Molecular Sciences*, 9(7), pp.1131–1141.
Pannu, J. et al., 2015. Ubiquitin specific protease 21 is dispensable for normal development, hematopoiesis and lymphocyte differentiation. *PloS one*, 10(2), p.e0117304.
Parsons, J.L. et al., 2009. Ubiquitin ligase ARF-BP1/Mule modulates base excision repair. *The EMBO journal*, 28(20), pp.3207–3215.
Patterson-Fortin, J. et al., 2010. Differential regulation of JAMM domain deubiquitinating enzyme activity within the RAP80 complex. *The Journal of biological chemistry*, 285(40), pp.30971–30981.
Pattle, S.B. & Farrell, P.J., 2006. The role of Epstein – Barr virus. , pp.1193–1205.
Pelzer, C. et al., 2007. UBE1L2, a novel E1 enzyme specific for ubiquitin. *The Journal of biological chemistry*, 282(32), pp.23010–23014.
Pfoh, R., Lacdao, I.K., Georges, A.A., et al., 2015. Crystal Structure of USP7 Ubiquitin-like Domains with an ICP0 Peptide Reveals a Novel Mechanism Used by Viral and Cellular

Proteins to Target USP7. *PLoS pathogens*, 11(6), p.e1004950.
Pfoh, R., Lacdao, I.K. & Saridakis, V., 2015. Deubiquitinases and the new therapeutic opportunities offered to cancer. *Endocrine-Related Cancer*, 22(1), pp.T35–T54.
Phillips, A.H. & Corn, J.E., 2015. Using protein motion to read, write, and erase ubiquitin signals. *Journal of Biological Chemistry*, 290(44), pp.26437–26444.
Platta, H.W. et al., 2014. The peroxisomal receptor dislocation pathway: to the exportomer and beyond. *Biochimie*, 98, pp.16–28.
Popp, M.W., Artavanis-Tsakonas, K. & Ploegh, H.L., 2009. Substrate filtering by the active site crossover loop in UCHL3 revealed by sortagging and gain-of-function mutations. *The Journal of biological chemistry*, 284(6), pp.3593–3602.
Qiao, R. et al., 2016. Mechanism of APC/C(CDC20) activation by mitotic phosphorylation. *Proceedings of the National Academy of Sciences of the United States of America*, 113(19), pp.E2570–E2578.
Ramamoorthy, S. et al., 2012. Overexpression of ligase defective E6-associated protein, E6-AP, results in mammary tumorigenesis. *Breast cancer research and treatment*, 132(1), pp.97–108.
Ravid, T. & Hochstrasser, M., 2007. Autoregulation of an E2 enzyme by ubiquitin-chain assembly on its catalytic residue. *Nature cell biology*, 9(4), pp.422–427.
Reddy, B.A. et al., 2014. Nucleotide biosynthetic enzyme GMP synthase is a TRIM21-controlled relay of p53 stabilization. *Molecular cell*, 53(3), pp.458–470.
Reed, B.J., Locke, M.N. & Gardner, R.G., 2015. A Conserved Deubiquitinating Enzyme Uses Intrinsically Disordered Regions to Scaffold Multiple Protein Interaction Sites. *The Journal of biological chemistry*, 290(33), pp.20601–20612.
Rego, M.A. et al., 2012. Regulation of the activation of the Fanconi anemia pathway by the p21 cyclin-dependent kinase inhibitor. *Oncogene*, 31(3), pp.366–375.
Reyes-Turcu, F.E. et al., 2008. Recognition of polyubiquitin isoforms by the multiple ubiquitin binding modules of isopeptidase T. *The Journal of biological chemistry*, 283(28), pp.19581–19592.
Reyes-Turcu, F.E., Ventii, K.H. & Wilkinson, K.D., 2009. Regulation and Cellular Roles of Ubiquitin-specific Deubiquitinating Enzymes. *Annu Rev Biochem*, 78, pp.363–397.
Rhodes, G., 2006. *Crystallography Made Crystal Clear* 3rd ed. J. Hayhurst, ed., Burlington, MA, USA: Academic Press.
Rodrigo-Brenni, M.C. & Morgan, D.O., 2007. Sequential E2s drive polyubiquitin chain assembly on APC targets. *Cell*, 130(1), pp.127–139.
Ronau, J.A., Beckmann, J.F. & Hochstrasser, M., 2016. Substrate specificity of the ubiquitin and Ubl proteases. *Cell Research*, 26(4), pp.441–456.
Rupp, B., 2010. *Biomolecular Crystallography: Principles, Practice, and Application to Structural Biology* 1st ed., New York, NY, USA: Garland Publishing.
Sahtoe, D.D. et al., 2016. BAP1/ASXL1 recruitment and activation for H2A deubiquitination. *Nature communications*, 7, p.10292.
Sahtoe, D.D. et al., 2015. Mechanism of UCH-L5 activation and inhibition by DEUBAD domains in RPN13 and INO80G. *Molecular cell*, 57(5), pp.887–900.
Sahtoe, D.D. & Sixma, T.K., 2015. Layers of DUB regulation. *Trends in Biochemical Sciences*, 40(8), pp.456–467.
Salsman, J. et al., 2012. Proteomic profiling of the human cytomegalovirus UL35 gene products reveals a role for UL35 in the DNA repair response. *Journal of virology*, 86(2), pp.806–20.

Sanchez-Barcelo, E.J. et al., 2016. COP1 and COP9 signalosome, evolutionarily conserved photomorphogenic proteins as possible targets of melatonin. *Journal of pineal research*, 61, pp.41–51.
Sandoval, D. et al., 2015. Ubiquitin-conjugating enzyme Cdc34 and ubiquitin ligase Skp1-cullin-F-box ligase (SCF) interact through multiple conformations. *The Journal of biological chemistry*, 290(2), pp.1106–1118.
Saridakis, V. et al., 2005. Structure of the p53 binding domain of HAUSP/USP7 bound to epstein-barr nuclear antigen 1: Implications for EBV-mediated immortalization. *Molecular Cell*, 18(1), pp.25–36.
Sarkari, F. et al., 2010. Further Insight into Substrate Recognition by USP7: Structural and Biochemical Analysis of the HdmX and Hdm2 Interactions with USP7. *Journal of Molecular Biology*, 402(5), pp.825–837.
Sarkari, F. et al., 2011. The herpesvirus associated ubiquitin specific protease, USP7, is a negative regulator of PML proteins and PML nuclear bodies. *PloS one*, 6(1), p.e16598.
Sato, Y. et al., 2015. Structures of CYLD USP with Met1- or Lys63-linked diubiquitin reveal mechanisms for dual specificity. *Nature structural & molecular biology*, 22(3), pp.222–229.
Saunier, R. et al., 2013. Integrity of the *Saccharomyces cerevisiae* Rpn11 protein is critical for formation of proteasome storage granules (PSG) and survival in stationary phase. *PloS one*, 8(8), p.e70357.
Schaeffer, V. et al., 2014. Binding of OTULIN to the PUB domain of HOIP controls NF-kappaB signaling. *Molecular cell*, 54(3), pp.349–361.
Scheffner, M. & Kumar, S., 2014. Mammalian HECT ubiquitin-protein ligases: biological and pathophysiological aspects. *Biochimica et biophysica acta*, 1843(1), pp.61–74.
Schimke, R.T., 1973. Control of enzyme levels in mammalian tissues. *Advances in enzymology and related areas of molecular biology*, 37, pp.135–187.
Schulman, B.A. & Harper, J.W., 2009. Ubiquitin-like protein activation by E1 enzymes: the apex for downstream signalling pathways. *Nature reviews. Molecular cell biology*, 10(5), pp.319–331.
Schwartz, Y.B. & Pirrotta, V., 2013. A new world of Polycombs: unexpected partnerships and emerging functions. *Nature reviews. Genetics*, 14(12), pp.853–864.
Seki, T. et al., 2013. JosD1, a membrane-targeted deubiquitinating enzyme, is activated by ubiquitination and regulates membrane dynamics, cell motility, and endocytosis. *The Journal of biological chemistry*, 288(24), pp.17145–17155.
Sekiguchi, S. et al., 2006. Localization of ubiquitin C-terminal hydrolase L1 in mouse ova and its function in the plasma membrane to block polyspermy. *The American journal of pathology*, 169(5), pp.1722–1729.
Selvaraju, K. et al., 2015. Inhibition of proteasome deubiquitinase activity: A strategy to overcome resistance to conventional proteasome inhibitors? *Drug Resistance Updates*, 21-22, pp.20–29.
Sette, P. et al., 2013. Ubiquitin conjugation to Gag is essential for ESCRT-mediated HIV-1 budding. *Retrovirology*, 10, p.79.
Shadfan, M., Lopez-Pajares, V. & Yuan, Z.-M., 2012. MDM2 and MDMX: Alone and together in regulation of p53. *Translational cancer research*, 1(2), pp.88–89.
Shapiro, L. & Harris, T., 2000. Finding function through structural genomics. *Current opinion in biotechnology*, 11(1), pp.31–35.
Sharma, N. et al., 2014. USP3 counteracts RNF168 via deubiquitinating H2A and gammaH2AX

at lysine 13 and 15. *Cell cycle (Georgetown, Tex.)*, 13(1), pp.106–114.
Sheng, Y. et al., 2006. Molecular recognition of p53 and MDM2 by USP7/HAUSP. *Nature structural & molecular biology*, 13(3), pp.285–291.
Shi, D. & Grossman, S.R., 2010. Ubiquitin becomes ubiquitous in cancer: emerging roles of ubiquitin ligases and deubiquitinases in tumorigenesis and as therapeutic targets. *Cancer biology & therapy*, 10(8), pp.737–747.
Shi, Y. et al., 2016. Rpn1 provides adjacent receptor sites for substrate binding and deubiquitination by the proteasome. *Science (New York, N.Y.)*, 351(6275).
Shrestha, R.K. et al., 2014. Insights into the Mechanism of Deubiquitination by JAMM Deubiquitinases from Cocrystal Structures of the Enzyme with the Substrate and Product. *Biochemistry*, 53, pp.3199–3217.
Sivachandran, N., Cao, J.Y. & Frappier, L., 2010. Epstein-Barr virus nuclear antigen 1 Hijacks the host kinase CK2 to disrupt PML nuclear bodies. *Journal of virology*, 84(21), pp.11113–11123.
Sloper-Mould, K.E. et al., 2001. Distinct functional surface regions on ubiquitin. *The Journal of biological chemistry*, 276(32), pp.30483–30489.
Sokolik, C.W. & Cohen, R.E., 1991. The structures of ubiquitin conjugates of yeast Iso-2-cytochrome c. *The Journal of biological chemistry*, 266(14), pp.9100–9107.
Song, M.S. et al., 2008. The deubiquitinylation and localization of PTEN are regulated by a HAUSP-PML network. *Nature*, 455(7214), pp.813–817.
Soucy, T.A., Smith, P.G. & Rolfe, M., 2009. Targeting NEDD8-activated cullin-RING ligases for the treatment of cancer. *Clinical cancer research : an official journal of the American Association for Cancer Research*, 15(12), pp.3912–3916.
Sowa, M.E. et al., 2009. Defining the human deubiquitinating enzyme interaction landscape. *Cell*, 138(2), pp.389–403.
Spratt, D.E., Walden, H. & Shaw, G.S., 2014. RBR E3 ubiquitin ligases: new structures, new insights, new questions. *The Biochemical journal*, 458(3), pp.421–37.
Stewart, M.D. et al., 2016. E2 enzymes: more than just middle men. *Nature Publishing Group*, 26(4), pp.423–440.
Stoll, K.E. et al., 2011. The essential Ubc4/Ubc5 function in yeast is HECT E3-dependent, and RING E3-dependent pathways require only monoubiquitin transfer by Ubc4. *The Journal of biological chemistry*, 286(17), pp.15165–15170.
Sun, X.-X. & Dai, M.-S., 2014. Deubiquitinating enzyme regulation of the p53 pathway: A lesson from Otub1. *World journal of biological chemistry*, 5(2), pp.75–84.
Suryadinata, R. et al., 2014. Mechanisms of generating polyubiquitin chains of different topology. *Cells*, 3(3), pp.674–89.
Swatek, K.N. & Komander, D., 2016. Ubiquitin modifications. *Cell research*, 26(4), pp.399–422.
Tang, J. et al., 2006. Critical role for Daxx in regulating Mdm2. *Nature cell biology*, 8(8), pp.855–862.
Tang, J. et al., 2010. Daxx is reciprocally regulated by Mdm2 and Hausp. *Biochem Biophys Res Commun.*, 393(3), pp.542–545.
Tang, J. et al., 2013. Phosphorylation of Daxx by ATM Contributes to DNA Damage-Induced p53 Activation. *PLoS ONE*, 8(2), pp.1–7.
van Tijn, P. et al., 2011. Alzheimer-associated mutant ubiquitin impairs spatial reference memory. *Physiology & behavior*, 102(2), pp.193–200.

van Tijn, P. et al., 2007. Dose-dependent inhibition of proteasome activity by a mutant ubiquitin associated with neurodegenerative disease. *Journal of cell science*, 120(Pt 9), pp.1615–1623.
van Voorhis, V.A. & Morgan, D.O., 2014. Activation of the APC/C Ubiquitin Ligase by Enhanced E2 Efficiency. *Current biology : CB*, 24(13), pp.1556–1562.
Tran, H. et al., 2008. Trabid, a new positive regulator of Wnt-induced transcription with preference for binding and cleaving K63-linked ubiquitin chains. *Genes & development*, 22(4), pp.528–542.
Trempe, J.F., 2011. Reading the ubiquitin postal code. *Current Opinion in Structural Biology*, 21(6), pp.792–801.
Tsou, W.-L. et al., 2013. Ubiquitination regulates the neuroprotective function of the deubiquitinase ataxin-3 in vivo. *The Journal of biological chemistry*, 288(48), pp.34460–34469.
VanderLinden, R.T. et al., 2015. Structural Basis for the Activation and Inhibition of the UCH37 Deubiquitylase. *Molecular Cell*, 57(5), pp.901–911.
Varshavsky, A., 2012. The ubiquitin system, an immense realm. *Annual review of biochemistry*, 81, pp.167–176.
Ventii, K.H. & Wilkinson, K.D., 2008. Protein partners of deubiquitinating enzymes. *The Biochemical journal*, 414(2), pp.161–175.
Vidal, M., 2009. Role of polycomb proteins Ring1A and Ring1B in the epigenetic regulation of gene expression. *The International journal of developmental biology*, 53(2-3), pp.355–370.
Villamil, M.A., Chen, J., et al., 2012. A noncanonical cysteine protease USP1 is activated through active site modulation by USP1-associated factor 1. *Biochemistry*, 51(13), pp.2829–2839.
Villamil, M.A., Liang, Q., et al., 2012. Serine phosphorylation is critical for the activation of ubiquitin-specific protease 1 and its interaction with WD40-repeat protein UAF1. *Biochemistry*, 51(45), pp.9112–9123.
Villamil, M.A., Liang, Q. & Zhuang, Z., 2013. The WD40-repeat protein-containing deubiquitinase complex: catalysis, regulation, and potential for therapeutic intervention. *Cell biochemistry and biophysics*, 67(1), pp.111–126.
Viswanathan, J. et al., 2011. Alzheimer's disease-associated ubiquilin-1 regulates presenilin-1 accumulation and aggresome formation. *Traffic (Copenhagen, Denmark)*, 12(3), pp.330–348.
Wada, K. & Kamitani, T., 2006. UnpEL/Usp4 is ubiquitinated by Ro52 and deubiquitinated by itself. *Biochemical and biophysical research communications*, 342(1), pp.253–258.
Wang, L. et al., 2014. High expression of UCH37 is significantly associated with poor prognosis in human epithelial ovarian cancer. *Tumour biology : the journal of the International Society for Oncodevelopmental Biology and Medicine*, 35(11), pp.11427–11433.
Wen, K.W. & Damania, B., 2010. Kaposi sarcoma-associated herpesvirus (KSHV): molecular biology and oncogenesis. *Cancer letters*, 289(2), pp.140–50.
Wernimont, A. & Edwards, A., 2009. In Situ proteolysis to generate crystals for structure determination: An update. *PLoS ONE*, 4(4).
Wickliffe, K.E. et al., 2011. The mechanism of linkage-specific ubiquitin chain elongation by a single-subunit E2. *Cell*, 144(5), pp.769–781.
Wiener, R. et al., 2012. The mechanism of OTUB1-mediated inhibition of ubiquitination. *Nature*, 483(7391), pp.618–622.

Wilkinson, K.D. et al., 1986. Structure and activities of a variant ubiquitin sequence from bakers' yeast. *Biochemistry*, 25(18), pp.4999–5004.
Wilkinson, K.D., 2005. The discovery of ubiquitin-dependent proteolysis. *Proceedings of the National Academy of Sciences of the United States of America*, 102(43), pp.15280–2.
Williams, C. et al., 2007. A conserved cysteine is essential for Pex4p-dependent ubiquitination of the peroxisomal import receptor Pex5p. *The Journal of biological chemistry*, 282(31), pp.22534–22543.
Wolberger, C., 2014. Mechanisms for regulating deubiquitinating enzymes. *Protein Science*, 23(4), pp.344–353.
Won, M. et al., 2016. Post-translational control of NF-kappaB signaling by ubiquitination. *Archives of pharmacal research*, 39(8), pp.1075–1084.
Wooh, J.W. et al., 2003. Comparison of three commercial sparse-matrix crystallization screens. *Acta crystallographica. Section D, Biological crystallography*, 59(Pt 4), pp.769–772.
Wu, N. et al., 2014. MiR-4782-3p inhibited non-small cell lung cancer growth via USP14. *Cellular physiology and biochemistry : international journal of experimental cellular physiology, biochemistry, and pharmacology*, 33(2), pp.457–467.
Wu, N. et al., 2013. Over-expression of deubiquitinating enzyme USP14 in lung adenocarcinoma promotes proliferation through the accumulation of beta-catenin. *International journal of molecular sciences*, 14(6), pp.10749–10760.
Wyce, A. et al., 2007. H2B ubiquitylation acts as a barrier to Ctk1 nucleosomal recruitment prior to removal by Ubp8 within a SAGA-related complex. *Molecular cell*, 27(2), pp.275–288.
Xu, G. et al., 2010. Ubiquitin-specific peptidase 21 inhibits tumor necrosis factor alpha-induced nuclear factor kappaB activation via binding to and deubiquitinating receptor-interacting protein 1. *The Journal of biological chemistry*, 285(2), pp.969–978.
Xu, P. et al., 2009. Quantitative proteomics reveals the function of unconventional ubiquitin chains in proteasomal degradation. *Cell*, 137(1), pp.133–145.
Xu, W. et al., 2013. Targeting the ubiquitin E1 as a novel anti-cancer strategy. *Current pharmaceutical design*, 19(18), pp.3201–3209.
Yang, B. et al., 2013. Network-based inference framework for identifying cancer genes from gene expression data. *BioMed research international*, 2013, p.401649.
Yang, K. et al., 2011. Regulation of the Fanconi anemia pathway by a SUMO-like delivery network. *Genes & development*, 25(17), pp.1847–1858.
Ye, Y. et al., 2009. Dissection of USP catalytic domains reveals five common insertion points. *Molecular bioSystems*, 5, pp.1797–1808.
Ye, Y. & Rage, M., 2011. Building ubiquitin chains: E2 enzymes at work. *Nat Rev Mol Cell Biol*, 10(11), pp.755–764.
Yin, H. et al., 2010. Dependence of phospholipase D1 multi-monoubiquitination on its enzymatic activity and palmitoylation. *The Journal of biological chemistry*, 285(18), pp.13580–13588.
Yu, H. et al., 2014. Tumor suppressor and deubiquitinase BAP1 promotes DNA double-strand break repair. *Proceedings of the National Academy of Sciences of the United States of America*, 111(1), pp.285–290.
Yuan, W.-C. et al., 2014. K33-Linked Polyubiquitination of Coronin 7 by Cul3-KLHL20 Ubiquitin E3 Ligase Regulates Protein Trafficking. *Molecular cell*, 54(4), pp.586–600.
Yun, S.-I. et al., 2015. Ubiquitin specific protease 4 positively regulates the WNT/beta-catenin signaling in colorectal cancer. *Molecular oncology*, 9(9), pp.1834–1851.

Zhang, J. et al., 2014. ABRO1 suppresses tumourigenesis and regulates the DNA damage response by stabilizing p53. *Nature communications*, 5, p.5059.
Zhang, J. et al., 2014. The regulation of TGF-beta/SMAD signaling by protein deubiquitination. *Protein & cell*, 5(7), pp.503–517.
Zhang, L. et al., 2012. USP4 is regulated by AKT phosphorylation and directly deubiquitylates TGF-beta type I receptor. *Nature cell biology*, 14(7), pp.717–726.
Zhang, Q. et al., 2016. Structural Basis of the Recruitment of Ubiquitin-Specific Protease USP15 by Spliceosome Recycling Factor SART3. *The Journal of biological chemistry*, 291(33), pp.17283–17292.
Zhang, X.-F. et al., 2016. Expression and prognostic role of ubiquitination factor E4B in primary hepatocellular carcinoma. *Molecular carcinogenesis*, 55(1), pp.64–76.
Zhang, Z. et al., 2013. USP49 deubiquitinates histone H2B and regulates cotranscriptional pre-mRNA splicing. *Genes & development*, 27(14), pp.1581–1595.
Zhang, Z.M. et al., 2015. An Allosteric Interaction Links USP7 to Deubiquitination and Chromatin Targeting of UHRF1. *Cell Reports*, 12(9), pp.1400–1406.
Zhao, Y., Morgan, M.A. & Sun, Y., 2014. Targeting Neddylation pathways to inactivate cullin-RING ligases for anticancer therapy. *Antioxidants & redox signaling*, 21(17), pp.2383–2400.
Zhao, Y. & Sun, Y., 2013. Cullin-RING Ligases as attractive anti-cancer targets. *Current pharmaceutical design*, 19(18), pp.3215–3225.
Zheng, N. et al., 2016. Recent advances in {SCF} ubiquitin ligase complex: clinical implications. *Biochimica et Biophysica Acta (BBA) - Reviews on Cancer*, 1866(1), pp.12-22.
Zhou, Z.-R. et al., 2012. Length of the active-site crossover loop defines the substrate specificity of ubiquitin C-terminal hydrolases for ubiquitin chains. *The Biochemical journal*, 441(1), pp.143–149.
Zlatanou, A. et al., 2016. USP7 is essential for maintaining Rad18 stability and DNA damage tolerance. *Oncogene*, 35(8), pp.965–976.
Zuin, A., Isasa, M. & Crosas, B., 2014. Ubiquitin Signaling: Extreme Conservation as a Source of Diversity. *Cells*, 3(3), pp.690–701.

Chapter 2:

Abdul Rehman, S.A. et al., 2016. MINDY-1 Is a Member of an Evolutionarily Conserved and Structurally Distinct New Family of Deubiquitinating Enzymes. *Molecular cell*, 63(1), pp.146–155.

Amerik, A.Y. et al., 1997. In vivo disassembly of free polyubiquitin chains by yeast Ubp14 modulates rates of protein degradation by the proteasome. *The EMBO journal*, 16(16), pp.4826–38.

Amerik, A.Y. et al., 2000. The Doa4 deubiquitinating enzyme is functionally linked to the vacuolar protein-sorting and endocytic pathways. *Molecular biology of the cell*, 11(10), pp.3365–80.

Amerik, a Y., Li, S.J. & Hochstrasser, M., 2000. Analysis of the deubiquitinating enzymes of the yeast *Saccharomyces cerevisiae*. *Biological chemistry*, 381(October), pp.981–992.

Anon, 2008. Protein production and purification. *Nature methods*, 5(2), pp.135–146.

Anton, F. et al., 2013. Two Deubiquitylases Act on Mitofusin and Regulate Mitochondrial Fusion along Independent Pathways. *Molecular Cell*, 49(3), pp.487–498.

Aufderheide, A. et al., 2015. Structural characterization of the interaction of Ubp6 with the 26S proteasome. *Proceedings of the National Academy of Sciences of the United States of America*, 112(28), pp.8626–31.

Avvakumov, G. V et al., 2012. Two ZnF-UBP domains in isopeptidase T (USP5). *Biochemistry*, 51(6), pp.1188–1198.

Bashore, C. et al., 2016. Ubp6 deubiquitinase controls conformational dynamics and substrate degradation of the 26S proteasome. *Nat Struct Mol Biol.*, 22(9), pp.712–719.

Baxter, B.K. et al., 2005. Atg19p ubiquitination and the cytoplasm to vacuole trafficking pathway in yeast. *The Journal of biological chemistry*, 280(47), pp.39067–39076.

Bhattacharya, S. & Ghosh, M.K., 2014. HAUSP, a novel deubiquitinase for Rb - MDM2 the critical regulator. *The FEBS journal*, 281(13), pp.3061–78.

Botstein, D. & Fink, G.R., 2011. Yeast: An experimental organism for 21st century biology. *Genetics*, 189(3), pp.695–704.

Bozza, W.P. & Zhuang, Z., 2011. Biochemical characterization of a multidomain deubiquitinating enzyme Ubp15 and the regulatory role of its terminal domains. *Biochemistry*, 50, pp.6423–6432.

Brooks, C.L. et al., 2007. The p53--Mdm2--HAUSP complex is involved in p53 stabilization by HAUSP. *Oncogene*, 26(51), pp.7262–6.

Brunger, A.T., 2007. Version1.2 of the Crystallography and NMR system. *Nature Protocols*, 2, pp.2728–2733.

Callis, J., 2014. The ubiquitination machinery of the ubiquitin system. *The Arabidopsis book / American Society of Plant Biologists*, 12, p.e0174.

Cao, J. & Yan, Q., 2012. Histone ubiquitination and deubiquitination in transcription, DNA damage response, and cancer. *Frontiers in oncology*, 2(March), p.26.

Chavoshi, S. et al., 2016. Identification of KSHV vIRF1 as a novel interaction partner of human deubiquitinase USP7. *Journal of Biological Chemistry*, 291(12), pp.6281–6291.

Chernova, T.A. et al., 2003. Pleiotropic effects of Ubp6 loss on drug sensitivities and yeast prion are due to depletion of the free ubiquitin pool. *The Journal of biological chemistry*, 278(52), pp.52102–52115.

Clague, M.J., Coulson, J.M. & Urbe, S., 2012. Cellular functions of the DUBs. *J Cell Sci*, 125(Pt

2), pp.277–286.
Clague, M.J., Liu, H. & Urbe, S., 2012. Governance of endocytic trafficking and signaling by reversible ubiquitylation. *Developmental cell*, 23(3), pp.457–467.
Clinkenbeard, K.D., Clinkenbeard, P.A. & Waurzyniak, B.J., 1995. Chaotropic agents cause disaggregation and enhanced activity of Pasteurella haemolytica leukotoxin. *Veterinary Microbiology*, 45(2–3), pp.201–209.
Cohen, M. et al., 2003. Ubp3 requires a cofactor, Bre5, to specifically de-ubiquitinate the COPII protein, Sec23. *Nature Cell Biology*, 5(7), pp.661–667.
Cohen, M., Stutz, F. & Dargemont, C., 2003. Deubiquitination, a new player in Golgi to endoplasmic reticulum retrograde transport. *The Journal of biological chemistry*, 278(52), pp.51989–51992.
Costa, S. et al., 2014. Fusion tags for protein solubility, purification and immunogenicity in Escherichia coli: the novel Fh8 system. *Frontiers in Microbiology*, 5, p.63.
Costanzo, M. et al., 2010. The Genetic Landscape of a Cell. *Science*, 327(5964), pp.425–431.
Crosas, B. et al., 2006. Ubiquitin Chains Are Remodeled at the Proteasome by Opposing Ubiquitin Ligase and Deubiquitinating Activities. *Cell*, 127(7), pp.1401–1413.
D'Arcy, P., Wang, X. & Linder, S., 2015. Deubiquitinase inhibition as a cancer therapeutic strategy. *Pharmacology & therapeutics*, 147, pp.32–54.
Ding, H. et al., 2002. Parallel cloning, expression, purification and crystallization of human proteins for structural genomics. *Acta Cryst D*, 58, pp.2102–2108.
Dupre, S. & Haguenauer-Tsapis, R., 2001. Deubiquitination Step in the Endocytic Pathway of Yeast Plasma Membrane Proteins : Crucial Role of Doa4p Ubiquitin Isopeptidase. *Molecular and cellular biology*, 21(14), pp.4482–4494.
Dyson, M.R. et al., 2004. Production of soluble mammalian proteins in Escherichia coli: identification of protein features that correlate with successful expression. *BMC biotechnology*, 4, p.32.
Eisele, F. et al., 2006. Mutants of the deubiquitinating enzyme Ubp14 decipher pathway diversity of ubiquitin-proteasome linked protein degradation. *Biochemical and Biophysical Research Communications*, 350(2), pp.329–333.
Eletr, Z.M. & Wilkinson, K.D., 2014. Regulation of Proteolysis by Human Deubiquitinating Enzymes. *Biochim Biophys Acta.*, 1843(1), pp.114–128.
Elliott, P.R. et al., 2011. Structural variability of the ubiquitin specific protease DUSP-UBL double domains. *FEBS letters*, 585(21), pp.3385–3390.
Emre, N.C.T. et al., 2005. Maintenance of low histone ubiquitylation by Ubp10 correlates with telomere-proximal Sir2 association and gene silencing. *Molecular cell*, 17(4), pp.585–594.
Emsley, P. & Cowtan, K., 2004. Coot: model-building tools for molecular graphics. *Acta crystallographica. Section D, Biological crystallography*, 60(Pt 12 Pt 1), pp.2126–2132.
Faggiano, S., Alfano, C. & Pastore, A., 2016. The missing links to link ubiquitin: Methods for the enzymatic production of polyubiquitin chains. *Analytical Biochemistry*, 492, pp.82–90.
Finley, D., 2009. Recognition and processing of ubiquitin-protein conjugates by the proteasome. *Annual review of biochemistry*, 78, pp.477–513.
Finley, D. et al., 2012. The ubiquitin-proteasome system of *Saccharomyces cerevisiae*. *Genetics*, 192(2), pp.319–360.
Finley, J.B. et al., 2004. Structural genomics for Caenorhabditis elegans: high throughput protein expression analysis. *Protein expression and purification*, 34(1), pp.49–55.
Graslund, S. et al., 2008. The use of systematic N- and C-terminal deletions to promote

production and structural studies of recombinant proteins. *Protein expression and purification*, 58(2), pp.210–221.
Guterman, A. & Glickman, M.H., 2004. Complementary Roles for Rpn11 and Ubp6 in Deubiquitination and Proteolysis by the Proteasome. *Journal of Biological Chemistry*, 279(3), pp.1729–1738.
Hadjivassiliou, H., Rosenberg, O.S. & Guthrie, C., 2014. The crystal structure of *S. cerevisiae* Sad1, a catalytically inactive deubiquitinase that is broadly required for pre-mRNA splicing. *RNA (New York, N.Y.)*, 20(5), pp.656–669.
Hanna, J. et al., 2006. Deubiquitinating enzyme Ubp6 functions noncatalytically to delay proteasomal degradation. *Cell*, 127(1), pp.99–111.
Hanna, J., Leggett, D.S. & Finley, D., 2003. Ubiquitin depletion as a key mediator of toxicity by translational inhibitors. *Molecular and Cellular Biology*, 23(24), pp.9251–9261.
Heinicke, S. et al., 2007. The Princeton Protein Orthology Database (P-POD): a comparative genomics analysis tool for biologists. *PloS one*, 2(8), p.e766.
Henry, K.W. et al., 2003. Transcriptional activation via sequential histone H2B ubiquitylation and deubiquitylation, mediated by SAGA-associated Ubp8. *Genes and Development*, 17(21), pp.2648–2663.
Hershko, A., 2005. The ubiquitin system for protein degradation and some of its roles in the control of the cell division cycle. *Cell death and differentiation*, 12(9), pp.1191–7.
Hochstrasser, M. & Amerik, A.Y., 2004. Mechanism and function of deubiquitinating enzymes. *Biochimica et Biophysica Acta (BBA) - Molecular Cell Research*, 1695(1–3), pp.189–207.
Hoeijmakers, J.H., 2001. Genome maintenance mechanisms for preventing cancer. *Nature*, 411(6835), pp.366–374.
Hoi, P.M. et al., 2015. Recent advances in structure-based drug design and virtual screening of VEGFR tyrosine kinase inhibitors. *Methods (San Diego, Calif.)*, 71, pp.85–91.
Holowaty, M.N. et al., 2003. Protein Interaction Domains of the Ubiquitin-specific Protease, USP7/HAUSP. *Journal of Biological Chemistry*, 278(48), pp.47753–47761.
van der Horst, A. et al., 2006. FOXO4 transcriptional activity is regulated by monoubiquitination and USP7/HAUSP. *Nature cell biology*, 8(10), pp.1064–1073.
Hu, M. et al., 2002. Crystal structure of a UBP-family deubiquitinating enzyme in isolation and in complex with ubiquitin aldehyde. *Cell*, 111(7), pp.1041–1054.
Hu, M. et al., 2005. Structure and mechanisms of the proteasome-associated deubiquitinating enzyme USP14. *The EMBO Journal*, 24(21), pp.3747–3756.
Jagannathan, M. et al., 2014. A role for USP7 in DNA replication. *Molecular and cellular biology*, 34(1), pp.132–145.
Jeffrey, G.A., 1997. *An Introduction to Hydrogen Bonding*, Oxford: Oxford University Press.
De Jong, R.N. et al., 2006. Solution structure of the human ubiquitin-specific protease 15 DUSP domain. *Journal of Biological Chemistry*, 281(8), pp.5026–5031.
Kahana, A. & Gottschling, D.E., 1999. DOT4 links silencing and cell growth in *Saccharomyces cerevisiae*. *Molecular and cellular biology*, 19(10), pp.6608–6620.
Kane, J.F., 1995. Effects of rare codon clusters on high-level expression of heterologous proteins in Escherichia coli. *Current opinion in biotechnology*, 6(5), pp.494–500.
Katz, E.J., Isasa, M. & Crosas, B., 2010. A new map to understand deubiquitination. *Biochemical Society transactions*, 38(Pt 1), pp.21–28.
Kelley, L.A. et al., 2015. The Phyre2 web portal for protein modeling, prediction and analysis. *Nat. Protocols*, 10(6), pp.845–858.

Khan, M.S. et al., 2016. Denaturation induced aggregation in alpha-crystallin: differential action of chaotropes. *Journal of molecular recognition : JMR*, 29(11), pp.536–543.
Kinner, A. & Kölling, R., 2003. The yeast deubiquitinating enzyme Ubp16 is anchored to the outer mitochondrial membrane. *FEBS Letters*, 549(1–3), pp.135–140.
Kolaj, O. et al., 2009. Use of folding modulators to improve heterologous protein production in Escherichia coli. *Microbial cell factories*, 8, p.9.
Kolling, R. & Hollenberg, C.P., 1994. The ABC-transporter Ste6 accumulates in the plasma membrane in a ubiquitinated form in endocytosis mutants. *The EMBO journal*, 13(14), pp.3261–3271.
Komander, D., Clague, M.J. & Urbé, S., 2009. Breaking the chains: structure and function of the deubiquitinases. *Nature*, 10, pp.550–563.
Kowalski, J.R. & Juo, P., 2012. The role of deubiquitinating enzymes in synaptic function and nervous system diseases. *Neural plasticity*, 2012, p.892749.
Kulathu, Y. & Komander, D., 2012. Atypical ubiquitylation — the unexplored world of polyubiquitin beyond Lys48 and Lys63 linkages. *Nature Reviews Molecular Cell Biology*, 13(8), pp.508–523.
Kvint, K. et al., 2008. Reversal of RNA polymerase II ubiquitylation by the ubiquitin protease Ubp3. *Molecular cell*, 30(4), pp.498–506.
Lam, M.H.Y., 2010. *Proteomic and Molecular Genetic Investigation of Deubiquitinating Enzymes in the Budding Yeast Saccharomyces cerevisiae (Doctoral dissertation)*. University of Toronto, Canada. Retrieved from: https://tspace.library.utoronto.ca
Lee, B.-H. et al., 2010. Enhancement of proteasome activity by a small-molecule inhibitor of USP14. *Nature*, 467(7312), pp.179–184.
Lee, M.J. et al., 2011. Trimming of ubiquitin chains by proteasome-associated deubiquitinating enzymes. *Molecular & cellular proteomics : MCP*, 10(5), p.R110.003871.
Leggett, D.S. et al., 2002. Multiple associated proteins regulate proteasome structure and function. *Molecular Cell*, 10(3), pp.495–507.
Li, K. et al., 2007. Molecular Basis for Bre5 Cofactor Recognition by the Ubp3 Deubiquitylating Enzyme. *Journal of Molecular Biology*, 372, pp.194–204.
Li, K. et al., 2005. Structural basis for interaction between the Ubp3 deubiquitinating enzyme and its Bre5 cofactor. *Journal of Biological Chemistry*, 280(32), pp.29176–29185.
Lionta, E. et al., 2014. Structure-Based Virtual Screening for Drug Discovery: Principles, Applications and Recent Advances. *Current Topics in Medicinal Chemistry*, 14(16), pp.1923–1938.
Liti, G. et al., 2009. Population genomics of domestic and wild yeasts. *Nature*, 458(7236), pp.337–341.
Livnat-Levanon, N. & Glickman, M.H., 2011. Ubiquitin-proteasome system and mitochondria - reciprocity. *Biochimica et biophysica acta*, 1809(2), pp.80–87.
Luna-Vargas, M.P. a et al., 2011. Enabling high-throughput ligation-independent cloning and protein expression for the family of ubiquitin specific proteases. *Journal of Structural Biology*, 175(2), pp.113–119.
Ma, J. et al., 2010. C-terminal region of USP7/HAUSP is critical for deubiquitination activity and contains a second mdm2/p53 binding site. *Archives of biochemistry and biophysics*, 503(2), pp.207–212.
Malawski, G.A. et al., 2006. Identifying protein construct variants with increased crystallization propensity--a case study. *Protein science : a publication of the Protein Society*, 15(12),

pp.2718–28.
Mandawe, J.C., 2010. *Interaction studies of yeast Ubiquitin Specific Processing Protease 15 (UBP15) N-terminal domain (Master's thesis)*. York University, Canada. Retrieved from: https://www.library.yorku.ca
Mao, P. & Smerdon, M.J., 2010. Yeast deubiquitinase Ubp3 interacts with the 26 S proteasome to facilitate Rad4 degradation. *Journal of Biological Chemistry*, 285(48), pp.37542–37550.
Maiti, R. et al., 2004. SuperPose: a simple server for sophisticated structural superposition. *Nucleic Acids Research*, 32(Web Server issue), pp.W590–W594.
Martinez-Hackert, E. & Hendrickson, W.A., 2009. Promiscuous substrate recognition in folding and assembly activities of the trigger factor chaperone. *Cell*, 138(5), pp.923–934.
Meulmeester, E. et al., 2005. Loss of HAUSP-mediated deubiquitination contributes to DNA damage-induced destabilization of HdmX and Hdm2. *Molecular cell*, 18(5), pp.565–576.
Min, J.-H. & Pavletich, N.P., 2007. Recognition of DNA damage by the Rad4 nucleotide excision repair protein. *Nature*, 449(7162), pp.570–575.
Mohammadi, S. et al., 2015. Scope and limitations of yeast as a model organism for studying human tissue-specific pathways. *BMC systems biology*, 9, p.96.
Nijman, S.M.B. et al., 2005. A genomic and functional inventory of deubiquitinating enzymes. *Cell*, 123(5), pp.773–86.
Nostramo, R. et al., 2015. The catalytic activity of the Ubp3 deubiquitinating protease is required for efficient stress granule assembly in *S. cerevisiae*. *Molecular and cellular biology*, 36(1), pp.173–83.
Oling, D., Masoom, R. & Kvint, K., 2014. Loss of Ubp3 increases silencing, decreases unequal recombination in rDNA, and shortens the replicative life span in *Saccharomyces cerevisiae*. *Molecular biology of the cell*, 25, pp.1916–24.
Ostapenko, D., Burton, J.L. & Solomon, M.J., 2015. The Ubp15 deubiquitinase promotes timely entry into S phase in *Saccharomyces cerevisiae*. *Molecular biology of the cell*, 26(12), pp.2205–2216.
Parenteau, J. et al., 2008. Deletion of many yeast introns reveals a minority of genes that require splicing for function. *Molecular biology of the cell*, 19(5), pp.1932–1941.
Park, K.C. et al., 1997. Purification and characterization of UBP6, a new ubiquitin-specific protease in *Saccharomyces cerevisiae*. *Archives of biochemistry and biophysics*, 347(1), pp.78–84.
Patrushev, M. V et al., 2015. Mitochondrial Fission and Fusion. *Biochemistry. Biokhimiia*, 80(11), pp.1457–1464.
Peng, J. et al., 2003. A proteomics approach to understanding protein ubiquitination. *Nature biotechnology*, 21(8), pp.921–926.
Peth, A., Besche, H.C. & Goldberg, A.L., 2009. Ubiquitinated proteins activate the proteasome by binding to Usp14/Ubp6, which causes 20S gate opening. *Molecular cell*, 36(5), pp.794–804.
Piper, R.C., Dikic, I. & Lukacs, G.L., 2014. Ubiquitin-dependent sorting in endocytosis. *Cold Spring Harbor perspectives in biology*, 6(1), pp.a016808–a016808.
Polo, S. et al., 2002. A single motif responsible for ubiquitin recognition and monoubiquitination in endocytic proteins. *Nature*, 416(6879), pp.451–455.
Qin, S. et al., 2009. Sem1p and Ubp6p orchestrate telomeric silencing by modulating histone H2B ubiquitination and H3 acetylation. *Nucleic Acids Research*, 37(6), pp.1843–1853.
Reyes-Turcu, F.E. et al., 2008. Recognition of polyubiquitin isoforms by the multiple ubiquitin

binding modules of isopeptidase T. *The Journal of biological chemistry*, 283(28), pp.19581–19592.
Reyes-Turcu, F.E., Ventii, K.H. & Wilkinson, K.D., 2009. Regulation and Cellular Roles of Ubiquitin-specific Deubiquitinating Enzymes. *Annu Rev Biochem*, 78, pp.363–397.
Richter, C., West, M. & Odorizzi, G., 2007. Dual mechanisms specify Doa4-mediated deubiquitination at multivesicular bodies. *The EMBO journal*, 26(10), pp.2454–2464.
Rosano, G.L. & Ceccarelli, E.A., 2014. Recombinant protein expression in Escherichia coli: Advances and challenges. *Frontiers in Microbiology*, 5(APR), pp.1–17.
Sahtoe, D.D. & Sixma, T.K., 2015. Layers of DUB regulation. *Trends in Biochemical Sciences*, 40(8), pp.456–467.
Saridakis, V. et al., 2005. Structure of the p53 binding domain of HAUSP/USP7 bound to epstein-barr nuclear antigen 1: Implications for EBV-mediated immortalization. *Molecular Cell*, 18(1), pp.25–36.
Sarkari, F. et al., 2010. Further Insight into Substrate Recognition by USP7: Structural and Biochemical Analysis of the HdmX and Hdm2 Interactions with USP7. *Journal of Molecular Biology*, 402(5), pp.825–837.
Sawyer, W.H. & Puckridge, J., 1973. The dissociation of proteins by chaotropic salts. *The Journal of biological chemistry*, 248(24), pp.8429–8433.
Schaefer, J.B. & Morgan, D.O., 2011. Protein-linked ubiquitin chain structure restricts activity of deubiquitinating enzymes. *Journal of Biological Chemistry*, 286(52), pp.45186–45196.
Schellman, J.A., 1997. Temperature, stability, and the hydrophobic interaction. *Biophysical journal*, 73(6), pp.2960–2964.
Schmitz, C., Kinner, A. & Kolling, R., 2005. The Deubiquitinating Enzyme Ubp1 Affects Sorting of the ATP-binding Cassette-Transporter Ste6 in the Endocytic Pathway Carolin. *Molecular biology of the cell*, 16(8), pp.1319–1329.
Schrödinger, L.L.., 2010. The PyMOL Molecular Graphics System.
Schulze, J.M. et al., 2011. Splitting the task: Ubp8 and ubp10 deubiquitinate different cellular pools of H2BK123. *Genes and Development*, 25(21), pp.2242–2247.
Sezonov, G., Joseleau-Petit, D. & D'Ari, R., 2007. Escherichia coli physiology in Luria-Bertani broth. *Journal of bacteriology*, 189(23), pp.8746–8749.
Shapiro, L. & Harris, T., 2000. Finding function through structural genomics. *Current opinion in biotechnology*, 11(1), pp.31–35.
Sheng, Y. et al., 2006. Molecular recognition of p53 and MDM2 by USP7/HAUSP. *Nature structural & molecular biology*, 13(3), pp.285–291.
Shirayama, M. et al., 1999. APC(Cdc20) promotes exit from mitosis by destroying the anaphase inhibitor Pds1 and cyclin Clb5. *Nature*, 402(6758), pp.203–207.
Shrestha, R.K. et al., 2014. Insights into the Mechanism of Deubiquitination by JAMM Deubiquitinases from Cocrystal Structures of the Enzyme with the Substrate and Product. *Biochemistry*, 53, pp.3199–3217.
Smyth, M.S., 2000. x Ray crystallography. *Molecular Pathology*, 53(1), pp.8–14.
Song, M.S. et al., 2008. The deubiquitinylation and localization of PTEN are regulated by a HAUSP-PML network. *Nature*, 455(7214), pp.813–817.
Swaminathan, S., Amerik, A.Y. & Hochstrasser, M., 1999. The Doa4 deubiquitinating enzyme is required for ubiquitin homeostasis in yeast. *Molecular biology of the cell*, 10(8), pp.2583–2594.
Tencer, A.H., Liang, Q. & Zhuang, Z., 2016. Divergence in Ubiquitin Interaction and Catalysis

among the Ubiquitin-Specific Protease Family Deubiquitinating Enzymes. *Biochemistry*, 55(33), pp.4708–4719.
Trempe, J.F., 2011. Reading the ubiquitin postal code. *Current Opinion in Structural Biology*, 21(6), pp.792–801.
Varshavsky, A., 2012. The ubiquitin system, an immense realm. *Annual review of biochemistry*, 81, pp.167–176.
Vera, A. et al., 2007. The conformational quality of insoluble recombinant proteins is enhanced at low growth temperatures. *Biotechnology and bioengineering*, 96(6), pp.1101–1106.
Visintin, R., Prinz, S. & Amon, A., 1997. CDC20 and CDH1: a family of substrate-specific activators of APC-dependent proteolysis. *Science (New York, N.Y.)*, 278(5337), pp.460–463.
Wang, Y. et al., 2005. Differential regulation of G protein α subunit trafficking by mono- and polyubiquitination. *Journal of Biological Chemistry*, 280(1), pp.284–291.
Wang, Y. et al., 2008. Down-regulation of Pkc1-mediated signaling by the deubiquitinating enzyme Ubp3. *The Journal of biological chemistry*, 283(4), pp.1954–1961.
Wernimont, A. & Edwards, A., 2009. In Situ proteolysis to generate crystals for structure determination: An update. *PLoS ONE*, 4(4).
Wojtowicz, A. et al., 2005. Expression of yeast deubiquitination enzyme UBP1 analogues in E. coli. *Microbial cell factories*, 4(1), p.17.
Wyndham, a M., Baker, R.T. & Chelvanayagam, G., 1999. The Ubp6 family of deubiquitinating enzymes contains a ubiquitin-like domain: SUb. *Protein science : a publication of the Protein Society*, 8, pp.1268–1275.
Xu, P. et al., 2009. Quantitative proteomics reveals the function of unconventional ubiquitin chains in proteasomal degradation. *Cell*, 137(1), pp.133–145.
Ye, T. et al., 2012. "Add to subtract": a simple method to remove complex background signals from the 1H nuclear magnetic resonance spectra of mixtures. *Analytical chemistry*, 84(2), pp.994–1002.
Yoshida, N. & Sato, M., 2009. Plasmid uptake by bacteria: a comparison of methods and efficiencies. *Applied microbiology and biotechnology*, 83(5), pp.791–798.

Chapter 3:

Alibek, K. et al., 2014. Implication of human herpesviruses in oncogenesis through immune evasion and supression. *Infectious agents and cancer*, 9(1), p.3.

Angeletti, P.C., Zhang, L. & Wood, C., 2008. The viral etiology of AIDS-associated malignancies. *Advances in pharmacology (San Diego, Calif.)*, 56, pp.509–57.

Bernardi, R. & Pandolfi, P.P., 2007. Structure, dynamics and functions of promyelocytic leukaemia nuclear bodies. *Nature reviews. Molecular cell biology*, 8(12), pp.1006–1016.

Boutell, C. et al., 2005. Reciprocal activities between herpes simplex virus type 1 regulatory protein ICP0, a ubiquitin E3 ligase, and ubiquitin-specific protease USP7. *Journal of virology*, 79(19), pp.12342–12354.

Boutell, C. & Everett, R.D., 2003. The herpes simplex virus type 1 (HSV-1) regulatory protein ICP0 interacts with and Ubiquitinates p53. *The Journal of biological chemistry*, 278(38), pp.36596–36602.

de Castro, E. et al., 2006. ScanProsite: detection of PROSITE signature matches and ProRule-associated functional and structural residues in proteins. *Nucleic acids research*, 34(Web Server issue), pp.W362–5.

Chang, Y. et al., 1994. Identification of herpesvirus-like DNA sequences in AIDS-associated Kaposi's sarcoma. *Science (New York, N.Y.)*, 266(5192), pp.1865–1869.

Chehab, N.H. et al., 1999. Phosphorylation of Ser-20 mediates stabilization of human p53 in response to DNA damage. *Proceedings of the National Academy of Sciences of the United States of America*, 96(24), pp.13777–13782.

Chen, W. et al., 2010. Distinct p53, p53:LANA, and LANA complexes in Kaposi's Sarcoma--associated Herpesvirus Lymphomas. *Journal of virology*, 84(8), pp.3898–3908.

Cummins, J.M. et al., 2004. Tumour suppression: disruption of HAUSP gene stabilizes p53. *Nature*, 428(6982), p.1 p following 486.

Edelman, D.C., 2005. Human herpesvirus 8--a novel human pathogen. *Virology journal*, 2, p.78.

Emsley, P. & Cowtan, K., 2004. Coot: model-building tools for molecular graphics. *Acta crystallographica. Section D, Biological crystallography*, 60(Pt 12 Pt 1), pp.2126–2132.

Everett, R.D. et al., 1997. A novel ubiquitin-specific protease is dynamically associated with the PML nuclear domain and binds to a herpesvirus regulatory protein. *The EMBO journal*, 16(7), pp.1519–1530.

Faesen, A.C. et al., 2011. Article Mechanism of USP7 / HAUSP Activation by Its C-Terminal Ubiquitin-like Domain and Allosteric Regulation by GMP-Synthetase. *Molecular Cell*, 44(1), pp.147–159.

Feng, J. et al., 2004. Stabilization of Mdm2 via decreased ubiquitination is mediated by protein kinase B/Akt-dependent phosphorylation. *Journal of Biological Chemistry*, 279(34), pp.35510–35517.

Gillen, J. et al., 2015. A Survey of the Interactome of Kaposi's Sarcoma-Associated Herpesvirus ORF45 Revealed Its Binding to Viral ORF33 and Cellular USP7, Resulting in Stabilization of ORF33 That Is Required for Production of Progeny Viruses K. Frueh, ed. *Journal of Virology*, 89(9), pp.4918–4931.

Hew, K. et al., 2013. The crystal structure of the DNA-binding domain of vIRF-1 from the oncogenic KSHV reveals a conserved fold for DNA binding and reinforces its role as a transcription factor. *Nucleic acids research*, 41(7), pp.4295–306.

Holowaty, M.N. et al., 2003. Protein Interaction Domains of the Ubiquitin-specific Protease,

USP7/HAUSP. *Journal of Biological Chemistry*, 278(48), pp.47753–47761.
Hu, M. et al., 2002. Crystal structure of a UBP-family deubiquitinating enzyme in isolation and in complex with ubiquitin aldehyde. *Cell*, 111(7), pp.1041–1054.
Hu, M. et al., 2006. Structural basis of competitive recognition of p53 and MDM2 by HAUSP/USP7: Implications for the regulation of the p53-MDM2 pathway. *PLoS Biology*, 4(2), pp.228–239.
Jacobs, S.R. & Damania, B., 2011. The viral interferon regulatory factors of KSHV: Immunosuppressors or oncogenes. *Frontiers in Immunology*, 2(June), pp.1–11.
Jager, W. et al., 2012. The Ubiquitin-Specific Protease USP7 Modulates the Replication of Kaposi's Sarcoma-Associated Herpesvirus Latent Episomal DNA. *Journal of Virology*, 86(12), pp.6745–6757.
Lambert, P.F. et al., 1998. Phosphorylation of p53 serine 15 increases interaction with CBP. *The Journal of biological chemistry*, 273(49), pp.33048–33053.
Lee, H.-R. et al., 2011. Bilateral inhibition of HAUSP deubiquitinase by a viral interferon regulatory factor protein. *Nature structural & molecular biology*, 18(12), pp.1336–44.
Lee, H.-R. et al., 2009. Kaposi's sarcoma-associated herpesvirus viral interferon regulatory factor 4 targets MDM2 to deregulate the p53 tumor suppressor pathway. *Journal of virology*, 83(13), pp.6739–47.
Li, M. et al., 2002. Deubiquitination of p53 by HAUSP is an important pathway for p53 stabilization. *Nature*, 416(6881), pp.648–653.
Li, M. et al., 2000. Inhibition of p300 histone acetyltransferase by viral interferon regulatory factor. *Molecular and cellular biology*, 20(21), pp.8254–8263.
Maul, G.G. & Everett, R.D., 1994. The nuclear location of PML, a cellular member of the C3HC4 zinc-binding domain protein family, is rearranged during herpes simplex virus infection by the C3HC4 viral protein ICP0. *The Journal of general virology*, 75 (Pt 6), pp.1223–1233.
Meredith, M., Orr, A. & Everett, R., 1994. Herpes simplex virus type 1 immediate-early protein Vmw110 binds strongly and specifically to a 135-kDa cellular protein. *Virology*, 200(2), pp.457–469.
Meulmeester, E. et al., 2005. ATM-mediated phosphorylations inhibit Mdmx/Mdm2 stabilization by HAUSP in favor of p53 activation. *Cell cycle (Georgetown, Tex.)*, 4(9), pp.1166–1170.
Monleon, D. et al., 2002. Rapid analysis of protein backbone resonance assignments using cryogenic probes, a distributed Linux-based computing architecture, and an integrated set of spectral analysis tools. *Journal of structural and functional genomics*, 2(2), pp.93–101.
Moore, P.S. & Chang, Y., 1998. Antiviral activity of tumor-suppressor pathways: clues from molecular piracy by KSHV. *Trends in genetics : TIG*, 14(4), pp.144–150.
Nakagawa, K. et al., 1999. Requirement of ATM in phosphorylation of the human p53 protein at serine 15 following DNA double-strand breaks. *Molecular and cellular biology*, 19(4), pp.2828–2834.
Nakamura, H. et al., 2001. Inhibition of p53 tumor suppressor by viral interferon regulatory factor. *Journal of virology*, 75(16), pp.7572–7582.
Park, Y.C. et al., 1999. Structural basis for self-association and receptor recognition of human TRAF2. *Nature*, 398(6727), pp.533–538.
Pattle, S.B. & Farrell, P.J., 2006. The role of Epstein – Barr virus. , pp.1193–1205.
Pfoh, R. et al., 2015. Crystal Structure of USP7 Ubiquitin-like Domains with an ICP0 Peptide Reveals a Novel Mechanism Used by Viral and Cellular Proteins to Target USP7. *PLoS*

pathogens, 11(6), p.e1004950.
Pozharskaya, V.P. et al., 2004. Short duration of elevated vIRF-1 expression during lytic replication of human herpesvirus 8 limits its ability to block antiviral responses induced by alpha interferon in BCBL-1 cells. *Journal of virology*, 78(12), pp.6621–6635.
Salsman, J. et al., 2008. Genome-wide screen of three herpesviruses for protein subcellular localization and alteration of PML nuclear bodies. *PLoS Pathogens*, 4(7), p.e1000100.
Salsman, J. et al., 2012. Proteomic profiling of the human cytomegalovirus UL35 gene products reveals a role for UL35 in the DNA repair response. *Journal of virology*, 86(2), pp.806–20.
Saridakis, V. et al., 2005. Structure of the p53 binding domain of HAUSP/USP7 bound to epstein-barr nuclear antigen 1: Implications for EBV-mediated immortalization. *Molecular Cell*, 18(1), pp.25–36.
Sarkari, F. et al., 2010. Further Insight into Substrate Recognition by USP7: Structural and Biochemical Analysis of the Hdmx and Hdm2 Interactions with USP7. *Journal of Molecular Biology*, 402(5), pp.825–837.
Sarkari, F. et al., 2011. The herpesvirus associated ubiquitin specific protease, USP7, is a negative regulator of PML proteins and PML nuclear bodies. *PloS one*, 6(1), p.e16598.
Sarkari, F. et al., 2013. Ubiquitin-specific Protease 7 Is a Regulator of Ubiquitin-conjugating Enzyme UbE2E1. *Journal of Biological Chemistry*, 288(23), pp.16975–16985.
Schrödinger, L.L., 2010. The PyMOL Molecular Graphics System. Version 2.0.
Seo, T. et al., 2001. Viral interferon regulatory factor 1 of Kaposi's sarcoma-associated herpesvirus binds to p53 and represses p53-dependent transcription and apoptosis. *J. Virol.*, 75(13), pp.6193–6198.
Shadfan, M., Lopez-Pajares, V. & Yuan, Z.-M., 2012. MDM2 and MDMX: Alone and together in regulation of p53. *Translational cancer research*, 1(2), pp.88–89.
Sheng, Y. et al., 2006. Molecular recognition of p53 and MDM2 by USP7/HAUSP. *Nature structural & molecular biology*, 13(3), pp.285–291.
Shin, Y.C. et al., 2006. Inhibition of the ATM / p53 Signal Transduction Pathway by Kaposi ' s Sarcoma-Associated Herpesvirus Interferon Regulatory Factor 1. *Journal of virology*, 80(5), pp.2257–2266.
Sivachandran, N., Sarkari, F. & Frappier, L., 2008. Epstein-Barr nuclear antigen 1 contributes to nasopharyngeal carcinoma through disruption of PML nuclear bodies. *PLoS pathogens*, 4(10), p.e1000170.
Vonrhein, C. et al., 2011. Data processing and analysis with the autoPROC toolbox. *Acta crystallographica. Section D, Biological crystallography*, 67(Pt 4), pp.293–302.
Wen, K.W. & Damania, B., 2010. Kaposi sarcoma-associated herpesvirus (KSHV): molecular biology and oncogenesis. *Cancer letters*, 289(2), pp.140–50.
Ye, T. et al., 2012. "Add to subtract": a simple method to remove complex background signals from the 1H nuclear magnetic resonance spectra of mixtures. *Analytical chemistry*, 84(2), pp.994–1002.

Chapter 4:

Alibek, K. et al., 2014. Implication of human herpesviruses in oncogenesis through immune evasion and supression. *Infectious agents and cancer*, 9(1), p.3.

Bakkenist, C.J. & Kastan, M.B., 2003. DNA damage activates ATM through intermolecular autophosphorylation and dimer dissociation. *Nature*, 421(6922), pp.499–506.

Boeckh, M. & Geballe, A.P., 2011. Cytomegalovirus : pathogen , paradigm , and puzzle. *The Journal of Clinical Investigation*, 121(5), pp.1673–1680.

Boutell, C. et al., 2005. Reciprocal activities between herpes simplex virus type 1 regulatory protein ICP0, a ubiquitin E3 ligase, and ubiquitin-specific protease USP7. *Journal of virology*, 79(19), pp.12342–12354.

Boutell, C. & Everett, R.D., 2003. The herpes simplex virus type 1 (HSV-1) regulatory protein ICP0 interacts with and Ubiquitinates p53. *The Journal of biological chemistry*, 278(38), pp.36596–36602.

Boutell, C., Orr, A. & Everett, R.D., 2003. PML residue lysine 160 is required for the degradation of PML induced by herpes simplex virus type 1 regulatory protein ICP0. *Journal of virology*, 77(16), pp.8686–8694.

Bresnahan, W. a & Shenk, T.E., 2000. UL82 virion protein activates expression of immediate early viral genes in human cytomegalovirus-infected cells. *Proceedings of the National Academy of Sciences of the United States of America*, 97(26), pp.14506–14511.

Brooks, C.L. et al., 2007. The p53--Mdm2--HAUSP complex is involved in p53 stabilization by HAUSP. *Oncogene*, 26(51), pp.7262–7266.

Brunger, A.T., 2007. Version1.2 of the Crystallography and NMR system. *Nature Protocols*, 2, pp.2728–2733.

Cantrell, S.R. & Bresnahan, W.A., 2006. Human Cytomegalovirus (HCMV) UL82 Gene Product (pp71) Relieves hDaxx-Mediated Repression of HCMV Replication. *Journal of Virology*, 80(12), pp.6188–6191.

Cazzalini, O. et al., 2010. Multiple roles of the cell cycle inhibitor p21(CDKN1A) in the DNA damage response. *Mutation research*, 704(1–3), pp.12–20.

Chavoshi, S. et al., 2016. Identification of KSHV vIRF1 as a novel interaction partner of human deubiquitinase USP7. *Journal of Biological Chemistry*, 291(12), pp.6281–6291.

Chee, M.S. et al., 1990. Analysis of the protein-coding content of the sequence of human cytomegalovirus strain AD169. *Current topics in microbiology and immunology*, 154, pp.125–169.

Chehab, N.H. et al., 2000. Chk2/hCds1 functions as a DNA damage checkpoint in G(1) by stabilizing p53. *Genes & development*, 14(3), pp.278–288.

Craig, a L. et al., 1999. Novel phosphorylation sites of human tumour suppressor protein p53 at Ser20 and Thr18 that disrupt the binding of mdm2 (mouse double minute 2) protein are modified in human cancers. *The Biochemical journal*, 342 (Pt 1), pp.133–141.

Davison, A.J. & Stow, N.D., 2005. New genes from old: redeployment of dUTPase by herpesviruses. *Journal of virology*, 79(20), pp.12880–12892.

Emsley, P. & Cowtan, K., 2004. Coot: model-building tools for molecular graphics. *Acta crystallographica. Section D, Biological crystallography*, 60(Pt 12 Pt 1), pp.2126–2132.

Everett, R.D. et al., 1997. A novel ubiquitin-specific protease is dynamically associated with the PML nuclear domain and binds to a herpesvirus regulatory protein. *The EMBO journal*, 16(7), pp.1519–1530.

Everett, R.D., 2001. DNA viruses and viral proteins that interact with PML nuclear bodies. *Oncogene*, 20(49), pp.7266–7273.
Everett, R.D. et al., 2013. The replication defect of ICP0-null mutant herpes simplex virus 1 can be largely complemented by the combined activities of human cytomegalovirus proteins IE1 and pp71. *Journal of virology*, 87(2), pp.978–990.
Feng, J. et al., 2004. Stabilization of Mdm2 via decreased ubiquitination is mediated by protein kinase B/Akt-dependent phosphorylation. *Journal of Biological Chemistry*, 279(34), pp.35510–35517.
Frappier, L., 2011. Viral disruption of promyelocytic leukemia (PML) nuclear bodies by hijacking host PML regulators. *Virulence*, 2(1), pp.58–62.
Friborg, J.J. et al., 1999. p53 inhibition by the LANA protein of KSHV protects against cell death. *Nature*, 402(6764), pp.889–894.
Gaspar, M. & Shenk, T., 2006. Human cytomegalovirus inhibits a DNA damage response by mislocalizing checkpoint proteins. *Proceedings of the National Academy of Sciences of the United States of America*, 103(8), pp.2821–2826.
Gillen, J. et al., 2015. A Survey of the Interactome of Kaposi's Sarcoma-Associated Herpesvirus ORF45 Revealed Its Binding to Viral ORF33 and Cellular USP7, Resulting in Stabilization of ORF33 That Is Required for Production of Progeny Viruses K. Frueh, ed. *Journal of Virology*, 89(9), pp.4918–4931.
Goderis, J. et al., 2016. Hearing in Children with Congenital Cytomegalovirus Infection: Results of a Longitudinal Study. *The Journal of pediatrics*, 172, p.110–115.e2.
Griffiths, P., Baraniak, I. & Reeves, M., 2015. The pathogenesis of human cytomegalovirus. *The Journal of pathology*, 235(2), pp.288–297.
Grosse, S.D., Ross, D.S. & Dollard, S.C., 2008. Congenital cytomegalovirus (CMV) infection as a cause of permanent bilateral hearing loss: a quantitative assessment. *Journal of clinical virology*, 41(2), pp.57–62.
He, Q. et al., 2016. The Daxx/Atrx Complex Protects Tandem Repetitive Elements during DNA Hypomethylation by Promoting H3K9 Trimethylation. *Cell Stem Cell*, 17(3), pp.273–286.
Hensel, G.M. et al., 1996. Intracellular localization and expression of the human cytomegalovirus matrix phosphoprotein pp71 (ppUL82): evidence for its translocation into the nucleus. *The Journal of general virology*, 77 (Pt 12, pp.3087–3097.
Hofmann, H., Sindre, H. & Stamminger, T., 2002. Functional interaction between the pp71 protein of human cytomegalovirus and the PML-interacting protein human Daxx. *Journal of virology*, 76(11), pp.5769–5783.
Holowaty, M.N. et al., 2003. Protein Interaction Domains of the Ubiquitin-specific Protease, USP7/HAUSP. *Journal of Biological Chemistry*, 278(48), pp.47753–47761.
Ishov, A.M., Vladimirova, O. V & Maul, G.G., 2002. Daxx-Mediated Accumulation of Human Cytomegalovirus Tegument Protein pp71 at ND10 Facilitates Initiation of Viral Infection at These Nuclear Domains. *Journal of Virology*, 76(15), pp.7705–7712.
Iyer, N.G. et al., 2004. p300 regulates p53-dependent apoptosis after DNA damage in colorectal cancer cells by modulation of PUMA/p21 levels. *Proceedings of the National Academy of Sciences*, 101(19), pp.7386–7391.
Jagannathan, M. et al., 2014. A role for USP7 in DNA replication. *Molecular and cellular biology*, 34(1), pp.132–145.
Jager, W. et al., 2012. The Ubiquitin-Specific Protease USP7 Modulates the Replication of Kaposi's Sarcoma-Associated Herpesvirus Latent Episomal DNA. *Journal of Virology*,

86(12), pp.6745–6757.
Kalejta, R.F., 2008. Tegument proteins of human cytomegalovirus. *Microbiology and molecular biology reviews : MMBR*, 72(2), pp.249–265.
Kalejta, R.F., Bechtel, J.T. & Shenk, T., 2003. Human cytomegalovirus pp71 stimulates cell cycle progression by inducing the proteasome-dependent degradation of the retinoblastoma family of tumor suppressors. *Molecular and cellular biology*, 23(6), pp.1885–1895.
Kalejta, R.F. & Shenk, T., 2003. The human cytomegalovirus UL82 gene product (pp71) accelerates progression through the G1 phase of the cell cycle. *Journal of virology*, 77(6), pp.3451–3459.
Kawauchi, K. & Wolf, S.J., 2014. Understanding p53: new insights into tumor suppression. *Expert review of anticancer therapy*, 14(10), pp.1101–1103.
Lambert, P.F. et al., 1998. Phosphorylation of p53 serine 15 increases interaction with CBP. *The Journal of biological chemistry*, 273(49), pp.33048–33053.
Lee, H.-R. et al., 2011. Bilateral inhibition of HAUSP deubiquitinase by a viral interferon regulatory factor protein. *Nature structural & molecular biology*, 18(12), pp.1336–1344.
Lee, H.-R. et al., 2009. Kaposi's sarcoma-associated herpesvirus viral interferon regulatory factor 4 targets MDM2 to deregulate the p53 tumor suppressor pathway. *Journal of virology*, 83(13), pp.6739–6747.
Lee, H.R. et al., 2014. Kaposi's Sarcoma-Associated Herpesvirus Viral Interferon Regulatory Factor 4 (vIRF4) Targets Expression of Cellular IRF4 and the Myc Gene To Facilitate Lytic Replication. *Journal of Virology*, 88(4), pp.2183–2194.
Li, M. et al., 2002. Deubiquitination of p53 by HAUSP is an important pathway for p53 stabilization. *Nature*, 416(6881), pp.648–653.
Li, M. et al., 2000. Inhibition of p300 histone acetyltransferase by viral interferon regulatory factor. *Molecular and cellular biology*, 20(21), pp.8254–8263.
Lukashchuk, V. et al., 2008. Human cytomegalovirus protein pp71 displaces the chromatin-associated factor ATRX from nuclear domain 10 at early stages of infection. *Journal of virology*, 82(24), pp.12543–12554.
Maul, G.G., 1998. Nuclear domain 10, the site of DNA virus transcription and replication. *BioEssays : news and reviews in molecular, cellular and developmental biology*, 20(8), pp.660–667.
Maul, G.G. & Everett, R.D., 1994. The nuclear location of PML, a cellular member of the C3HC4 zinc-binding domain protein family, is rearranged during herpes simplex virus infection by the C3HC4 viral protein ICP0. *The Journal of general virology*, 75 (Pt 6), pp.1223–1233.
Maya, R., 2001. ATM-dependent phosphorylation of Mdm2 on serine 394: role in p53 activation by DNA damage. *Genes Dev.*, pp.1067–1077.
Mayo, L.D. & Donner, D.B., 2001. A phosphatidylinositol 3-kinase/Akt pathway promotes translocation of Mdm2 from the cytoplasm to the nucleus. *Proceedings of the National Academy of Sciences of the United States of America*, 98(20), pp.11598–11603.
McFarlane, S. & Preston, C.M., 2011. Human cytomegalovirus immediate early gene expression in the osteosarcoma line U2OS is repressed by the cell protein ATRX. *Virus Research*, 157(1), pp.47–53.
Meredith, M., Orr, A. & Everett, R., 1994. Herpes simplex virus type 1 immediate-early protein Vmw110 binds strongly and specifically to a 135-kDa cellular protein. *Virology*, 200(2), pp.457–469.

Moll, U.M. & Petrenko, O., 2003. The MDM2-p53 Interaction. *Molecular Cancer Research*, 1(14), pp.1001–1008.
Monleon, D. et al., 2002. Rapid analysis of protein backbone resonance assignments using cryogenic probes, a distributed Linux-based computing architecture, and an integrated set of spectral analysis tools. *Journal of structural and functional genomics*, 2(2), pp.93–101.
Parkinson, J. & Everett, R.D., 2000. Alphaherpesvirus proteins related to herpes simplex virus type 1 ICP0 affect cellular structures and proteins. *Journal of virology*, 74(21), pp.10006–10017.
Pearson, M. et al., 2000. PML regulates p53 acetylation and premature senescence induced by oncogenic Ras. *Nature*, 406(6792), pp.207–210.
Penkert, R.R. & Kalejta, R.F., 2010. Nuclear localization of tegument-delivered pp71 in human cytomegalovirus-infected cells is facilitated by one or more factors present in terminally differentiated fibroblasts. *Journal of virology*, 84(19), pp.9853–9863.
Penkert, R.R. & Kalejta, R.F., 2012. Tale of a tegument transactivator: the past, present and future of human CMV pp71. *Future Virology*, 7(9), pp.855–869.
Pfoh, R. et al., 2015. Crystal Structure of USP7 Ubiquitin-like Domains with an ICP0 Peptide Reveals a Novel Mechanism Used by Viral and Cellular Proteins to Target USP7. *PLoS pathogens*, 11(6), p.e1004950.
Reed, S.M. & Quelle, D.E., 2015. p53 Acetylation: Regulation and Consequences R. S. Hartley, ed. *Cancers*, 7(1), pp.30–69.
Reeves, M. & Sinclair, J., 2013. Regulation of Human Cytomegalovirus Transcription in Latency: Beyond the Major Immediate-Early Promoter. *Viruses*, 5(6), pp.1395–1413.
Reeves, M.B. & Sinclair, J.H., 2010. Analysis of latent viral gene expression in natural and experimental latency models of human cytomegalovirus and its correlation with histone modifications at a latent promoter. *The Journal of general virology*, 91(Pt 3), pp.599–604.
Rieder, F.J.J. et al., 2017. Human cytomegalovirus phosphoproteins are hypophosphorylated and intrinsically disordered. *The Journal of general virology*, 98(3), pp.471–485.
Saffert, R.T. & Kalejta, R.F., 2007. Human cytomegalovirus gene expression is silenced by Daxx-mediated intrinsic immune defense in model latent infections established in vitro. *Journal of virology*, 81(17), pp.9109–9120.
Salsman, J. et al., 2012. Proteomic profiling of the human cytomegalovirus UL35 gene products reveals a role for UL35 in the DNA repair response. *Journal of virology*, 86(2), pp.806–20.
Sancar, A. et al., 2004. Molecular mechanisms of mammalian DNA repair and the DNA damage checkpoints. *Annual review of biochemistry*, 73, pp.39–85.
Saridakis, V. et al., 2005. Structure of the p53 binding domain of HAUSP/USP7 bound to epstein-barr nuclear antigen 1: Implications for EBV-mediated immortalization. *Molecular Cell*, 18(1), pp.25–36.
Sarkari, F. et al., 2010. Further Insight into Substrate Recognition by USP7: Structural and Biochemical Analysis of the HdmX and Hdm2 Interactions with USP7. *Journal of Molecular Biology*, 402(5), pp.825–837.
Sarkari, F. et al., 2011. The herpesvirus associated ubiquitin specific protease, USP7, is a negative regulator of PML proteins and PML nuclear bodies. *PloS one*, 6(1), p.e16598.
Sarkari, F. et al., 2013. Ubiquitin-specific Protease 7 Is a Regulator of Ubiquitin-conjugating Enzyme UbE2E1. *Journal of Biological Chemistry*, 288(23), pp.16975–16985.
Schrödinger, L.L.., 2010. The PyMOL Molecular Graphics System. Version 2.0.
Seo, T. et al., 2001. Viral interferon regulatory factor 1 of Kaposi's sarcoma-associated

herpesvirus binds to p53 and represses p53-dependent transcription and apoptosis. *J. Virol.*, 75(13), pp.6193–6198.
Shen, W. et al., 2008. Nuclear trafficking of the Human Cytomegalovirus pp71 (ppUL82) tegument protein. *Virology*, 376(1), pp.42–52.
Sheng, Y. et al., 2006. Molecular recognition of p53 and MDM2 by USP7/HAUSP. *Nature structural & molecular biology*, 13(3), pp.285–291.
Shiloh, Y. & Ziv, Y., 2013. The ATM protein kinase: regulating the cellular response to genotoxic stress, and more. *Nature Reviews Molecular Cell Biology*, 14(4), pp.197–210.
Shin, Y.C. et al., 2006. Inhibition of the ATM / p53 Signal Transduction Pathway by Kaposi ' s Sarcoma-Associated Herpesvirus Interferon Regulatory Factor 1. *Journal of virology*, 80(5), pp.2257–2266.
Sivachandran, N., Sarkari, F. & Frappier, L., 2008. Epstein-Barr nuclear antigen 1 contributes to nasopharyngeal carcinoma through disruption of PML nuclear bodies. *PLoS pathogens*, 4(10), p.e1000170.
Smith, R.M., Kosuri, S. & Kerry, J.A., 2014. Role of human cytomegalovirus tegument proteins in virion assembly. *Viruses*, 6(2), pp.582–605.
Sun, Y., 2006. p53 and its downstream proteins as molecular targets of cancer. *Molecular carcinogenesis*, 45(6), pp.409–415.
Tang, J. et al., 2006. Critical role for Daxx in regulating Mdm2. *Nature cell biology*, 8(8), pp.855–862.
Tang, J. et al., 2010. Daxx is reciprocally regulated by Mdm2 and Hausp. *Biochem Biophys Res Commun.*, 393(3), pp.542–545.
Tang, J. et al., 2013. Phosphorylation of Daxx by ATM Contributes to DNA Damage-Induced p53 Activation. *PLoS ONE*, 8(2), pp.1–7.
Tavalai, N. & Stamminger, T., 2011. Intrinsic cellular defense mechanisms targeting human cytomegalovirus. *Virus research*, 157(2), pp.128–133.
Tomtishen III, J., 2012. Human cytomegalovirus tegument proteins (pp65, pp71, pp150, pp28). *Virology Journal*, 9(1), p.22.
Torres, L. & Tang, Q., 2015. Immediate–Early (IE) gene regulation of cytomegalovirus: IE1- and pp71-mediated viral strategies against cellular defenses. *Virol Sin.*, 29(6), pp.343–352.
Uddin, S. et al., 2005. Inhibition of phosphatidylinositol 3'-kinase/AKT signaling promotes apoptosis of primary effusion lymphoma cells. *Clinical cancer research : an official journal of the American Association for Cancer Research*, 11(8), pp.3102–3108.
Varnum, S.M. et al., 2004. Identification of Proteins in Human Cytomegalovirus (HCMV) Particles : the HCMV Proteome Identification of Proteins in Human Cytomegalovirus (HCMV) Particles : the HCMV Proteome †. *Journal of virology*, 78(20), pp.10960–10966.
Voon, H.P.J. & Wong, L.H., 2016. New players in heterochromatin silencing: histone variant H3.3 and the ATRX/DAXX chaperone. *Nucleic Acids Research*, 44(4), pp.1496–1501.
Wagner, M.J. & Smiley, J.R., 2011. Herpes simplex virus requires VP11/12 to activate Src family kinase-phosphoinositide 3-kinase-Akt signaling. *Journal of virology*, 85(6), pp.2803–2812.
Wang, L. et al., 2011. Interplay between MDM2, MDMX, Pirh2 and COP1: The negative regulators of p53. *Molecular Biology Reports*, 38(1), pp.229–236.
Weber, J.D. et al., 2000. Cooperative signals governing ARF-mdm2 interaction and nucleolar localization of the complex. *Molecular and cellular biology*, 20(7), pp.2517–2528.
Winkler, L.L., Hwang, J. & Kalejta, R.F., 2013. Ubiquitin-independent proteasomal degradation

of tumor suppressors by human cytomegalovirus pp71 requires the 19S regulatory particle. *Journal of virology*, 87(8), pp.4665–4671.

Xia, L. et al., 2017. Human Cytomegalovirus vaccine development: Immune responses to look into vaccine strategy. *Human vaccines & immunotherapeutics*, 14(2), pp.292–303.

Ye, T. et al., 2012. "Add to subtract": a simple method to remove complex background signals from the 1H nuclear magnetic resonance spectra of mixtures. *Analytical chemistry*, 84(2), pp.994–1002.

Chapter 5:

Ashizawa, A. et al., 2012. The ubiquitin system and Kaposi's sarcoma-associated herpesvirus. *Frontiers in Microbiology*, 3(February), pp.1–10.

Baresova, P., Pitha, P.M. & Lubyova, B., 2013. Distinct roles of Kaposi's sarcoma-associated herpesvirus-encoded viral interferon regulatory factors in inflammatory response and cancer. *Journal of virology*, 87, pp.9398–9410.

Bashore, C. et al., 2016. Ubp6 deubiquitinase controls conformational dynamics and substrate degradation of the 26S proteasome. *Nat Struct Mol Biol.*, 22(9), pp.712–719.

Boeckh, M. & Geballe, A.P., 2011. Cytomegalovirus : pathogen , paradigm , and puzzle. *The Journal of Clinical Investigation*, 121(5), pp.1673–1680.

Bozza, W.P. & Zhuang, Z., 2011. Biochemical characterization of a multidomain deubiquitinating enzyme Ubp15 and the regulatory role of its terminal domains. *Biochemistry*, 50, pp.6423–6432.

Bresnahan, W. a & Shenk, T.E., 2000. UL82 virion protein activates expression of immediate early viral genes in human cytomegalovirus-infected cells. *Proceedings of the National Academy of Sciences of the United States of America*, 97(26), pp.14506–14511.

Chavoshi, S. et al., 2016. Identification of KSHV vIRF1 as a novel interaction partner of human deubiquitinase USP7. *Journal of Biological Chemistry*, 291(12), pp.6281–6291.

Choi, Y.B. & Nicholas, J., 2010. Bim nuclear translocation and inactivation by viral interferon regulatory factor. *PLoS pathogens*, 6(8), p.e1001031.

Coen, N. et al., 2014. KSHV Targeted Therapy: An Update on Inhibitors of Viral Lytic Replication. *viruses*, 6, pp.4731–4759.

Cohen, B.E., Durstenfeld, A. & Roehm, P.C., 2014. Viral Causes of Hearing Loss: A Review for Hearing Health Professionals. *Trends in Hearing*, 18, p.2331216514541361.

Deng, H., Liang, Y. & Sun, R., 2007. Regulation of KSHV lytic gene expression. *Current topics in microbiology and immunology*, 312, pp.157–183.

Dittmer, D.P. & Damania, B., 2016. Kaposi sarcoma–associated herpesvirus: immunobiology, oncogenesis, and therapy. *The Journal of Clinical Investigation*, 126(9), pp.3165–3175.

Dyson, M.R. et al., 2004. Production of soluble mammalian proteins in Escherichia coli: identification of protein features that correlate with successful expression. *BMC biotechnology*, 4, p.32.

el-Deiry, W.S. et al., 1993. WAF1, a potential mediator of p53 tumor suppression. *Cell*, 75(4), pp.817–825.

Evensen, L., Link, W. & Lorens, J.B., 2010. Imaged-based high-throughput screening for anti-angiogenic drug discovery. *Current pharmaceutical design*, 16(35), pp.3958–3963.

Everett, R.D. et al., 1997. A novel ubiquitin-specific protease is dynamically associated with the PML nuclear domain and binds to a herpesvirus regulatory protein. *The EMBO journal*, 16(7), pp.1519–1530.

Feldman, G. et al., 2004. Detection of tetracysteine-tagged proteins using a biarsenical fluorescein derivative through dry microplate array gel electrophoresis. *Electrophoresis*, 25(15), pp.2447–2451.

Fowotade, A., 2017. *Molecular Virology of KSHV: Elucidating VIRF2 AND VIRF4 Function*. University of Surrey, U.S.A. Retrieved from: http://epubs.surrey.ac.uk/id/eprint/813233

Gaspar, M. & Shenk, T., 2006. Human cytomegalovirus inhibits a DNA damage response by mislocalizing checkpoint proteins. *Proceedings of the National Academy of Sciences of the*

United States of America, 103(8), pp.2821–2826.
Gelperin, D.M. et al., 2005. Biochemical and genetic analysis of the yeast proteome with a movable ORF collection. *Genes and Development*, 19(23), pp.2816–2826.
Gillen, J. et al., 2015. A Survey of the Interactome of Kaposi's Sarcoma-Associated Herpesvirus ORF45 Revealed Its Binding to Viral ORF33 and Cellular USP7, Resulting in Stabilization of ORF33 That Is Required for Production of Progeny Viruses K. Frueh, ed. *Journal of Virology*, 89(9), pp.4918–4931.
Gomez, T.A. et al., 2011. Identification of a functional docking site in the Rpn1 LRR domain for the UBA-UBL domain protein Ddi1. *BMC biology*, 9, p.33.
Grosse, S.D., Ross, D.S. & Dollard, S.C., 2008. Congenital cytomegalovirus (CMV) infection as a cause of permanent bilateral hearing loss: a quantitative assessment. *Journal of clinical virology*, 41(2), pp.57–62.
Hainaut, P. et al., 1997. Database of p53 gene somatic mutations in human tumors and cell lines: updated compilation and future prospects. *Nucleic acids research*, 25(1), pp.151–157.
Hanpude, P. et al., 2015. Deubiquitinating enzymes in cellular signaling and disease regulation. *IUBMB life*, 67(7), pp.544–555.
He, M. et al., 2016. The emerging role of deubiquitinating enzymes in genomic integrity, diseases, and therapeutics. *Cell & bioscience*, 6, p.62.
Heinicke, S. et al., 2007. The Princeton Protein Orthology Database (P-POD): a comparative genomics analysis tool for biologists. *PloS one*, 2(8), p.e766.
Hong, C.W. & Zeng, Q., 2014. Tapping the treasure of intracellular oncotargets with immunotherapy. *FEBS Letters*, 588(2), pp.350–355.
Hu, M. et al., 2005. Structure and mechanisms of the proteasome-associated deubiquitinating enzyme USP14. *The EMBO Journal*, 24(21), pp.3747–3756.
Ishov, A.M., Vladimirova, O. V & Maul, G.G., 2002. Daxx-Mediated Accumulation of Human Cytomegalovirus Tegument Protein pp71 at ND10 Facilitates Initiation of Viral Infection at These Nuclear Domains. *Journal of Virology*, 76(15), pp.7705–7712.
Jager, W. et al., 2012. The Ubiquitin-Specific Protease USP7 Modulates the Replication of Kaposi's Sarcoma-Associated Herpesvirus Latent Episomal DNA. *Journal of Virology*, 86(12), pp.6745–6757.
Kalejta, R.F., Bechtel, J.T. & Shenk, T., 2003. Human cytomegalovirus pp71 stimulates cell cycle progression by inducing the proteasome-dependent degradation of the retinoblastoma family of tumor suppressors. *Molecular and cellular biology*, 23(6), pp.1885–1895.
Kalejta, R.F. & Shenk, T., 2003. The human cytomegalovirus UL82 gene product (pp71) accelerates progression through the G1 phase of the cell cycle. *Journal of virology*, 77(6), pp.3451–3459.
Lam, M.H.Y., 2010. *Proteomic and Molecular Genetic Investigation of Deubiquitinating Enzymes in the Budding Yeast Saccharomyces cerevisiae (Doctoral dissertation)*. University of Toronto, Canada. Retrieved from: https://tspace.library.utoronto.ca
Lane, D.P. & Verma, C., 2012. Mdm2 in Evolution. *Genes & Cancer*, 3, pp.320–324.
Lee, H.-R. et al., 2011. Bilateral inhibition of HAUSP deubiquitinase by a viral interferon regulatory factor protein. *Nature structural & molecular biology*, 18(12), pp.1336–1344.
Lin, R. et al., 2001. HHV-8 encoded vIRF-1 represses the interferon antiviral response by blocking IRF-3 recruitment of the CBP/p300 coactivators. *Oncogene*, 20(7), pp.800–811.
Liu, Z. et al., 2012. Different expression systems for production of recombinant proteins in *Saccharomyces cerevisiae. Biotechnology and Bioengineering*, 109(5), pp.1259–1268.

Luna-Vargas, M.P. a et al., 2011. Enabling high-throughput ligation-independent cloning and protein expression for the family of ubiquitin specific proteases. *Journal of Structural Biology*, 175(2), pp.113–119.
Ma, Z. et al., 2015. Modulation of the cGAS-STING DNA sensing pathway by gammaherpesviruses. *Proceedings of the National Academy of Sciences of the United States of America*, 112(31), pp.E4306–E4315.
Mallery, D.L. et al., 2010. Antibodies mediate intracellular immunity through tripartite motif-containing 21 (TRIM21). *Proceedings of the National Academy of Sciences*, 107(46), pp.19985–19990.
Mariggiò, G., Koch, S. & Schulz, T.F., 2017. Kaposi sarcoma herpesvirus pathogenesis. *Philosophical transactions of the Royal Society of London. Series B, Biological sciences*, 372(1732), p. 20160275.
Meredith, M., Orr, A. & Everett, R., 1994. Herpes simplex virus type 1 immediate-early protein Vmw110 binds strongly and specifically to a 135-kDa cellular protein. *Virology*, 200(2), pp.457–469.
Mesri, E. a., Feitelson, M. a. & Munger, K., 2014. Human viral oncogenesis: A cancer hallmarks analysis. *Cell Host and Microbe*, 15(3), pp.266–282.
Mitchell, D. a, Marshall, T.K. & Deschenes, R.J., 1993. Vectors for the inducible overexpression of glutathione S-transferase fusion proteins in yeast. *Yeast (Chichester, England)*, 9(7), pp.715–722.
Nakamura, H. et al., 2003. Global changes in Kaposi's sarcoma-associated virus gene expression patterns following expression of a tetracycline-inducible Rta transactivator. *Journal of virology*, 77(7), pp.4205–4220.
Nakamura, H. et al., 2001. Inhibition of p53 tumor suppressor by viral interferon regulatory factor. *Journal of virology*, 75(16), pp.7572–7582.
Nickischer, D. et al., 2018. Challenges and Opportunities in Enabling High-Throughput, Miniaturized High Content Screening. *Methods in molecular biology (Clifton, N.J.)*, 1683, pp.165–191.
Olivier, M., Hollstein, M. & Hainaut, P., 2010. TP53 mutations in human cancers: origins, consequences, and clinical use. *Cold Spring Harbor perspectives in biology*, 2(1), p.a001008.
Ostapenko, D., Burton, J.L. & Solomon, M.J., 2015. The Ubp15 deubiquitinase promotes timely entry into S phase in *Saccharomyces cerevisiae*. *Molecular biology of the cell*, 26(12), pp.2205–2216.
Pomorski, A. & Krezel, A., 2011. Exploration of biarsenical chemistry--challenges in protein research. *Chembiochem : a European journal of chemical biology*, 12(8), pp.1152–1167.
Rasmussen, a et al., 2011. A new expression vector for production of enzymes in the yeast Saccharomyces (Lachancea) kluyveri. *Nucleosides, nucleotides & nucleic acids*, 30(12), pp.1227–1232.
Romanos, M. a, Scorer, C. a & Clare, J.J., 1992. Foreign gene expression in yeast: a review. *Yeast (Chichester, England)*, 8(6), pp.423–488.
Salsman, J. et al., 2012. Proteomic profiling of the human cytomegalovirus UL35 gene products reveals a role for UL35 in the DNA repair response. *Journal of virology*, 86(2), pp.806–820.
Sancar, A. et al., 2004. Molecular mechanisms of mammalian DNA repair and the DNA damage checkpoints. *Annual review of biochemistry*, 73, pp.39–85.
Saridakis, V. et al., 2005. Structure of the p53 binding domain of HAUSP/USP7 bound to

epstein-barr nuclear antigen 1: Implications for EBV-mediated immortalization. *Molecular Cell*, 18(1), pp.25–36.
Sarkari, F., 2010. *Functions of Ubiquitin Specific Protease 7 (USP7) in Epstein- Barr Virus Infection and Associated Cancers*. University of Toronto, Canada. Retrieved from: https://tspace.library.utoronto.ca
Sarkari, F. et al., 2010. Further Insight into Substrate Recognition by USP7: Structural and Biochemical Analysis of the HdmX and Hdm2 Interactions with USP7. *Journal of Molecular Biology*, 402(5), pp.825–837.
Seo, T. et al., 2001. Viral interferon regulatory factor 1 of Kaposi's sarcoma-associated herpesvirus binds to p53 and represses p53-dependent transcription and apoptosis. *J. Virol.*, 75(13), pp.6193–6198.
Seo, T. et al., 2002. Viral interferon regulatory factor 1 of Kaposi's sarcoma-associated herpesvirus interacts with a cell death regulator, GRIM19, and inhibits interferon/retinoic acid-induced cell death. *Journal of virology*, 76(17), pp.8797–8807.
Sheng, Y. et al., 2006. Molecular recognition of p53 and MDM2 by USP7/HAUSP. *Nature structural & molecular biology*, 13(3), pp.285–291.
Shi, Y. et al., 2016. Rpn1 provides adjacent receptor sites for substrate binding and deubiquitination by the proteasome. *Science (New York, N.Y.)*, 351(6275), p.aad9421.
Shin, Y.C. et al., 2006. Inhibition of the ATM / p53 Signal Transduction Pathway by Kaposi's Sarcoma-Associated Herpesvirus Interferon Regulatory Factor 1. *Journal of virology*, 80(5), pp.2257–2266.
Smith, L.R. et al., 2013. Clinical Development of a Cytomegalovirus DNA Vaccine: From Product Concept to Pivotal Phase 3 Trial. *Vaccines*, 1(4), pp.398–414.
Stinski, M.F. & Isomura, H., 2008. Role of the cytomegalovirus major immediate early enhancer in acute infection and reactivation from latency. *Medical microbiology and immunology*, 197(2), pp.223–231.
Torres, L. & Tang, Q., 2015. Immediate–Early (IE) gene regulation of cytomegalovirus: IE1- and pp71-mediated viral strategies against cellular defenses. *Virol Sin.*, 29(6), pp.343–352.
Turnbull, A.P. et al., 2017. Molecular basis of USP7 inhibition by selective small molecule 1 inhibitors. *Nature Publishing Group*, 550(7677), pp.481–486.
Vu, B.T. & Vassilev, L., 2011. Small-molecule inhibitors of the p53-MDM2 interaction. *Current topics in microbiology and immunology*, 348, pp.151–172.
Wahl, G.M. & Carr, A.M., 2001. The evolution of diverse biological responses to DNA damage : insights from yeast and p53. *Nature Cell Biology*, 3(12), pp.277–286.
Wang, L. et al., 2011. Interplay between MDM2, MDMX, Pirh2 and COP1: The negative regulators of p53. *Molecular Biology Reports*, 38(1), pp.229–236.
Wen, K.W. & Damania, B., 2010. Kaposi sarcoma-associated herpesvirus (KSHV): molecular biology and oncogenesis. *Cancer letters*, 289(2), pp.140–50.
Winkler, L.L., Hwang, J. & Kalejta, R.F., 2013. Ubiquitin-independent proteasomal degradation of tumor suppressors by human cytomegalovirus pp71 requires the 19S regulatory particle. *Journal of virology*, 87(8), pp.4665–4671.
Xia, L. et al., 2017. Human Cytomegalovirus vaccine development: Immune responses to look into vaccine strategy. *Human vaccines & immunotherapeutics*, 14(2), pp.292–303.
Yu, Y. et al., 2017. USP7 is associated with greater disease activity in systemic lupus erythematosus via stabilization of the IFNalpha receptor. *Molecular medicine reports*, 16(2), pp.2274–2280.

Yu, Y. & Hayward, G.S., 2010. The ubiquitin E3 ligase RAUL negatively regulates type i interferon through ubiquitination of the transcription factors IRF7 and IRF3. *Immunity*, 33(6), pp.863–877.
Zhu, H. et al., 2001. Global analysis of protein activities using proteome chips. *Science (New York, N.Y.)*, 293(5537), pp.2101–2105.
Zhu, Y. et al., 2014. Nanoliter-scale protein crystallization and screening with a microfluidic droplet robot. *Scientific reports*, 4, p.5046.
Zhu, Y. & Fang, Q., 2013. Analytical detection techniques for droplet microfluidics--a review. *Analytica chimica acta*, 787, pp.24–35.
Zlatanou, A. et al., 2015. USP7 is essential for maintaining Rad18 stability and DNA damage tolerance. *Oncogene*, 35(8), pp.965–976.

Appendix

Appendix A: List of Primers Used in Chapter 2 for p15TVL Cloning.

UBP	Residues	Forward Primer	Reverse Primer
1	1-809	ttgtatttccagggcatggatttgtttattgaaagc	caagcttcgtcatcagtttacatctttaccaga
	92-741	ttgtatttccagggcgagatcttgaaaagaggt	caagcttcgtcatcattcatcaaagtcatattcg
	92-809	ttgtatttccagggcgagatcttgaaaagaggt	caagcttcgtcatcagtttacatctttaccaga
	93-753	ttgtatttccagggcatgatcttgaaaagaggtggt	caagcttcgtcatcaaatagcttccaaatcatc
	97-741	ttgtatttccagggcggtggtttcattgctggt	caagcttcgtcatcattcatcaaagtcatattcg
	97-809	ttgtatttccagggcggtggtttcattgctggt	caagcttcgtcatcagtttacatctttaccaga
	101-739	ttgtatttccagggcatggctggtttagttaatgat	ttgtatttccagggcatggctggtttagttaatgat
2	1-735	ttgtatttccagggcatgatgccgaacgaagataat	caagcttcgtcatcatggccaattttctggcgg
	434-832	ttgtatttccagggcatgaatgagcaaactcattcg	caagcttcgtcatcatgccaaatatgctagctc
	724-1271	ttgtatttccagggcatgatagatccaaattccttg	caagcttcgtcatcatagaattcttttcaatgg
	725-1271	ttgtatttccagggcgatccaaattccttgccg	caagcttcgtcatcatagaattcttttcaatggctc
	725-1259	ttgtatttccagggcgatccaaattccttgccg	caagcttcgtcatcatccttgtttgacatatac
	731-1271	ttgtatttccagggcccagaaaattggccaact	caagcttcgtcatcatagaattcttttcaatggctc
	731-1259	ttgtatttccagggcccagaaaattggccaact	caagcttcgtcatcatccttgtttgacatatac
	736-1259	ttgtatttccagggcatgactggcattaataatatc	caagcttcgtcatcatccttgtttgacatatac
For cloning in pET-28b vector	1-912	gcgcccatgggcatgaacatgcaagacgctaac	gcgctcgagatttctcttttgatacattaaaatataggc
	148-912	gcgcccatgggcaacagtggcagcaatgcg	gcgctcgagatttctcttttgatacattaaaatataggc
	189-912	gcgcccatgggcgatgtcactaaattaaagaatctc	gcgctcgagatttctcttttgatacattaaaatataggc
3	1-912	ttgtatttccagggcatgaacatgcaagacgctaac	caagcttcgtcatcaatttctcttttgatacat
	1-459	ttgtatttccagggcatgatgaacatgcaagacgct	caagcttcgtcatcatggaataatggaatggac
	50-912	ttgtatttccagggctaccccacacaaatacct	caagcttcgtcatcaatttctcttttgatacat
	104-912	ttgtatttccagggcggcattaccaataacaatgga	caagcttcgtcatcaatttctcttttgatacat
	148-912	ttgtatttccagggcaacagtggcagcaatgcg	caagcttcgtcatcaatttctcttttgatacat
	189-912	ttgtatttccagggcgatgtcactaaattaaagaatctc	caagcttcgtcatcaatttctcttttgatacat
	412-912	ttgtatttccagggcatgaaatacgttccaccttct	caagcttcgtcatcaatttctcttttgatacat
	426-909	ttgtatttccagggcggttcgattgcgttaaga	caagcttcgtcatcattgatacattaaaatataggc
	426-912	ttgtatttccagggcggttcgattgcgttaaga	caagcttcgtcatcaatttctcttttgatacat
	429-909	ttgtatttccagggcgcgttaagaatgtgttttg	caagcttcgtcatcattgatacattaaaatataggc
	429-912	ttgtatttccagggcgcgttaagaatgtgttttg	caagcttcgtcatcaatttctcttttgatacat
	445-909	ttgtatttccagggcaataaagatgttgaaaac	caagcttcgtcatcattgatacattaaaatataggc
	445-912	ttgtatttccagggcaataaagatgttgaaaac	caagcttcgtcatcaatttctcttttgatacat
	447-909	ttgtatttccagggcgatgttgaaaacaaaatacca	caagcttcgtcatcattgatacattaaaatataggc
	447-912	ttgtatttccagggcgatgttgaaaacaaaatacca	caagcttcgtcatcaatttctcttttgatacat
	449-909	ttgtatttccagggcgaaaacaaaataccagtc	caagcttcgtcatcattgatacattaaaatataggc
	449-912	ttgtatttccagggcgaaaacaaaataccagtc	caagcttcgtcatcaatttctcttttgatacat
	454-912	ttgtatttccagggcgtccattccattattcca	caagcttcgtcatcaatttctcttttgatacat
	459-912	ttgtatttccagggcatgagaggcataattaacaga	caagcttcgtcatcaatttctcttttgatacat

UBP	Residues	Forward Primer	Reverse Primer
4	1-323	ttgtatttccagggcatgatggagcagaatattatt	caagcttcgtcatcaatttgacttaagccaacc
	1-330	ttgtatttccagggcatggagcagaatattattagt	caagcttcgtcatcatgatgatacttgcctccc
	1-561	ttgtatttccagggcatgatggagcagaatattatt	caagcttcgtcatcacgcgaaatcaaggtcata
	2-315	ttgtatttccagggcgagcagaatattattagtacc	caagcttcgtcatcaaccagattccagaatga
	324-561	ttgtatttccagggcatgtatgggaggcaagtatca	caagcttcgtcatcacgcgaaatcaaggtcata
	545-926	ttgtatttccagggcatgcatacagatgttacacca	caagcttcgtcatcaaacaccgtagacgcggtg
	551-926	ttgtatttccagggcacttcttctcataattatgac	caagcttcgtcatcaaacaccgtagacgcggt
	556-926	ttgtatttccagggctatgaccttgatttcgcg	caagcttcgtcatcaaacaccgtagacgcggt
	562-924	ttgtatttccagggcatggttggtttggaaaatcta	caagcttcgtcatcagtagacgcggtgataaaa
5	1-280	ttgtatttccagggcatgatgggctcagaacaagcc	caagcttcgtcatcatataagatctagatcaag
	1-289	ttgtatttccagggcatgggctcagaacaagcc	caagcttcgtcatcacgctgtttcactgacaga
	1-445	ttgtatttccagggcatgatgggctcagaacaagcc	caagcttcgtcatcatataagatctagatcaag
	3-270	ttgtatttccagggctcagaacaagccttaagt	caagcttcgtcatcacccattttccaaaatgag
	3-280	ttgtatttccagggctcagaacaagccttaagt	caagcttcgtcatcatataagatctagatcaag
	281-445	ttgtatttccagggcatgtatcaatcatctgtcagt	caagcttcgtcatcatataagatctagatcaag
	431-805	ttgtatttccagggcatgaccatcctaaacaac	caagcttcgtcatcatcaaaaaattctttcgta
	434-805	ttgtatttccagggcctaaacaactcacaagtg	caagcttcgtcatcatcaaaaaattctttcgta
	440-805	ttgtatttccagggccttgatctagatcttatag	caagcttcgtcatcatcaaaaaattctttcgta
	446-805	ttgtatttccagggcatggtaggattggaaaatata	caagcttcgtcatcaaaaaattctttcgtaaaa
6	1-499	ttgtatttccagggcatgatgagcggagaaacgttt	caagcttcgtcatcacagaccaaatcctttata
	109-488	ttgtatttccagggcatggttggtttcaagaatatg	caagcttcgtcatcaactatcactttcgccccc
7	1-460	ttgtatttccagggcatgatgctagacgatgataag	caagcttcgtcatcacaagtaatcttcaataga
	1-608	ttgtatttccagggcatgatgagcggagaaacgttt	caagcttcgtcatcacagaccaaatcctttata
	593-1071	ttgtatttccagggcatgattccaactattgaacgc	caagcttcgtcatcactagtcataaaccctttc
	598-1070	ttgtatttccagggccgcagtccaaacgtatac	caagcttcgtcatcaataaaccctttcataaaa
	598-1071	ttgtatttccagggccgcagtccaaacgtatac	caagcttcgtcatcactagtcataaaccctttc
	603-1070	ttgtatttccagggctacgtttcgttgtccatc	caagcttcgtcatcaataaaccctttcataaaa
	603-1071	ttgtatttccagggctacgtttcgttgtccatc	caagcttcgtcatcactagtcataaaccctttc
	608-1070	ttgtatttccagggcatgacgggactaagaaatttg	caagcttcgtcatcaataaaccctttcataaaa
8	1-136	ttgtatttccagggcatgatgagcatttgtccacat	caagcttcgtcatcaaagcccatctcttctttc
	137-469	ttgtatttccagggcatgtctggcctgatcaacatg	caagcttcgtcatcattgacgaatggtgtagaa

UBP	Residues	Forward Primer	Reverse Primer
9	1-754	ttgtatttccagggcatgatgataaaaagatggtta	caagcttcgtcatcatttgatgaagctcaatat
	122-671	ttgtatttccagggcatgccatatggggatggt	caagcttcgtcatcaattttcggtcttatcagc
	122-707	ttgtatttccagggcgatttaatgccatatggg	caagcttcgtcatcatttacgatcccttaacca
	124-674	ttgtatttccagggcatgccatatggggatggt	caagcttcgtcatcaattttcggtcttatcagc
	128-671	ttgtatttccagggcgatggttccaataaagtg	caagcttcgtcatcacttatcagcctgtgtttc
	128-707	ttgtatttccagggcgatggttccaataaagtg	caagcttcgtcatcatttacgatcccttaacca
	134-668	ttgtatttccagggcatgtttggttatgaaaatttt	caagcttcgtcatcactgtgtttctttatagaa
	311-668	ttgtatttccagggcatggcttcaactacagattgt	caagcttcgtcatcactgtgtttctttatagaa
10	1-361	ttgtatttccagggcatgatgaccactcaagaatcg	caagcttcgtcatcaaggcttcaaattggtgaa
	336-746	ttgtatttccagggcatgatcaatgatcgtggttct	caagcttcgtcatcaggcagatttcgccaatgg
	351-734	ttgtatttccagggcaattggggcgacaaattc	caagcttcgtcatcaagttagcctcgtgtatag
	351-746	ttgtatttccagggcaattggggcgacaaattc	caagcttcgtcatcaagatttcgccaatggcaa
	356-734	ttgtatttccagggcttcaccaatttgaagcct	caagcttcgtcatcaagttagcctcgtgtatag
	356-746	ttgtatttccagggcttcaccaatttgaagcct	caagcttcgtcatcaagatttcgccaatggcaa
	362-734	ttgtatttccagggcatgcgtggccttttgaatcat	caagcttcgtcatcaagttagcctcgtgtatag
11	1-297	ttgtatttccagggcatgatgttattaaacccagat	caagcttcgtcatcaaatagataactctgataa
	1-135	ttgtatttccagggcatgatgttattaaacccagat	caagcttcgtcatcatcttttttcttttttatggt
	297-710	ttgtatttccagggcatgactggcctgcaaaatcca	caagcttcgtcatcaatccattctttcgtagaa
	283-713	ttgtatttccagggcatgccagtaattgaagattct	caagcttcgtcatcattcatagttctcttcatc
	287-717	ttgtatttccagggcgaagattctaatgatctg	caagcttcgtcatcaacagaattcttcttcatag
	291-717	ttgtatttccagggcctgttatcagagttatct	caagcttcgtcatcaacagaattcttcttcatag
12	1-1123	ttgtatttccagggcatgggttcttcagatgtttca	caagcttcgtcatcactgtagtttagagctgcc
	1-345	ttgtatttccagggcatgggttcttcagatgtttca	caagcttcgtcatcagtgattcccttctatagg
	1-361	ttgtatttccagggcatgggttcttcagatgtttca	caagcttcgtcatcatgatgctggttcgagttt
	1-367	ttgtatttccagggcatgggttcttcagatgtttca	caagcttcgtcatcagaccaaaccagtagtacc
	90-361	ttgtatttccagggcatgaatggtcaagatggaaga	caagcttcgtcatcatgatgctggttcgagttt
	98-345	ttgtatttccagggcgtcttagaacaacaaaga	caagcttcgtcatcagtgattcccttctatagg
	98-361	ttgtatttccagggcgtcttagaacaacaaaga	caagcttcgtcatcatgatgctggttcgagttt
	90-1123	ttgtatttccagggcatgaatggtcaagatggaaga	caagcttcgtcatcactgtagtttagagctgcc
	98-1123	ttgtatttccagggcgtcttagaacaacaaaga	caagcttcgtcatcactgtagtttagagctgcc
	101-1119	ttgtatttccagggcatgggtactactggtttggtc	caagcttcgtcatcaatgacggcgaatgtaaaa
	353-1123	ttgtatttccagggcgcttataataaactcgaac	caagcttcgtcatcactgtagtttagagctgcc
	358-1123	ttgtatttccagggcgaaccagcatcaggtact	caagcttcgtcatcactgtagtttagagctgcc
	362-1119	ttgtatttccagggcatgggtactactggtttggtc	caagcttcgtcatcaatgacggcgaatgtaaaa

UBP	Residues	Forward Primer	Reverse Primer
13	1-747	ttgtatttccagggcatgatgatcagaagatggcta	caagcttcgtcatcagcttttcctaaaactaaa
	139-669	ttgtatttccagggcatgtttggatacgaaaatttt	caagcttcgtcatcaatacatcgctttataaaa
	129-673	ttgtatttccagggctcaatgccctatggagac	caagcttcgtcatcaagcgtttgaatacatcgc
	129-682	ttgtatttccagggctcaatgccctatggagac	caagcttcgtcatcatgccatattttcacgatc
	134-673	ttgtatttccagggcatggacggctccaacaaagtt	caagcttcgtcatcaagcgtttgaatacatcgc
	134-682	ttgtatttccagggcatggacggctccaacaaagtt	caagcttcgtcatcatgccatattttcacgatc
	329-669	ttgtatttccagggcatgaataacctggacttgaaa	caagcttcgtcatcaatacatcgctttataaaa
14	1-781	ttgtatttccagggcatggcagaagcagtactagaa	caagcttcgtcatcagcatcttgtatagaaata
	1-322	ttgtatttccagggcatggcagaagcagtactagaa	caagcttcgtcatcagccataattcttactagc
	40-277	ttgtatttccagggccattcattgaatatatgc	caagcttcgtcatcattcttgtatgttaattccg
	312-781	ttgtatttccagggctttgaaaaattatccgct	caagcttcgtcatcagcatcttgtatagaaata
	316-781	ttgtatttccagggcatggctagtaagaattatggc	caagcttcgtcatcagcatcttgtatagaaata
	317-781	ttgtatttccagggcgctagtaagaattatggc	caagcttcgtcatcagcatcttgtatagaaata
	322-781	ttgtatttccagggcatgtgtggtctgatcaatttg	caagcttcgtcatcagcatcttgtatagaaata
15	215-537	ttgtatttccagggcatggttggcttccgaaatcag	caagcttcgtcatcattcttgacgtatataaac
	1-204	ttgtatttccagggcatgatgagctctgaagacgaa	caagcttcgtcatcaatagcccgtgactttctt
	538-1230	ttgtatttccagggcatgcaagaggaggatttgctg	caagcttcgtcatcagtttttaatgatcattgg
16	41-497	ttgtatttccagggcggggattctaagcagagt	caagcttcgtcatcaatttacacgttcgtagtatag
	46-499	ttgtatttccagggcatgagtattgggaagtacacg	caagcttcgtcatcatttatttacacgttcgta
	47-497	ttgtatttccagggcattgggaagtacacgaca	caagcttcgtcatcaatttacacgttcgtagtatag
	53-499	ttgtatttccagggcatggtgggcttaattaatcgt	caagcttcgtcatcatttatttacacgttcgta
SAD1	1-149	ttgtatttccagggcatgatggaggttgataacaaa	caagcttcgtcatcaaaatccattcagatatgt
	44-448	ttgtatttccagggctctgagaaaatttgctgc	caagcttcgtcatcactcttgcttttcccatac
	150-448	ttgtatttccagggcatgatagggttcaccaatgcg	caagcttcgtcatcactcttgcttttcccatac
PAN2	1-504	ttgtatttccagggcatgatgaataattggcaacat	caagcttcgtcatcaatactcagtgttattaaa
	493-826	ttgtatttccagggcaattttgattttacgccc	caagcttcgtcatcaaggttttcgtaattcttcc
	505-846	ttgtatttccagggcatgtcaggattggatccagat	caagcttcgtcatcatgttttccaagggtatgt
	847-1115	ttgtatttccagggcatgccagaaattatcatatat	caagcttcgtcatcatccctttgaagtttctgg